frontiers | Research Topics

Clinical management of cardiac ventricular arrhythmias: Mapping and ablation

Edited by
Feifan Ouyang, Tom Wong, Minglong Chen, Kyoung-Ryul Julian Chun and Andreas Metzner

Published in
Frontiers in Cardiovascular Medicine

ISSN 1664-8714
ISBN 978-2-83251-612-6
DOI 10.3389/978-2-83251-612-6

About Frontiers

Frontiers is more than just an open access publisher of scholarly articles: it is a pioneering approach to the world of academia, radically improving the way scholarly research is managed. The grand vision of Frontiers is a world where all people have an equal opportunity to seek, share and generate knowledge. Frontiers provides immediate and permanent online open access to all its publications, but this alone is not enough to realize our grand goals.

Frontiers journal series

The Frontiers journal series is a multi-tier and interdisciplinary set of open-access, online journals, promising a paradigm shift from the current review, selection and dissemination processes in academic publishing. All Frontiers journals are driven by researchers for researchers; therefore, they constitute a service to the scholarly community. At the same time, the *Frontiers journal series* operates on a revolutionary invention, the tiered publishing system, initially addressing specific communities of scholars, and gradually climbing up to broader public understanding, thus serving the interests of the lay society, too.

Dedication to quality

Each Frontiers article is a landmark of the highest quality, thanks to genuinely collaborative interactions between authors and review editors, who include some of the world's best academicians. Research must be certified by peers before entering a stream of knowledge that may eventually reach the public - and shape society; therefore, Frontiers only applies the most rigorous and unbiased reviews. Frontiers revolutionizes research publishing by freely delivering the most outstanding research, evaluated with no bias from both the academic and social point of view. By applying the most advanced information technologies, Frontiers is catapulting scholarly publishing into a new generation.

What are Frontiers Research Topics?

Frontiers Research Topics are very popular trademarks of the *Frontiers journals series*: they are collections of at least ten articles, all centered on a particular subject. With their unique mix of varied contributions from Original Research to Review Articles, Frontiers Research Topics unify the most influential researchers, the latest key findings and historical advances in a hot research area.

Find out more on how to host your own Frontiers Research Topic or contribute to one as an author by contacting the Frontiers editorial office: frontiersin.org/about/contact

Clinical management of cardiac ventricular arrhythmias: Mapping and ablation

Topic editors

Feifan Ouyang — University Medical Center Hamburg-Eppendorf, Germany
Tom Wong — The Royal Brompton and Harefield NHS Foundation Trust, National Heart and Lung Institute, Imperial College London, China
Minglong Chen — The First Affiliated Hospital of Nanjing Medical University, China
Kyoung-Ryul Julian Chun — CCB Frankfurt, Med. III, Kardiologie, Markuskrankenhaus, Germany
Andreas Metzner — University Heart and Vascular Center, University Medical Center Hamburg-Eppendorf, Germany

Citation

Ouyang, F., Wong, T., Chen, M., Chun, K.-R. J., Metzner, A., eds. (2023). *Clinical management of cardiac ventricular arrhythmias: Mapping and ablation*. Lausanne: Frontiers Media SA. doi: 10.3389/978-2-83251-612-6

Table of contents

frontiers in Cardiovascular Medicine

ORIGINAL RESEARCH
published: 20 October 2021
doi: 10.3389/fcvm.2021.747858

Cardiopulmonary Support During Catheter Ablation of Ventricular Arrhythmias With Hemodynamic Instability: The Role of Inducibility

*Massimo Grimaldi[1], Maria Monica Marino[2], Nicola Vitulano[1], Federico Quadrini[1], Federica Troisi[1], Nicola Caporusso[3], Vera Perniciaro[1], Rosa Caruso[1], Nicola Duni[1], Giacomo Cecere[1], Alberto Martinelli[1], Pietro Guida[1], Vito Del Monte[3], Tommaso Langialonga[1], Luigi Di Biase[4,5] and Antonio Di Monaco[1,6]**

[1] Ospedale Generale Regionale "F. Miulli," Dipartimento di Cardiologia, Bari, Italy, [2] Policlinico Tor Vergata, Dipartimento di Cardiologia, Rome, Italy, [3] Ospedale Generale Regionale "F. Miulli," Dipartimento di Anestesia e Rianimazione, Bari, Italy, [4] St. David's Medical Center, Texas Cardiac Arrhythmia Institute, Austin, TX, United States, [5] Montefiore Medical Center, Albert Einstein College of Medicine, Bronx, NY, United States, [6] Dipartimento di Medicina Clinica e Sperimentale, Universitá di Foggia, Foggia, FG, Italy

OPEN ACCESS

Edited by:
Minglong Chen,
The First Affiliated Hospital of Nanjing Medical University, China

Reviewed by:
Vikas Kataria,
University of Delhi, India
Hui-Nam Pak,
Yonsei University Health System, South Korea

***Correspondence:**
Antonio Di Monaco
a.dimonaco@gmail.com

Specialty section:
This article was submitted to Cardiac Rhythmology, a section of the journal Frontiers in Cardiovascular Medicine

Received: *26 July 2021*
Accepted: *20 September 2021*
Published: *20 October 2021*

Citation:
Grimaldi M, Marino MM, Vitulano N, Quadrini F, Troisi F, Caporusso N, Perniciaro V, Caruso R, Duni N, Cecere G, Martinelli A, Guida P, Del Monte V, Langialonga T, Di Biase L and Di Monaco A (2021) Cardiopulmonary Support During Catheter Ablation of Ventricular Arrhythmias With Hemodynamic Instability: The Role of Inducibility. Front. Cardiovasc. Med. 8:747858. doi: 10.3389/fcvm.2021.747858

Background: Catheter ablation is a treatment option for sustained ventricular tachycardias (VTs) that are refractory to pharmacological treatment; however, patients with fast VT and electrical storm (ES) are at risk for cardiogenic shock. We report our experience using cardiopulmonary support with extracorporeal membrane oxygenation (ECMO) during catheter ablation of VT.

Methods: Sixty-two patients (mean age 68 ± 9 years; 94% male) were referred to our center for catheter ablation of repeated episodes of hemodynamically unstable ventricular arrhythmias. ES was defined as the occurrence of three or more VT/ventricular fibrillation episodes requiring electrical cardioversion or defibrillation in a 24-h period. All patients had hemodynamically unstable VTs.

Results: Thirty-one patients (group 1) performed catheter ablation without ECMO support and 31 patients (group 2) with ECMO support. At the end of the procedure, ventricular inducibility was not performed in 16 patients of group 1 (52%) due to significant hemodynamic instability. Ventricular inducibility was performed in the other 15 patients (48%); polymorphic VTs were inducible in eight patients. In group 2, VTs were not inducible in 29 patients (93%); polymorphic VTs were inducible in two patients. The median follow-up duration was 24 months. Four patients of group 1 (13%) and five patients of group 2 (16%) died due to refractory heart failure. An implantable cardioverter-defibrillator intervention (shock or antitachycardia pacing) was documented in 13 patients of group 1 (42%) and six patients of group 2 (19%).

Conclusions: Extracorporeal membrane oxygenation support during catheter ablation for hemodynamically unstable VTs is a useful tool to prevent acute procedural heart failure and to reduce arrhythmic burden.

Keywords: catheter ablation, electrical storm, extracorporeal membrane oxygenation, ventricular arrhythmia, ventricular inducibility

INTRODUCTION

Electrical storm (ES) is a life-threatening syndrome that consists of repeated episodes of ventricular tachycardia (VT) or ventricular fibrillation (VF) occurring over a short period of time. Termination of ES requires an appropriate external or implantable cardioverter-defibrillator (ICD) intervention (1). Previous studies have described poor outcomes associated with ES as well as an up to 3-fold increased risk of mortality in patients with ES (1–3).

Catheter ablation for ES can reduce recurrent episodes of ventricular arrhythmias (VAs) and improve patient prognoses (4–7); however, patients with hemodynamically unstable VAs have a rate of procedural complications and mortality. Recent data suggest that cardiopulmonary support with extracorporeal membrane oxygenation (ECMO) can provide valuable support during catheter ablation procedures in this setting (8–14). In particular, the ECMO system is useful for managing intraoperative acute hemodynamic decompensation and can facilitate the accurate mapping and ablation of unstable VAs.

In this study, we report our experience regarding the ablation of hemodynamically unstable VAs with or without ECMO support.

METHODS

Study Population

A total of 62 patients (mean age 68 ± 9 years; 94% male) were referred to Miulli Hospital for catheter ablation of repeated episodes of hemodynamically unstable sustained VAs between January 2015 and December 2019. All patients had ES and hemodynamically unstable VAs symptomatic for syncope or presyncope. ES was defined as the occurrence of three or more VT/VF episodes requiring electrical cardioversion or defibrillation in a 24-h period (1). All arrhythmias were unresponsive to amiodarone antiarrhythmic therapy. ECMO support was available at our center from January 2017. Thirty-one patients (group 1) performed catheter ablation without ECMO support (from January 2015 to December 2016) and 31 patients (group 2) with ECMO support (from January 2017 to December 2019).

All procedures were performed by expert operators; the surgical team consisted of two electrophysiologists, one interventional cardiologist, one anesthesiologist, two perfusion technicians, and two nurses. Two vascular surgeons were also present if a patient required femoral artery isolation. All patients underwent preoperative Doppler ultrasound and/or angiocomputed tomography of the lower leg to assess the femoral arteries. The study was approved by the local Ethics Committee.

Electrophysiological Study and Ablation With ECMO Support

All procedures were initiated under conscious sedation with an intravenous infusion of diazepam (10 mg) and fentanyl (0.2 mg) under the supervision of an anesthesiologist; general anesthesia was administered at the discretion of the anesthesiologist. Antibiotic prophylaxis (cefazolin 2 g and teicoplanin 400–600 mg) was administered immediately before the procedure. Intra-arterial blood pressure monitoring and digital pulse oximetry were monitored continuously during the procedure and ICD therapies were inactivated for the duration of the procedure.

In group 2 patients, before inserting ablation catheters into the heart, cannulas for ECMO support were positioned under the supervision of two expert perfusionists. The circuit (Cardiohelp System, Maquet, Rastatt, Germany) consisted of a centrifugal pump, polymethylpentene gas exchanger, heat exchanger, tubing, and variously sized cannulas for venous and arterial cannulation. The appropriate cannula sizes were selected based on an evaluation of vascular diameter from Doppler ultrasound or angiocomputed tomography of the lower leg and on patient weight. The left femoral artery was cannulated and a guidewire was positioned in the right femoral artery. Angiography was performed to visualize the right common femoral artery and the artery was cannulated under fluoroscopic guidance using the Seldinger technique. Two Perclose Proglide (Abbot, North Chicago, United States) suture-mediated closure systems were positioned in the femoral arteries to facilitate closure of the arteries at the end of the procedure. The right femoral vein was also cannulated. The arterial cannula was inserted into the common femoral artery and advanced up to the iliac artery. The venous cannula was advanced up to the right atrium under fluoroscopic guidance. In patients with a small right femoral artery, a small sheath was placed in the superficial femoral artery to permit distal flow and prevent limb ischemia. In three patients with significant femoral arterial atherosclerosis, the ECMO cannulas were positioned by vascular surgeons. ECMO support was started at 3 L and adjusted following the patient's hemodynamics. During support, heparin was administered to a target-activated clotting time of 300 s in cases of endocardial left VA or 250 s in cases of endocardial right or epicardial VA.

In patients with VA of suspected epicardial origin, a pericardial approach was guaranteed before positioning the ECMO circuit. This workflow was adopted so that the pericardial approach was performed before heparin administration. We performed the pericardial approach as described previously (15) and placed a steerable sheath (Agilis, St. Jude Medical) in the pericardial space to allow catheter stability and maneuverability.

In all patients, the ablation catheter was inserted through the femoral artery/vein and located inside of the left/right ventricle or epicardium through the pericardial sheath. Mapping and ablation were performed with a 3.5-mm irrigated catheter with a contact force sensor (Thermocool Smartouch Surround Flow, Biosense Webster, CA, USA) and a three-dimensional mapping system (CARTO, Biosense Webster, Inc., CA, USA). Substrate maps were obtained using a multipolar mapping catheter (Pentaray; Biosense Webster, CA, USA) in 27 patients.

At first, a geometry of the chamber of interest was created using the Thermocool Smartouch Surround Flow or Pentaray catheters (Biosense Webster, CA, USA); then, a substrate map was acquired during sinus rhythm or right ventricular pacing in pacing-dependent patients. In those patients with cardiac resynchronization therapy devices, left ventricular pacing was turned off.

Initially, an accurate substrate ablation was performed targeting the areas of local abnormal ventricular activity and late potentials (16, 17). In patients with a spontaneous induction of clinical VTs during substrate mapping or ablation, activation mapping was attempted if hemodynamic stability. Activation and entrainment mapping were performed to identify critical sites of the VT reentrant circuit as previously described (18–20). In particular, the window of interest was opened from the termination of the first QRS to the onset of the second QRS of the VT cycle, to define the diastolic interval. The last step was ventricular inducibility. Programmed ventricular stimulation after ablation was performed at the right ventricular apex (basal drive 600/500/400 ms up to three extra stimuli). In the case of inducible VTs, a new mapping and ablation was performed until the non-inducibility was obtained.

Extracorporeal membrane oxygenation (ECMO) support was increased during acute hemodynamic decompensation due to spontaneous or induced VT to permit optimal mapping and ablation of arrhythmias. Radiofrequency energy was delivered with a maximum power of 45 W and a targeted impedance decrease of at least 10% from baseline. Ablation was delivered when the contact force was between 7 and 30 g; when the contact force was > 20 g, we used a maximum power of 35 W. Procedural success was defined as an inability to induce sustained VTs and the disappearance of frequent spontaneous premature ventricular complexes.

In all the patients of group 2, the arterial and venous cannulas were removed at the end of the procedure. The right femoral artery was closed using the previously positioned Perclose Proglide closure system and the vein was closed with manual compression. In three patients, ECMO cannulas were removed by vascular surgeons. After ECMO cannula removal, right femoral artery angiography was performed to exclude the possibility of procedural damage (the angiography catheter was inserted through the left femoral artery). Blood inside of the circuit was recovered using an autologous blood recovery machine (Cell Saver®5+, Haemonetics Corporation) and infused into the patient.

Clinical follow-up was performed every month after catheter ablation for the first year than every 3 months. Clinical recurrence, ICD therapy, and procedural complications were recorded for all patients.

Statistical Analysis

Descriptive statistics are summarized as the mean ± SD for continuous variables and the number or percentages for categorical variables. The Kaplan–Meier method was used to show graphically survival postprocedure. Statistical analyses were performed using STATA software version 14 (Stata, College Station, TX, USA).

RESULTS

General Findings and Procedural Data

The main clinical characteristics of patients are reported in **Table 1**. There were no significant differences regarding most clinical characteristics parameters except for hypertension, coronary artery bypass graft surgery, and pharmacological therapy (antiplatelets, anticoagulants, and statins). No significant differences were found regarding PAINESD risk score, previous catheter ablations for VT, mean length cycle of VTs, and mean left ventricular ejection fraction (**Table 1**). All patients were refractory to treatment with at least one antiarrhythmic drug. None of the patients presented with ES in the context of acute myocardial infarction. Reversible ischemia was excluded by left heart catheterization in each patient the same day of the procedure or the day before the procedure. None of the patients exhibited alterations in serum electrolytes.

Electrophysiological Study and Ablation With ECMO Support

Two patients of group 2 required urgent ECMO support for acute heart decompensation, the other 29 patients underwent the ablation with prophylactic ECMO support considering the hemodynamically unstable VAs. General anesthesia was used in 14 (45%) patients of group 1 and 16 (51%) patients of group 2. We performed epicardial access without complications in one patient of group 1 (3%) and three patients of group 2 (10%); in all these patients, epicardial ablation was performed without complications. In three cases of significant femoral arterial atherosclerosis, ECMO cannulas were positioned by vascular surgeons. In all patients of group 2, the diameters of the arterial and venous cannulas were 15 and 25 Fr, respectively.

The left ventricle was mapped in all patients of group 1. In 21 patients of group 1 (68%), spontaneous clinical VTs were documented during substrate mapping. All VTs were not mapped and they were interrupted with electrical cardioversion due to hemodynamic instability. A median of three electrical shock applications (range 1–5) was used per patient. At the end of substrate ablation, the programmed ventricular stimulation was not performed in 16 patients (52%) due to significant hemodynamic instability. Ventricular inducibility was performed in the other 15 patients (48%); polymorphic VTs were inducible in eight patients and the operator decided to stop the procedure for the hemodynamic instability.

In group 2, the left ventricle was mapped in all patients and the right ventricle was mapped in five patients. In 23 patients of group 2 (74%), 37 VTs induced during substrate mapping were successfully mapped and ablated in all patients. A median of two VTs (range, 1–3) was targeted per patient. ECMO support preserved hemodynamic stability during all VTs permitting an accurate mapping. After substrate ablation, VTs were not inducible in 20 patients of group 2 (64%). In nine patients, the induced VTs were successfully mapped and ablated thus obtaining the absence of ventricular inducibility at the end of the procedure. Polymorphic VTs were inducible in two patients of group 2 and the operator decided to stop the procedure after a mean time of 3.4 h. Among these two patients, electrocardiographic analysis of QRS morphologies was consistent with an epicardial origin of VTs and the operator did not get the pericardial access due to a previous coronary

TABLE 1 | Patient characteristics by study groups.

	All $n = 62$	No ECMO $n = 31$	ECMO $n = 31$	p
Age (years)	68 ± 9	69 ± 8	66 ± 10	0.135
Male sex	58 (94%)	30 (97%)	28 (90%)	0.612
Smoking history	33 (53%)	19 (61%)	14 (45%)	0.203
Body mass index (Kg/m^2)	25.9 ± 3.4	26.6 ± 3.8	25.2 ± 2.8	0.085
Body mass index >30 Kg/m^2	6 (10%)	5 (16%)	1 (3%)	0.195
Hypertension	38 (61%)	23 (74%)	15 (48%)	0.037
Dyslipidemia	42 (68%)	24 (77%)	18 (58%)	0.103
Diabetes mellitus	15 (24%)	9 (29%)	6 (19%)	0.374
Chronic renal failure	14 (23%)	6 (19%)	8 (26%)	0.544
Familiarity for cardiovascular disease	25 (40%)	15 (48%)	10 (32%)	0.196
Chronic obstructive pulmonary disease	33 (53%)	18 (58%)	15 (48%)	0.445
Dysthyroidism	15 (24%)	8 (26%)	7 (23%)	0.767
Coronary artery disease	47 (76%)	25 (81%)	22 (71%)	0.374
Percutaneous coronary intervention	37 (60%)	18 (58%)	19 (61%)	0.796
Coronary artery bypass graft surgery	14 (23%)	11 (35%)	3 (10%)	0.015
Valve surgery	2 (3%)	2 (6%)	0 (0%)	0.492
NYHA classification III-IV	47 (76%)	23 (74%)	24 (77%)	0.767
Stroke	3 (5%)	1 (3%)	2 (6%)	1.000
Hypertrophic cardiomyopathy	1 (2%)	0 (0%)	1 (3%)	1.000
Idiopathic ventricular fibrillation	2 (3%)	0 (0%)	2 (6%)	0.492
Idiopathic dilated cardiomyopathy	10 (16%)	3 (10%)	7 (23%)	0.167
ARVD	1 (2%)	1 (3%)	0 (0%)	1.000
Previous catheter ablation for VT	15 (24%)	9 (29%)	6 (19%)	0.374
Number of shock/ATP	6.8 ± 2.6	5.7 ± 2.8	7.5 ± 2.3	0.055
Mean length cycle of VT (m)	296 ± 32	285 ± 34	307 ± 30	0.16
Left ventricular ejection fraction (%)	30 ± 9	30 ± 8	30 ± 10	1.000
Left ventricular ejection fraction <25%	32 (52%)	14 (45%)	18 (58%)	0.309
Left ventricular diameter (mm)	61 ± 7	60 ± 5	62 ± 8	0.233
PAINESD risk score	21 ± 6	22 ± 5	21 ± 7	0.373
ACE-inhibitors	26 (42%)	13 (42%)	13 (42%)	1.000
Angiotensin-II-receptor antagonists	12 (19%)	6 (19%)	6 (19%)	1.000
Sacubitril plus valsartan	19 (31%)	10 (32%)	9 (29%)	0.783
Beta-blocker	61 (98%)	31 (100%)	30 (97%)	1.000
Diuretics	52 (84%)	26 (84%)	26 (84%)	1.000
Calcium channel blocker	7 (11%)	5 (16%)	2 (6%)	0.425
Antiplatelet	40 (65%)	24 (77%)	16 (52%)	0.034
Anticoagulant	26 (42%)	7 (23%)	19 (61%)	0.002
Amiodarone	57 (92%)	30 (97%)	27 (87%)	0.354
Statins	41 (66%)	25 (81%)	16 (52%)	0.016
Tapazole	6 (10%)	3 (10%)	3 (10%)	1.000
Levotiroxin	10 (16%)	6 (19%)	4 (13%)	0.490

Mean ± SD or absolute frequency (percentage). ACE, angiotensin converting enzyme; ARVD, arrhythmogenic right ventricular dysplasia; ATP, antitachycardia pacing; NYHA, New York Heart Association; VT, ventricular tachycardia.

TABLE 2 | Procedural data by thre study groups.

	All $n = 62$	No ECMO $n = 31$	ECMO $n = 31$	p
Total procedure duration (min)	200 ± 68	198 ± 74	201 ± 62	0.882
Fluoroscopy times (min)	8 ± 6	5 ± 3	12 ± 10	<0.001
Dose area product (Gy*cm^2)	34 ± 46	13 ± 17	55 ± 56	<0.001
Radiofrequency time (min)	49 ± 18	49 ± 18	48 ± 17	0.83
Periprocedural complications	2 (3%)	0 (0%)	2 (6%)	0.492
Epicardial ablation	4 (6%)	1 (3%)	3 (10%)	0.612

Mean ± SD or absolute frequency (percentage).

artery bypass graft. ECMO support was removed at the end of the procedure in 30 patients (97%); one patient required long-term ECMO support and died due to refractory heart failure after 5 days. An accurate substrate mapping and ablation was performed in all patients without procedural differences in the two study groups. The mean duration of the ablation procedure and fluoroscopy time were significantly higher in group 2 than in group 1 (**Table 2**). **Figure 1** shows the electroanatomic mapping and ablation in a patient of group 2.

Procedural Complications

In group 1, five patients had femoral artery damage (three pseudoaneurysms resolved with arterial compression and two dissections resolved with surgery). In group 2, one patient had the dislodgment of ECMO arterial cannula with hemorrhagic shock and recovered without sequelae, three patients had femoral artery dissection treated by percutaneous angioplasty with stenting.

Follow-Up

The median follow-up duration was 25 months in group 1 and 24 months in group 2 (range 6–36 months). During follow-up, four patients of group 1 (13%) and five patients of group 2 (16%) died due to refractory heart failure ($p = 0.45$). Furthermore, one patient of group 1 (3%) and one patient of group 2 (3%) died from treatment-refractory ES. The patients with ES recurrence had a VT inducible at the end of the procedure. At final follow-up, an ICD intervention for sustained VT (shock or antitachycardia pacing) was documented in 13 patients of group 1 (42%) and six patients of group 2 (19%) ($p = 0.017$). In both groups,

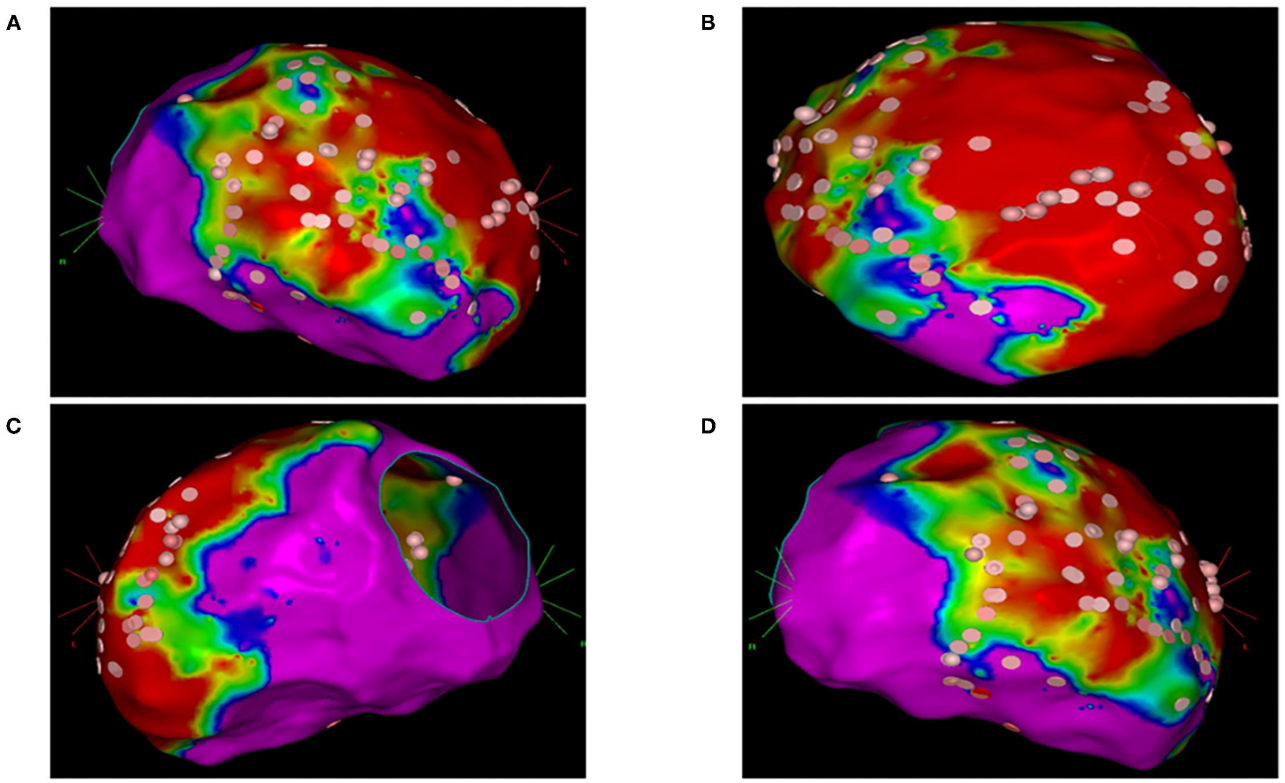

FIGURE 1 | Electroanatomic mapping and ablation of the left ventricle using the CARTO system. **(A)** Anterior-posterior view. **(B)** Left anterior oblique view. **(C)** Left lateral view. **(D)** Right anterior oblique view. Areas with normal voltage (>1.5 mV) are represented with purple color. Areas with low voltage (>0.5 mV) are represented with red color. Border zone areas are represented with blue and green colors (between 0.5 and 1.5 mV). Pink tags represent areas exposed to radiofrequency ablation.

an ICD intervention was documented in all patients with the inducibility of VTs at the end of the procedure. Furthermore, in patients without inducibility of VTs at the end of the procedure (seven patients in group 1 and 29 patients in group 2), an ICD intervention was documented in one patient of group 1 (14%) and four patients of group 2 (13%).

In group 2, three patients were implanted with left ventricular assist devices and one patient underwent heart transplantation. The Kaplan–Meier curve regarding mortality for refractory heart failure and ICD interventions was reported in **Figures 2**, **3**.

DISCUSSION

The findings of this study indicate that ECMO support during catheter ablation for ES and hemodynamically unstable VTs is a useful tool to prevent acute procedural heart failure and to reduce arrhythmic burden during follow-up.

Catheter ablation is an important treatment option that can achieve VT/VF suppression and provide long-term arrhythmia control in patients with treatment-refractory ES and fast VA (1, 4–7). However, catheter ablation procedures have a high risk of complications: fast VA induced by radiofrequency delivery, catheter movements and pacing maneuvers, multiple electrical cardioversions, and fluid overload can lead to cardiac stunning and acute hemodynamic decompensation.

Most published articles investigated outcomes of emergent cardiopulmonary support with ECMO to rescue acute heart decompensation in patients undergoing catheter ablation of ES showing that ECMO support was associated with poor outcomes when used as a rescue intervention for acute heart decompensation despite hemodynamic stabilization and effective acute arrhythmia suppression (8, 10–14). In particular, the majority of patients studied died of refractory heart failure in the short-term follow-up.

In a recent article (9), we reported data of patients who presented with ES and hemodynamically unstable VTs showing that preemptive ECMO support for patients with ES and hemodynamically unstable VTs was useful to prevent acute heart failure and to reduce procedural complications. A recent article, moreover, reported that the preemptive use of ECMO support for high-risk patients undergoing catheter ablation for VT storm was found to be effective in maintaining hemodynamic status and allowing successful mapping and catheter ablation for VT (14).

In this study, we showed that patients ablated with ECMO support had a reduction in the arrhythmic burden at long-term follow-up. This finding is probably related to the ability in performing safe ventricular inducibility at the end of the procedure without the risk of acute heart failure due to pacing or VT induction. Previous studies, in fact, reported

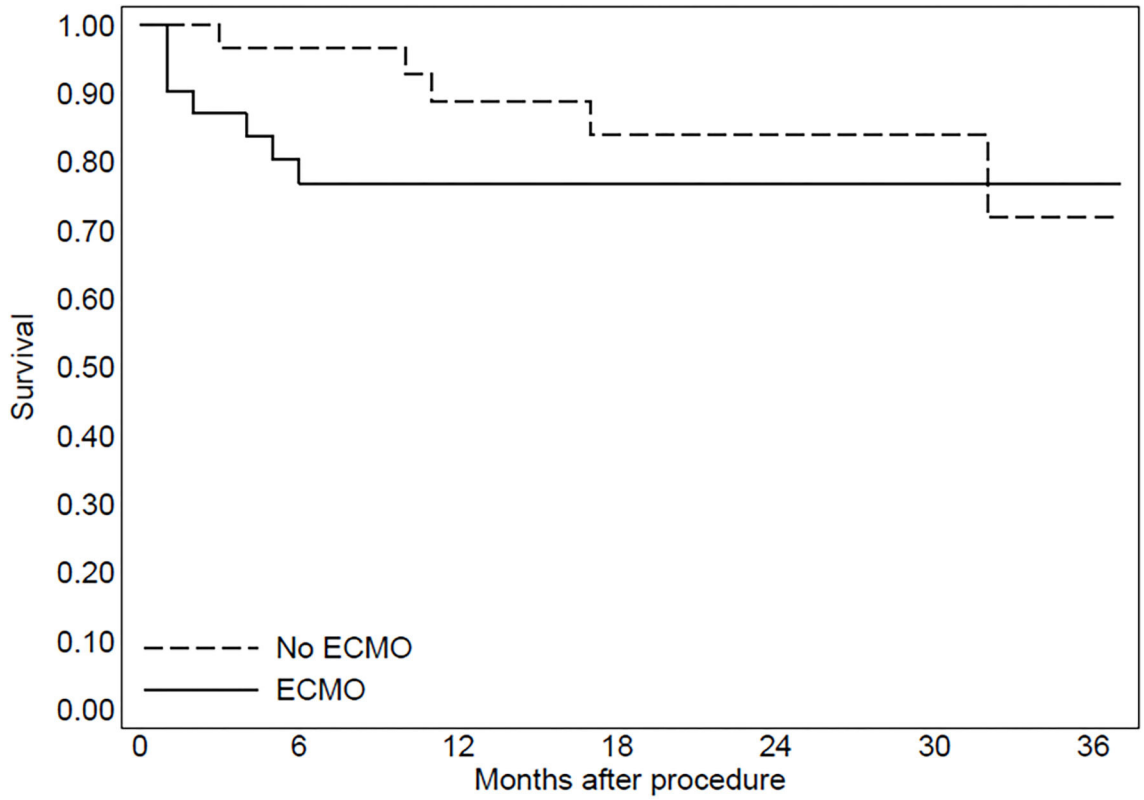

FIGURE 2 | The Kaplan-Meier curve to evaluate mortality due to refractory heart failure after the procedure.

that non-inducibility of VT at the end of the procedure was associated with reduced recurrences during follow-up (21, 22). Recent data reported that the adoption of an extensive induction protocol improved prognosis after VT ablation (23). In particular, patients who were deemed non-inducible for any VT with an extensive induction protocol after the final ablation (up to four extra stimuli ± burst pacing) had a better prognosis compared to patients who were deemed non-inducible for any VT after a limited induction protocol (three extra stimuli). Ventricular inducibility is generally limited in patients with a poor hemodynamic state for the risk of acute heart failure due to pacing and VT induction. Our data, for the first time, reported that ECMO support is useful to perform a safe VT inducibility after ablation avoiding acute heart failure in this population of frail patients.

Furthermore, previous studies investigated the best ablation strategy in patients with unstable VTs. Substrate ablation approach in sinus rhythm is a good strategy of VT ablation but previous data reported that in some cases the hemodynamic support was required because of persistent induction of unstable VTs (12). One study by Bunch et al. (24) provided evidence that hemodynamic support might allow activation mapping of VT with comparable outcomes and complications to an exclusive substrate mapping in sinus rhythm. A meta-analysis including six retrospective observational studies showed that activation/entrainment-guided ablation strategy and substrate-based ablation strategy had similar acute results, long-term outcome and complications rate (25). These results support our hypothesis that in the ECMO group the reduction of arrhythmic burden was not related to the ablation strategy but to the possibility to obtain a non-inducibility of VTs at the end of the procedure.

Finally, no significant reduction of mortality for refractory heart failure was found in patients ablated with ECMO support. Previous studies correlated the reduction of arrhythmic burden to a better survival (26) but the lack of this data in our study is probably because the study population was composed of critical patients with severe heart failure and a worse prognosis. ECMO support, however, improved the quality of life of these patients reducing shock interventions during long-term Follow-up.

The major limitations to this study are the relatively small number of patients and the lack of a randomized design. Another limitation is the low number of patients performing epicardial ablation. Finally, although the procedures were performed by experienced operators, results may have been influenced by the development of mapping and catheter technology over time.

CONCLUSION

In this experience, ECMO support facilitated mapping and ablation in patients with ES and hemodynamic instability. The

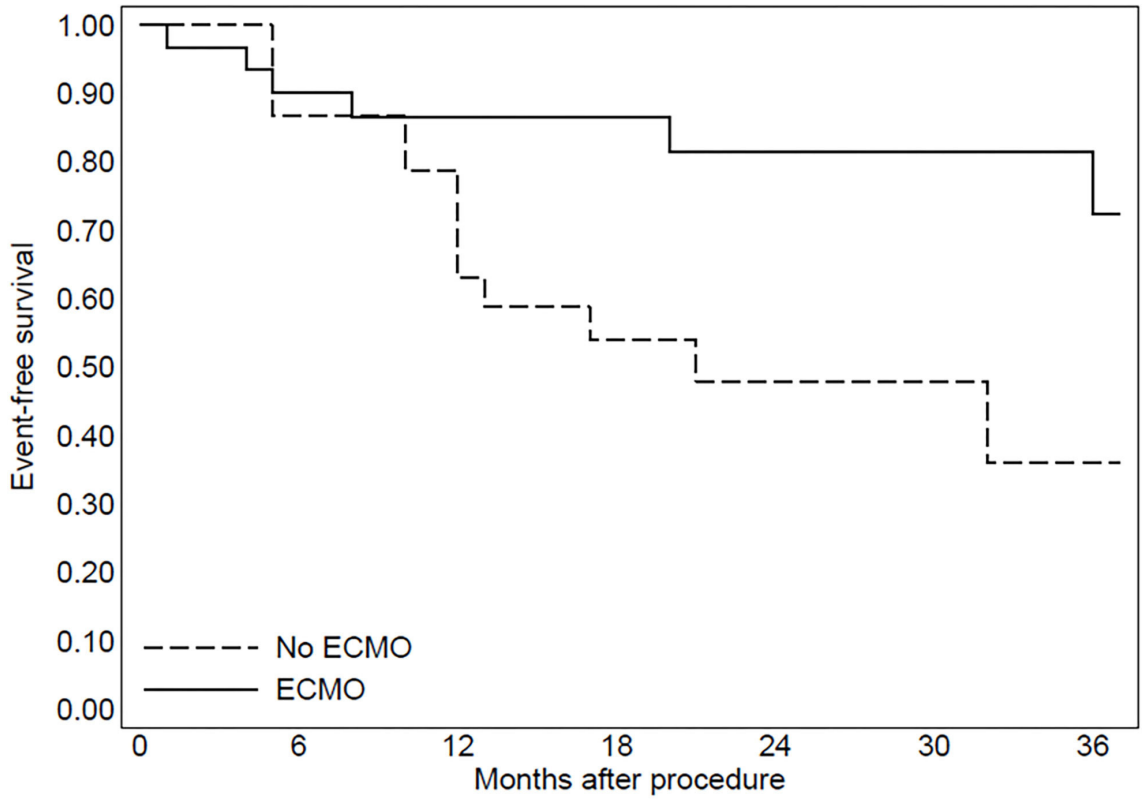

FIGURE 3 | The Kaplan-Meier curve to evaluate ICD interventions after the procedure.

safety in performing ventricular inducibility after ablation is probably the explaining of reduced arrhythmic burden in patients ablated with the ECMO support.

DATA AVAILABILITY STATEMENT

The raw data supporting the conclusions of this article will be made available by the authors, without undue reservation.

ETHICS STATEMENT

The studies involving human participants were reviewed and approved by Comitato Etico Policlinico Di Bari. Written informed consent for participation was not required for this study in accordance with the national legislation and the institutional requirements.

AUTHOR CONTRIBUTIONS

AD, MG, and PG contributed to conception and design of the study. MM organized the database. PG performed the statistical analysis. AD wrote the first draft of the manuscript. NV, FQ, FT, NC, VP, RC, ND, GC, and AM wrote sections of the manuscript. VD, TL, and LD revised the manuscript. All authors contributed to manuscript revision, read, and approved the submitted version.

REFERENCES

1. Priori SG, Blomström-Lundqvist C, Mazzanti A, Blom N, Borggrefe M, Camm J, et al. 2015 ESC Guidelines for the management of patients with ventricular arrhythmias and the prevention of sudden cardiac death: The Task Force for the Management of Patients with Ventricular Arrhythmias and the Prevention of Sudden Cardiac Death of the European Society of Cardiology (ESC). Endorsed by: Association for European Paediatric and Congenital Cardiology (AEPC). *Eur Heart J.* (2015) 36:2793–867. doi: 10.1093/eurheartj/ehv316
2. Conti S, Pala S, Biagioli V, Del Giorno G, Zucchetti M, Russo E, et al. Electrical storm: a clinical and electrophysiological overview. *World J Cardiol.* (2015) 7:555–61. doi: 10.4330/wjc.v7.i9.555
3. Exner DV, Pinski SL, Wyse DG, Renfroe EG, Follmann D, Gold M, et al. Antiarrhythmics versus implantable defibrillators. Electrical storm presages nonsudden death: the antiarrhythmics versus implantable defibrillators (AVID) trial. *Circulation.* (2001) 103:2066–71. doi: 10.1161/01.CIR.103.16.2066
4. Carbucicchio C, Santamaria M, Trevisi N, Maccabelli G, Giraldi F, Fassini G, et al. Catheter ablation for the treatment of electrical storm in patients with implantable cardioverter defibrillators: short- and long-term outcomes in a prospective single-center study. *Circulation.* (2008) 117:462–9. doi: 10.1161/CIRCULATIONAHA.106.686534
5. Deneke T, Shin DI, Lawo T, Bösche L, Balta O, Anders H, et al. Catheter ablation of electrical storm in a collaborative hospital

network. *Am J Cardiol.* (2011) 108:233–9. doi: 10.1016/j.amjcard.2011.03.030
6. Kozeluhova M, Peichl P, Cihak R, Wichterle D, Vancura V, Bytesnik J, et al. Catheter ablation of electrical storm in patients with structural heart disease. *Europace.* (2011) 13:109–13. doi: 10.1093/europace/euq364
7. Vergara P, Tung R, Vaseghi M, Brombin C, Frankel DS, Di Biase L, et al. Successful ventricular tachycardia ablation in patients with electrical storm reduces recurrences and improves survival. *Heart Rhythm.* (2018) 15:48–55. doi: 10.1016/j.hrthm.2017.08.022
8. Ballout JA, Wazni OM, Tarakji KG, Saliba WI, Kanj M, Diab M, et al. Catheter ablation in patients with cardiogenic shock and refractory ventricular tachycardia. *Circ Arrhythm Electrophysiol.* (2020) 13:e007669. doi: 10.1161/CIRCEP.119.007669
9. Di Monaco A, Quadrini F, Troisi F, Vitulano N, Caruso R, Duni N, et al. Cardiopulmonary support in patients undergoing catheter ablation of poorly tolerated ventricular arrhythmias and electrical storm. *J Cardiovasc Electrophysiol.* (2019) 30:1281–6. doi: 10.1111/jce.13995
10. Enriquez A, Liang J, Gentile J, Schaller RD, Supple GE, Frankel DS, et al. Outcomes of rescue cardiopulmonary support for periprocedural acute hemodynamic decompensation in patients undergoing catheter ablation of electrical storm. *Heart Rhythm.* (2018) 15:75–80. doi: 10.1016/j.hrthm.2017.09.005
11. Carbucicchio C, Della Bella P, Fassini G, Trevisi N, Riva S, Giraldi F, et al. Percutaneous cardiopulmonary support for catheter ablation of unstable ventricular arrhythmias in high-risk patients. *Herz.* (2009) 34:545–52. doi: 10.1007/s00059-009-3289-3
12. Baratto F, Pappalardo F, Oloriz T, Bisceglia C, Vergara P, Silberbauer J, et al. Extracorporeal membrane oxygenation for hemodynamic support of ventricular tachycardia ablation. *Circ Arrhythm Electrophysiol.* (2016) 9:e004492. doi: 10.1161/CIRCEP.116.004492
13. Mathuria N, Wu G, Rojas-Delgado F, Shuraih M, Razavi M, Civitello A, et al. Outcomes of pre-emptive and rescue use of percutaneous left ventricular assist device in patients with structural heart disease undergoing catheter ablation of ventricular tachycardia. *J Interv Card Electrophysiol.* (2017) 48:27–34. doi: 10.1007/s10840-016-0168-8
14. Campbell T, Bennett RG, Lee V, Turnbull S, Eslick A, Kruit N, et al. Ventricular tachycardia storm ablation with pre-emptive circulatory support by extracorporeal membrane oxygenation: Australian experience. *Heart Lung Circ.* (2021) 30:555–66. doi: 10.1016/j.hlc.2020.09.926
15. Lim HS, Sacher F, Cochet H, Berte B, Yamashita S, Mahida S, et al. Safety and prevention of complications during percutaneous epicardial access for the ablation of cardiac arrhythmias. *Heart Rhythm.* (2014) 11:1658–65. doi: 10.1016/j.hrthm.2014.05.041
16. Jaïs P, Maury P, Khairy P, Sacher F, Nault I, Komatsu Y, et al. Elimination of local abnormal ventricular activities: a new end point for substrate modification in patients with scar-related ventricular tachycardia. *Circulation.* (2012) 125:2184–96. doi: 10.1161/CIRCULATIONAHA.111.043216
17. Vergara P, Trevisi N, Ricco A, Petracca F, Baratto F, Cireddu M, et al. Late potentials abolition as an additional technique for reduction of arrhythmia recurrence in scar related ventricular tachycardia ablation. *J Cardiovasc Electrophysiol.* (2012) 23:621–7. doi: 10.1111/j.1540-8167.2011.02246.x
18. Mathuria N. Catheter ablation of ventricular tachycardia. *Tex Heart Inst J.* (2018) 45:166–7. doi: 10.14503/THIJ-18-6679
19. Dukkipati SR, Choudry S, Koruth JS, Miller MA, Whang W, Reddy VY. Catheter ablation of ventricular tachycardia in structurally normal hearts: indications, strategies, and outcomes-part I. *J Am Coll Cardiol.* (2017) 70:2909–23. doi: 10.1016/j.jacc.2017.10.031
20. Dukkipati SR, Koruth JS, Choudry S, Miller MA, Whang W, Reddy VY. Catheter ablation of ventricular tachycardia in structural heart disease: indications, strategies, and outcomes-part II. *J Am Coll Cardiol.* (2017) 70:2924–41. doi: 10.1016/j.jacc.2017.10.030
21. Ghanbari H, Baser K, Yokokawa M, Stevenson W, Della Bella P, Vergara P, et al. Noninducibility in postinfarction ventricular tachycardia as an end point for ventricular tachycardia ablation and its effects on outcomes: a meta-analysis. *Circ Arrhythm Electrophysiol.* (2014) 7:677–83. doi: 10.1161/CIRCEP.113.001404
22. Hu J, Zeng S, Zhou Q, Zhu W, Xu Z, Yu J, et al. Can ventricular tachycardia noninducibility after ablation predict reduced ventricular tachycardia recurrence and mortality in patients with non-ischemic cardiomyopathy? A meta-analysis of twenty-four observational studies. *Int J Cardiol.* (2016) 222:689–95. doi: 10.1016/j.ijcard.2016.07.200
23. Campbell T, Bennett RG, Garikapati K, Turnbull S, Bhaskaran A, De Silva K, et al. Prognostic significance of extensive versus limited induction protocol during catheter ablation of scar-related ventricular tachycardia. *J Cardiovasc Electrophysiol.* (2020) 31:2909–19. doi: 10.1111/jce.14740
24. Bunch TJ, Darby A, May HT, Ragosta M, Lim DS, Taylor AM, et al. Efficacy and safety of ventricular tachycardia ablation with mechanical circulatory support compared with substrate-based ablation techniques. *Europace.* (2012) 14:709–14. doi: 10.1093/europace/eur347
25. Kumar S, Baldinger SH, Romero J, Fujii A, Mahida SN, Tedrow UB, et al. Substrate-based ablation versus ablation guided by activation and entrainment mapping for ventricular tachycardia: a systematic review and meta-analysis. *J Cardiovasc Electrophysiol.* (2016) 27:1437–47. doi: 10.1111/jce.13088
26. Tung R, Vaseghi M, Frankel DS, Vergara P, Di Biase L, Nagashima K, et al. Freedom from recurrent ventricular tachycardia after catheter ablation is associated with improved survival in patients with structural heart disease: an International VT Ablation Center Collaborative Group study. *Heart Rhythm.* (2015) 12:1997–2007. doi: 10.1016/j.hrthm.2015.05.036

Conflict of Interest: The authors declare that the research was conducted in the absence of any commercial or financial relationships that could be construed as a potential conflict of interest.

frontiers in Cardiovascular Medicine

ORIGINAL RESEARCH
published: 26 October 2021
doi: 10.3389/fcvm.2021.744779

Late Gadolinium Enhancement Cardiovascular Magnetic Resonance Assessment of Substrate for Ventricular Tachycardia With Hemodynamic Compromise

John Whitaker[1], Radhouene Neji[1,2], Steven Kim[3], Adam Connolly[1], Thierry Aubriot[3], Justo Juliá Calvo[4], Rashed Karim[1], Caroline H. Roney[1], Brendan Murfin[5], Carla Richardson[5], Stephen Morgan[5], Tevfik F. Ismail[1,5], James Harrison[1], Judith de Vos[6], Maurice C. G. Aalders[6], Steven E. Williams[1,7†], Rahul Mukherjee[1], Louisa O'Neill[1], Henry Chubb[1], Cory Tschabrunn[8], Elad Anter[9], Luigi Camporota[5], Steven Niederer[1], Sébastien Roujol[1], Martin J. Bishop[1], Matthew Wright[5], John Silberbauer[4], Reza Razavi[1] and Mark O'Neill[1]*

[1] School of Biomedical Engineering and Imaging Sciences, King's College, London, United Kingdom, [2] Siemens Healthcare, Frimley, United Kingdom, [3] Abbott Medical, St Paul, MN, United States, [4] Brighton and Sussex University Hospitals NHS Trust, Brighton, United Kingdom, [5] Guy's and St Thomas' NHS Foundation Trust, London, United Kingdom, [6] Department of Biomedical Engineering and Physics, Amsterdam UMC, University of Amsterdam, Amsterdam, Netherlands, [7] Centre for Cardiovascular Science, University of Edinburgh, Edinburgh, United Kingdom, [8] Division of Cardiovascular Medicine, University of Pennsylvania, Philadelphia, PA, United States, [9] Cleveland Clinic, Cleveland, OH, United States

Background: The majority of data regarding tissue substrate for post myocardial infarction (MI) VT has been collected during hemodynamically tolerated VT, which may be distinct from the substrate responsible for VT with hemodynamic compromise (VT-HC). This study aimed to characterize tissue at diastolic locations of VT-HC in a porcine model.

Methods: Late Gadolinium Enhancement (LGE) cardiovascular magnetic resonance (CMR) imaging was performed in eight pigs with healed antero-septal infarcts. Seven pigs underwent electrophysiology study with venous arterial-extra corporeal membrane oxygenation (VA-ECMO) support. Tissue thickness, scar and heterogeneous tissue (HT) transmurality were calculated at the location of the diastolic electrograms of mapped VT-HC.

Results: Diastolic locations had median scar transmurality of 33.1% and a median HT transmurality 7.6%. Diastolic activation was found within areas of non-transmural scar in 80.1% of cases. Tissue activated during the diastolic component of VT circuits was thinner than healthy tissue (median thickness: 5.5 mm vs. 8.2 mm healthy tissue, $p < 0.0001$) and closer to HT (median distance diastolic tissue: 2.8 mm vs. 11.4 mm healthy tissue, $p < 0.0001$). Non-scarred regions with diastolic activation were closer to steep gradients in thickness than non-scarred locations with normal EGMs (diastolic locations distance = 1.19 mm vs. 9.67 mm for non-diastolic locations, $p < 0.0001$). Sites activated late in diastole were closest to steep gradients in tissue thickness.

OPEN ACCESS

Edited by:
Andreas Metzner, University Heart and Vascular Center Hamburg (UHZ), Germany

Reviewed by:
Martin Stiles, The University of Auckland, New Zealand
Christian Sohns, Heart and Diabetes Center North Rhine-Westphalia, Germany

***Correspondence:**
John Whitaker
john.whitaker@kcl.ac.uk

†ORCID:
Steven E. Williams
orcid.org/0000-0002-7266-2084

Specialty section:
This article was submitted to Cardiac Rhythmology, a section of the journal Frontiers in Cardiovascular Medicine

Received: *20 July 2021*
Accepted: *20 September 2021*
Published: *26 October 2021*

Citation:
Whitaker J, Neji R, Kim S, Connolly A, Aubriot T, Calvo JJ, Karim R, Roney CH, Murfin B, Richardson C, Morgan S, Ismail TF, Harrison J, de Vos J, Aalders MCG, Williams SE, Mukherjee R, O'Neill L, Chubb H, Tschabrunn C, Anter E, Camporota L, Niederer S, Roujol S, Bishop MJ, Wright M, Silberbauer J, Razavi R and O'Neill M (2021) Late Gadolinium Enhancement Cardiovascular Magnetic Resonance Assessment of Substrate for Ventricular Tachycardia With Hemodynamic Compromise. Front. Cardiovasc. Med. 8:744779. doi: 10.3389/fcvm.2021.744779

Conclusions: Non-transmural scar, mildly decreased tissue thickness, and steep gradients in tissue thickness represent the structural characteristics of the diastolic component of reentrant circuits in VT-HC in this porcine model and could form the basis for imaging criteria to define ablation targets in future trials.

Keywords: ventricular tachycardia, late gadolinium enhancement, cardiovascular magnetic resonance, mechanical circulatory support, venous-arterial extra corporeal membrane oxygenation (VA-ECMO)

INTRODUCTION

Viable myocytes within and on the border of dense scar display abnormal electrophysiological characteristics that promote reentrant arrhythmias (1–3). In most clinical VT ablation procedures, electrophysiological criteria alone are normally used to identify arrhythmogenic tissue (4–6). Even with a combination of ablation of clinical VT identified through activation and entrainment mapping and pace-mapping as well as substrate-based ablation (7), medium term outcomes remain modest with up to 50% of patients experiencing a recurrence of VT within a year of ablation (8).

When imaged *ex-vivo* at the near-cellular level, late-gadolinium enhanced (LGE) cardiovascular magnetic resonance (CMR) accurately identifies peri-infarct heterogeneous tissue (HT) as regions of intermediate signal intensity (ISI) (9). This tissue represents the critical substrate responsible for post-MI reentrant VT (10). These observations have been extended to *in-vivo* imaging where it has been reported that regions of ISI may also display abnormal electrophysiological properties (11, 12) described as the peri-infarct borderzone (BZ). This suggests that *in-vivo* LGE-CMR may offer a low-risk option for generating a 3D assessment of substrate that may have utility in guiding substrate-based VT ablation.

Pre-procedural cross-sectional imaging has been proposed as a non-invasive approach that may facilitate more comprehensive arrhythmogenic substrate identification and ablation (13). Effective substrate identification, either using electrophysiological or structural criteria, may be of particular importance in the context of the growing population of patients presenting with VT with hemodynamic compromise (VT-HC) (14, 15), in which only a substrate-guided approach is usually possible (6).

We hypothesized that under idealized experimental conditions the quality of LGE-CMR could be optimized in order provide accurate anatomic information about the tissue substrate for VT-HC. We aimed to characterize the tissue substrate responsible for VT-HC using high-resolution *in-vivo* 3D LGE-CMR and acquiring high-density activation mapping under hemodynamic support to identify the location of diastolic electrograms during post-MI VT-HC in a chronic porcine infarct model.

MATERIALS AND METHODS

Animal studies complied with French law and were performed at the Institut de Chirurgie Guidée par l'image (IHU), Strasbourg, France. The experimental protocol was approved by the local and national institutional animal care and ethics committee. Eight domestic pigs underwent a 180 minute balloon occlusion of the mid left anterior descending (LAD) artery to create experimental ischemia-reperfusion myocardial infarction (MI) as previously described (16). Seven weeks following MI each pig underwent late-gadolinium enhanced (LGE) cardiovascular magnetic resonance (CMR) imaging. One week later each pig underwent electrophysiology study with prophylactic hemodynamic support during which VT was induced and assessed using high-density activation mapping.

CARDIOVASCULAR MAGNETIC RESONANCE IMAGING DATA ACQUISITION

All imaging was performed on 1.5T scanner (MAGNETOM Aera, Siemens Healthineers, Erlangen, Germany) with an 18-channel body matrix coil and a 32-channel spine coil.

Clinical Standard 2D Late Gadolinium Enhanced Cardiovascular Magnetic Resonance Imaging

Ten min after 0.1 mmol/kg gadobutrol (Gadovist, Bayer Plc, Reading, UK) bolus, 2D LGE-CMR imaging was acquired. Inversion-time (TI) scout was acquired in a single mid ventricular short axis slice [free breathing, balanced steady state free precession (bSSFP); linear k-space reordering; echo time/repetition time/flip angle (TE/TR/α): 1.11 ms/2.6 ms/30°; slice thickness: 8 mm; in plane resolution: 1.8 x 1.8 mm^2; field of view (FOV): 340 x 276 mm^2]. Clinical standard 2D LGE-CMR imaging was acquired using an inversion recovery (IR) sequence with phase-sensitive IR (PSIR) reconstruction (bSSFP; linear k-space reordering; TE/TR/α: 1.21 ms/3 ms/45°; slice thickness: 6 mm; in plane resolution: 1.4 x 1.4 mm^2; FOV: 360 x 281 mm^2). Fifteen min after Gd bolus, 0.0011 mmol/kg/min Gd infusion was commenced. TI-scout was repeated at regular intervals following Gd bolus and during infusion.

3D Late Gadolinium Enhanced Cardiovascular Magnetic Resonance Imaging

Isotropic navigator-gated ECG-triggered 3D IR sequence was acquired in the mid-diastolic phase as identified from cine imaging (fat saturation prepared; bSSFP; coronal orientation; linear k-space reordering; TE/TR/α: 1.58ms/3.6ms/90°; gating

window = 7 mm; parallel imaging using GRAPPA with acceleration factor 2; resolution 1.2 x 1.2 x 1.2 mm^3; FOV: 400 x 257 x 96 mm^3; 2 R-R interval ECG triggering) with full ventricular coverage. Subjective and objective parameters of image quality were compared between 2D and 3D LGE CMR imaging (further details in **Supplementary Figure 1**).

CARDIOVASCULAR MAGNETIC RESONANCE IMAGING DATA ANALYSIS

Image Segmentation

Each 3D LGE-CMR scan was manually segmented by a single observer within Seg3D2 [University of Utah, Utah, USA, https://www.sci.utah.edu/cibc-software/seg3d.html]. Based on previously reported analysis of LGE-CMR imaging from patients undergoing VT ablation (17), the segmented myocardium was thresholded for scar signal intensity (SI_{scar}) at 60% and intermediate SI ($SI_{intermediate}$) at 40% of the highest SI within the segmentation.

Tissue Thickness and Scar Transmurality Assessment

Field lines between the endocardial and epicardial surfaces were derived by solving the Laplace equation as previously described (18). Briefly, the endocardial and epicardial surfaces were tagged. To calculate the distance from endocardial to epicardial surface, the Laplace equation ($\nabla^2 u = 0$) was solved with Dirichlet boundary conditions assigned at the endocardial ($u = 0$) and epicardial ($u = 1$) surfaces. Wall thickness was evaluated as the total length of the continuous path from the endocardium to the epicardium when moving orthogonally between adjacent iso-potential surfaces. Tissue thickness gradients were assessed using a radial basis function to identify the gradient in tissue thickness (further details in **Supplementary Materials**). Transmurality of scar and HT was defined as the proportion of nodes along the path between endocardium and epicardium corresponding to each tissue type. The distance of each endocardial node to the nearest neighboring node assigned as heterogeneous tissue (HT) was automatically calculated.

Segmentations were processed to generate a surface mesh containing endocardial and epicardial surfaces, scar and aorta in the Digital Image Fusion (DIF) format for import into the Precision Electroanatomic Mapping System (EAMS, Abbott, St Paul, MN, USA) within which they were registered with the EAMS geometry, as described below.

Electrophysiology Study and Hemodynamic Support

Electrophysiology procedures were conducted 8 weeks after MI under general anesthetic (further details in **Supplementary Materials**) using the Precision electro-anatomic mapping system (EAMS, Abbott, Chicago, IL).

Prior to the EP study pigs were established on venous-arterial extra-corporeal membrane oxygenation (VA-ECMO) via the left femoral artery and vein and hemodynamic support was prophylactically instituted using a Maquet Cardiohelp machine (Maquet Getinge group, Rastatt, Germany, see **Supplementary Figure 1**). Venous and arterial access was established for the EP study and hemodynamic monitoring/drug administration. Hemodynamic compromise (HC) was defined as a rhythm associated with a mean arterial pressure (MAP) below 50 mmHg or a pulse pressure lower than 20 mmHg. During rhythms not associated with HC, VA-ECMO circuit flow was reduced to 0.5 L/min. During rhythms associated with HC, VA-ECMO flow ranged between 0.5 and 1 L to 4 L depending on hemodynamic status to maintain a MAP of 65–70 mmHg. Further details are provided in the **Supplementary Materials**.

A sensor-enabled Abbott FlexAbility™ ablation catheter was advanced to the aorta via the right femoral artery and used to acquire aortic root and coronary ostia geometry prior to gaining retrograde left ventricular (LV) access across the aortic valve. A multipolar mapping catheter [HD Grid™ or LiveWire™ duo-deca (Abbott, Chicago, IL)] was advanced through an Agilis sheath via the aorta to acquire LV endocardial geometry.

LV endocardial activation maps were acquired while pacing from the RV apex at 500 ms and then 300 ms.

An attempt was made to induce ventricular tachycardia (VT) using an adapted Wellen's VT stimulation protocol (19) with up to four extra-stimuli from right and then left ventricular sites. In the event that no VT was induced, the non-selective beta agonist isoproterenol was commenced as an infusion at an initial rate of 2 μg/min and up titrated to a maximum rate of infusion of 20 μg/min during which programmed electrical stimulation was repeated.

Activation maps were acquired using the Automap function within Precision™ using the initial deflection seen on any lead of the surface ECG leads as the timing reference with strict settings applied (EAMS, Abbott, St Paul, MN, USA) (Score = 85; speed limit = 10 mm/s; distance 1 mm; enhanced noise rejection: off). Each individual bipolar and unipolar EGM from the mapped VTs and maps during pacing were subsequently reviewed offline and the activation time reassigned when necessary. Following spontaneous or pace-termination, VT induction and mapping was subsequently repeated. Final activation maps were reviewed by at least two experienced electrophysiologists.

The extent of conduction block (identified as regions with tightly spaced isochrones in which > 15 ms separated adjacent activation points; in which activation on either side of tightly spaced isochrones from wave fronts moving in different directions, and in which double potentials identified in proximity to the boundary between adjacent waves of conduction) during RV pacing and during each mapped VT was estimated using the surface distance function within the EAMS.

Co-registration of Imaging and Electrophysiological Data

After the EP study, using the re-map function within the EAMS, a surface mesh generated from the LGE-CMR scan was imported into the EAMS in the digital image fusion (DIF) format. The EAMS LV geometry was registered to the DIF

model with an initial landmark-based registration with the aorta, coronary ostia and LV apex as initial fiducial landmarks, followed by surface registration using the proprietary surface registration function within the EAMS. EAMS points manually identified as having healthy EGMs during RVP_{500} and those demonstrating diastolic activation during VT were exported from the EAMS. The location of these points from the EAMS mesh were automatically mapped to nodes on the CMR derived mesh within a 1 mm radius, to allow a node-wise assessment of the structural characteristics of tissue demonstrating diastolic activation during VT and healthy tissue could be made.

Episcopic Auto-Fluorescence Cryomicrotome Imaging

Following euthanasia, each heart was processed and then imaged using episcopic auto-fluorescence cryomicrotome imaging as previously described (20) (see **Supplementary Figure 2**).

Statistical Analysis

Normality of distribution of variables was assessed using the Shapiro-Wilks test. Normally distributed continuous variables are expressed as mean ± SD, otherwise variables are reported as medians with interquartile ranges. Normally distributed data were compared using a two tailed, paired sample *t*-test.

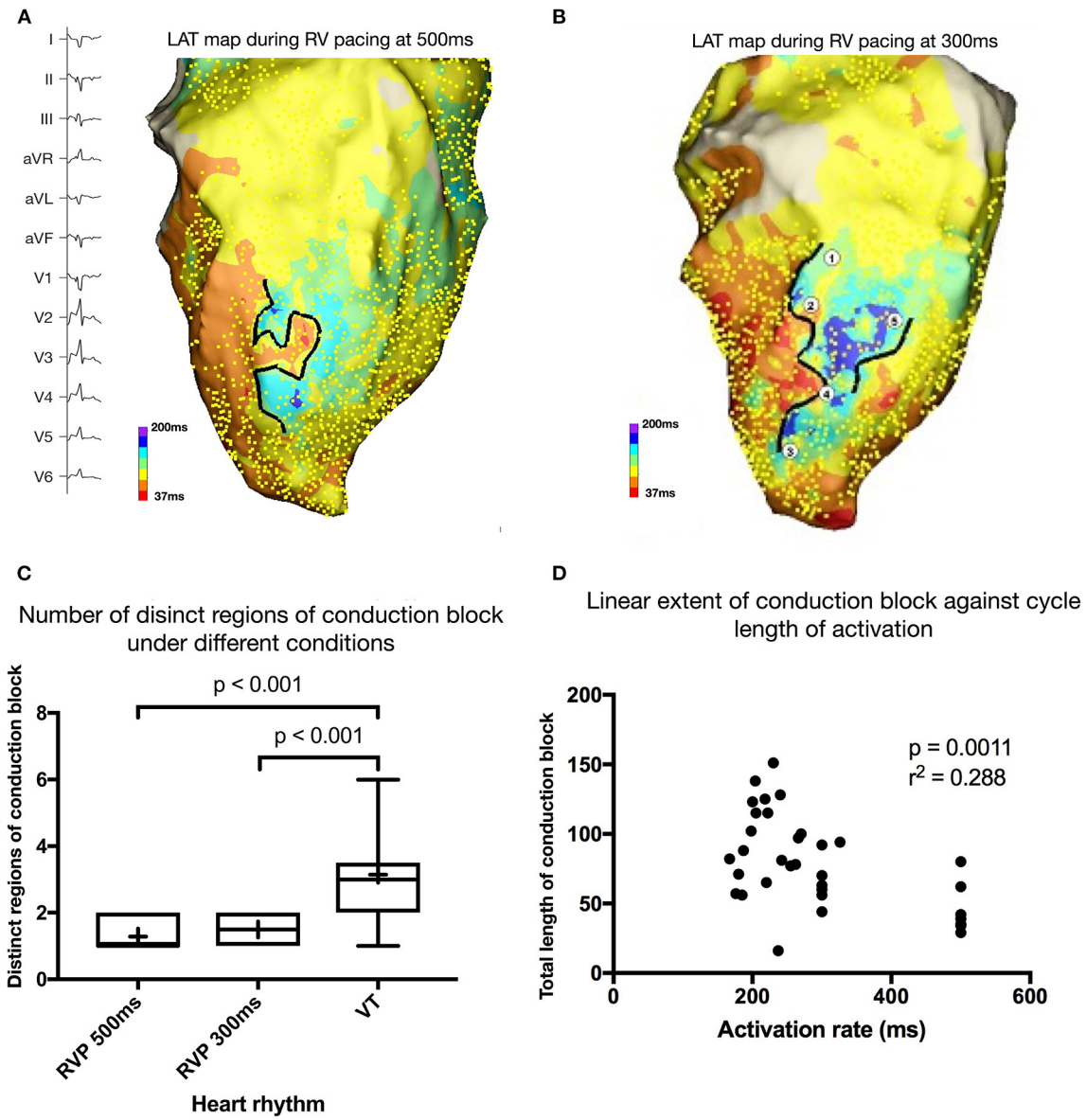

FIGURE 1 | (A) Activation map during right ventricular (RV) pacing at 500 ms. Yellow dots mark the point at which activation time was recorded. Black line represents linear conduction block during pacing at this cycle length. **(B)** Activation map during right ventricular (RV) pacing at 300 ms. **(C)** Number of distinct regions of conduction block during different heart rhythms (RV pacing at 500 ms and 300 ms and during VT). **(D)** Scatter plot of extent of linear endocardial conduction block and activation rate during pacing or VT.

Ordinal and non-parametric continuous data were compared using a Mann-Whitney U test or Kruskal-Wallis H-test as appropriate, with pairwise comparisons performed using Dunn's (1964) procedure with a Bonferroni correction for multiple comparisons where appropriate in which case adjusted p-values are presented. Two-tailed values of $p<0.05$ were considered significant. Statistical analysis was carried out in SPSS (v24, IBM Corporation, New York).

RESULTS

One post-MI pig died after CMR imaging and prior to EP study. The study protocol was completed in the remaining seven post-MI pigs and two control pigs who did not undergo CMR imaging. During this study all the VT that was induced was associated with hemodynamic compromise as defined above.

Late Gadolinium Enhanced Imaging Under Contrast Steady State

3D LGE-CMR imaging was acquired in eight animals (weight 62.6+/−3.7 kg) in the supine position under general anesthesia and CSS achieved in seven animals. In a single animal failure of the peripheral cannula interrupted the continuous Gd infusion, which prevented CSS during imaging. In the remaining seven animals 3D LGE-CMR imaging was acquired using a total Gd dose of <0.2 mmol/kg. 3D LGE-CMR was acquired in mid-diastole with a data acquisition duration of 83–104 ms, 23–42 segments, and a total imaging time of 50+/−12 min. Under conditions of CSS mean variation in $TI_{myocardium}$ was 5.2% (±3.1%, range 2.6–9.3%) and mean variation in TI_{blood} was 9.8% (±2.1%, range 6.7–13.5%). Representative imaging examples and demonstration of CSS are shown in **Figure 1**. All 3D LGE-CMR imaging is available for review online (**Supplementary Material**).

A comparison of the image quality with clinical standard 2D LGE-CMR imaging was undertaken and is included in the **Supplementary Materials.**

Induced Ventricular Tachycardia

Twenty episodes of VT-HC demonstrating a macro reentrant pattern of activation were mapped (18 complete maps, 2 incomplete) and the locations of diastolic electrograms (EGMs) assessed to be part of the reentrant circuit were identified and Labeled. A summary of the characteristics of the induced VTs is shown in **Table 1**. All mapped VTs were dependent on at least one region of conduction block that was not evident during RVP_{500}. All VTs with a complete activation map demonstrated at least two distinct regions of conduction block.

There was an increase in the extent of conduction block between RVP_{500} and VT (mean increase = 45 mm, 95% CI 27–63 mm, $p < 0.001$) and between RVP_{300} and VT (mean increase 23 mm, 95% CI 5–42 mm, $p = 0.016$), and a trend toward, an increase in conduction block between RVP_{500} and RVP_{300} (mean increase = 22 mm, 95% CI−1–45 mm, $p = 0.059$). Pearson correlation coefficient demonstrated a negative correlation between activation rate and total extent of conduction block ($r^2 = 0.288$, $p = 0.001$). These data are illustrated in **Figure 1**. Entrainment mapping was attempted in a subset of the induced VT-HC but was not successful due to failure to entrain or degeneration of the VT to ventricular fibrillation (VF).

TABLE 1 | Number of tachyarrhythmias observed and mapped per animal.

Pig	Number of episodes of non-sustained VT	Number of sustained, unmapped VTs	Number of mapped VTs	Number of episodes VF
1	67	3	0	7
2	-	-	-	-
3	27	2	4	1
4	100	3	9	4
5	22	2	2	6
6	16	3	2	10
7	88	2	2	1
8	47	3	2	8

Tissue Structure Assessment With *in-vivo* CMR at Locations With Diastolic Activation

Representative examples of diastolic EGMs recorded during VT are shown with their corresponding locations on *in-vivo* CMR in **Figure 2**. As shown in these examples, diastolic EGMs were visualized in regions with subendocardial HT (location 1), near-transmural scar (location 2) and pure HT (location 3). Tissue thinning is also seen in all locations.

A representative example of the position of a diastolic EGM, corresponding *in-vivo* imaging and episcopic auto-fluorescence cryomicrotome imaging (EACI) data is shown in **Figure 3**.

Non-enhanced tissue adjacent to regions of enhancement on *in-vivo* CMR were frequently observed in the septal area and corresponded to regions where muscle fibers traversing the RV cavity, including the moderator band, inserted into the septum. An example of this is shown in **Figure 4**, in which a corridor of preserved myocardium surrounded by dense scar forms the principal path of the diastolic isthmus of one VT, which in this case is approximately aligned with the direction of the long axis of the left ventricle.

The structural characteristics of locations at which diastolic EGMs occurred during the observed VTs were systematically examined and compared with locations at which normal EGMs were recorded. The normal EGMs were all recorded at positions with 0% scar/HT transmurality. Diastolic locations had a median scar transmurality of 33.1%, [IQR 0–77.3%, mean 37.4(±36.3) %, $p < 0.001$] and a median HT transmurality 7.6% [IQR 0–30.3%, mean 18.3(±22.9)% $p < 0.001$]. The majority (80.1%) of diastolic locations were found within areas with non-transmural scar or HT. Tissue activated in the diastolic component of VT circuits was thinner than healthy tissue (median thickness tissue with diastolic activation = 5.5 mm vs. 8.2 mm healthy tissue, $p < 0.001$) and was closer to HT (median distance from HT diastolically activated tissue 2.8 mm vs. 11.4 mm healthy tissue, $p < 0.001$). Of those diastolic locations that were in regions without scar or HT, all were within 15 mm of HT and

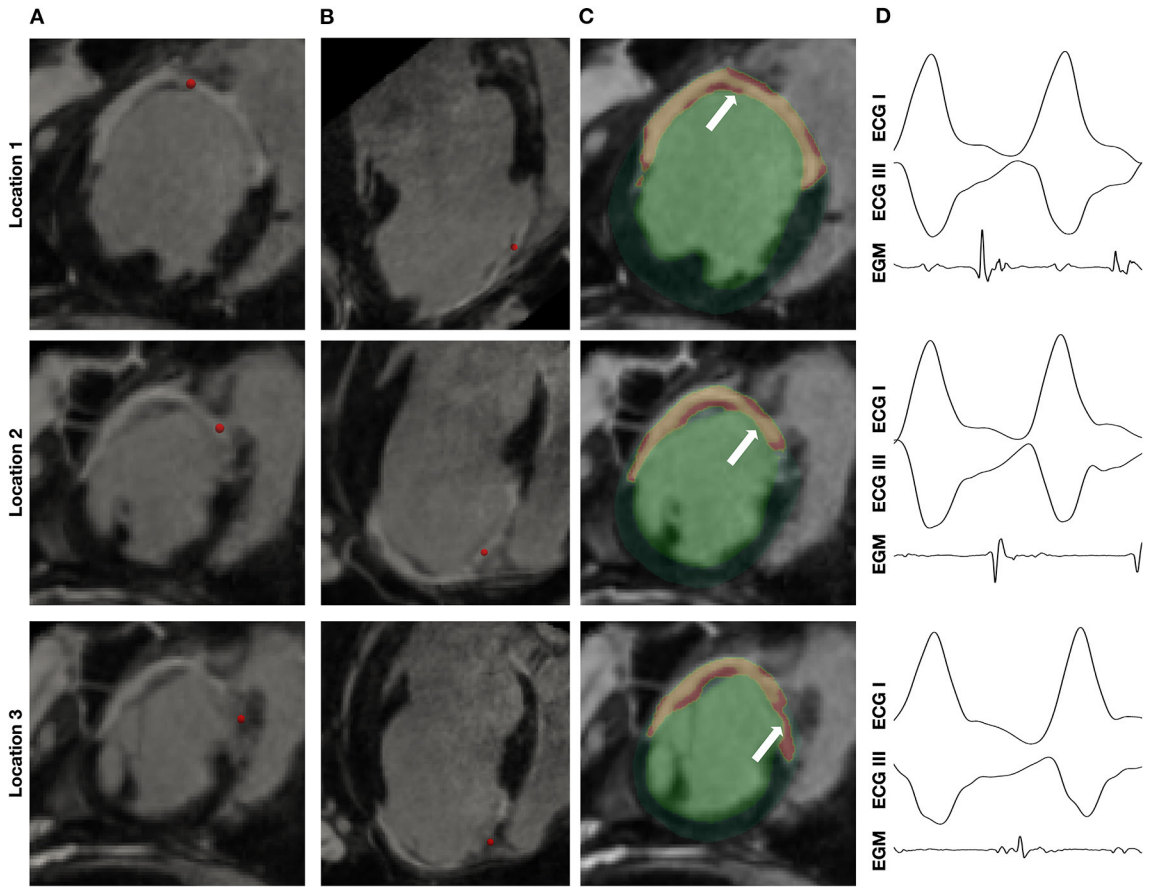

FIGURE 2 | Visualization of location of diastolic EGMs on *in-vivo* CMR. Column **(A)** and column **(B)** show short axis (SAX) and long axis (LAX) multiplanar reconstruction (MPR) of *in-vivo* CMR with the location of the corresponding diastolic EGM [column **(D)**] indicated by a red sphere. Column **(C)** shows SAX MPR of *in-vivo* CMR with segmentation of scar (yellow) and heterogeneous tissue (HT) (red) superimposed.

89% lay within 10 mm of HT. These results are illustrated in **Figure 5.**

Non-scarred Regions With Diastolic Activation During Ventricular Tachycardia

Approximately 20% of diastolic points had 0% scar/HT on *in-vivo* CMR. As noted, all regions activated during diastole during VT-HC were within 15 mm of HT. An example of EGMs recorded from a reentrant VT-HC is shown in **Figure 6**. In this example, early diastolic activation is identified within non-scarred tissue, before the wavefront continues into a region demonstrating non-transmural scar in which the remainder of the isthmus is located. On the corresponding *in-vivo* CMR and EACI data the EGMs are located adjacent to a sharp gradient in tissue thickness just outside the thinned scar region. When all locations without scar were considered, locations with diastolic activation were closer to steep gradients in tissue thickness than non-diastolic locations (diastolic locations distance = 1.2 mm (IQR 0–3.6 mm) vs. 9.7 mm (IQR 2.9–18.6 mm) for non-diastolic locations, $p < 0.001$). When diastolic locations were classified according to whether they demonstrated early, mid or late activation within the diastolic window, defined as being from the end of the QRS complex on the surface ECG, the median distance to regions of steep gradient in tissue thickness was lowest at late-diastolic sites (distance = 1.5 mm), followed by early-diastolic sites (distance = 2.8 mm) and greatest at mid-diastolic sites (distance = 3.9 mm, $p < 0.001$ for group differences and $p < 0.001$ for all pairwise comparisons).

DISCUSSION

In a chronic porcine infarct model high resolution 3D LGE-CMR acquired during contrast steady state can be used to define the structural characteristics of components of post-infarct reentrant VT circuits. Our data demonstrate that the majority of diastolic locations in this model of VT-HC are located in regions with non-transmural (<95%) scar/HT with lower tissue thickness than healthy tissue. In addition, ∼20% of diastolic points during VT-HC are in non-scarred tissue that is adjacent to steep gradients in tissue thickness.

Late-Gadolinium Enhanced Imaging Under Conditions of Contrast Steady State

Establishing CSS was technically feasible and resulted in stable $TI_{myocardium}$ for prolonged periods during image acquisition. For high-resolution 3D imaging sequences used in previous

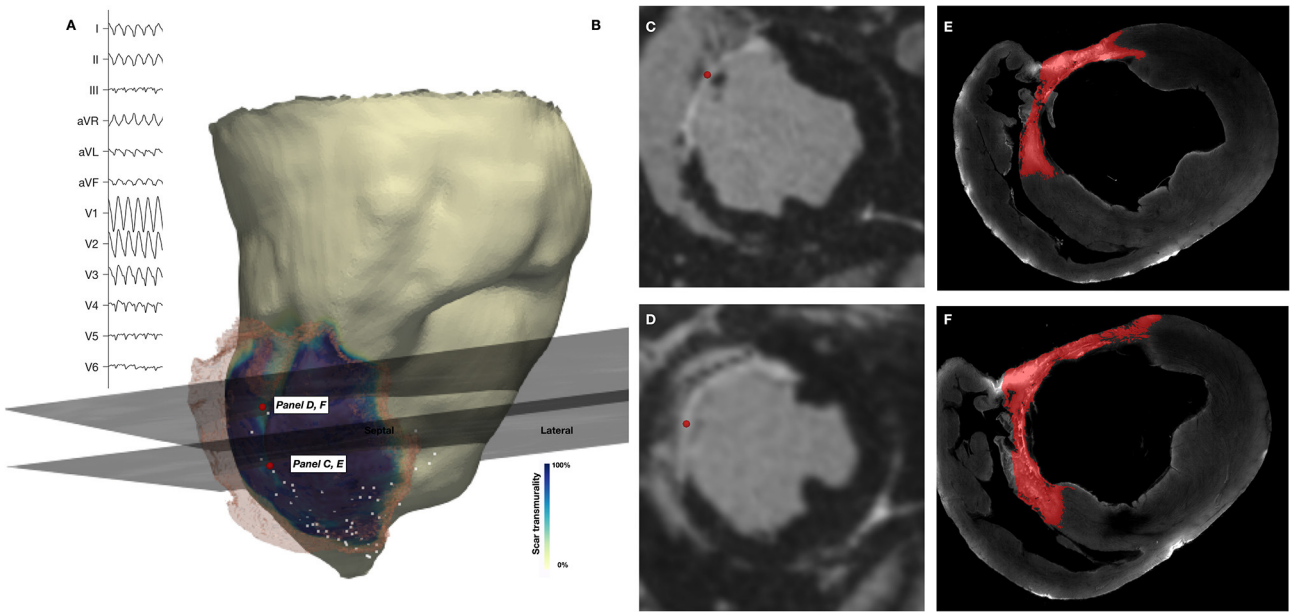

FIGURE 3 | Co-localization of diastolic locations from Electroanatomic Mapping System and *in-vivo* imaging and episcopic auto-fluorescence cryomicrotome imaging. **(A)** Surface 12-lead ECG of induced VT. **(B)** *In-vivo* CMR derived shell color coded according to scar transmurality, with translucent mesh derived from scar also shown. Location of 2 diastolic EGMs is shown (red spheres) and corresponding short axis (SAX) *in-vivo* LGE CMR slice. **(C,D)** SAX slices shown in **(B)**, with location of recorded EGM (red sphere). **(E,F)** Corresponding EACI data with segmented scar (red) superimposed.

imaging-supported VT ablation studies, $TI_{myocardium}$ drift during acquisition routinely necessitated 30–80 ms being added to the $TI_{myocardium}$ prior to the start of a 3D acquisition, which may be of up to 29 min in duration (21–23). In the present data, drift in $TI_{myocardium}$ across the course of an extended acquisition duration was always <10% and the mean was 5.2%, corresponding to an average change in $TI_{myocardium}$ of approximately 12 ms. In clinical practice, establishing CSS for 3D image acquisition even during scans of routine duration would minimize the drift in $TI_{myocardium}$ and may be helpful for optimizing image quality.

The non-standard approach to contrast delivery has not been robustly validated in this study. However, it is noted that the strategy of continuous contrast infusion, on which the protocol for the current study was based, has been validated against histological samples during extra-cellular volume mapping for the assessment of fibrosis (24). There is no consensus regarding the optimal method for thresholding LGE-CMR for scar (25), and the optimal strategy may depend on the contrast administration protocol used during imaging. The Full Width-Half Maximum technique represents a strategy with robust histological validation (26), however, clinical studies have suggested that thresholding for dense scar at 60% of the maximum SI best identifies electrophysiologically relevant left ventricular substrate. This consideration led to the current strategy being chosen for this study (17). The current study does address the unresolved issue of the optimal thresholding strategy for LGE-CMR.

The 3D LGE-CMR imaging in this study was acquired with a FA of 90° which likely resulted in reduced blood-scar contrast due to the higher T2 weighting that resulted (see **Supplementary Figure 3**). While in this study we did not feel low contrast between blood pool and scar prohibited confident identification of the blood-myocardial interface, the differentiation of endocardial scar from the blood pool could be improved in subsequent studies through using a lower flip angle. We note that this issue is encountered to some degree in all bright-blood LGE sequences and represents a motivation to the development of dark blood sequences to overcome this effect (27).

Transmurality of Scar

The calculated transmurality of scar in locations with diastolic activation reported here is lower than has been reported previously. In previous reports, mean scar transmurality at VT isthmus sites assessed using 2D 1.4 x 1.4 x 8 mm^3 LGE-CMR with scar segmented according to a Full-width at half-maximum (FWHM) threshold was 60 ± 38% (28) or using a similar 2D LGE-CMR imaging 66 ± 22%, which rose to 76 ± 16% at sites of concealed entrainment and to 70 ± 21% at termination sites (29). The use of 2D imaging, bolus contrast administration and different image analysis protocols used in previous experiments is likely to contribute to observed differences in scar transmurality. In addition, there may be mechanistic differences between the VT-HC described here and VTs studied previously, both of which included at least some hemodynamically tolerated VTs. Early reports of hemodynamically tolerated scar-mediated VT often localized the isthmus to within a thin walled LV aneurysm, which would likely be identified on CMR imaging as transmural scar (30, 31). In contrast, the re-entrant VT-HC observed in this study displayed a greater dependence on

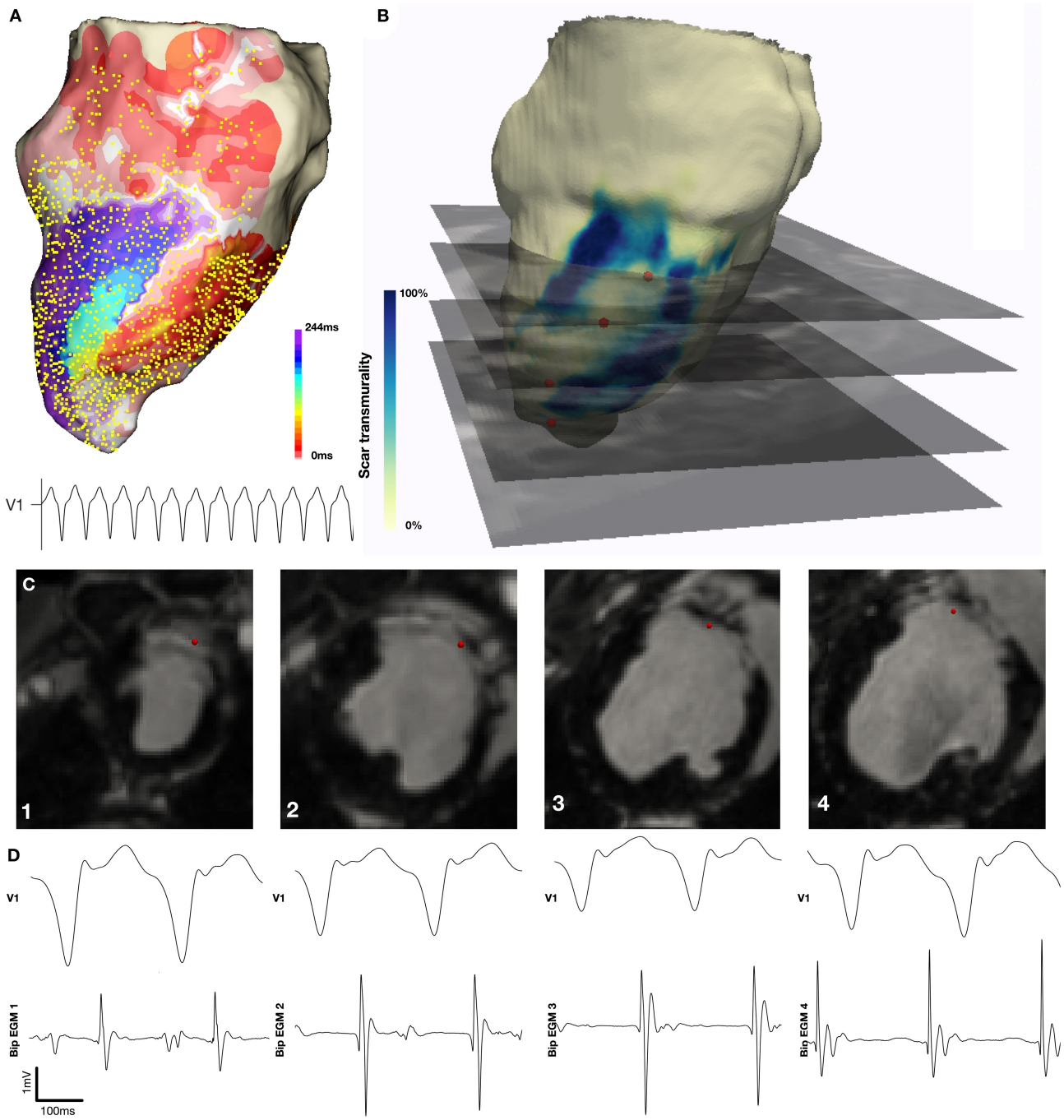

FIGURE 4 | Localization of diastolic locations on *in-vivo* CMR imaging. **(A)** Activation map demonstrating re-entrant VT with a figure 8 pattern of re-entry. **(B)** CMR derived mesh color coded according to scar transmurality with location of selected diastolic EGMs indicated by red sphere and corresponding *in-vivo* LGE CMR imaging indicated. **(C)** Diastolic EGM and corresponding location on *in-vivo* CMR at four sequential points along the diastolic isthmus of this VT.

functional rather than fixed conduction block, suggesting that the structural substrate of VT-HC may be distinct from slower and hemodynamically tolerated VTs. In addition, the use of high-resolution imaging and the measures taken to minimize artifact in this report may have contributed to an increased sensitivity for the identification of tissue with preserved viability and reduced the calculated scar transmurality at sites with diastolic activation.

Tissue Thickness

Tissue thickness has been demonstrated to be a sensitive structural marker for arrhythmogenic tissue in the post-MI

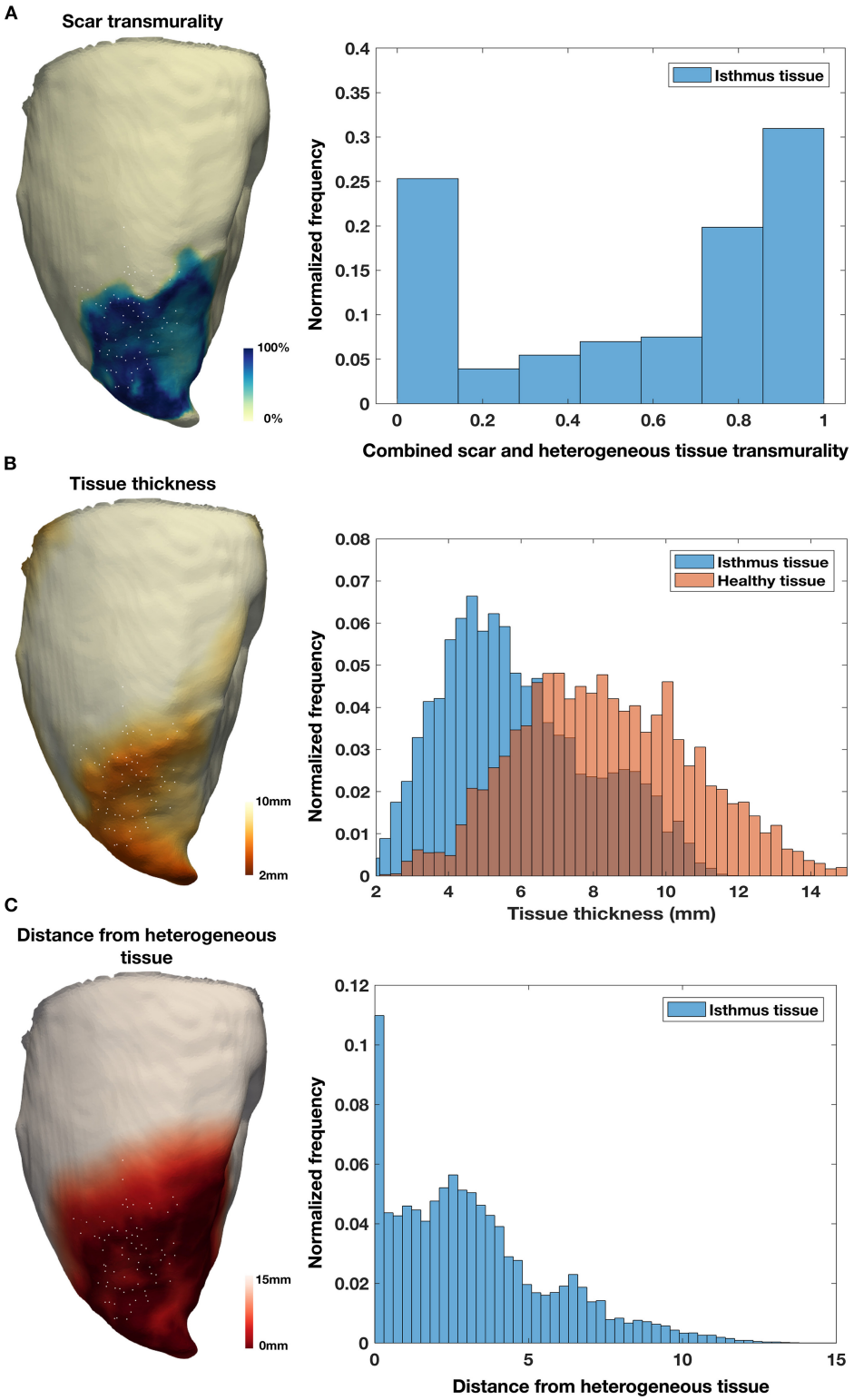

FIGURE 5 | Tissue characteristics of diastolic locations. **(A)** Example of LGE CMR derived endocardial shell color coded according to scar transmurality and demonstrating antero-septal infarction. Histogram shows combined scar/heterogeneous tissue (HT) transmurality pooled from all locations activated during diastole in all pigs. **(B)** Example of LGE CMR derived endocardial shell color coded according to tissue thickness. Histogram shows tissue thickness pooled from all diastolic locations (blue) in all pigs compared with tissue thickness at the location of normal EGMs pooled from all pigs (red). **(C)** Example of LGE CMR derived endocardial shell color coded according to distance from HT. Histogram shows distance from HT pooled from all diastolic locations in six pigs.

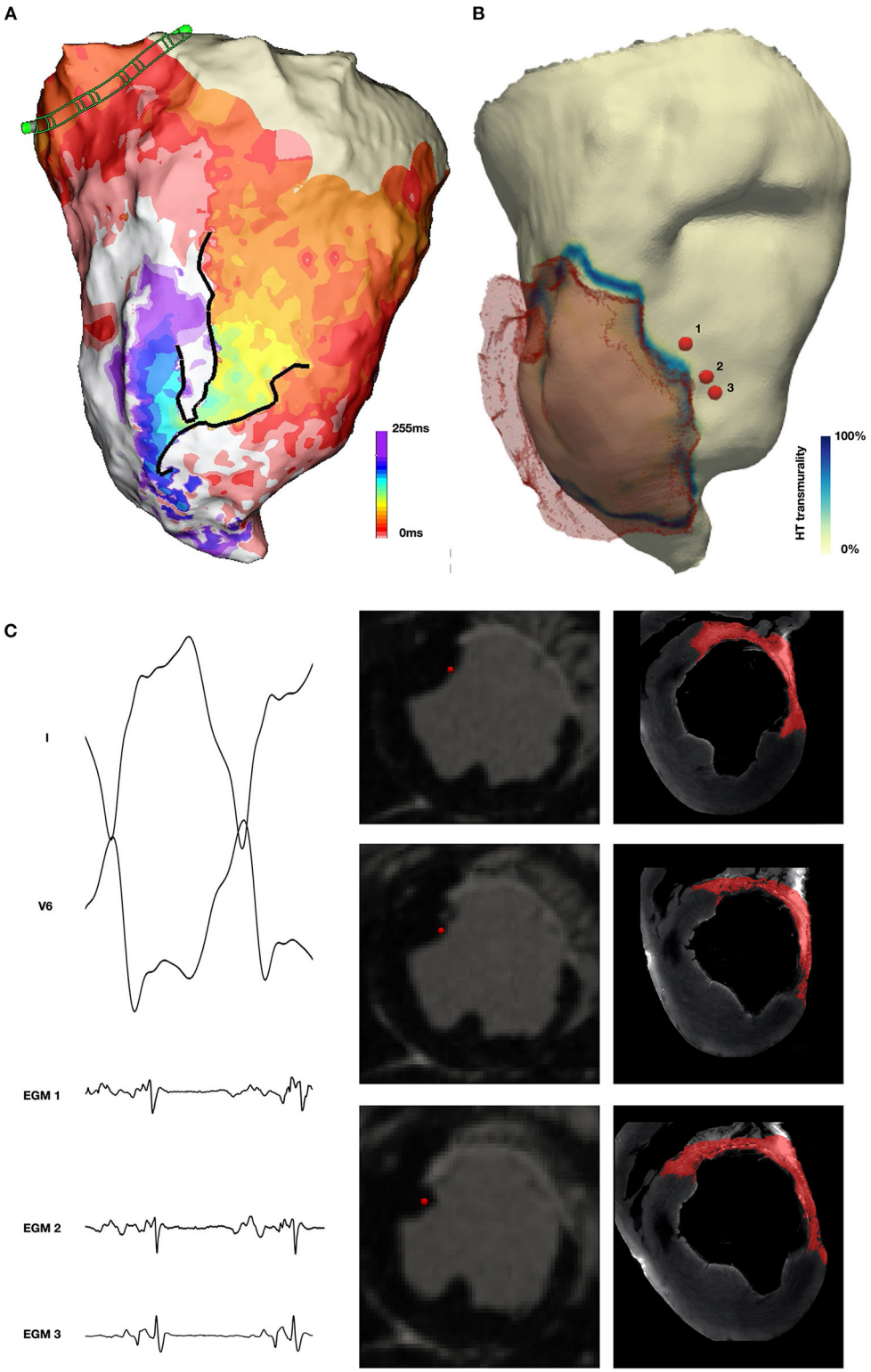

FIGURE 6 | Non-scarred tissue demonstrating diastolic activation during VT. **(A)** Activation map during VT demonstrating diastolic activation during VT (yellow to purple) with a converging pattern of activation toward a narrow channel (green) which subsequently widens prior to multiple systolic breakouts (red). **(B)** *In-vivo* CMR derived shell with translucent mesh of scar overlaid and color coded according to HT transmurality. The location of 3 early diastolic EGMs is indicated by red spheres. **(C)** Early diastolic EGM, short axis (SAX) *in-vivo* CMR and corresponding EACI imaging at locations 1, 2 and 3 demonstrating location of EGMs in tissue proximal to scar, but without enhancement in the wall at this location.

LV when assessed using coronary computed tomographic angiography (CCTA) (32). Among patients undergoing catheter ablation of drug refractory post-MI scar-related VT, 98% have been reported to demonstrate wall thinning on CCTA (32). As well as demonstrating a strong relationship between low voltage regions and local abnormal ventricular activations (LAVA), 89% of RF termination sites were located within the imaging substrate [defined as regions of wall thinning (tissue thickness < 5 mm) or severe wall thinning (tissue thickness < 2 mm)], with the majority of these located within 10 mm of the margin. The data presented here also indicate that regions of diastolic activation during VT-HC tend to be thinner than healthy tissue. However, examination of the histograms shown in Figure demonstrates that there is significant overlap between the tissue thickness assessed with diastolic activation and healthy tissue, and therefore tissue thickness alone would not adequately differentiate regions of diastolic activation during VT from healthy tissue. In the present study, the shorter VT cycle length and dependence of the VTs on functional rather than fixed anatomical conduction block, as might be expected in an aneurysm demonstrating severe wall thinning, suggests a possible explanation for why diastolic activation during VT was observed in tissue with a wider range of thicknesses than in previous reports which have used CT imaging.

Non-enhancing Tissue Activated During Diastole in VT

Approximately 20% of diastolic locations present were found in locations with no scar/HT identified on *in-vivo* imaging. This tissue was located in close proximity to HT and adjacent to steep gradients in tissue thickness. The diastolic activation of such tissue has not been previously demonstrated in the reentrant paths of hemodynamically tolerated VT. This tissue may include regions of tissue with microscopic fibrosis that occurs adjacent to scar and that is not identified by *in-vivo* LGE-CMR imaging but is likely to demonstrate distinct electrophysiological properties that promote its participation in VT-HC. Intrinsic tissue anisotropy at the scar interface, which may be enhanced in diseased ventricular tissue (33), is also likely to affect conduction behavior in this region. In canine models of scar related re-entry, it is established that the arc of functional conduction block responsible for the initiation of reentry localizes to regions of sharp gradients in tissue thickness and previous experiments have demonstrated that conduction velocity during pacing in this model is slower in regions of steep gradients in tissue thickness (34). In addition, the lowest conduction velocity (CV) in the re-entrant circuits of VTs in the same model may be found at exit sites (35). A wave of depolarization slows when transitioning from a small to a larger body of tissue due to the dispersion of the small source transmembrane current to a large number of downstream cells (source-sink mismatch) (36) and due to wavefront curvature that is a consequence of the geometric expansion of tissue encountered by a propagating wavefront. These observations suggest a mechanistic explanation for the diastolic activation of non-scarred tissue adjacent to steep gradients in tissue thickness in the reentrant path of VT-HC defined by functional conduction block, and the greatest proximity of the late diastolic component to these areas.

Unique Anatomical Characteristics of the Isthmus

In this study, tissue with scar/HT transmurality and tissue thickness across a wide range has been identified as activated during the diastolic component of the reentrant VT-HC studied. In a previous study of porcine post-MI VT-HC (10), despite high-resolution *ex-vivo* CMR (0.4 x 0.4 x 0.4 mm^3), anatomic features distinguishing HT harboring diastolic activation during VT from non-participating HT were not identified. At a histological level, structural differences exist between regions harboring a critical diastolic isthmus that distinguish this tissue from other HT (37). However, since it was impossible to identify these differences using high resolution *ex-vivo* CMR, it is extremely unlikely that such arrhythmogenic HT would be distinguishable from non-arrhythmogenic HT with CMR at current *in-vivo* resolution. The tissue in which the diastolic isthmus of VT-HC is expected to be located has been characterized in this model, however the current data does not indicate that within regions of non-transmural scar/HT, arrhythmogenic and non-arrhythmogenic substrate may be differentiated.

Limitations

Activation mapping alone was used to characterize the VT-HC circuits in this study. Entrainment mapping to confirm participation of the regions with diastolic activation was attempted but not routinely achieved and this represents a limitation of the presented data. The registration of electrophysiology and imaging data represents a major challenge when attempting to establish the structural basis for observed electrophysiological phenomena. Despite meticulous care in the registration between LGE-CMR and EAMS data, it is acknowledged that registration error has not been avoided entirely. Establishing the correct rotation around the long axis of the LV remains a significant challenge even with the use of coronary ostia and other anatomical landmarks as guidance. Change in the shape of the LV between the time of electrophysiology procedures and imaging are expected due to differences in the loading conditions, which represents an additional challenge, as do absolute limitations in the accuracy of the localization of EGM signals. The degree to which registration error affects the accuracy of results is difficult to quantify and is not accurately described by surface distance between EAMS and imaging data. There is no consensus regarding the optimal threshold to apply in order to accurately identify scar on LGE-CMR (25). The challenge of quantitatively assessing scar and fibrosis are compounded by differences in imaging parameters and contrast administration protocols, which will affect degree of hyperenhancement of tissue. The absence of standard histological data from this study due to the destructive nature of the EACI process is a further limitation of the current study and prohibits formal validation of the imaging data. Common to most large animal pre-clinical studies, this study included a relatively small number of animals, in consideration of minimizing the use of animals in experiments and cost. Despite

these limitations, the comparison between LGE-CMR and high density electrophysiological mapping data demonstrate that the imaging acquired and processing strategy reliably identified electrophysiologically relevant tissue in this model.

CONCLUSIONS

The structural characteristics of the tissue demonstrating diastolic activation during reentrant VT-HC, including non-transmural scar, mildly decreased tissue thickness and steep gradients in tissue thickness, are likely to promote functional conduction block which is demonstrated to be an important mechanism underlying the VT-HC observed in this model. The late diastolic segment of activation during VT-HC is closest to steep gradients in tissue thickness which may be a contributory factor to the maximal wavefront slowing seen in this region. The characterization of the myocardial substrate for post-MI scar mediated VT-HC could form the basis for imaging criteria to define ablation targets during future trials.

DATA AVAILABILITY STATEMENT

The raw data supporting the conclusions of this article will be made available by the authors, without undue reservation.

ETHICS STATEMENT

The animal study was reviewed and approved by Animal studies complied with French law and were performed at the Institut de Chirurgie Guidée par l'image (IHU), Strasbourg, France. The experimental protocol was approved by the Local and National Institutional Animal Care and Ethics Committee.

AUTHOR CONTRIBUTIONS

JW: conceived and designed study, analyzed data and prepared first draft and subsequent modifications of the manuscript. RN and SR: designed and implemented CMR protocols, assisted in acquisition of imaging and contributed to analysis of data. SK: contributed to experimental design, assisted with acquisition of electroanatomic mapping data, and contributed to analysis of data. AC: key contribution to analysis of electrophysiologic data. TA: planning and acquisition of electrophysiological data. JC, MW, and JS: electrophysiologist who acquired electro-anatomic mapping data. RK: developed computational tools for registration of imaging and electrophysiologic data. BM, CRi, SM, and LC: development of VA-ECMO protocol for hemodynamic support, delivery of hemodynamic support during electrophysiology studies. TI and JH: CMR reader. JV and MA: development of cryomicrotome imaging protocol and processing of tissue to acquire cryomicrotome imaging and approved submitted version of manuscript. SW, LO'N, RM, HC, RR, and MO'N: involved in acquisition of CMR and electrophysiological data. RM: repeat segmentation of 3d LGE CMR imaging for inter-observer reproducibility. HC, RR, and MO'N: funding holder for study. SW, LO'N, RM, HC, RR, MO'N, CT, EA, SN, and MB: planning and study design. RR and MO'N: supervisory oversight of project. CT, EA, SN, MB, HC, RR, MO'N, RM, SW, LO'N, TI, JH, BM, CRi, SM, LC, CRo, RK, JC, MW, JS, TA, AC, SK, RN and SR: substantial modifications to previous drafts of manuscript and approved submitted version of manuscript. TA, JC, MW, JS, BM, CRi, SM, LC, CRo, TI, JH, RK, SW, LO'N, RM, CT, EA, SN, MB, HC, RR, and MO'N: analysis and interpretation of data. All authors contributed to the article and approved the submitted version.

FUNDING

This work was supported by a Medical Research Council UK Clinical Research Training Fellowship (grant code MR/N001877/1) which funded JW; the Health Innovation Challenge Fund (HICF-R10-698), a parallel funding partnership between the Department of Health and the Wellcome Trust, the Wellcome Engineering and Physical Sciences Research Council (EPSRC) Centre for Medical Engineering at King's College London (WT203148/Z/16/Z); EPSRC grant (EP/R010935/1); National Institute for Health Research (NIHR) Biomedical Research Centre award to Guy's and St Thomas' National Health Service (NHS) Foundation Trust in partnership with King's College London, and by the NIHR Healthcare Technology Co-operative for Cardiovascular Disease at Guy's and St Thomas' NHS Foundation Trust. The views expressed are those of the author(s) and not necessarily those of the NHS, the NIHR or the Department of Health. The CardioHelp machine and all ECMO consumables were donated by Maquet, Getinge Group without conditions on their use. The Precision and Claris system and all EP mapping consumables were donated by Abbott without conditions on their use. This research was funded in whole, or in part, by the Wellcome Trust [Grant Number WT203148/Z/16/Z]. For the purpose of open access, the author has applied a CC BY public copyright licence to any Author Accepted manuscript version arising from this submission. This project was supported by the National Institute of General Medical Sciences of the National Institutes of Health [Grant Numbers P41 GM103545 and R24 GM136986]. SW was supported by British Heart Foundation [Grant Number FS/20/26/34952].

ACKNOWLEDGMENTS

We are grateful to the Abbott UK, France and US teams who generously loaned the Precision and Claris systems for these experiments, provided outstanding technical support and donated all the EP mapping catheters, cables and consumables, Sagar Haval, Lynn Calvert and the Maquet, Getinge Group who generously provided a CardioHelp machine, provided technical support and donated all the ECMO consumables as well as Sophie Pernot and the staff at the Institute de Chirurgie Guidée par

l'image (IHU), Strasbourg, France for their support for these experiments and the outstanding animal care they provided. We are grateful to Professor Maria Siebes for her assistance with establishing the protocol for and assistance with the processing of the cryomicrotome imaging.

SUPPLEMENTARY MATERIAL

The Supplementary Material for this article can be found online at: https://www.frontiersin.org/articles/10.3389/fcvm.2021.744779/full#supplementary-material

REFERENCES

1. Mehra R, Zeiler RH, Gough WB, El-Sherif N. Reentrant ventricular arrhythmias in the late myocardial infarction period. 9 electrophysiologic-anatomic correlation of reentrant circuits. *Circulation.* (1983) 67:11–24. doi: 10.1161/01.CIR.67.1.11
2. El-Sherif N, Smith RA, Evans K. Canine ventricular arrhythmias in the late myocardial infarction period. 8 epicardial mapping of reentrant circuits. *Circ Res.* (1981) 49:255–65. doi: 10.1161/01.RES.49.1.255
3. Qin D, Zhang Z-H, Caref EB, Boutjdir M, Jain P, El-Sherif N. Cellular and ionic basis of arrhythmias in postinfarction remodeled ventricular myocardium. *Circ Res*. (1996) 79:461–73. doi: 10.1161/01.RES.79.3.461
4. Stevenson WG, Friedman PL, Sager PT, Saxon LA, Kocovic D, Harada T, et al. Exploring postinfarction reentrant ventricular tachycardia with entrainment mapping. *J Am Coll Cardiol.* (1997) 29:1180–9. doi: 10.1016/S0735-1097(97)00065-X
5. Tung R, Mathuria N, Michowitz Y, Yu R, Buch E, Bradfield J, et al. Functional pace-mapping responses for identification of targets for catheter ablation of scar-mediated ventricular tachycardia. *Circ Arrhythmia Electrophysiol.* (2012) 5:264–72. doi: 10.1161/CIRCEP.111.967976
6. Jaïs P, Maury P, Khairy P, Sacher F, Nault I, Komatsu Y, et al. Elimination of local abnormal ventricular activities : a new end point for substrate modification in patients with scar-related ventricular tachycardia. *Circulation.* (2012) 125:2184–96. doi: 10.1161/CIRCULATIONAHA.111.043216
7. Al-Khatib SM, Stevenson WG, Ackerman MJ, Bryant WJ, Callans DJ, Curtis AB, et al. 2017 AHA/ACC/HRS guideline for management of patients with ventricular arrhythmias and the prevention of sudden cardiac death: a report of the American College of Cardiology/American Heart Association Task Force on Clinical Practice Guidelines and the Heart Rhythm Society. *Circulation*. (2018) 138:e272–391. doi: 10.1016/j.hrthm.2017.10.036
8. Dukkipati SR, Koruth JS, Choudry S, Miller MA, Whang W, Reddy VY. Catheter ablation of ventricular tachycardia in structural heart disease: indications, strategies, and outcomes—part II. *J Am Coll Cardiol.* (2017) 70:2924–41. doi: 10.1016/j.jacc.2017.10.030
9. Schelbert EB, Hsu LY, Anderson SA, Mohanty BD, Karim SM, Kellman P, et al. Late gadolinium-enhancement cardiac magnetic resonance identifies postinfarction myocardial fibrosis and the border zone at the near cellular level in ex vivo rat heart. *Circ Cardiovasc Imaging.* (2010) 3:743–52. doi: 10.1161/CIRCIMAGING.108.835793
10. Ashikaga H, Sasano T, Dong J, Zviman MM, Evers R, Hopenfeld B, et al. Magnetic resonance-based anatomical analysis of scar-related ventricular tachycardia: implications for catheter ablation. *Circ Res.* (2007) 101:939–47. doi: 10.1161/CIRCRESAHA.107.158980
11. Piers SRD, Tao Q, De Riva Silva M, Siebelink HM, Schalij MJ, Van Der Geest RJ, et al. CMR-based identification of critical isthmus sites of ischemic and nonischemic ventricular tachycardia. *JACC Cardiovasc Imaging.* (2014) 7:774–84. doi: 10.1016/j.jcmg.2014.03.013
12. Androulakis A, Zeppenfeld K, Paiman E, Venlet J, CA G, Schalij M, et al. Scar transmurality and composition derived from LGE MRI predicts VT. *Eur Heart J.* (2017) 38:Supplement:4088314. doi: 10.1093/eurheartj/ehx502.2017
13. Andreu D, Penela D, Acosta J, Fernández-Armenta J, Perea RJ, Soto-Iglesias D, et al. Cardiac magnetic resonance–aided scar dechanneling: influence on acute and long-term outcomes. *Hear Rhythm.* (2017) 14:1121–8. doi: 10.1016/j.hrthm.2017.05.018
14. Sacher F, Tedrow UB, Field ME, Raymond JM, Koplan BA, Epstein LM, et al. Ventricular tachycardia ablation: evolution of patients and procedures over 8 years. *Circ Arrhythm Electrophysiol.* (2008) 1:153–61. doi: 10.1161/CIRCEP.108.769471
15. Josephson ME, Anter E. Substrate mapping for ventricular tachycardia assumptions and misconceptions. *JACC Clin Electrophysiol.* (2015) 1:341–52. doi: 10.1016/j.jacep.2015.09.001
16. Whitaker J, Tschabrunn CM, Jang J, Leshem E, O'Neill M, Manning WJ, et al. Cardiac MR characterization of left ventricular remodeling in a swine model of infarct followed by reperfusion. *J Magn Reson Imaging.* (2018) 48:808–17. doi: 10.1002/jmri.26005
17. Andreu D, Berruezo A, Ortiz-Pérez JT, Silva E, Mont L, Borràs R, et al. Integration of 3D electroanatomic maps and magnetic resonance scar characterization into the navigation system to guide ventricular tachycardia ablation. *Circ Arrhythmia Electrophysiol.* (2011) 4:674–83. doi: 10.1161/CIRCEP.111.961946
18. Bishop M, Rajani R, Plank G, Gaddum N, Carr-White G, Wright M, et al. Three-dimensional atrial wall thickness maps to inform catheter ablation procedures for atrial fibrillation. *Europace.* (2016) 18:376–83. doi: 10.1093/europace/euv073
19. Wellens H, Brugada P, Stevenson WG. Programmed electrical stimulation of the heart in patients with life-threatening ventricular arrhythmias: what is the significance of induced arrhythmias and what is the correc stimulation protocol? *Circulation.* (1985) 72:1–8. doi: 10.1161/01.CIR.72.1.1
20. van Horssen P, van den Wijngaard JPHM, Brandt MJ, Hoefer IE, Spaan JAE, Siebes M. Perfusion territories subtended by penetrating coronary arteries increase in size and decrease in number toward the subendocardium. *Am J Physiol Circ Physiol.* (2013) 306:H496–504. doi: 10.1152/ajpheart.00584.2013
21. Fernández-Armenta J, Berruezo A, Andreu D, Camara O, Silva E, Serra L, et al. Three-dimensional architecture of scar and conducting channels based on high resolution ce-CMR: insights for ventricular tachycardia ablation. *Circ Arrhythmia Electrophysiol.* (2013) 6:528–37. doi: 10.1161/CIRCEP.113.000264
22. Andreu D, Ortiz-Pérez JT, Fernández-Armenta J, Guiu E, Acosta J, Prat-González S, et al. 3D delayed-enhanced magnetic resonance sequences improve conducting channel delineation prior to ventricular tachycardia ablation. *Europace.* (2015) 17:938–45. doi: 10.1093/europace/euu310
23. Bizino MB, Tao Q, Amersfoort J, Siebelink HJ, Bogaard PJ, Van RJ, et al. High spatial resolution free-breathing 3D late gadolinium enhancement cardiac magnetic resonance imaging in ischaemic and non-ischaemic cardiomyopathy : quantitative assessment of scar mass and image quality. *Eur Radiol.* (2018) 28:4027–35. doi: 10.1007/s00330-018-5361-y
24. Flett AS, Hayward MP, Ashworth MT, Hansen MS, Taylor AM, Elliott PM, et al. Equilibrium contrast cardiovascular magnetic resonance for the measurement of diffuse myocardial fibrosis: preliminary validation in humans. *Circulation.* (2010) 122:138–44. doi: 10.1161/CIRCULATIONAHA.109.930636
25. Schulz-Menger J, Bluemke DA, Bremerich J, Flamm SD, Fogel MA, Friedrich MG, et al. Standardized image interpretation and post-processing in cardiovascular magnetic resonance-2020 update. *J Cardiovasc Magn Reson.* (2020) 22:1–22. doi: 10.1186/s12968-020-00610-6
26. Amado LC, Gerber BL, Gupta SN, Rettmann DW, Szarf G, Schock R, et al. Accurate and objective infarct sizing by contrast-enhanced magnetic resonance imaging in a canine myocardial infarction model. *J Am Coll Cardiol.* (2004) 44:2383–9. doi: 10.1016/j.jacc.2004.09.020
27. Ginami G, Neji R, Rashid I, Chiribiri A, Ismail TF, Botnar RM, et al. 3D whole-heart phase sensitive inversion recovery CMR for simultaneous black-blood late gadolinium enhancement and bright-blood coronary CMR angiography. *J Cardiovasc Magn Reson.* (2017) 19:1–14. doi: 10.1186/s12968-017-0405-z
28. Desjardins B, Crawford T, Good E, Oral H, Chugh A, Pelosi F, et al. Infarct architecture and characteristics on delayed enhanced magnetic resonance imaging and electroanatomic mapping in patients with postinfarction ventricular arrhythmia. *Hear Rhythm.* (2009) 6:644–51. doi: 10.1016/j.hrthm.2009.02.018

29. Piers SRD, Everaerts K, Van Der Geest RJ, Hazebroek MR, Siebelink HM, Pison LAFG, et al. Myocardial scar predicts monomorphic ventricular tachycardia but not polymorphic ventricular tachycardia or ventricular fibrillation in nonischemic dilated cardiomyopathy. *Hear Rhythm.* (2015) 12:2106–14. doi: 10.1016/j.hrthm.2015.05.026
30. Josephson ME, Horowitz LN, Farshidi A, Spear JF, Kastor JA, Moore EN. Recurrent sustained ventricular tachycardia. 2 endocardial mapping. *Circulation.* (1978) 57:431–40. doi: 10.1161/01.CIR.57.3.440
31. Okumura K, Olshansky B, Henthorn RW, Epstein AE, Plumb VJ, Waldo AL. Demonstration of the presence of slow conduction during sustained ventricular tachycardia in man: use of transient entrainment of the tachycardia. *Circulation.* (1987) 75:369–78. doi: 10.1161/01.CIR.75.2.369
32. Yamashita S, Sacher F, Mahida S, Berte B, Lim HS, Komatsu Y, et al. Image integration to guide catheter ablation in scar-related ventricular tachycardia. *J Cardiovasc Electrophysiol.* (2016) 27:699–708. doi: 10.1111/jce.12963
33. Glukhov AV, Fedorov VV, Kalish PW, Ravikumar VK, Lou Q, Janks D, et al. Conduction remodeling in human end-stage nonischemic left ventricular cardiomyopathy. *Circulation.* (2012) 125:1835–47. doi: 10.1161/CIRCULATIONAHA.111.047274
34. Jang J, Whitaker J, Leshem E, Ngo L, Neisus U, Nakamori S, et al. Local conduction velocity in the presence of late gadolinium enhancement and myocardial wall thinning: a cardiac magnetic resonance study in a swine model of healed left ventricular infarction. *Circ Arrhythm Electrophysiol.* (2019) 12:e007175. doi: 10.1161/CIRCEP.119.007175
35. Anter E, Tschabrunn CM, Buxton AE, Josephson ME. High-resolution mapping of postinfarction reentrant ventricular tachycardia: electrophysiological characterization of the circuit. *Circulation.* (2016) 134:314–27. doi: 10.1161/CIRCULATIONAHA.116.021955
36. Fast VG, Klkber AG. Cardiac tissue geometry as a determinant of unidirectional conduction block: assessment of microscopic excitation spread by optical mapping in patterned cell cultures and in a computer model. *Cardiovasc Res.* (1995) 29:697–707.
37. Dhanjal TS, Lellouche N, von Ruhland CJ, Abehsira G, Edwards DH, Dubois-Randé JL, et al. Massive accumulation of myofibroblasts in the critical isthmus is associated with ventricular tachycardia inducibility in post-infarct swine heart. *JACC Clin Electrophysiol.* (2017) 3:703–14. doi: 10.1016/j.jacep.2016.11.010

Conflict of Interest: The CardioHelp machine and all ECMO consumables were donated by Maquet, Getinge Group without conditions on their use. The Precision and Claris system and all EP mapping consumables were donated by Abbott without conditions on their use. The authors declare a potential conflict of interest and state it below. RN was employed by the company Siemens Healthcare. SK and TA were employed by the company Abbott Medical.

The remaining authors declare that the research was conducted in the absence of any commercial or financial relationships that could be construed as a potential conflict of interest.

frontiers in Cardiovascular Medicine

CASE REPORT
published: 22 November 2021
doi: 10.3389/fcvm.2021.748194

Case Report: A Rare Complication Following Catheter Ablation of Scar-Related Ventricular Tachycardia

Xiaoyong Xu[1†], Ming Ye[2†], Yaxun Sun[3], Qiang Liu[3], Fusheng Ma[1] and Chenyang Jiang[3]*

[1] Department of Cardiology, Ningbo Medical Treatment Centre Li Huili Hospital, Ningbo, China, [2] Department of Electrophysiology, Ningbo Medical Treatment Centre Li Huili Hospital, Ningbo, China, [3] Department of Cardiology, Sir Run Run Shaw Hospital, School of Medicine, Zhejiang University, Hangzhou, China

Background: The substrate for ventricular tachycardia (VT) in patients with structural heart disease is usually complex and often requires extensive ablation. As a result, the incidence of major procedure-related complications has been reported to be higher when compared to patients without structural heart disease. In this study, we present a rare complication after extensive substrate modification of scar-related VT.

Case: A 65-year-old man with ischemic cardiomyopathy was referred to the electrophysiology laboratory for radiofrequency ablation of VT following repetitive implantable cardioverter defibrillator shocks within a short period. As with hemodynamic intolerance of induced VT, an approach involving extensive endocardial substrate modification to reduce the arrhythmogenicity of the scars was adopted. After the procedure, the heart function of the patient deteriorated significantly. The postprocedural ECG showed a bizarre, extremely wide surface QRS complex (360 ms), termed as homologous ventricular separation. The pronounced dyssynchrony of the ventricle was corrected by an upgrade to cardiac resynchronization therapy with defibrillation (CRT-D). As a result, the symptoms of the patient improved significantly. The width of the intrinsic QRS complex was not recovered during an 18-month follow-up.

Conclusion: Homologous ventricular separation is a rare arrhythmia, manifested as two separated QRS waves. This case report demonstrates, for the first time, that homologous ventricular separation may occur after extensive substrate modification of scar-related VT. CRT-D can correct the dyssynchronous ventricle caused by homologous ventricular separation.

Keywords: ventricular tachycardia, homologous ventricular separation, catheter ablation, complication, substrate modification

OPEN ACCESS

Edited by:
Kyoung-Ryul Julian Chun, CCB Frankfurt, Med. III, Kardiologie, Markuskrankenhaus, Germany

Reviewed by:
Hussam Ali, MultiMedica (IRCCS), Italy
Christian Hendrik Heeger, University Heart Center Luebeck, Germany

****Correspondence:***
Fusheng Ma
mfs732@163.com

† These authors have contributed equally to this work and share first authorship

Specialty section:
This article was submitted to Cardiac Rhythmology, a section of the journal Frontiers in Cardiovascular Medicine

Received: *27 July 2021*
Accepted: *20 October 2021*
Published: *22 November 2021*

Citation:
Xu XY, Ye M, Sun YX, Liu Q, Ma FS and Jiang CY (2021) Case Report: A Rare Complication Following Catheter Ablation of Scar-Related Ventricular Tachycardia. Front. Cardiovasc. Med. 8:748194. doi: 10.3389/fcvm.2021.748194

INTRODUCTION

For patients with structural heart disease, catheter ablation is indicated as adjunctive treatment when recurrent ventricular tachycardia (VT) leads to repetitive implantable cardioverter defibrillator (ICD) therapies within a short time. Catheter ablation of VT has been shown to improve VT-free survival at long-term follow-up in the setting of ischemic cardiomyopathy (1). Although the complication rate of catheter ablation is higher than that of patients without structural

heart disease, it is still within an accepted range (2, 3). In this study, we present a rare complication after extensive substrate modification of scar-related VT.

CASE DESCRIPTION

A 65-year-old man with ischemic cardiomyopathy was referred to the electrophysiology laboratory for radiofrequency (RF) ablation of VT following repetitive ICD shocks, even after appropriate antiarrhythmic therapy (**Figure 1A**). A baseline ECG showed sinus rhythm with a QRS duration of 112 ms (**Figure 1B**). The transthoracic echocardiogram (TTE) demonstrated a dilated left ventricle (left ventricular end-diastolic diameter of 68 mm) and left ventricular ejection fraction (LVEF) of 40%. As with hemodynamic intolerance of induced VT, an approach involving extensive endocardial substrate modification to reduce the arrhythmogenicity of scars was adopted. Endocardial electroanatomical high-density mapping was performed by using the 20-polar PentaRay catheter and the CARTO mapping system (Biosense Webster, Diamond Bar, California, USA), with the fast-anatomical mapping reconstruction resolution set at a high level. Arrhythmia substrates were identified in the basal septal endocardium of the left ventricular (**Figure 2**). RF current at a power setting of 40–50 W was applied to eliminate all the potential arrhythmia substrates including ventricular late potentials and local abnormal ventricular activity. The right ventricular endocardium was subsequently mapped with no low voltage area (<0.5 mV). For potential intramural arrhythmia substrate in the ventricular septum, we used bipolar RF of combining both the left and right ventricular septal surface ablation. Extensive substrate ablation was performed until: (1) no monomorphic VT was inducible and (2) only unstable VTs that were different from those previously induced. After the procedure, the heart function of the patient deteriorated significantly. The repeated TTE demonstrated an LVEF of 34%, with paradoxical motion of the left and right ventricle during both the diastole and systole. The postprocedural ECG is shown in **Figure 3A**. Upon close examination of the ECG, what are the unusual findings? How should the patient can be managed?

Upon close examination of the limb leads, we found a bizarre, extremely wide surface QRS complex (360 ms), which was composed of two independent QRS complexes separated by an isoelectric baseline. The first QRS complex in this sequence, highlighted in **Figure 3A** in a blue color, mimicked atrial depolarization in the limb leads. The second QRS complex in this sequence, highlighted in **Figure 3A** in a purple color, resembled a left bundle branch block (LBBB) pattern and the wave highlighted in **Figure 3A** in orange was a T wave.

This evaluation led to the recommendation of an upgrade to cardiac resynchronization therapy with defibrillation (CRT-D). Due to the deterioration of heart function, even after appropriate heart failure therapy, the patient consented to the upgrade. The procedure was successfully performed with extracorporeal membrane oxygenation support (**Figure 4**). The intracardiac recordings from the right and left ventricle showed marked intraventricular conduction delay (200 ms)

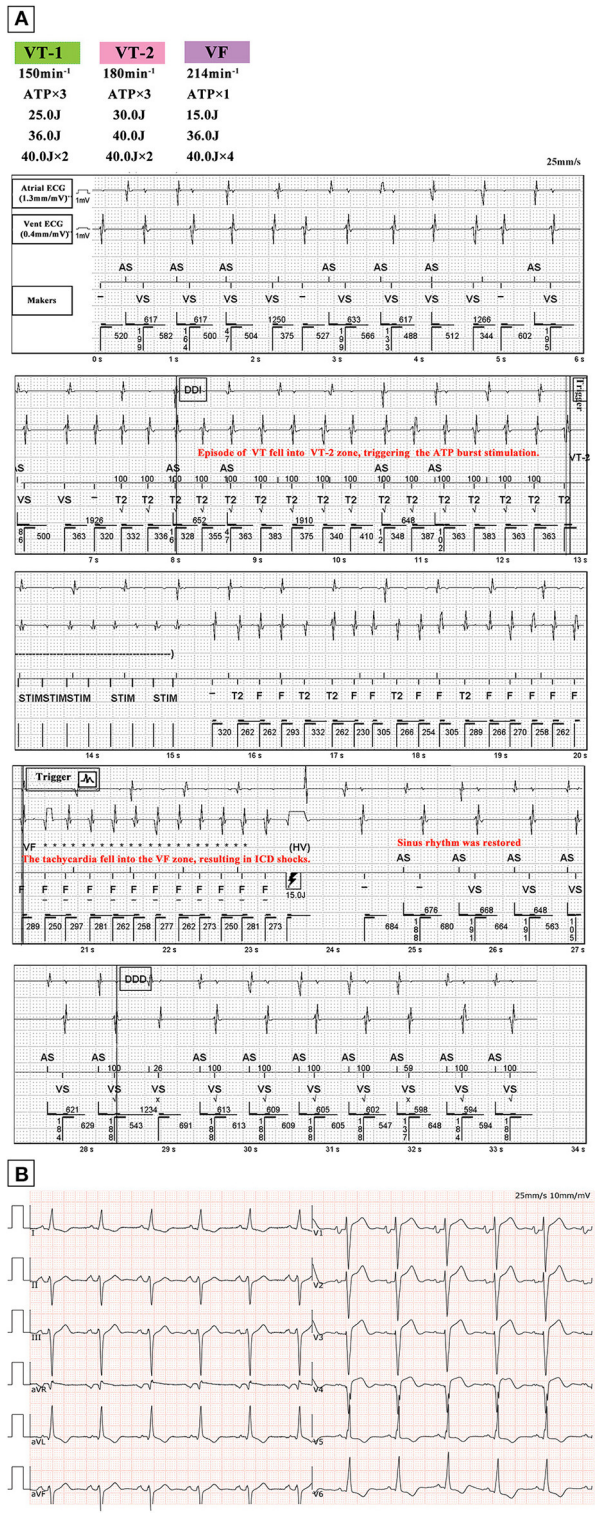

FIGURE 1 | (A) Episode of VT detected by ICD. Sinus rhythm is restored following one attempt of ATP burst stimulation with subsequent shock application according to the ICD programming protocol shown on the upper left corner. **(B)** ECG of the patient in sinus rhythm after shock therapy, with a QRS duration of 112 ms. Abbreviations: VT, ventricular tachycardia; ICD, implantable cardioverter defibrillator; VF, ventricular fibrillation; ATP, antitachycardia pacing; vent, ventricular.

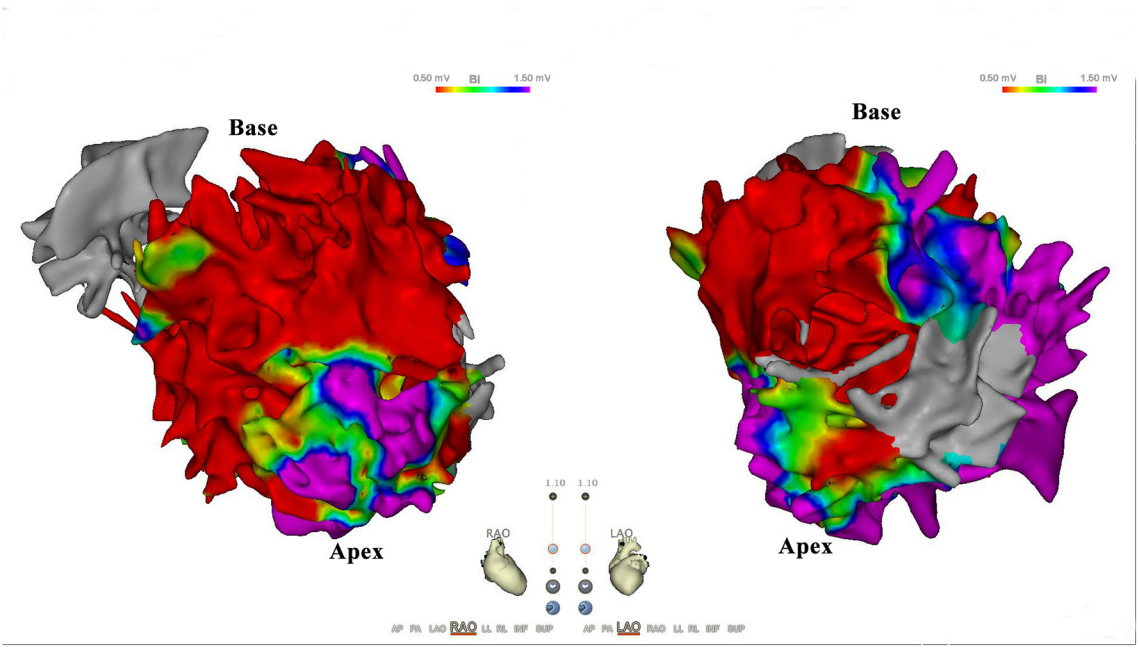

FIGURE 2 | Scar distribution in endocardium. Bipolar voltage map of the left ventricular endocardium. Scar cutoff is set at <0.5 mV (red area); border zone is set at 0.5–1.5 mV. Note predilection of scar distribution to basal septal endocardium of left ventricular.

(**Figure 3B**). When the ECG was recorded simultaneously with intracardiac recording, we found that the first QRS complex in surface ECG was the result of depolarization of the right ventricle and the second QRS complex was due to depolarization of the left ventricle. Following postimplant ECG optimization, the interventricular interval was narrowed from 200 ms in intrinsic intraventricular conduction to 20 ms in biventricular pacing (**Figures 3B,C**). After turning on CRT-D, the fused E/A waves were separated in TTE, which suggested that the heart responded well to the CRT-D therapy (**Figure 5**). As a result, the symptoms of the patient improved significantly. The width of the intrinsic QRS complex was not recovered during an 18-month follow-up. The detailed timeline of the clinical course of this patient is displayed in **Table 1**.

DISCUSSION

Cardiac resynchronization therapy with defibrillation has demonstrated improved outcomes in selected patients with heart failure. The therapeutic benefit of CRT-D is achieved by the mechanical correction of the dyssynchronous left ventricle. Therefore, the greater the intraventricular dyssynchrony, which manifested as a widened surface QRS complex, the greater the benefit of CRT-D (4). To improve CRT-D response rates, the guideline emphasizes attention to the electrical parameters, especially before implant (i.e., LBBB and QRS duration $\geq$150 ms) (5). LBBB morphology is required in the class I recommendation (5). In this case, the postablation ECG shows ventricular activation separation, producing two QRS complexes that do not interfere with each other and are separated by an isoelectric baseline, resulting in pronounced ventricular dyssynchronization. However, after CRT-D corrects the dyssynchronous ventricle, the patient experienced an improvement in symptoms significantly. By means of a thorough literature review, we find that this rare arrhythmia, first reported in 1975, known as homologous ventricular separation and defined as a partial ventricular myocardium depolarized significantly later than others because of a complete myocardial conduction block (6). Homologous ventricular separation has been sporadically reported (6–9). According to previous case reports, it seems that homologous ventricular separation can occur in patients with acute deterioration of heart function (7), procainamide toxicity (6), cardiac arrest (8), and myocardial infarction (9). In the patient described in this report, ventricular separation was due to extensive ventricular ablation.

There are two strategies for the ablation of scar-related VT: (1) standard strategy: selective targeting the critical isthmus that supports the development and maintenance of VT (as identified by activation, entrainment, and pace mapping techniques) and (2) substrate modification: extensive substrate modification to reduce the arrhythmogenicity of scarring without any specific arrhythmia targeting. In a meta-analysis, Briceno et al. found that complete substrate modification results in a lower risk of long-term ventricular arrhythmia recurrence and all-cause mortality than standard ablation and incomplete substrate modification (3). In addition, the complication rate of substrate modification-related was approximately 7% including complete atrioventricular block, acute hemodynamic

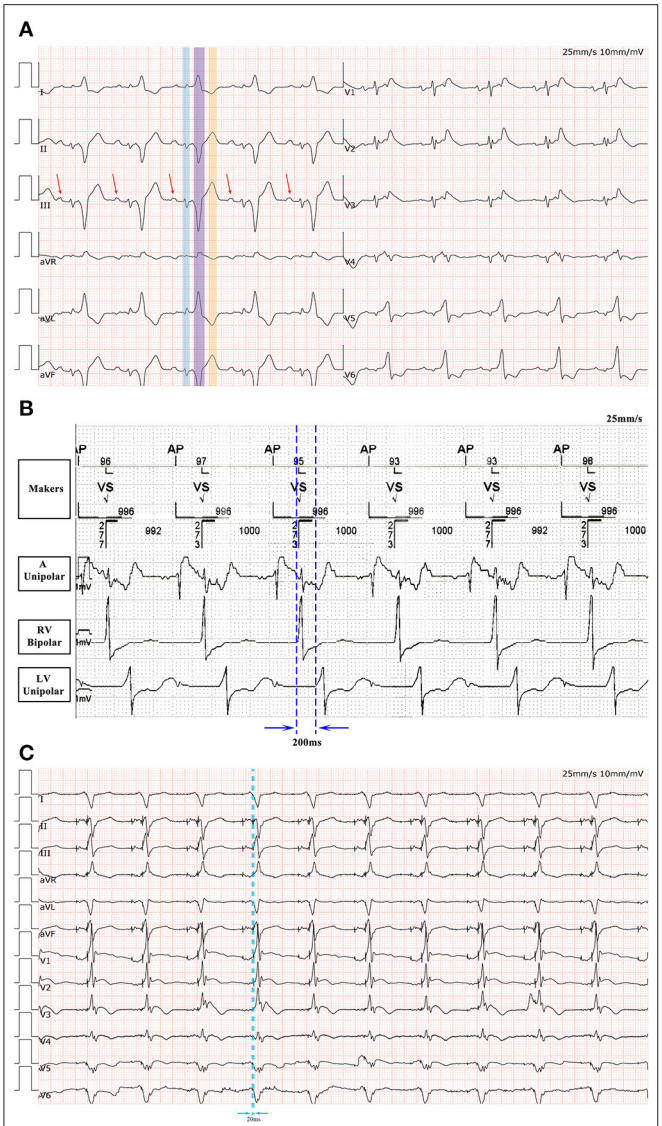

FIGURE 3 | (A) A 12-lead ECG after ablation. The underlying rhythm is sinus rhythm with QRS duration of 360 ms. Note the initial QRS complex mimicking atrial electrical activity in standard (highlighted in blue). The real P wave is indicated by the arrow. Another QRS complex in this sequence is highlighted in purple. The wave highlighted in orange is the T wave. **(B)** The right ventricular-left ventricular interval is 200 ms in the absence of ventricular pacing. **(C)** Following ECG optimization by CRT-P programming, the QRS complex is significantly narrowed.

decompensation, puncture hematoma, cardiac tamponade, stroke/transient ischemic attack, phrenic nerve palsy, transient ST-segment elevation, and death (2, 10). To date, no homologous ventricular separation cases after substrate modification of scar-related VT have been reported. Chambers electrical isolation by catheter ablation is not uncommon. This entails isolation of the atriums from the ventricles by atrioventricular nodal ablation for rapid atrial fibrillation that cannot be controlled. In addition, the left atrium can be unintentionally isolated from the right atrium after extensive left atrium ablation (11). Due to many muscle-to-muscle connections between the right and left ventricles, it seems impossible to electrically isolate the two ventricles by catheter ablation. This case report demonstrated that ventricular separation may occur after extensive substrate modification of scar-related VT. In this case, as with hemodynamic intolerance of induced VT, we attempt to homogenize all the tissues in a low voltage area. After eliminating most of the ventricular late potentials and local abnormal ventricular activity, VT is still inducible. This suggests the presence of an intramural substrate. Empirically, we use bipolar RF of combining both the left and right ventricular septal surface ablation. During the procedure, the QRS complex suddenly separated into two parts. The potential mechanisms may include the extensive lesions in many parts of the left ventricle, especially aggressive ablation in the ventricular septum, resulting in the obstruction of electrical conduction of the ventricular muscle and Purkinje conduction system in the septum. Therefore, the spread of depolarizations from the atrium went to the right ventricle firstly, subsequently conducted to the left ventricle via apical myocardium (activation maps in sinus rhythm before and after ablation was not shown). In order to prevent this rare complication, we believe that extensive endocardial substrate modification in the ventricular septum needs to be very careful.

DATA AVAILABILITY STATEMENT

The original contributions presented in this study are included in the article. Further inquiries can be directed to the corresponding author.

ETHICS STATEMENT

Written informed consent was obtained from the participant for the publication of this case report (including all the data and images).

AUTHOR CONTRIBUTIONS

XYX, MY, YXS, QL, CYJ, and FSM: contribute to conceptualization. XYX, YXS, QL, and MY: were involved in data collection, validation, and formal analysis. XYX: wrote the manuscript. All authors reviewed and approved the final manuscript for publication.

FUNDING

This study was supported in part by the Natural Science Foundation of Ningbo 2017A610200 and 2014A610270 for open access publication fees.

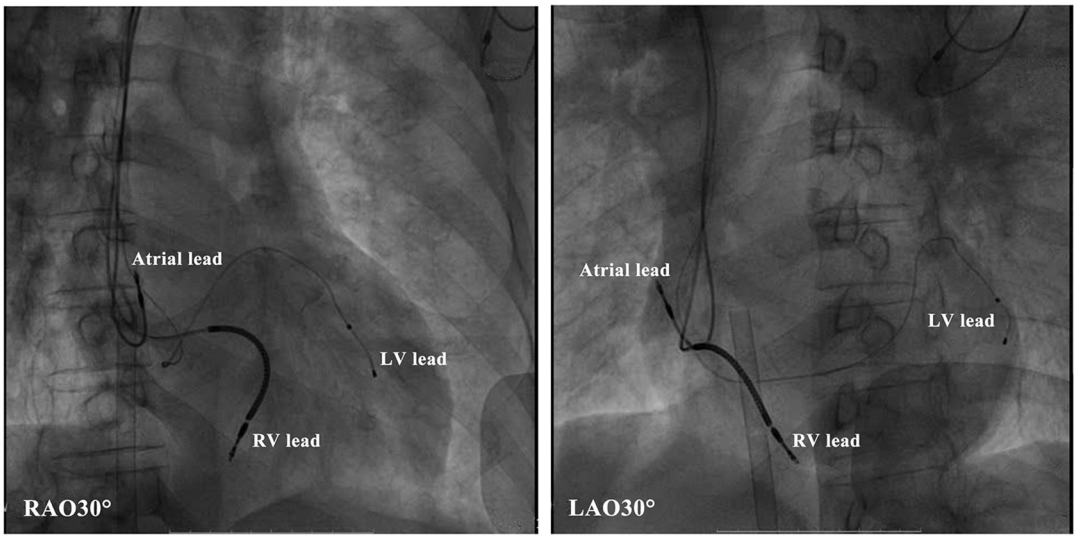

FIGURE 4 | Radiologic images of the cardiac resynchronization therapy system showing lead positioning. LV, left ventricular; RV, right ventricular.

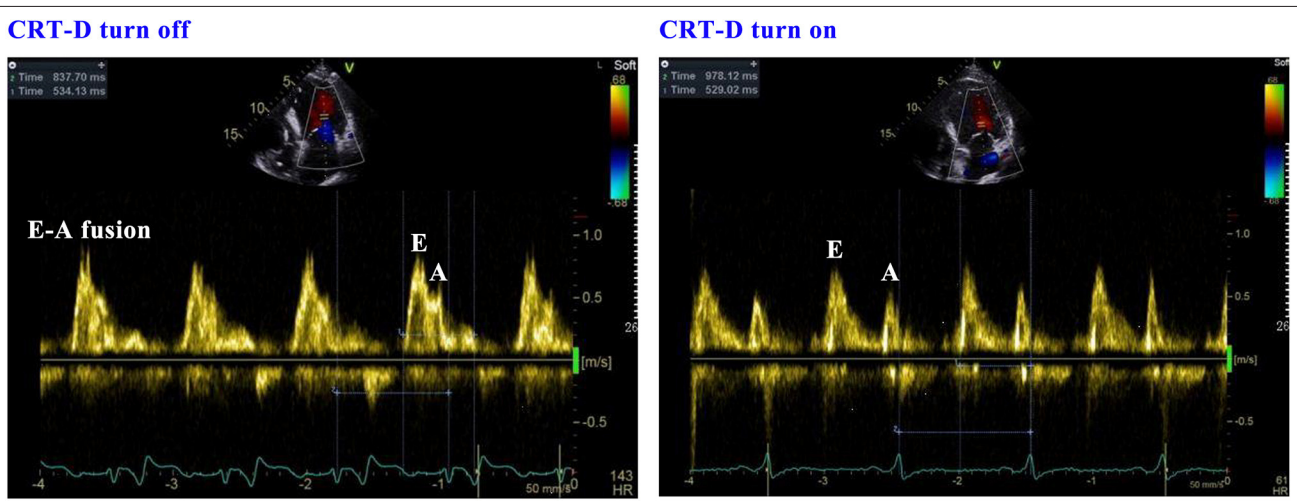

FIGURE 5 | The response of echocardiography when the CRT-D is turned on and off. CRT-D, cardiac resynchronization therapy with defibrillation.

TABLE 1 | Detailed timeline of clinical course of the patient.

12/3/2013	The patient was diagnosed with ischemic cardiomyopathy and given the guideline-directed medical treatment of heart failure.
7/27/2017	An episode of hemodynamically unstable ventricular tachycardia (VT) resulted in treatment with implantable cardioverter-defibrillator (ICD) to prevent sudden cardiac death.
12/19/2019	The occurrence of VT electrical storm led to repetitive ICD therapies within a short period of time.
12/28/2019	The patient was referred for VT ablation. Following the procedure, the heart function of the patient deteriorated. The postprocedural ECG showed homologous ventricular separation.
1/3/2020	After an upgrade to biventricular pacing, the patient's symptoms improved significantly.
01/03/2020 to present	Follow-up period

REFERENCES

1. Muser D, Liang JJ, Pathak RK, Magnani S, Castro SA, Hayashi T, et al. Long-Term Outcomes of Catheter Ablation of Electrical Storm in Nonischemic Dilated Cardiomyopathy Compared With Ischemic Cardiomyopathy. *JACC Clin Electrophysiol.* (2017) 3:767–78. doi: 10.1016/j.jacep.2017.01.020
2. Fernandez J-Armenta, Soto D-Iglesias, Silva E, Penela D, Jauregui B, Linhart M, et al. Safety and Outcomes of Ventricular Tachycardia Substrate Ablation During Sinus Rhythm: A Prospective Multicenter Registry. *JACC Clin Electrophysiol.* (2020) 6:1435–48. doi: 10.1016/j.jacep.2020.07.028
3. Briceno DF, Romero J, Villablanca PA, Londono A, Diaz JC, Maraj I, et al. Long-term outcomes of different ablation strategies for ventricular tachycardia in patients with structural heart disease: systematic review and meta-analysis. *Europace.* (2018) 20:104–15. doi: 10.1093/europace/eux109
4. Kuznetsov VA, Soldatova AM, Kasprzak JD, Krinochkin DV, Melnikov NN. Echocardiographic markers of dyssynchrony as predictors of super-response to cardiac resynchronisation therapy - a pilot study. *Cardiovasc Ultrasound.* (2018) 16:24. doi: 10.1186/s12947-018-0140-0
5. Brignole M, Auricchio A, Baron G-Esquivias, Bordachar P, Boriani G, Breithardt OA, et al. 2013 ESC guidelines on cardiac pacing and cardiac resynchronization therapy: the task force on cardiac pacing and resynchronization therapy of the european society of cardiology (ESC). developed in collaboration with the european heart rhythm association (EHRA). *Eur Heart J.* (2013) 34:2281–329. doi: 10.1093/eurheartj/eht150
6. Gay RJ, Brown DF. Pacemaker failure due to procainamide toxicity. *Am J Cardiol.* (1974) 34:728–32. doi: 10.1016/0002-9149(74)90164-7
7. Yan S, Yu J, Xia Z, Zhu B, Hu J, and Li J. A rare form of extremely wide QRS complex due to reversed homologous electrical ventricular separation of acute heart failure. *Ann Noninvasive Electrocardiol.* (2018) 23:e12482. doi: 10.1111/anec.12482
8. Castellanos A, Sung RJ, Myerburg RJ. Intraventricular dissociation due to complete intraventricular block. *Chest.* (1975) 68:833–4. doi: 10.1378/chest.68.6.833
9. Algeo SS, Ewy GA. Pseudo-atrial rhythm due to electrical ventricular separation. *Am Heart J.* (1985) 109:900–2. doi: 10.1016/0002-8703(85)90656-8
10. Wolf M, Sacher F, Cochet H, Kitamura T, Takigawa M, Yamashita S, et al. Long-Term Outcome of Substrate Modification in Ablation of Post-Myocardial Infarction Ventricular Tachycardia. *Circ Arrhythm Electrophysiol.* (2018) 11:e005635. doi: 10.1161/CIRCEP.117.005635
11. Jain S, Mirza S, Shukla G. Inadvertent atrial dissociation following catheter ablation: A demonstration of cardiac anisotropy and functional block. *HeartRhythm Case Rep.* (2019) 5:201–4. doi: 10.1016/j.hrcr.2018.12.010

Conflict of Interest: The authors declare that the research was conducted in the absence of any commercial or financial relationships that could be construed as a potential conflict of interest.

frontiers in Cardiovascular Medicine

ORIGINAL RESEARCH
published: 07 December 2021
doi: 10.3389/fcvm.2021.767514

Predictors and Long-Term Outcome of Ablation of Discrete Pre-potentials in Patients With Idiopathic Ventricular Arrhythmias Originating From the Aortic Sinuses of Valsalva

*Hui-Qiang Wei[1,2], Xiao-Gang Guo[2], Gong-Bu Zhou[3], Qi Sun[2], Jian-Du Yang[2], Hai-Yang Xie[2], Jackson Liang[4], Shu Zhang[2], Shulin Wu[1] and Jian Ma[2]**

[1] Department of Cardiology, Guangdong Cardiovascular Institute, Guangdong Provincial People's Hospital, Guangdong Academy of Medical Sciences, Guangzhou, China, [2] State Key Laboratory of Cardiovascular Disease, Arrhythmia Center, National Center for Cardiovascular Diseases, Fuwai Hospital, Chinese Academy of Medical Sciences and Peking Union Medical College, Beijing, China, [3] Department of Cardiology, Peking University Third Hospital, Beijing, China, [4] Division of Cardiovascular Medicine, Electrophysiology Service, University of Michigan Health System, Ann Arbor, MI, United States

OPEN ACCESS

Edited by:
Minglong Chen,
The First Affiliated Hospital of Nanjing Medical University, China

Reviewed by:
Neal Kay,
University of Alabama at Birmingham, United States
Hongwu Chen,
Nanjing Medical University, China

***Correspondence:**
Jian Ma
majian_fuwai@126.com

Specialty section:
This article was submitted to Cardiac Rhythmology, a section of the journal Frontiers in Cardiovascular Medicine

Received: 30 August 2021
Accepted: 09 November 2021
Published: 07 December 2021

Citation:
Wei H-Q, Guo X-G, Zhou G-B, Sun Q, Yang J-D, Xie H-Y, Liang J, Zhang S, Wu S and Ma J (2021) Predictors and Long-Term Outcome of Ablation of Discrete Pre-potentials in Patients With Idiopathic Ventricular Arrhythmias Originating From the Aortic Sinuses of Valsalva. Front. Cardiovasc. Med. 8:767514. doi: 10.3389/fcvm.2021.767514

Background: The predictability and long-term outcome of the discrete pre-potential (DPP) of idiopathic ventricular arrhythmias (VAs) arising from the aortic sinuses of Valsalva (ASV) have not been fully identified.

Methods: Of 687 consecutive patients undergoing ablation of outflow tract VAs, there were 105 (15.3%) patients with VAs originating from the ASV region who were included. Detailed mapping was performed within the ASV in all patients. Electrocardiographic, electrophysiological parameters, and long-term success rate were compared between patients with and without the DPPs.

Results: A DPP was recorded in 67 of 105 (63.8%) patients, including 38 left sinus of Valsalva (LSV)-VAs (38/105, 36.2%) and 29 right sinus of Valsalva (RSV)-VAs (29/105, 27.6%). The patients with DPPs had wider QRS duration (152 ± 17 vs. 145 ± 14 ms, $p < 0.001$). The average of earliest activation time was significantly earlier in patients with DPPs (−38.6 ± 8.5 vs. −27.7 ± 5.7 ms, $p < 0.001$). Mean time from the first lesion to elimination of VAs was shorter in patients with DPPs (2.3 ± 2.1 s vs. 4.9 ± 1.0 s, $p < 0.001$). A stepwise logistic multivariable analysis identified only younger age as a significant predictor of DPP (age ≤ 35.5 years predicted DPP with 92.9% positive predictive value). During a follow-up duration of 42.5 ± 22.3 months, 63 (94.0%) patients with DPPs and 30 (78.9%) patients without DPPs remained free of recurrent VAs ($p = 0.027$).

Conclusion: Discrete pre-potentials were observed in 63.8% of patients with VAs arising from the ASV. Ablation in patients with DPPs was associated with higher long-term success. DPPs were seen more commonly in younger (age ≤ 35.5 years) patients.

Keywords: ventricular arrhythmia, catheter ablation, sinus of Valsalva, discrete pre-potential, outcome

INTRODUCTION

The right or left ventricular outflow tracts (RVOTs or LVOTs) are the most common sites of origin for idiopathic ventricular tachycardia (VT) or premature ventricular contractions (PVCs). Radiofrequency (RF) catheter ablation has been considered as a safe and effective method to treat outflow tract ventricular arrhythmias (VAs), and arrhythmias from these sites are being increasingly recognized (1–3). Several studies have reported that a discrete pre-potential (DPP) can sometimes be recorded at the successful ablation sites within the aortic sinuses of Valsalva (ASV), and the presence of the DPPs has been considered to be useful in guiding ablation within the ASV (4–6). However, there remains a paucity of comparative data on the prevalence and predictability of identifying DPPs during mapping and ablation of idiopathic VAs arising from the ASV. Consequently, the aim of this study was to identify the electrocardiographic and electrophysiological predictors of DPPs of idiopathic VAs arising from the ASV.

METHODS

The data that support the findings of this study are available from the corresponding author upon reasonable request.

Study Population

A total of 687 patients underwent ablation of ventricular outflow tract VAs between January 2012 and December 2018 at our center (**Figure 1**). Patients who underwent repeat ablation or ablation failed were excluded in this study (the anatomic location of their VA origin could not be determined). All patients had cardiac imaging with transthoracic echocardiography to confirm the absence of structural heart disease. All patients provided written informed consent before the catheter ablation. This study was approved by the institutional review board of Fuwai Hospital.

ECG Analysis

Detailed analysis of clinical VT or PVCs was performed offline using an electrophysiological data acquisition system (LabSystem PRO, Bard Electrophysiology, Lowell, MA, USA). The following measurements were assessed during the clinical VT or PVCs using the measurement tool: (1) R- and S-wave amplitudes in leads I, II, III, and V_1 to V_3; (2) Q-wave amplitude in leads aVL, aVR, and the Q-wave ratio in lead aVL/aVR; (3) QRS duration; and (4) the precordial transitional zone (TZ); In addition, the precordial TZ was analyzed during the sinus rhythm. The TZ index was calculated as follows: TZ index = TZ score of the clinical VAs minus the TZ score of sinus rhythm (7). In cases with a QS pattern in lead I, we defined the R-amplitude as being 0 mV. The T-P segment was considered the isoelectric baseline for the measurement of R- and S-wave amplitude. All measurements were independently performed by two cardiac electrophysiologists.

Electrophysiological Study

After the withdrawal of all antiarrhythmic drugs for at least five half-lives, all patients underwent electrophysiological evaluation. An electrophysiological study was performed with the patient in the fasting, non-sedated state. Catheters were inserted into the heart under fluoroscopy *via* the femoral vessels. If clinical VAs did not appear simultaneously, programmed stimulation or intravenous isoproterenol was performed to provoke the clinical arrhythmias. Bipolar signals were filtered at 30–500 Hz, and unipolar signals were filtered at 0.05–500 Hz. Intravenous heparin was administered to maintain an activated clotting time of 250 s.

Mapping and Catheter Ablation

Three-dimensional electroanatomic mapping was applied in all patients using the CARTO mapping system (Biosense Webster, Inc., Diamond Bar, CA). Mapping and ablation were performed using a NaviStar ThermoCool catheter (Biosense Webster, Diamond Bar, California) *via* the femoral vessels. Point-by-point mapping was performed to create anatomic maps, and activation mapping was always used to identify the earliest activation site during the PVCs or VT as previously described (8). Pace mapping was also performed in some cases. An ideal target for ablation was selected based on the earliest activation time during the PVCs or VT. DPP was defined as sharp high-frequency potentials occurring after or during the local ventricular electrogram in sinus rhythm or preceding the local ventricular electrogram during PVCs that sometimes displayed double or multiple components.

When mapping and ablation were attempted in ASV, selective angiography through the irrigated catheter tip or aortic arteriography using a pigtail catheter was performed to locate the position of the ASVs. Detailed mapping in the ASV was achieved using the ablation catheter. RF energy was delivered using an initial power of 25 W with an irrigation rate of 17 mL/min. During RF delivery, if a decreased frequency or elimination of VAs occurred within the initial 15 s, the application was maintained and titrated for 60–90 s. If the earliest activation time of VAs was <20 ms, then additional mapping was performed below the valve, coronary venous system or retried in RVOT. After successful ablation, intravenous administration of isoproterenol and programmed ventricular stimulation were performed to reinduce clinical VAs. Acute procedural success was defined as elimination and non-inducibility of the clinical PVCs or VT with isoproterenol infusion and programmed stimulation after at least a 30-min waiting period after the last ablation lesion.

Follow-Up

Continuous telemetric monitoring was performed for 24 h in all patients postablation. Long-term success was defined as no recurrence of the clinical VAs during a Holter monitoring. After hospital discharge, patients were seen in outpatient clinic every 3 months for the 1st year postablation, and every 6 months thereafter. All patients underwent 24-h Holter monitoring and transthoracic echocardiography during follow-up. If the patients had any rhythm-related symptoms, a 12-lead ECG or 24-h 12-lead Holter monitoring was performed to document the cause of the symptoms.

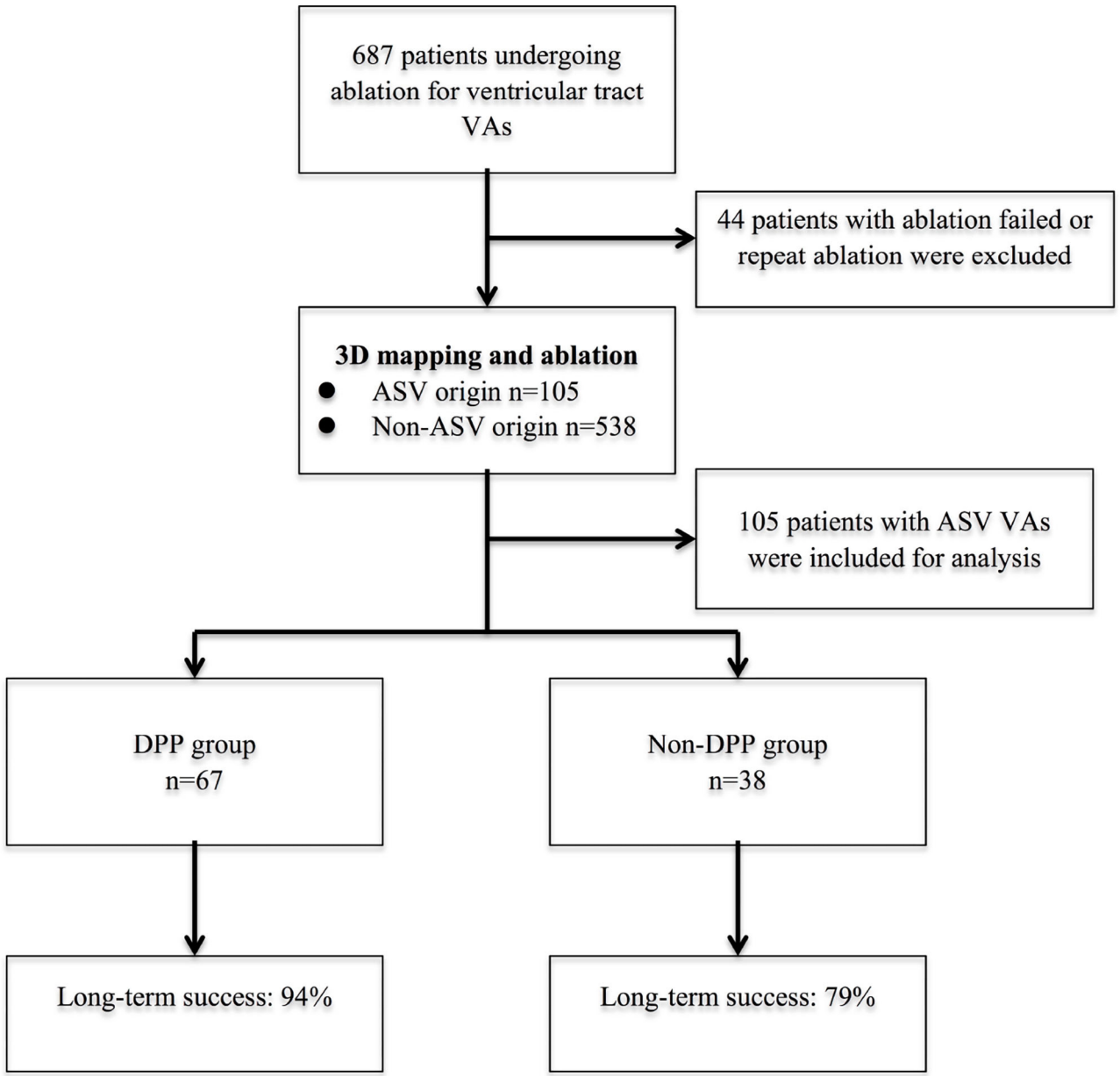

FIGURE 1 | The flow diagram of the study and long-term success rate. 3D, 3-dimensional; ASV, aortic sinus of Valsalva; DPP, discrete pre-potential; VA, ventricular arrhythmia.

Statistical Analysis

All continuous variables are expressed as mean ± SD. The categorical variables are presented as numbers and percentages. Categorical variables were compared using chi-squared analysis. Continuous variables were compared using the Student's *t*-test or Mann–Whitney *U*-test, depending on data distribution. Significant clinical characteristics and ECG parameters predicting predictors of DPPs were tested by univariately, and multivariable logistic regression models were constructed using a backward procedure with $p > 0.1$ as the default criterion for eliminating all variables. Independent variables were tested for collinearity, but no collinearity was present. Receiver operating characteristic (ROC) curves corresponding to the selected logistic regression models were constructed, and the area under the curve (AUC) was calculated to access the diagnostic value of the variables. The optimal cutoff equaled the maximum of Youden's index J, calculated from the ROC data as the cutoff with the greatest sum of sensitivity and specificity (J = sensitivity + specificity−1). A two-tailed value of $p < 0.05$ was considered statistically significant. All statistical

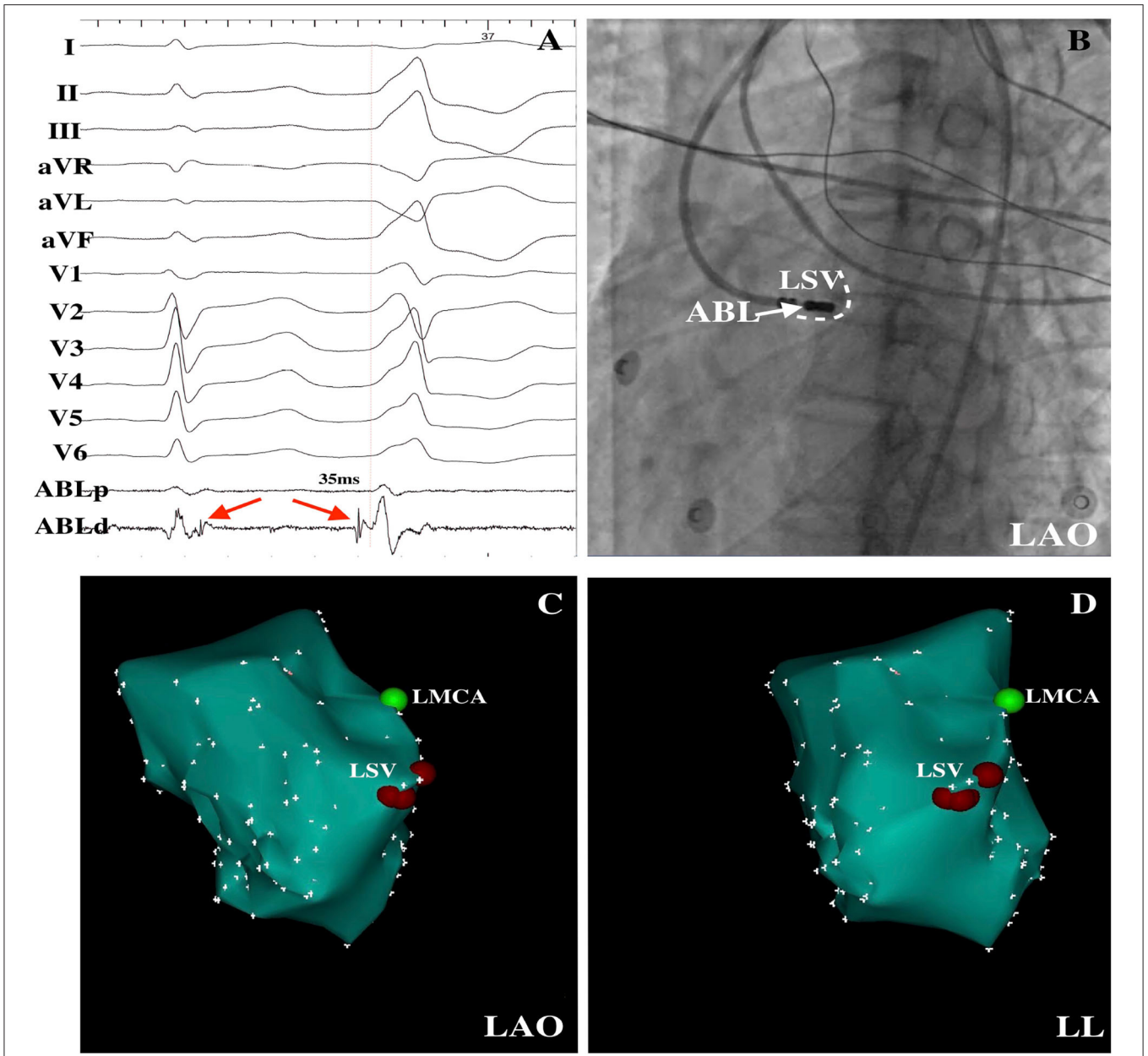

FIGURE 2 | PVCs were successfully ablated within the LSV. **(A)** Delayed potential (red arrow) was observed during the sinus rhythm, and a DPP on the LSV preceded the QRS by 35 ms at the successful ablation site was recorded. **(B)** LAO radiographic view revealed the mapping catheter within the LSV. LAO **(C)** and LL **(D)** electroanatomical maps demonstrated the successful ablation points within the LSV. LSV, left sinus of Valsalva; DPP, discrete pre-potential; LAO, left anterior oblique; LL, left lateral; ABL, ablation catheter; LMCA, left main coronary artery.

analyses were performed using SPSS 19.0 (SPSS, Inc., Chicago, IL, USA).

RESULTS

Baseline Characteristics

The successful ablation site was located within the ASV region in 105 (15.3%) of the 687 patients: 64 (61.0%) from the left sinus of Valsalva (LSV) and 41 (39.0%) from the right sinus of Valsalva (RSV). Of the 105 patients whose successful target site was from the ASV, a DPP was recorded in 67 of 105 (63.8%) patients, including 38 LSV-VAs (38/64, 59.4%) (**Figure 2**) and 29 RSV-VAs (29/41, 70.7%) (**Figure 3**). Baseline clinical and demographic data are presented in **Table 1**. Patients in whom DPPs were identified were younger in age than those without DPPs (37.6 ± 17.3 years vs. 52.2 ± 12.8 years, $p < 0.001$), and patients with DPPs were more likely to be male gender (62.7%) whereas those without DPPs were more likely to be female gender (57.9%) ($p = 0.042$)

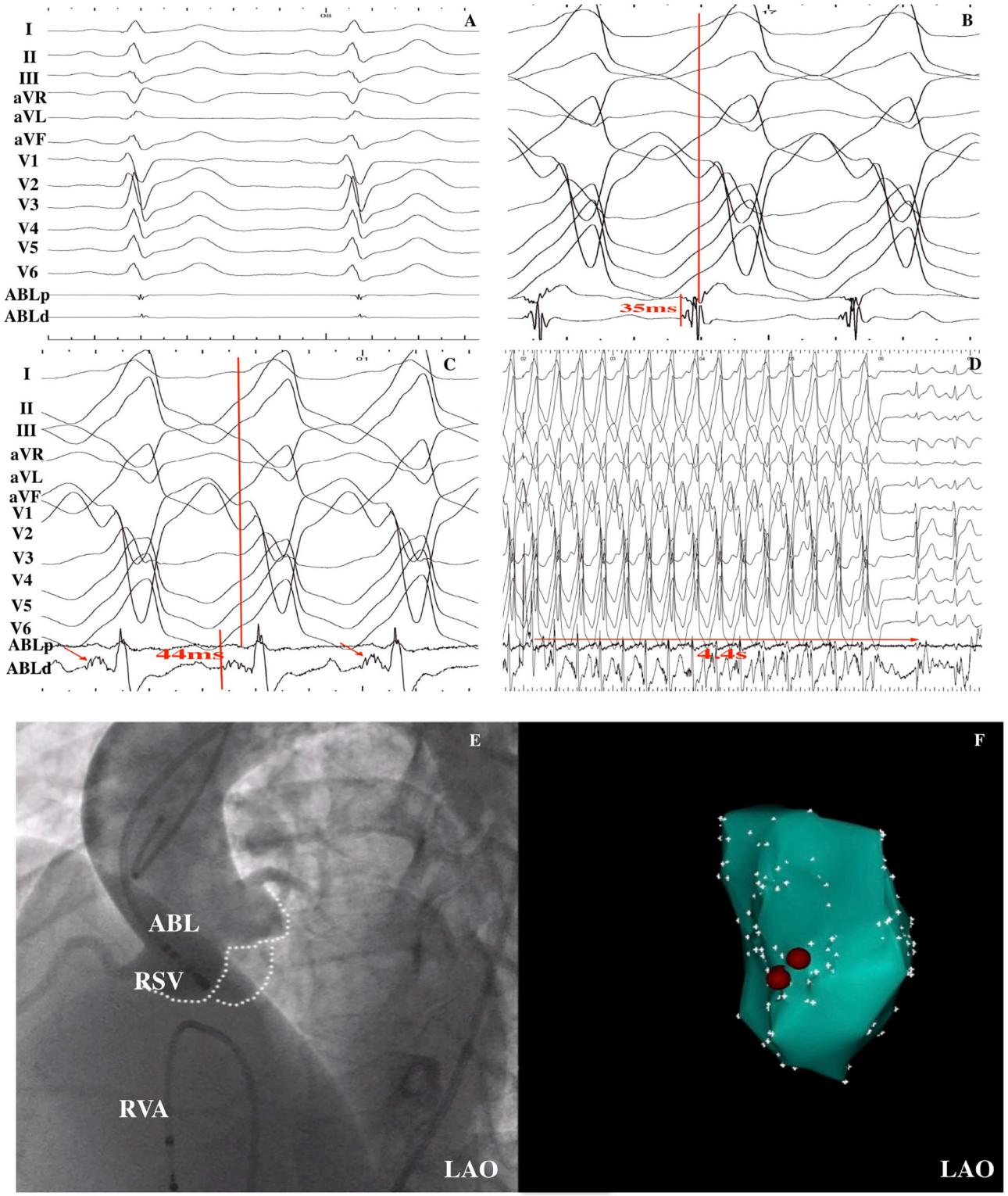

FIGURE 3 | VT was successfully ablated within the RSV in a 15-year-old male patient. **(A)** Baseline 12-lead ECG was shown; **(B)** An early ventricular activation preceded by QRS by 35 ms during the VT was recorded at the RVOT, but ablation was ineffective. **(C)** Fragmented potential (red arrow) was found at the RSV, and the interval from the potential to QRS onset was 44 ms. **(D)** After RF energy delivery, VT was terminated after 4.4 s. **(E)** LAO fluoroscopic view of the mapping catheter at the successful ablation site as demonstrated by aortic artery angiography. **(F)** Electroanatomical CARTO map of the VT in the LAO view. Red points indicate ablation points. RSV, right sinus of Valsalva; RF, radiofrequency ablation; VT, ventricular tachycardia; LAO, left anterior oblique; ABL, ablation catheter; RVA, right ventricular apex.

TABLE 1 | Baseline clinical characteristics in patients with and without DPP.

	DPP+ ($n = 67$)	DPP− ($n = 38$)	p-value
Age (years)	37.6 ± 17.3	52.2 ± 12.8	<0.001
Male	42 (62.7%)	16 (42.1%)	0.042
LVEF (%)	60.4 ± 7.5	61.3 ± 6.8	0.828
PVC burden on 24-h Holter monitoring	30,754 ± 14,740	28,466 ± 13,575	0.456
Clinical arrhythmias			0.01
Frequent PVCs	53 (79.1%)	37 (97.4%)	
Non-sustained or sustained VT	14 (20.9%)	1 (2.6%)	
Number of failed AADs	0.9 ± 0.8	1.2 ± 0.7	0.098
Structural heart disease	0	0	-

Values are described as mean ± SD or n.
DPP, discrete pre-potential; LVEF, left ventricular ejection fraction; PVC, premature ventricular contraction; VT, ventricular tachycardia; AAD, antiarrhythmic drug.

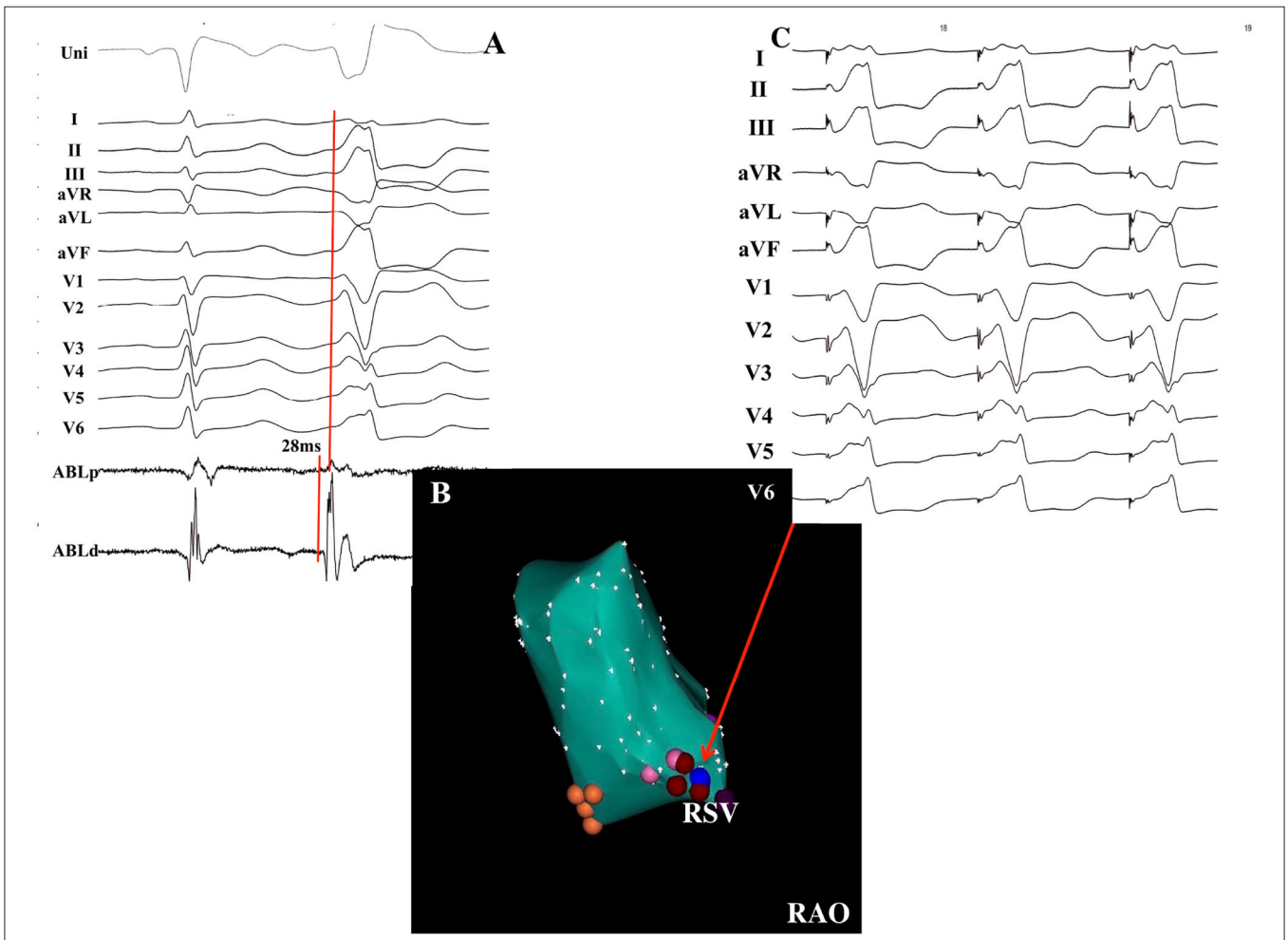

FIGURE 4 | Successful ablation of PVCs without DPPs in a 63-year-old female patient. **(A)** The earliest activation recorded at the RSV preceded the QRS complex onset by 28 ms without DPPs. **(B)** Electroanatomical CARTO map of the PVCs in the RAO view. Red points indicate the ablation points. Blue point indicates the pacing site. Orange points indicate the non-coronary sinus of Valsalva. **(C)** Pacing mapping was excellent when pacing was delivered at the ablation site. RSV, right sinus of Valsalva; DPP, discrete pre-potential; RAO, right anterior oblique.

(**Figure 4**). In addition, patients with DPPs were more likely to have non-sustained or sustained VT rather than single PVC (20.9 vs. 2.6%, $p = 0.01$).

ECG Characteristics

The VA ECG characteristics are summarized in **Table 2**. Patients with DPPs had wider QRS (152 ± 17 vs. 145 ±14 ms, $p < 0.001$).

TABLE 2 | ECG parameters during the VAs between patients with and without DPP.

	DPP+ ($n = 67$)	DPP− ($n = 38$)	p-value
QRS duration (ms)	152 ± 17	145 ± 14	0.019
R-wave amplitude in lead I (mV)	0.20 ± 0.25	0.15 ± 0.15	0.248
R-wave amplitude in lead II (mV)	1.82 ± 0.47	1.63 ± 0.37	0.105
R-wave amplitude in lead III (mV)	1.77 ± 0.61	1.63 ± 0.37	0.194
R-wave amplitude in lead aVF (mV)	1.79 ± 0.54	1.62 ± 0.31	0.117
R-wave ratio in lead II/III	1.10 ± 0.37	1.02 ± 0.17	0.260
Q-wave amplitude in lead aVL (mV)	0.86 ± 0.40	0.80 ± 0.29	0.361
Q-wave amplitude in lead aVR (mV)	0.94 ± 0.26	0.81 ± 0.16	<0.001
Q-wave ratio in lead aVL/aVR	0.96 ± 0.46	1.02 ± 0.39	0.496
R-wave amplitude in lead V_1 (mV)	0.45 ± 0.32	0.39 ± 0.27	0.285
S-wave amplitude in lead V_1 (mV)	1.03 ± 0.55	0.57 ± 0.40	<0.001
R-wave amplitude in lead V_2 (mV)	0.91 ± 0.48	0.97 ± 0.51	0.478
S-wave amplitude in lead V_2 (mV)	1.47 ± 0.91	0.90 ± 0.58	<0.001
R-wave amplitude in lead V_3 (mV)	1.41 ± 0.65	1.65 ± 0.74	0.056
Precordial TZ index	−0.53	−1.22	0.005

Values are displayed as mean ± SD.
DPP, discrete pre-potential; TZ, transitional zone.

TABLE 3 | Electrophysiological characteristics during the VAs between patients with and without DPP.

	DPP+ ($n = 67$)	DPP− ($n = 38$)	p-value
Mean activation time (ms)	−38.6 ± 8.5	−27.7 ± 5.7	<0.001
Mean time from the first RF lesion to the elimination of VAs (s)	2.3 ± 2.1	4.9 ± 1.0	<0.001
Total Number of RF application	2.1 ± 1.0	2.7 ± 0.9	<0.001
Initial mapping of right side	33 (49.3%)	12 (31.6%)	0.101

Values are demonstrated as mean ± SD or n.
DPP, discrete pre-potential; RF, radiofrequency; VA, ventricular arrhythmia.

Q-wave amplitude in lead aVR was greater in patients with DPPs (0.94 ± 0.25 vs. 0.81 ± 0.16 mV, $p < 0.001$). S-wave amplitude in leads V_1 and V_2 was greater in patients with DPPs (1.03 ± 0.55 vs. 0.57 ± 0.40 mV, $p < 0.001$; 1.47 ± 0.91 vs. 0.90 ± 0.58 mV, $p < 0.001$, respectively). The TZ index was larger in patients with DPPs compared with those without DPPs (−0.53 vs. −1.22, $p = 0.005$).

Electrophysiological Characteristics

Detailed mapping of the ASVs was performed in all patients. The average of the earliest activation time was significantly earlier in patients with DPPs than in those without DPPs (−38.6 ± 8.5 vs. −27.7 ± 5.7 ms, $p < 0.001$). RVOT mapping was initially performed in 33 (49.3%) patients with DPPs and 12 (31.6%) patients without DPPs ($p = 0.101$). The mean time from the first RF lesion to the elimination of VAs was shorter in patients with DPPs than in those without DPPs (2.3 ± 2.1 vs. 4.9 ± 1.0 s, $p < 0.001$). The total number of RF applications in patients with DPPs was significantly less than in those without DPPs (2.1 ± 1.0 vs. 2.7 ± 0.9, $p < 0.001$) (**Table 3**).

Predictors of DPP

A stepwise logistic multivariable analysis identified only the age as a significant predictor of a DPP (OR 1.61; 95% confidence interval 1.03–2.74; $p < 0.001$). On the basis of ROC curve analysis, an age of ≤ 35.5 years produced an AUC of 0.731 with a sensitivity of 44.3% and specificity of 93.3%, with a 92.9% of positive predictive value and a 46.7% of negative predictive value (**Figure 5**).

Complications and Follow-Up

There were three peripheral vascular complications including two patients with pseudoaneurysm and one with arteriovenous fistula. There were no other major complications, including no coronary arterial damage or aortic valve injury in any patients. Over a total follow-up duration of 42.5 ± 22.3 months, 63 (94.0%) patients with DPPs and 30 (78.9%) patients without DPPs remained free of recurrent VAs in the absence of antiarrhythmic drugs. There was a significant difference in recurrent rate between patients with and without DPPs (6.0 vs. 21.1%, $p = 0.027$). Of these patients, Seven of 12 patients received repeat ablation. Successful ablation was achieved in the same location in two patients with DPPs. However, in the other five patients without DPPs, the distribution of ablation sites was as follows: RVOT in three patients, aorto-mitral continuity (AMC) in one patient, and below RSV-LSV commissure in one patient. Repeat ablation was successful in these five patients.

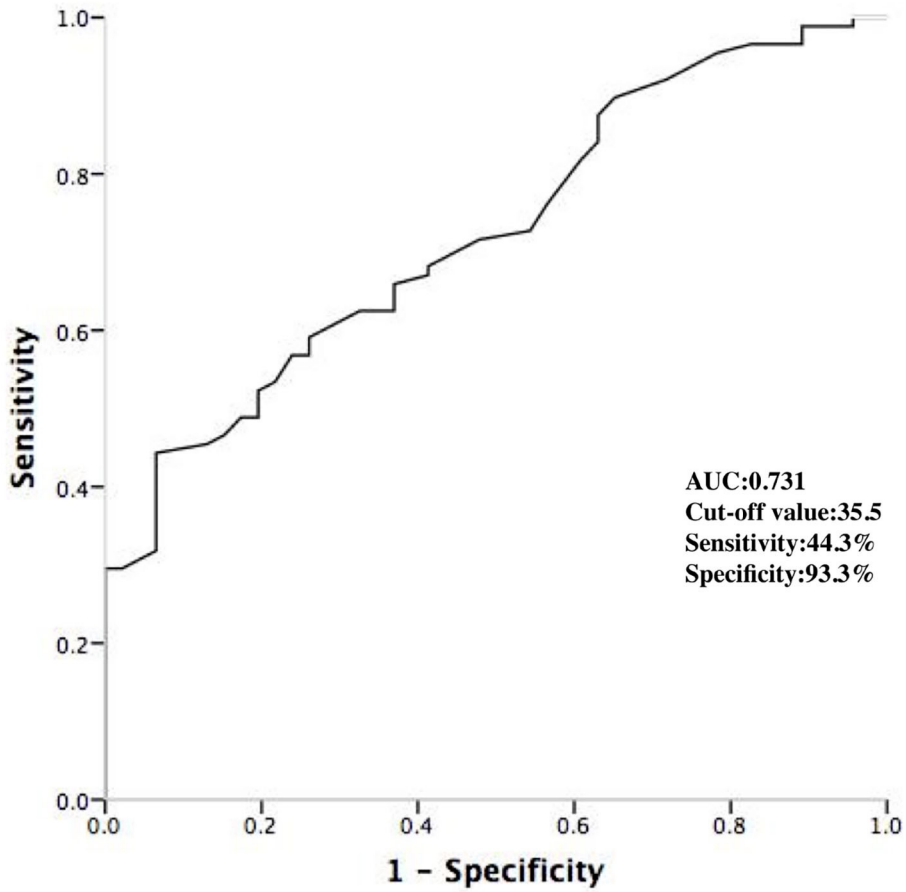

FIGURE 5 | ROC curve analyzing the age to predict the DPPs. DPP, discrete pre-potential; AUC, area under curve.

DISCUSSION

Major Findings

To the best of our knowledge, this is the first study to investigate the predictors of DPPs of VAs originating from the ASV. In this study, we found that (1) a DPP can be recorded in 63.8% of the patients whose successful ablation site locates in the LSV or RSV; (2) RF ablation in patients with DPPs was associated with a higher long-term success rate compared with those without DPPs; (3) the age is the only independent predictor of DPPs; and (4) the age $\leq$ 35.5 years can predict the presence of DPPs with a 92.9% of positive predictive value.

Presence of DPP

Previous studies have reported that extensions of the left ventricular myocardium frequently exist within the ASV (9–11). The fibrosis and fatty tissue among these muscular sleeves may create a possible VA substrate (11). The presence of DPPs of VAs originating from the ASV has been described in previous studies and considered to be useful in guiding ablation within the ASV (4–6). There has been a wide range in prevalence of DPPs during ASV and outflow tract VA ablation, ranging from 10% of all outflow tract VA ablations, 26% of all ASV ablations, and up to 100% of patients with ASV in a study by Ouyang et al. (4–6). In this study, DPPs were recorded in 67 (63.8%) of 105 patients in whom ablation from the ASV was successful in eliminating the VA. Non-sustained or sustained VT was commonly seen in the patients with DPPs, which is consistent with Ouyang's study. We surmise that the DPPs may be responsible for triggering the VA, similar to that observed from superior vena cava and pulmonary vein in patients with atrial fibrillation (12, 13). The low incidence of DPPs reported in previous studies may be due to decreased recognition of the low-amplitude DPP in some patients. The scale of the electrogram recorded in the ablation catheter should be magnified during the mapping within the ASV. In addition, small sample sizes may account for the low prevalence of the DPP.

ECG Characteristics

Few studies have described the ECG characteristics of DPPs of VAs originating from the ASV. Hachiya et al. (4) reported nine of 35 patients with DPPs and no specific ECG findings were found. In this study, using quantitative ECG analysis, several unique ECG characteristics were found in patients with DPPs. The patients with DPPs were associated with

wider QRS. Q-wave amplitude in lead aVR was greater in patients with DPPs. S-wave amplitude in leads V_1 and V_2 were greater in patients with DPPs. In addition, the TZ index was larger in patients with DPPs compared with those without DPPs. The extra-ventricular myocardium extensions may be responsible for these unique ECG characteristics. These myocardial extensions were asymmetrical, with sleeves routinely found along anterior portions of the RSV and LSV (14), which might produce a vector from anterior to posterior. This activation manner results in the terminal S-wave in leads V_1 and V_2.

Predictors of DPP

The DPPs have been considered to be an indicator of successful ablation site within the ASV (4, 6). As Ouyang reported, two ventricular activation components were always recorded at the successful site in patients with VT originating from the ASV (6). In Ouyang's study, the mean age of the patients was 36.6 years. In this study, we found that the age was the independent predictor of DPPs. An age of $\leq$ 35.5 years produced an AUC of 0.731 with a sensitivity of 44.3% and specificity of 93.3%, with a high-positive predictive value, which was consistent with Ouyang's study. Younger patients were more likely to have a DPP, which might be explained by the fact that degenerative fibrosis of the myocardial extensions may occur over time with advancing age (15).

Long-Term Clinical Outcome

Several investigators have demonstrated the favorable outcome in small series of patients with DPPs of VAs originating from the ASV (4–6). In this study, during a follow-up period of 42.5 $\pm$ 22.3 months, 94% of patients with DPPs remained free of recurrent VAs. However, a higher recurrent rate was observed in patients without DPPs. This may further prove that the DPPs represent the myocardial origin of VAs, and the presence of DPPs may help to identify successful ablation sites and improve long-term success. In some cases without DPPs, although successful ablation was initially achieved in ASC, the true arrhythmia origin may not be located in ASC due to the complexity of LVOT anatomy. The larger part of the RSV and the commissure between RSV and LSV are related to the interventricular septum which forms part of the subaortic valvular region and the RVOT septal wall. Similarly, the LSV is in close relationship with the LV summit, the interventricular vein, and the AMC (16). In our study, five patients without DPPs received repeat procedures. The final ablation sites were RVOT in three patients, AMC in one patient, and below RSV-LSV commissure in one patient. Therefore, careful mapping of all the neighbor structures around the ASC may be needed in some patients without DPPs undergoing the first procedure to reduce the recurrent rate.

Study Limitations

This was a retrospective single-center study with a limited sample size. First, pace mapping was not routinely performed in all patients. Second, VAs from RSV-LSV junction were also defined as RSV or LSV-VAs and were not analyzed separately in this study. Furthermore, no non-sinus Valsalva cases were included because only four cases were found in our study, and the value of statistical analysis in such a small case series might be questioned. Third, although successful ablation was achieved within ASV in all cases, the real arrhythmia origin still could not be 100% sure. Final successful ablation in the ASV could not necessarily mean that the VAs originated from this spot. Furthermore, intracardiac echocardiography was not available in all patients due to the cost.

CONCLUSION

Discrete pre-potentials were observed in 63.8% of the patients in whom VAs were successfully eliminated with ablation from the ASV region. Ablation in patients with DPPs was associated with higher long-term success. Younger age independently predicted the DPPs. A cutoff of 35.5 years of age indicated the presence of the DPPs with a 92.9% of positive predictive value.

DATA AVAILABILITY STATEMENT

The raw data supporting the conclusions of this article will be made available by the authors, without undue reservation.

ETHICS STATEMENT

The studies involving human participants were reviewed and approved by Institutional Review Board of Fuwai Hospital. The patients/participants provided their written informed consent to participate in this study. Written informed consent was obtained from the individual(s) for the publication of any potentially identifiable images or data included in this article.

AUTHOR CONTRIBUTIONS

All authors listed have made a substantial, direct, and intellectual contribution to the work and approved it for publication.

FUNDING

This study was supported by a grant from the National Natural Science Foundation of China (#81670309).

REFERENCES

1. Calkins H, Kalbfleisch SJ, el-Atassi R, Langberg JJ, Morady F. Relation between efficacy of radiofrequency catheter ablation and site of origin of idiopathic ventricular tachycardia. *Am J Cardiol.* (1993) 71:827–33. doi: 10.1016/0002-9149(93)90832-W
2. Morady F, Kadish AH, DiCarlo L, Kou WH, Winston S, deBuitlier M, et al. Long-term results of catheter ablation of idiopathic right ventricular tachycardia. *Circulation.* (1990) 82:2093–9. doi: 10.1161/01.CIR.82.6.2093
3. Tsai CF, Chen SA, Tai CT, Chiang CE, Lee SH, Wen ZC, et al. Idiopathic monomorphic ventricular tachycardia: Clinical outcome, electrophysiologic

characteristics and long-term results of catheter ablation. *Int J Cardiol.* (1997) 62:143–50. doi: 10.1016/S0167-5273(97)00198-8
4. Hachiya H, Yamauchi Y, Iesaka Y, Yagishita A, Sasaki T, Higuchi K, et al. Discrete prepotential as an indicator of successful ablation in patients with coronary cusp ventricular arrhythmia. *Circ Arrhythm Electrophysiol.* (2013) 6:898–904. doi: 10.1161/CIRCEP.113.000157
5. Srivathsan KS, Bunch TJ, Asirvatham SJ, Edwards WD, Friedman PA, Munger TM, et al. Mechanisms and utility of discrete great arterial potentials in the ablation of outflow tract ventricular arrhythmias. *Circ Arrhythm Electrophysiol.* (2008) 1:30–8. doi: 10.1161/CIRCEP.107.750315
6. Ouyang F, Fotuhi P, Ho SY, Hebe J, Volkmer M, Goya M, et al. Repetitive monomorphic ventricular tachycardia originating from the aortic sinus cusp: Electrocardiographic characterization for guiding catheter ablation. *J Am Coll Cardiol.* (2002) 39:500–8 doi: 10.1016/S0735-1097(01)01767-3
7. Yoshida N, Inden Y, Uchikawa T, Kamiya H, Kitamura K, Shimano M, et al. Novel transitional zone index allows more accurate differentiation between idiopathic right ventricular outflow tract and aortic sinus cusp ventricular arrhythmias. *Heart Rhythm.* (2011) 8:349–56. doi: 10.1016/j.hrthm.2010.11.023
8. Wei HQ, Guo XG, Liu X, Zhou GB, Sun Q, Yang JD, et al. Safety and efficacy of catheter ablation of ventricular arrhythmias with para-hisian origin via a systematic direct approach from the aortic sinus cusp. *Heart Rhythm.* (2018) 15:1626–33. doi: 10.1016/j.hrthm.2018.05.021
9. Ho SY. Structure and anatomy of the aortic root. *Eur J Echocardiogr.* (2009) 10:i3–10. doi: 10.1093/ejechocard/jen243
10. Gami AS, Noheria A, Lachman N, Edwards WD, Friedman PA, Talreja D, et al. Anatomical correlates relevant to ablation above the semilunar valves for the cardiac electrophysiologist: A study of 603 hearts. *J Interv Card Electrophysiol.* (2011) 30:5–15. doi: 10.1007/s10840-010-9523-3
11. Hasdemir C, Aktas S, Govsa F, Aktas EO, Kocak A, Bozkaya YT, et al. Demonstration of ventricular myocardial extensions into the pulmonary artery and aorta beyond the ventriculo-arterial junction. *Pacing Clin Electrophysiol.* (2007) 30:534–9. doi: 10.1111/j.1540-8159.2007.00704.x
12. Haissaguerre M, Jais P, Shah DC, Takahashi A, Hocini M, Quiniou G, et al. Spontaneous initiation of atrial fibrillation by ectopic beats originating in the pulmonary veins. *N Engl J Med.* (1998) 339:659–66. doi: 10.1056/NEJM199809033391003
13. Lin WS, Tai CT, Hsieh MH, Tsai CF, Lin YK, Tsao HM, et al. Catheter ablation of paroxysmal atrial fibrillation initiated by non-pulmonary vein ectopy. *Circulation.* (2003) 107:3176–83. doi: 10.1161/01.CIR.0000074206.52056.2D
14. Tabatabaei N, Asirvatham SJ. Supravalvular arrhythmia: Identifying and ablating the substrate. *Circ Arrhythm Electrophysiol.* (2009) 2:316–26. doi: 10.1161/CIRCEP.108.847962
15. Sahasakul Y, Edwards WD, Naessens JM, Tajik AJ. Age-related changes in aortic and mitral valve thickness: Implications for two-dimensional echocardiography based on an autopsy study of 200 normal human hearts. *Am J Cardiol.* (1988) 62:424–30. doi: 10.1016/0002-9149(88)90971-X
16. Di Biase L, Romero J, Zado ES, Diaz JC, Gianni C, Hranitzki PM, et al. Variant of ventricular outflow tract ventricular arrhythmias requiring ablation from multiple sites: Intramural origin. *Heart Rhythm.* (2019) 16:724–32. doi: 10.1016/j.hrthm.2018.11.028

Conflict of Interest: The authors declare that the research was conducted in the absence of any commercial or financial relationships that could be construed as a potential conflict of interest.

frontiers in Cardiovascular Medicine

ORIGINAL RESEARCH
published: 20 December 2021
doi: 10.3389/fcvm.2021.778866

Idiopathic Ventricular Arrhythmias Ablated in Different Subregions of the Aortic Sinuses of Valsalva: Anatomical Distribution, Precordial Electrocardiographic Notch Patterns, and Bipolar Electrographic Characteristics

Sixian Weng[1†], *Zhengqin Zhai*[1,2†], *Min Tang*[1*], *Bin Zhou*[1], *Lei Ding*[1], *Fengyuan Yu*[1], *Yingjie Qi*[1], *Hongda Zhang*[1], *Tianjie Feng*[1] *and Shu Zhang*[1]

[1] State Key Laboratory of Cardiovascular Disease, Department of Cardiology, Cardiovascular Institute, Fuwai Hospital, National Center for Cardiovascular Diseases, Chinese Academy of Medical Sciences and Peking Union Medical College, Beijing, China, [2] China-Japan Friendship Hospital, Beijing, China

Background: Little is known about the differences among ventricular arrhythmias (VAs) ablated in different subregions of the aortic sinuses of Valsalva (ASVs). We aim to investigate the distribution, precordial electrocardiographic patterns, and bipolar electrogram characteristics of VAs ablated in different subregions of the ASVs.

Methods: We divided the right ASV and the left ASV into a total of 6 subregions and studied 51 idiopathic VAs ablated first time successfully in the ASVs.

Results: These 51 VAs were inhomogeneously distributed among the 6 subregions, which comprised the right-lateral ASV (1/51), the right-anterior ASV (11/51), the regions along the right (13/51) and left (9/51) sides of the ASV junction, the left-anterior ASV (5/51), and the left-lateral ASV (12/51). Fractionated potentials were dominant (39/51, 76%) among the 3 types of target electrograms. From the right-lateral ASV to the left-lateral ASV, the percentage of fractionated potentials gradually decreased from 100 to 59%. A precordial rebound notch in V3-V4 or V4-V5 had sensitivity of 90.9%, specificity of 85.0%, and negative predictive value (NPV) of 97.1% to predict VAs ablated in the right-anterior ASV. A precordial rebound notch in V2-V3 had sensitivity of 50.0%, specificity of 94.9%, and NPV of 86.0% to predict VAs ablated in the left-lateral ASV.

Conclusion: VA targets were mainly distributed in the anterior and the left-lateral ASVs. Fractionated potentials were common among target electrograms, especially in theright-anterolateral ASV. Precordial electrocardiographic rebound notch has high predictive accuracy in identifying different subregions of the ASVs as target ablation sites.

Keywords: ventricular arrhythmias, aortic sinuses of Valsalva, bipolar electrogram, target distribution, precordial notch, radiofrequency catheter ablation

OPEN ACCESS

Edited by:
Feifan Ouyang,
University Medical Center Hamburg-Eppendorf, Germany

Reviewed by:
Yangjing Xue,
Wenzhou Medical University, China
Ardan Muammer Saguner,
University Hospital Zürich, Switzerland

***Correspondence:**
Min Tang
doctortangmin@yeah.net

†These authors have contributed equally to this work

Specialty section:
This article was submitted to Cardiac Rhythmology, a section of the journal Frontiers in Cardiovascular Medicine

Received: *17 September 2021*
Accepted: *22 November 2021*
Published: *20 December 2021*

Citation:
Weng S, Zhai Z, Tang M, Zhou B, Ding L, Yu F, Qi Y, Zhang H, Feng T and Zhang S (2021) Idiopathic Ventricular Arrhythmias Ablated in Different Subregions of the Aortic Sinuses of Valsalva: Anatomical Distribution, Precordial Electrocardiographic Notch Patterns, and Bipolar Electrographic Characteristics. Front. Cardiovasc. Med. 8:778866. doi: 10.3389/fcvm.2021.778866

INTRODUCTION

Idiopathic ventricular arrhythmias (VAs) with the electrocardiographic inferior axis frequently originate from the aortic sinuses of Valsalva (ASVs) (1, 2). Compared to VAs originating from the right ventricular outflow tract (RVOT), mapping and ablation are usually challenging for VAs from the ASV (ASV-VAs) due to the complicated anatomical construction of the ASVs, confusion of ECG locations, and the difficulty of confirming target electrograms. Thus, a lower radiofrequency catheter ablation (RFCA) success rate was observed for ASV-VAs than for VAs originating from the RVOT. Previous studies have described the electrocardiographic or electrophysiological characteristics of VAs from the left ASV (3), the right ASV (4), and the left-right commissure (5, 6), while little is known about the distributions of VAs in the subregions of the ASVs. In this study, we further divided the left and right ASVs into 6 subregions, with the aim of investigating the target distribution, the specific precordial electrocardiographic patterns, and the bipolar electrographic characteristics of VAs ablated in different subregions.

METHODS

Study Population

This single-center retrospective study enrolled 65 consecutive patients with inferior axis deviation and monomorphic VAs who had no RFCA history and were referred for a first acute successful RFCA in the ASVs from September 2016 to September 2020 in the Department of Cardiology, Fuwai Hospital. The exclusion criteria were as follows: (1) structural heart disease was diagnosed before RFCA and (2) VAs with the same ECG morphology that had been ablated in the 1st procedure recurred during a follow-period of at least 6 months. The clinical data that were analyzed in the study included baseline characteristics, standard 12-lead ECGs, intracardiac electrograms, 3-dimensional electroanatomic mapping data, imaging information, and follow-up outcomes. This study was approved by the Ethics Committee of Fuwai Hospital (approval no. 2021-1523), Chinese Academy of Medical Sciences, and followed the Declaration of Helsinki. A written informed consent was obtained from all the patients.

Three-Dimensional Mapping and RFCA

After discontinuing antiarrhythmic drugs for at least 5 half-lives and completing preoperative examinations, patients underwent mapping and RFCA procedures. We obtained the 12-lead ECGs (bandpass filter: 0.05–100 Hz) and intracardiac electrograms (bandpass filter: bipolar 30–500 Hz; unipolar 0.1–500 Hz) from a multichannel electrophysiology recorder (Bard Electrophysiology, Lowell, Massachusetts, USA). Activation mapping was performed using a 3-dimensional electroanatomic mapping system (CARTO3, Biosense Webster Incorporation, Diamond Bar, California, USA) with an irrigated catheter (NaviStar ThermoCool, Biosense Webster Incorporation, Diamond Bar, California, USA) or contact force catheter (Thermocool SmartTouch, Biosense Webster Incorporation, Diamond Bar, California, USA). The mapping catheter was advanced via an SL1 or SR0 long sheath, if necessary. Heparin was administered after accessing the femoral artery and was used to maintain an activated clotting time of 200–250 s. For patients with a transitional zone index (7) ≥ -0.5, we performed 3-dimensional mapping in the RVOT first; those with a transitional zone index < -0.5 underwent direct mapping in the ASVs by a transaortic approach. Electroanatomic maps were constructed via fast anatomic mapping, point-by-point mapping, or intracardiac echocardiography (ICE) reconstruction (Soundstar, Biosense Webster Incorporation, Diamond Bar, California, USA). An ideal target for ablation was based on 3 criteria: (1) the earliest activated site during mapping ($\geq$20 ms earlier than the QRS onset of VAs); (2) a synchronized onset of distal bipolar and unipolar (QS shape) electrogram; and (3) if possible, a pace mapping (match $\geq$ 95%) was performed to confirm the final target if the earliest activated site was unclear or showed little difference (<5 ms) from other sites. Before ablation, we used selective coronary angiography (using a pigtail catheter or irrigated catheter) or an ICE image to confirm that the distance between the target and the coronary ostia was greater than 5 mm. RFCA was delivered with a maximum power of 35 W and a maximum temperature of 55°C (irrigated flow rate: 2 ml/min) for up to 60–90 s. An effective RFCA was defined as reduction, disappearance, or acceleration with the same ECG morphology of VAs within the 1st 10 s. If RFCA did not influence VAs, it was discontinued and the catheter was repositioned. The endpoint for RFCA consisted of the disappearance of VAs for at least 20 min and the non-inducibility of VAs during isoproterenol infusion and/or programmed stimulation.

Subregions of the ASV

To determine the differences of VAs in electrocardiographic/electrophysiological characteristics from different regions in the ASVs, we further divided the right and left ASVs into 6 subregions (**Figure 1**): (1) Right-lateral ASV: the lateral and posterior portions of the right ASV, usually located behind the right coronary ostium; (2) Right-anterior ASV: the anterior portion (center section) of the right ASV, which contained the nadir of the semilunar hinges, usually located between the right coronary ostium and the adjacent left-right commissure; (3) Right side adjacent to the left-right commissure; (4) Left side adjacent to the left-right commissure; (5) Left-anterior ASV: the anterior portion (center section) of the left ASV, which contained the nadir of the semilunar hinges, usually located between the left coronary ostium and the adjacent left-right commissure; and (6) Left-lateral ASV: the lateral and posterior portions of the left ASV, usually located behind the left coronary ostium. The location of different subregions was based on 3-dimensional maps and imaging confirmation (ICE and/or angiography).

Analysis of ECG and Intracardiac Electrograms

A notch was defined as an extra deflection (not in initiation and termination) in downstroke or upstroke. A precordial electrocardiographic rebound notch of VAs was defined as a downstroke notch on the earlier lead followed by an upstroke

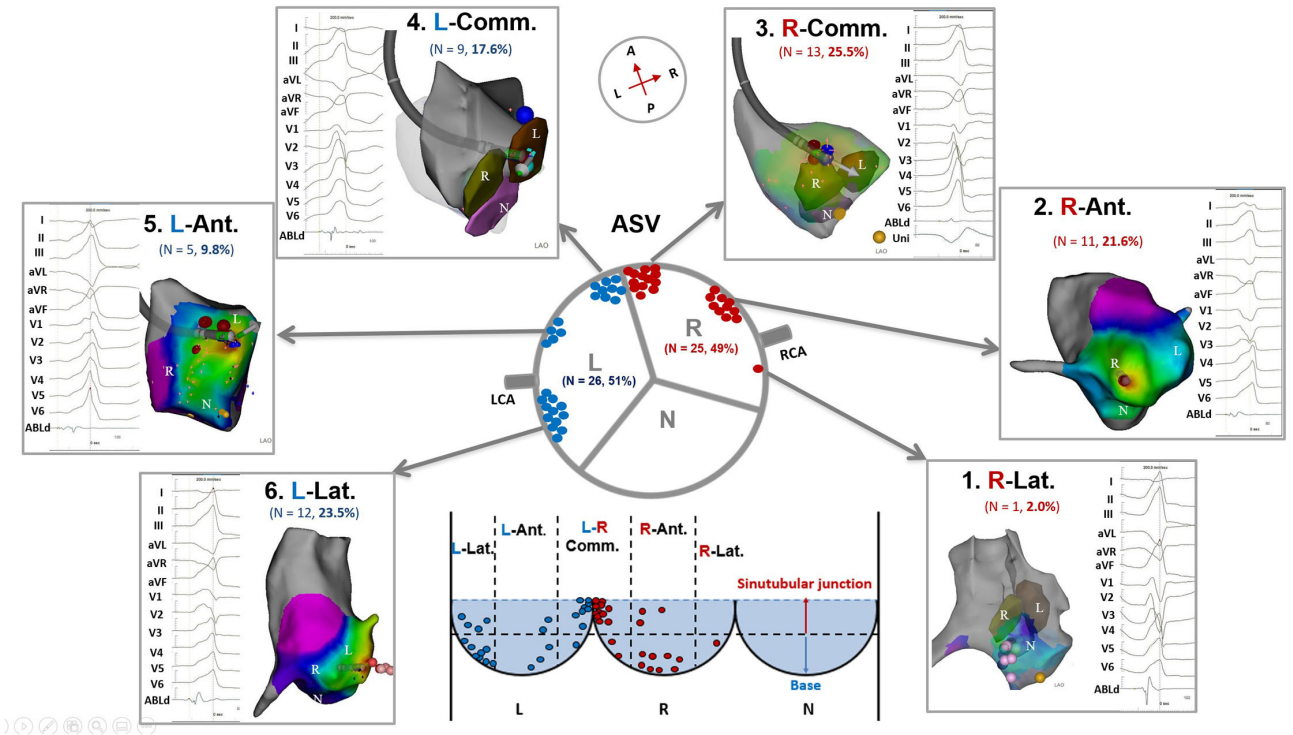

FIGURE 1 | Anatomic distributions of ventricular arrhythmias ablated in the ASVs. ASV, aortic sinus of Valsalva; N, non-coronary ASV; L, left ASV; R, right ASV; RCA, right coronary artery; LCA, left coronary artery; R-Lat., right-lateral ASV; R-Ant., right-anterior ASV; R-Comm., right side adjacent to the left-right commissure; L-Comm., left side adjacent to the left-right commissure; L-Ant., left-anterior ASV; L-Lat., left-lateral ASV.

notch on a later lead (**Figure 2**); this feature can also be quantified as the difference of peak R-wave deflection interval (from the earliest QRS onset to the peak R-wave deflection) (8) between the adjacent precordial leads (**Figure 3**). Data from the bipolar electrograms of the target in different ASV subregions were focused on amplitude, duration, and earliest activation. The bipolar electrogram characteristics of the target were reflected in the deflection and potential elements (**Figure 4**).

Follow-Up

All the patients underwent a 12-lead ECG and 24-h Holter monitoring on the same day, 1 month, 3 months, 6 months, and 12 months after the procedure. Meanwhile, outpatient or telehealth visits were performed when patients experienced clinical symptoms such as palpitation. Recurrence was defined as a clinical VA (same ECG morphology) burden $\geq$ 2% in 24-h Holter monitoring.

Statistical Analysis

Continuous variables are expressed as the mean $\pm$ SD (normal distribution) or median with interquartile range (non-normal distribution), while categorical variables are described as numbers or percentages. Continuous variables were compared using the one-way ANOVA (normal distribution) or the Mann–Whitney *U* test (abnormal distribution). Categorical variables were compared using the chi-squared test. The Bonferroni correction was applied to multiple comparisons among the different subregions. A box-and-whisker graph and the receiver operating characteristic curve were used to obtain the best diagnostic values. A two-sided p-value < 0.05 was considered as statistically significant. Data analysis was performed using the SPSS version 21 (IBM Corporation, Armonk, New York, USA). Graphs were obtained using the Prism version 8.0 (GraphPad Software Incorporation, La Jolla, California, USA).

RESULTS

Characteristics of the Patient

After excluding 14 patients (4 patients with structural heart disease and 10 patients with VA recurrence), a total of 51 patients with successfully ablated VAs in the ASVs were enrolled in this study. More than half of the patients were male. Most of them were middle aged (Q1–Q3, 39–59 years). All the patients presented with normal cardiac structure and function with the clinical symptoms of palpitation and/or presyncope before ablation. The details of the baseline characteristics are shown in **Table 1**.

Characteristics of Distribution and Bipolar Electrograms in Ablation Target

A total of 20 patients underwent remapping and reablation in the ASVs after failed attempts to find an ideal target and/or achieved

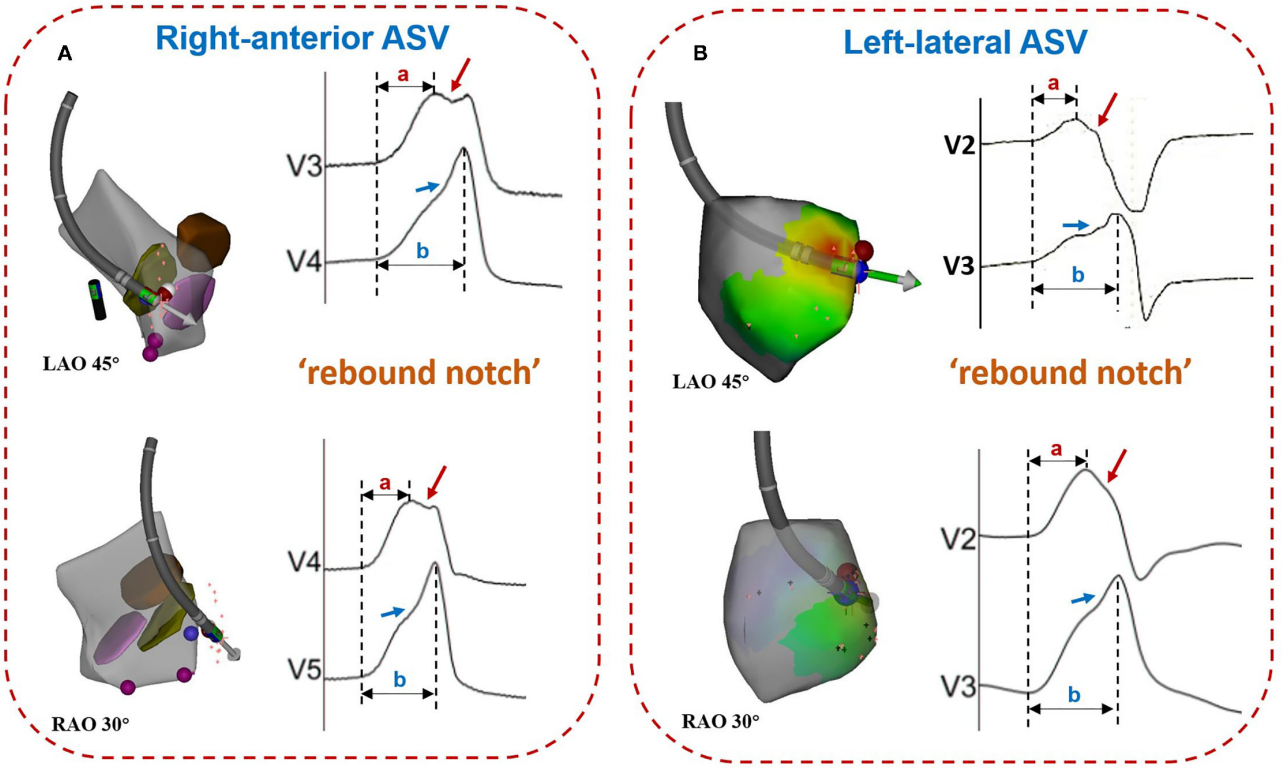

C

Rebound notch	Sensitivity (%)	Specificity (%)	PPV (%)	NPV (%)	P value
V3-4/4-5 (distinguish right-anterior ASV from others)	90.9	85.0	62.5	97.1	<.01
V2-3 (distinguish left-lateral ASV from others)	50.0	94.9	75.0	86.0	<.01

FIGURE 2 | Patterns of rebound notches on the precordial lead. **(A)** Left-sided (V3-V5) rebound notches (a downstroke notch on the earlier lead followed by an upstroke notch on a later lead; peak R-wave deflection interval: (a < b) is more common in ventricular arrhythmias ablated in the right-anterior ASV. **(B)** Right-sided (V2-V3) rebound notches are more common in ventricular arrhythmias ablated in the left-lateral ASV. **(C)** The accuracy of rebound notches in identifying ventricular arrhythmias originating from the right-anterior ASV and/or the left-lateral ASV. ASV, aortic sinus of Valsalva; PPV, positive predictive value; NPV, negative predictive value.

an effective RFCA (reduction, elimination, and morphology change of VAs) in the RVOT. All the VAs were eventually mapped and ablated successfully in the ASVs. Targets were most commonly (39/51, 76%) located in the anterior portion (in front of the coronary ostia) of the ASVs, which comprised the right-anterior ASV (11/51, 21.6%), the right side adjacent to the left-right commissure (13/51, 25.5%), the left side adjacent to the left-right commissure (9/51, 17.6%), and the left-anterior ASV (5/51, 9.8%). Only 1 VA was located in the right-lateral ASV, while 12 VAs (12/51, 23.5%) were located in the left-lateral ASV (**Figure 1**). The mean earliest activation on bipolar electrogram was 28 ms. As shown in **Table 2**, when compared to VAs in the left-right commissure, those in the left-anterior/lateral ASVs had lower amplitudes of the target bipolar electrogram (0.50–1.16 vs. 0.35–0.67, $p = 0.044$). A total of 3 kinds of target bipolar electrograms were found in this study including the single potential (6/51, 12%), the prepotential (6/51, 12%), and the fractionated potential (39/51, 76%). From the right-lateral ASV to the left-lateral ASV, the percentage of fractionated potential gradually decreased from 100 to 59% (**Figure 4** and **Supplementary Table 1**).

Electrocardiogram Characteristics of VAs Originating From Different Subregions of the ASV

A positive "R" wave in the initiation and termination of lead I was more common (91.7 vs. 40.9 vs. 11.8%, $p < 0.05$) in VAs from the right-anterior/lateral ASV than in those from other subregions. From the right-lateral ASV to the left-lateral

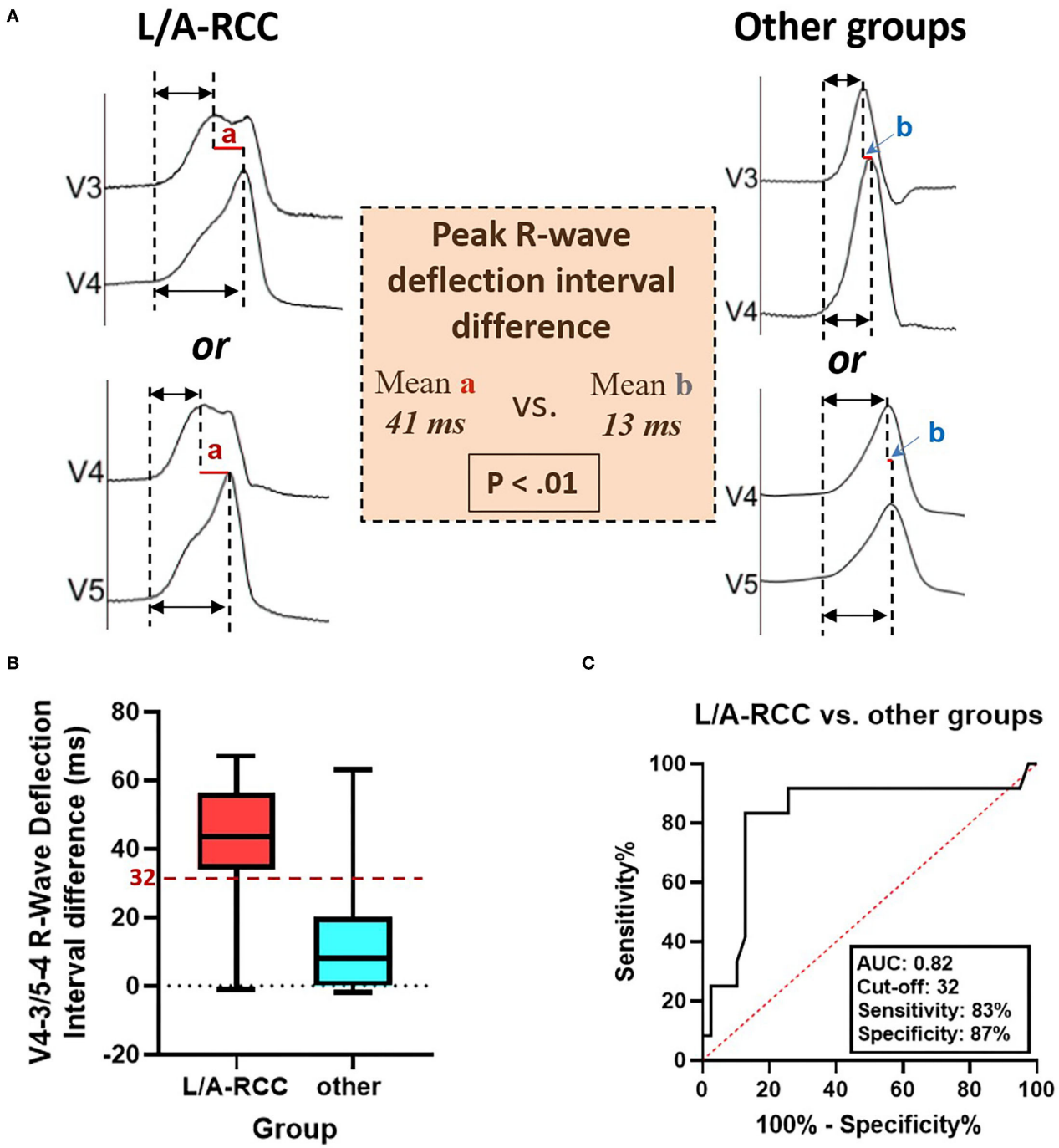

FIGURE 3 | The peak R-wave deflection interval difference between V4-V3 and V5-V4 during ventricular arrhythmias ablated in the ASVs. **(A)** The R-Ant./Lat. group had a longer peak R-wave deflection interval difference between V4-V3 and V5-V4 than other groups. **(B)** The box-and-whisker plots show the V4-V3 or V5-V4 peak R-wave deflection interval difference between R-Ant./Lat. and other groups. **(C)** The receiver operating characteristic analysis for peak R-wave deflection interval difference between V4-V3 and V5-V4 in patients with ventricular arrhythmias ablated in the ASVs. ASV, aortic sinus of Valsalva; R-Ant./Lat., right-lateral/anterior ASV; AUC, area under the curve.

ASV, the percentage of a negative "S/QS" in lead I increased gradually (8.3 vs. 13.6 vs. 52.9%, $p < 0.05$). More than 80% of VAs from the right-anterior/lateral ASV precordial transited ≥ V2. A precordial transition before V2 was most common in the left-right commissure and the left-anterior/lateral ASV (45.4 vs. 58.8%). A precordial electrocardiographic rebound notch was

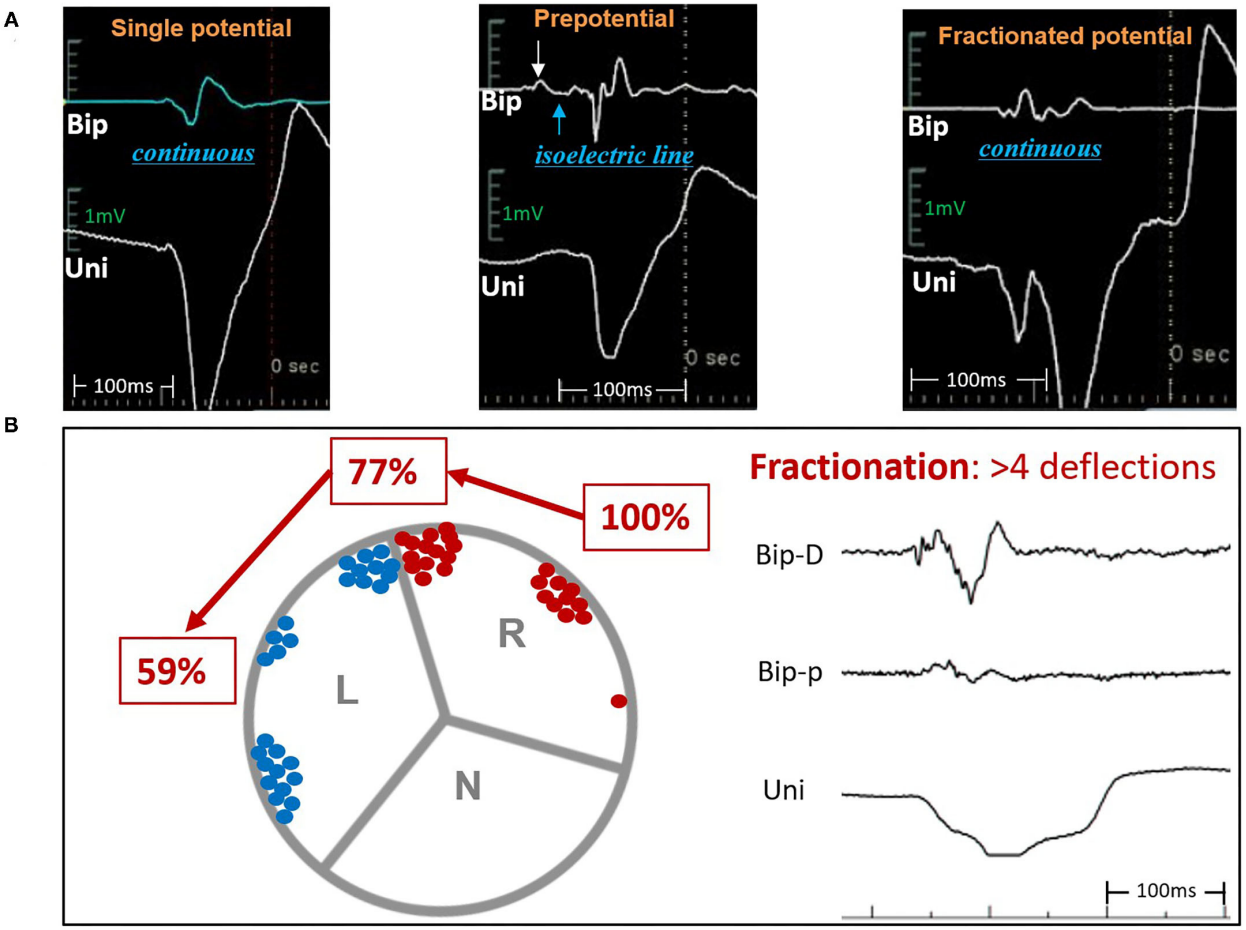

C

Target electrogram	R-Ant./Lat.	R-L Comm.	L-Ant./Lat.	Sum
Single potential	0	3	3	6
Prepotential	0	2	4	6
Fractionated potential	12 (100%)	17 (77%)	10 (59%)	39
Sum	12	22	17	51

FIGURE 4 | Distributions and characteristics of the target bipolar electrogram. **(A)** 3 types of target electrograms. **(B)** Distributions and **(C)** proportions of fractionated potentials. Bip, bipolar electrogram; Uni, unipolar electrogram; ASV, aortic sinus of Valsalva; N, non-coronary ASV; L, left ASV; R, right ASV; R-Ant./Lat., right-lateral/anterior ASV; R-L Comm., left-right commissure; L-Ant./Lat., left-lateral/anterior ASV.

more common in VAs from the right-anterior/lateral ASV (100 vs. 28.3 vs. 41.2%) than in those from the left-right commissure or the left-anterior/lateral ASV. The detailed ECG comparisons are shown in **Table 2**.

Diagnostic Value of Precordial Rebound Notch

A rebound notch in V3-V4 or V4-V5 (**Figure 5**) was observed in 91% (10/11) of VAs from the right-anterior ASV, while it was less likely to appear in other subregions (6/40, 15%). Among VAs ablated in the right and left ASV, a rebound notch in V3-V4 or V4-V5 had a sensitivity of 90.9%, a specificity of 85.0%, a positive predictive value (PPV) of 62.5%, and a negative predictive value (NPV) of 97.1% to predict VAs ablated in the right-anterior ASV (**Figure 2**). Meanwhile, the peak R-wave deflection interval difference between V4-V3 and V5-V4 during VAs was significant between the right-anterior/lateral ASV and other subregions (41 ± 19 vs. 13 ± 17, $p < 0.01$); a cutoff value of 32 ms (area under the curve, 0.82; CI, 0.67–0.98; $p < 0.01$) predicted an ablated target in the right-anterior/lateral

ASV with a sensitivity of 83.0% and a specificity of 87.0% (**Figure 3**).

A rebound notch in V2-V3 during VAs was more common in the left-lateral ASV (6/12; 50 vs. 5%, $p < 0.05$). Among VAs ablated in the right and left ASV, a rebound notch in V2-V3 had a sensitivity of 50.0%, a specificity of 94.9%, a PPV of 75.0%, and a NPV of 86.0% to predict VAs ablated in the left-lateral ASV (**Figure 2**). Meanwhile, the peak R-wave deflection interval difference between V3 and V2 during VAs seemed greater in the left-lateral ASV, but showed no significance when compared with other subregions (19 ± 16 vs. 12 ± 11, $p > 0.05$). A cutoff value of 31 ms had a sensitivity of 33.3% and a specificity of 92.3% to predict VAs ablated in the left-lateral ASV.

The details of different peak R-wave deflection intervals and precordial rebound notches are given in **Supplementary Table 2**.

TABLE 1 | Baseline characteristics.

Patient characteristics (*N* = 51)	
Age, y	53 (39–59)
Male, n (%)	31 (61)
Clinical symptoms, n (%)	
Palpitations	51 (100)
Presyncope	1 (2)
Syncope	0
Clinical VAs, n (%)	
Only PVCs	41 (80)
PVCs, non-sustained VT	8 (16)
PVCs, sustained VT	2 (4)
LVEDD (mm) before ablation	49 (45–54)
LVEF (%) before ablation	64 (60–65)
No. of patients LVEF < 50%	0
VA burden before ablation, beats/24 h	24445 (15000–36000)

Values are presented as the median (Q1–Q3) or n (%). VA, ventricular arrhythmia; PVC, premature ventricular contraction; LVEDD, left ventricular end-diastolic dimension; LVEF, left ventricular ejection fraction.

DISCUSSION

Major Findings

This study revealed the distribution and electrocardiographic/electrophysiological characteristics of VAs ablated in different subregions of the ASVs. The main findings are as follows:

1. Ventricular arrhythmias from the ASVs are mainly distributed in the anterior and the left lateral portions.
2. Among the 3 kinds of VAs targeting bipolar electrograms in the ASVs, the fractionated potential was in the majority, but its percentage decreased gradually from the right-lateral to the left-lateral ASV.
3. Precordial electrocardiographic rebound notch is a simple and distinct ECG pattern that has a high predictive accuracy for identifying VA origins in the right-anterior ASV or the left-lateral ASV.

TABLE 2 | Bipolar electrogram and ECG characteristics during ventricular arrhythmias.

	R-Ant./Lat. (*N* = 12)	**R-L comm.(*N* = 22)**	**L-Ant./Lat. (*N* = 17)**	***P* value**
Target amplitude, mV	0.56 (0.33–0.99)[a,b]	0.76 (0.50–1.16)[a]	0.41 (0.35–0.67)[b]	**0.044***
Target duration, ms	138.9 ± 14.5	139.1 ± 42.6	124.9 ± 35.4	0.416
Earliest activation, ms	25.8 ± 6.0	27.4 ± 7.4	29.5 ± 8.3	0.469
Lead I morphology, *n* (%)				
R/RR'/RSR'	11 (91.7)[a]	9 (40.9)[b]	2 (11.8)[b]	**<0.05***
Rs (R/S ≥ 1)	0	6 (27.3)	3 (17.6)	>0.05
rS (R/S <1)	0	4 (18.2)	3 (17.6)	>0.05
QS, QRS	1 (8.3)[a]	3 (13.6)[a]	9 (52.9)[b]	**<0.05***
Precordial transition, *n* (%)				
V1	1 (8.3)[a]	7 (31.8)[a,b]	9 (52.9)[b]	**<0.05***
V1-2	1 (8.3)	3 (13.6)	1 (5.9)	>0.05
V2	1 (8.3)	2 (9.1)	0	>0.05
V2-3	4 (33.3)	5 (22.7)	7 (41.2)	>0.05
≥V3	5 (41.7) [a]	5 (22.7) [a,b]	0[b]	**<0.05***
Precordial rebound notch, *n* (%)				
None	0[a]	16 (72.7)[b]	10 (58.8)[b]	**<0.05***
V1-2	1 (8.3)	0	0	>0.05
V2-3	0	2 (9.1)	6 (35.3)	>0.05
V3-4	9 (75) [a]	2 (9.1) [b]	1 (5.9) [b]	**<0.05***
V4-5	2 (16.7)	2 (9.1)	0	>0.05

Values are presented as the mean ± SD, median (Q1–Q3), or n (%). ASV, aortic sinus of Valsalva; R-Ant./Lat., right-lateral/anterior ASV; R-L Comm., left-right commissure; L-Ant./Lat., left-lateral/anterior ASV. [a or b] Different letters indicate intergroup significance; e.g., for the "target amplitude," significance is shown between R-L Comm. and L-Ant./Lat.
*The Bold values and the symbol * highlight the P value < 0.05.*

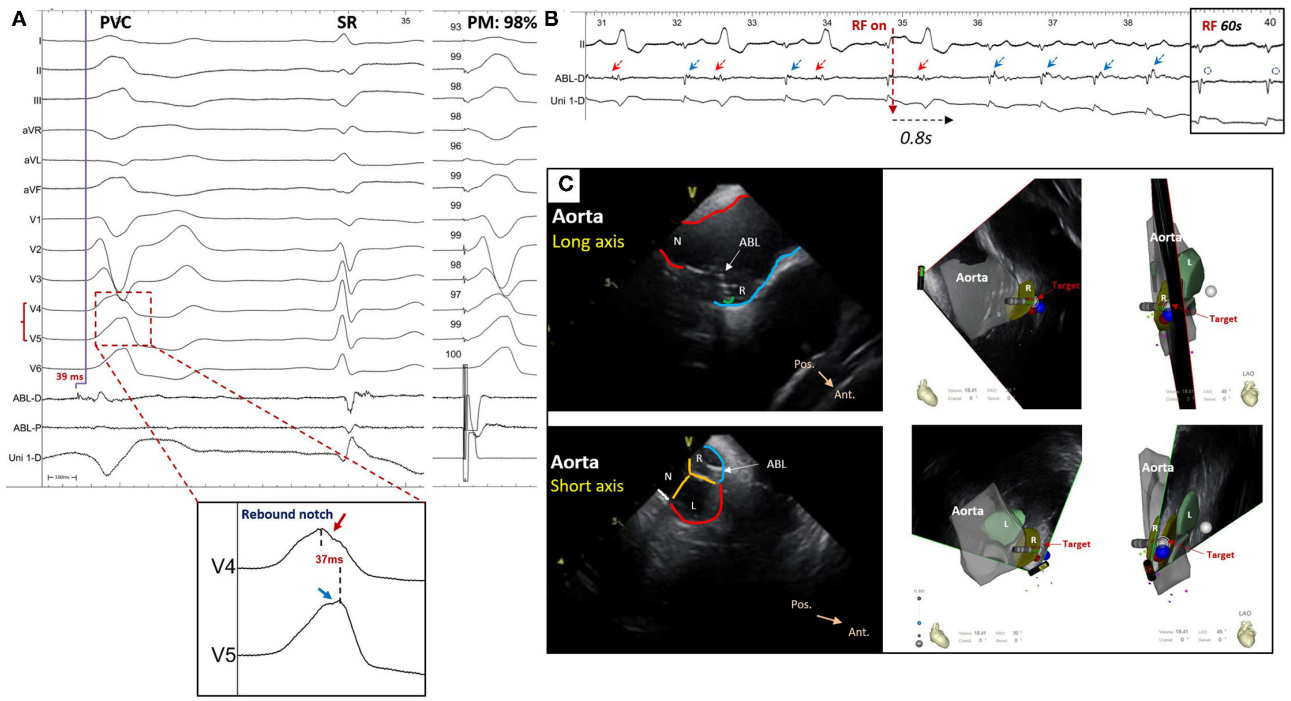

FIGURE 5 | A patient who suffered from premature ventricular contraction (PVC) with left bundle branch block morphology and inferior axis deviation ablated in the right-anterior ASV. **(A)** The ECG of PVC showed a rebound notch on leads V4-V5; the final target revealed a reversal potential (compared with sinus rhythm) that preceded the onset of QRS for 39 ms during PVC and the pace mapping showed a similarity of 98%. **(B)** The ventricular bigeminy rhythm disappeared immediately after radiofrequency (RF) initiation and the late potential (blue arrow) during sinus rhythm was eliminated after 60 s of RF. **(C)** The ablated target was located at the right-anterior ASV through intracardiac echocardiography. ABL-D/P, distal or proximal bipolar electrogram; Uni-D, distal unipolar electrogram; SR, sinus rhythm; PM, pace mapping; ABL, ablation catheter; ASV, aortic sinus of Valsalva; N, non-coronary ASV; L, left ASV; R, right ASV; Pos., posterior; Ant., anterior.

Correlation Between Anatomy and Electrophysiology of the ASV-VAs

As a part of the aortic root, the ASVs are located in the center of the heart, surrounded by the RVOT, the left ventricle, the right atrium, and the left atrium. As for the relative anatomic location, the right ASV forms the right anterior portion of the ASVs and abuts the RVOT, resulting in an electrogram that shows a large ventricular potential and a small (or absent) atrial potential; the left ASV located higher and lateral, which is stuck in the middle of the RVOT and the left atrium and usually shows a local ventricular and atrial electrogram; the non-coronary ASV, which is the lowest and most posterior part, is close to the interatrial septum and shows a large atrial potential (9). Meanwhile, histological study (10) found that ventricular musculature mainly extends into the anterior portion of the ASVs, while the non-coronary ASV, the right-lateral ASV, and the left-lateral ASV are embraced by the fibrous skeleton (11). In keeping with such anatomic substrate, the targets of the ASV-VAs in this study were mainly distributed in the anterior portion of the ASVs, while only a quarter (13/51) of the VA targets was located in the lateral ASVs. However, according to the distributional difference (left-lateral ASV, 13/51 vs. right-lateral ASV, 1/51), the left-lateral ASV should receive more attention than the right-lateral ASV during mapping and ablation, probably due to the anatomic proximity between the left-lateral ASV and the aortomitral continuity [another arrhythmogenic region (12)]. Similarly, Yang et al. (3) reported a case series about the ablation of VAs with predominant monophasic "R" waves in precordial leads from the left ASV. They found that those with small "s" waves in ECG-V2 and a single "V" electrogram in the target were located more inferior and lateral in the left ASV. This anatomic distribution (left-lateral ASV) and these target potential characteristics (lower amplitude and less fractionation) are similar to those in this study, which is why VA targets were more common in the left-lateral ASV than in the right-lateral ASV.

Electrocardiogram Characteristics of the ASV-VAs

Due to the distinct posterior-anterior and blurry left-right anatomic relationship between the pulmonary root and the aortic root, ECG differentiation of left- and right-sided outflow tract VAs is mainly based on the precordial lead (13). Many ECG signs and prediction algorithms, such as an R-wave duration index $\geq$ 50% and R/S-wave amplitude index $\geq$ 30% in V1 and/or V2 (1), a V2 transition ratio $\geq$ 0.60, a transitional zone index $<$ 0 (7), and an R-wave deflection interval of modified precordial lead (8), can

predict an origin of the left ventricular outflow tract VAs. Within the ASVs, different sinuses have different VA ECG characteristics. The right ASV is located inferior, anterior, and to the right of the left ASV, which usually presents as a lower amplitude in the inferior lead, a greater positive portion in lead I, and a later transition in the precordial lead (V2-V3) during VAs recorded in ECG. In contrast to VAs from the right ASV, VAs from the left ASV usually show a larger amplitude in the inferior lead, a greater negative portion in lead I, and an early transition in the precordial lead (before V2) (2). Moreover, some VAs from the left ASV could show predominant monophasic "R" waves in precordial leads with an "s" wave in lead V2 (3). In addition, a "QRS" pattern (5) in leads V1-V3 and/or a "QS" pattern plus a downstroke notch (6) in lead V1 with a precordial transition at lead V3 might suggest a site of VA origin in the left-right commissure. Occasionally, an ECG pattern of narrower QRS duration, "s" wave in lead III, and smaller III/II ratio indicate an ablation in the non-coronary ASV, which might be of a para-Hisian origin. However, none of those studies focused on subregions of the ASV. This study further divided the right and the left ASVs into 6 subregions according to the anatomic marks revealed by ICE or coronary angiography. In addition to the typical ECG characteristics of the ASV-VAs, such as a positive "R" wave in the initiation and termination of lead I being more common in the VAs from the right ASV, we also found that the contiguous precordial electrocardiographic notch patterns could be a novel ECG signature for locating different subregions of the ASV. A left precordial rebound notch (V3-V4/V4-V5) during VAs indicates a right-anterior subregion, while a right precordial rebound notch (V2-V3) during VAs indicates a left-lateral subregion. Above all, this novel precordial ECG sign could provide supplemental evidence for the localization of the ASV-VAs, thus improving the precision and efficiency of mapping in the ASVs.

Underlying Mechanism of the Precordial Electrocardiographic Rebound Notch

An electrocardiographic notch in VAs might be related to slow or prolonged conduction. Marchlinski et al. first reported that an R wave notch of the inferior lead was more common in the free wall than in the septum during RVOT pacing, which could be explained by the sequential activation of the right ventricle and the left ventricle during pacing from free-wall sites leading to prolonged activation time and causing the electrocardiographic inferior notch (14). Yamada et al. found that VAs originating from the parietal band always presented with a notch in the middle of any QRS in all the cases, which suggested prolonged time conduct from the VA origin to the Purkinje system (15). In addition, the "notch" could be a sign of epicardial VAs. A precordial pseudodelta wave (upstroke notch) $\geq$ 34 ms has a sensitivity of 83% and a specificity of 95% to predict an epicardial origin (16). Both the upstroke and downstroke notches of the R wave in lead III have a sensitivity of 40.6% and a specificity of 97.5% to predict VAs arising from the distal great cardiac vein (17). Similarly, this study showed that VAs located in the right-anterior ASV, which always show a fractionated potential (slow conduction) in the target bipolar electrogram, are covered by different kinds of precordial rebound notches (V1-V2, 8.3%; V3-V4, 75%; and V4-V5, 16.7%).

A precordial electrocardiographic rebound notch is defined as a downstroke notch on the earlier lead followed by an upstroke notch on the later lead, indicating that the adjacent precordial leads have shorter and longer peak R-wave deflection intervals, respectively. Thus, a precordial electrocardiographic rebound notch is always followed by a larger difference in the peak R-wave deflection interval between the adjacent precordial leads, which may reflect a difference in the local depolarized time. In summary, activations from different subregions of the ASVs are conducted by different vectors, resulting in different patterns of the precordial electrocardiographic rebound notch. Interestingly, we never found a precordial sequential notch (an upstroke notch on the earlier lead followed by a downstroke notch on the later lead) in the study population.

LIMITATIONS

This retrospective study is limited by the small sample size and single center, which prevented us from testing the diagnostic value of precordial electrocardiographic rebound notches in patients with the ASV-VAs in an external validation cohort. Meanwhile, the mechanism of the rebound notch remains speculative and unclear. High-density epicardial and endocardial electroanatomic mapping can reveal the activation pattern of the ASV-VAs and may explain this specific precordial electrocardiographic notch change. Moreover, any target that was confirmed by local activation mapping [28 ms (22–33 ms)] and matching pace mapping could not be definitively recognized as an origin site because we did not perform high-density epicardial and endocardial ventricular outflow tract mapping in all the patients. Thus, we used the verb "originate" prudently. In addition, ICE, considered the gold standard for the location of VAs, was used in only approximately 40% of the population due to the retrospective nature of this study. For the rest of the patients, detailed coronary angiography plus 3-dimensional maps can be an alternative solution. Finally, this study did not enroll patients with VAs originating from the non-coronary ASV because of their low incidence rate and uncertain origin (possibly para-Hisian origin).

CONCLUSION

The targets of the ASV-VAs were distributed mainly in the anterior and the left-lateral ASVs. The fractionated potential was dominant in the 3 types of target electrograms, while the percentage of target fractionation gradually decreased from the right-lateral to the left-lateral ASVs. A precordial electrocardiographic rebound notch has high predictive accuracy for the localization of VAs in the right-anterior or left-lateral ASVs.

DATA AVAILABILITY STATEMENT

The original contributions presented in the study are included in the article/**Supplementary Material**, further inquiries can be directed to the corresponding author/s.

ETHICS STATEMENT

The studies involving human participants were reviewed and approved by Ethics Committee of Fuwai Hospital. Written informed consent to participate in this study was provided by the participants' legal guardian/next of kin. Written informed consent was obtained from the individual(s) for the publication of any potentially identifiable images or data included in this article.

AUTHOR CONTRIBUTIONS

All the authors contributed to the study conception and design. Material preparation, data collection, and analysis were performed by SW, MT, and ZZ. The first draft of the manuscript was written by SW and all the authors commented on previous versions of the manuscript. All the authors read and approved the final version of the manuscript.

FUNDING

This work was supported by the National Natural Science Foundation of China (Grant No. 61527811).

SUPPLEMENTARY MATERIAL

The Supplementary Material for this article can be found online at: https://www.frontiersin.org/articles/10.3389/fcvm.2021.778866/full#supplementary-material

REFERENCES

1. Ouyang F, Fotuhi P, Ho SY, Hebe J, Volkmer M, Goya M, et al. Repetitive monomorphic ventricular tachycardia originating from the aortic sinus cusp: electrocardiographic characterization for guiding catheter ablation. *J Am Coll Cardiol.* (2002) 39:500–8. doi: 10.1016/S0735-1097(01)01767-3
2. Yamada T, McElderry HT, Doppalapudi H, Murakami Y, Yoshida Y, Yoshida N, et al. Idiopathic ventricular arrhythmias originating from the aortic root prevalence, electrocardiographic and electrophysiologic characteristics, and results of radiofrequency catheter ablation. *J Am Coll Cardiol.* (2008) 52:139–47. doi: 10.1016/j.jacc.2008.03.040
3. Yang JD, Sun Q, Guo XG, Zhou GB, Liu X, Luo B, et al. Ablation of ventricular arrhythmias with predominant monophasic "R" waves in precordial leads from the left sinus of Valsalva: Electrocardiographic and electrophysiologic characteristics. *J Cardiovasc Electrophysiol.* (2019) 30:541–9. doi: 10.1111/jce.13845
4. Wang Y, Liang Z, Wu S, Han Z, Ren X. Idiopathic ventricular arrhythmias originating from the right coronary sinus: Prevalence, electrocardiographic and electrophysiological characteristics, and catheter ablation. *Heart Rhythm.* (2018) 15:81–9. doi: 10.1016/j.hrthm.2017.09.008
5. Yamada T, Yoshida N, Murakami Y, Okada T, Muto M, Murohara T, et al. Electrocardiographic characteristics of ventricular arrhythmias originating from the junction of the left and right coronary sinuses of Valsalva in the aorta: the activation pattern as a rationale for the electrocardiographic characteristics. *Heart Rhythm.* (2008) 5:184–92. doi: 10.1016/j.hrthm.2007.09.029
6. Bala R, Garcia FC, Hutchinson MD, Gerstenfeld EP, Dhruvakumar S, Dixit S, et al. Electrocardiographic and electrophysiologic features of ventricular arrhythmias originating from the right/left coronary cusp commissure. *Heart Rhythm.* (2010) 7:312–22. doi: 10.1016/j.hrthm.2009.11.017
7. Yoshida N, Inden Y, Uchikawa T, Kamiya H, Kitamura K, Shimano M, et al. Novel transitional zone index allows more accurate differentiation between idiopathic right ventricular outflow tract and aortic sinus cusp ventricular arrhythmias. *Heart Rhythm.* (2011) 8:349–56. doi: 10.1016/j.hrthm.2010.11.023
8. Anderson RD, Kumar S, Binny S, Prabhu M, Al-Kaisey A, Parameswaran R, et al. Modified precordial lead R-wave deflection interval predicts left- and right-sided idiopathic outflow tract ventricular arrhythmias. *JACC Clin Electrophysiol.* (2020) 6:1405–19. doi: 10.1016/j.jacep.2020.07.011
9. Sasaki T, Hachiya H, Hirao K, Higuchi K, Hayashi T, Furukawa T, et al. Utility of distinctive local electrogram pattern and aortographic anatomical position in catheter manipulation at coronary cusps. *J Cardiovasc Electrophysiol.* (2011) 22:521–9. doi: 10.1111/j.1540-8167.2010.01957.x
10. Hasdemir C, Aktas S, Govsa F, Aktas EO, Kocak A, Bozkaya YT, et al. Demonstration of ventricular myocardial extensions into the pulmonary artery and aorta beyond the ventriculo-arterial junction. *Pacing Clin Electrophysiol PACE.* (2007) 30:534–9. doi: 10.1111/j.1540-8159.2007.00704.x
11. Saremi F, Sánchez-Quintana D, Mori S, Muresian H, Spicer DE, Hassani C, et al. Fibrous skeleton of the heart: anatomic overview and evaluation of pathologic conditions with CT and MR imaging. *Radiographics.* (2017) 37:1330–51. doi: 10.1148/rg.2017170004
12. Chen J, Hoff PI, Rossvoll O, De Bortoli A, Solheim E, Sun L, et al. Ventricular arrhythmias originating from the aortomitral continuity: an uncommon variant of left ventricular outflow tract tachycardia. *Europace.* (2012) 14:388–95. doi: 10.1093/europace/eur318
13. Anderson RD, Kumar S, Parameswaran R, Wong G, Voskoboinik A, Sugumar H, et al. Differentiating right- and left-sided outflow tract ventricular arrhythmias. *Circul Arrhythmia Electrophysiol.* (2019) 12:e007392. doi: 10.1161/CIRCEP.119.007392
14. Dixit S, Gerstenfeld EP, Callans DJ, Marchlinski FE. Electrocardiographic patterns of superior right ventricular outflow tract tachycardias: distinguishing septal and free-wall sites of origin. *J Cardiovasc Electrophysiol.* (2003) 14:1–7. doi: 10.1046/j.1540-8167.2003.02404.x
15. Yamada T, Yoshida N, Itoh T, Litovsky SH, Doppalapudi H, McElderry HT, et al. Idiopathic ventricular arrhythmias originating from the parietal band: electrocardiographic and electrophysiological characteristics and outcome of catheter ablation. *Circul Arrhythmia Electrophysiol.* (2017) 10:e005099. doi: 10.1161/CIRCEP.117.005099
16. Berruezo A, Mont L, Nava S, Chueca E, Bartholomay E, Brugada J. Electrocardiographic recognition of the epicardial origin of ventricular tachycardias. *Circulation.* (2004) 109:1842–7. doi: 10.1161/01.CIR.0000125525.04081.4B
17. Lin YN, Xu J, Pan YQ, Zheng C, Lin JX Li J, et al. An electrocardiographic sign of idiopathic ventricular tachycardia ablatable from the distal great cardiac vein. *Heart rhythm.* (2020) 17:905–14. doi: 10.1016/j.hrthm.2020.01.027

Conflict of Interest: The authors declare that the research was conducted in the absence of any commercial or financial relationships that could be construed as a potential conflict of interest.

Publisher's Note: All claims expressed in this article are solely those of the authors and do not necessarily represent those of their affiliated organizations, or those of the publisher, the editors and the reviewers. Any product that may be evaluated in this article, or claim that may be made by its manufacturer, is not guaranteed or endorsed by the publisher.

frontiers in Cardiovascular Medicine

ORIGINAL RESEARCH
published: 23 December 2021
doi: 10.3389/fcvm.2021.801441

Catheter Ablation of Ventricular Arrhythmias Originating From the Region of DGCV-AIV via a Swartz Sheath Support Approach

Cheng Zheng, Wei-Qian Lin, Yao-Ji Wang, Fang-Zhou Lv, Qi-Qi Jin, Jin Li and Jia-Feng Lin**

Department of Cardiology, The Second Affiliated Hospital and Yuying Children's Hospital of Wenzhou Medical University, Wenzhou, China

OPEN ACCESS

Edited by:
Feifan Ouyang, University Medical Center Hamburg-Eppendorf, Germany

Reviewed by:
Christian Hendrik Heeger, University Heart Center Luebeck, Germany
Yumei Xue, Guangdong Academy of Medical Sciences, China

***Correspondence:**
Jin Li
wyd0115@126.com
Jia-Feng Lin
linjiafeng_wzmcfey@163.com

Specialty section:
This article was submitted to Cardiac Rhythmology, a section of the journal Frontiers in Cardiovascular Medicine

Received: *25 October 2021*
Accepted: *26 November 2021*
Published: *23 December 2021*

Citation:
Zheng C, Lin W-Q, Wang Y-J, Lv F-Z, Jin Q-Q, Li J and Lin J-F (2021) Catheter Ablation of Ventricular Arrhythmias Originating From the Region of DGCV-AIV via a Swartz Sheath Support Approach. Front. Cardiovasc. Med. 8:801441. doi: 10.3389/fcvm.2021.801441

Aims: This study aimed to investigate an appropriate catheter manipulation approach for ventricular arrhythmias (VAs) originating from the left ventricular epicardium adjacent to the transitional area from the great cardiac vein to the anterior interventricular vein (DGCV-AIV).

Methods: A total of 123 patients with DGCV-AIV VAs were retrospectively analyzed. All these patients underwent routine mapping and ablation by conventional approach [Non-Swartz sheath support (NS) approach] firstly. In the situation of the distal portion of the coronary venous system (CVS) not being accessed or a good target site not being obtained, the Swartz sheath support (SS) approach was attempted alternatively. If this still failed, the hydrophilic coated guidewire and left coronary angiographic catheter-guided deep engagement of Swartz sheath in GCV to support ablation catheter was performed.

Results: A total of 103 VAs (103/123, 83.74%) were successfully eliminated in DGCV-AIV. By NS approach, the tip of the catheter reached DGCV in 39.84% VAs (49/123), reached target sites in 35.87% VAs (44/123), and achieved successful ablation in 30.89% VAs (38/123), which was significantly lower than by SS approach (88.61% (70/79), 84.81 % (67/79), and 75.95% (60/79), $P < 0.05$). There were no significant differences in complication occurrence between the NS approach and the SS approach (4/123, 3.25% vs. 7/79, 8.86%, $p > 0.05$). The angle between DGCV and AIV$<83^{\circ}$ indicated an inaccessible AIV by catheter tip with a predictive value of 94.5%. Width/height of coronary venous system>0.69 more favored a SS approach with a predictive value of 87%.

Conclusion: For radiofrequency catheter ablation (RFCA) of VAs arising from DGCV-AIV, the SS approach facilitates the catheter tip to achieve target sites and contributes to a successful ablation.

Keywords: distal great cardiac vein, anterior interventricular vein, summit-communicating vein, ventricular arrhythmias, radiofrequency catheter ablation, Swartz sheath

INTRODUCTION

Radiofrequency catheter ablation (RFCA) is an effective and safe therapy for idiopathic ventricular arrhythmias (VAs). However, the ablation of VAs originating from the left ventricular epicardium adjacent to the transitional area from the great cardiac vein to the anterior interventricular vein (DGCV-AIV) can be challenging because of the complex anatomic structures of this region (adjacent to coronary arteries) and difficulty in manipulation of the ablation catheter in the small-lumen and tortuous coronary venous system (1, 2).

It is reasonable to assume that any approach which could assist ablation catheter going through the anatomic obstacles in the coronary venous system and aid catheter tip reaching more distal portion of DGCV-AIV would improve the success rate of RFCA. Nevertheless, up to now, no systemic studies investigated the most appropriate manipulation approach for RFCA of VAs arising from DGCV-AIV.

Recent studies revealed that application of the Swartz sheath could improve the stability of catheter manipulation and enhance mapping and ablation efficiency in RFCA for VAs, for example, reversed U-curve technique of ablation catheter with the support of Swartz sheath for PSCs VAs (3), reversed S-curve technique of ablation catheter with the support of Swartz sheath close to the fossa ovalis for endocardial LV summit VAs (4). Thus, we doubt whether the Swartz sheath support approach could be utilized in the RFCA of DGCV-AIV VAs to achieve a more efficient ablation.

In this study, we aimed to evaluate the value and safety of the Swartz sheath support approach in the mapping and ablation of DGCV-AIV VAs.

METHODS

Study Population

A total of 2768 patients (mean age 49.07 ± 17.40 years) were referred for RFCA for symptomatic VAs in our center from December 2009 to December 2020. Among them, 123 consecutive VAs were confirmed arising from the DGCV-AIV based on systemic mapping results or successful ablation sites and enrolled in this retrospective study. All patients had a normal ECG during sinus rhythm. Complete physical examination, echocardiography, exercise stress testing, or coronary angiography proved no structural heart diseases in any patient. Ethical approval was obtained from the hospital's ethics committee, and all patients gave written informed consent before operation.

Mapping and Ablation

Electrophysiological study and ablation were performed after discontinuation of all anti-arrhythmic drugs for at least five half-lives. A 6F decapolar catheter (4-mm interelectrode spacing) was inserted from the right internal jugular vein and placed in the coronary sinus as distal as possible. If clinical arrhythmias failed to occur spontaneously, intravenous isoproterenol infusion (2–5 mg/min) was administered. An irrigated-tip ablation catheter was advanced to the right ventricle via antegrade transvenous approach and to the left ventricle via retrograde aortic approach. During VAs, the RV endocardium, LV endocardium, and aortic cusps were mapped cautiously and compared with the distal bipolar electrodes of the coronary sinus catheter, in order to identify the earliest site of ventricular activation. If comprehensive mapping results showed the earliest activation sites were in the distal portion of the coronary venous system (CVS), we would consider the VAs as arising from DGCV-AIV. For DGCV-AIV, the irrigated tip was applied with a flow rate of 30–60 ml/min, preset power of 25–30 W. CAG was performed in all cases to investigate the distance from the catheter tip to adjacent coronary arteries before RFCA. Energy delivery was forbidden when the distance was less than 5 mm. Coronary blood supply was routinely evaluated before and after ablation. If VAs were terminated or accelerated during the initial 10 s, radiofrequency delivery would be continued for 60 to 180 s. Otherwise, other targets were sought.

After successful ablation, intravenous administration of isoproterenol and programmed stimulation were performed to induce clinical VA. Acute success was defined as both an absence of spontaneous or provoked clinical VA at the end of the procedure and the latter 48-h period post-ablation on ECG Holter.

Swartz Sheath Support Approach and Non-Swartz Sheath Support Approach

When the DGCV-AIV was considered the origin of ventricular arrhythmias, detailed mapping in DGCV-AIV was performed. For mapping and ablation in DGCV-AIV, two catheter manipulation approaches could be adopted, as shown in **Figure 1**. The conventional approach, the non-Swartz sheath support (NS) approach, was facilitated by delivering the tip of the ablation catheter directly from the ostium of the coronary sinus to DGCV-AIV to perform mapping and ablation. The Swartz sheath support (SS) approach was facilitated by engagement of Swartz sheath in GCV from the ostium of coronary sinus by ablation catheter. Then the ablation catheter and Swartz sheath were advanced alternately in GCV to reach the distal portion of DGCV-AIV to perform mapping and ablation. If the Swartz sheath still could not go through the GCV, the hydrophilic coated guide wire and left coronary angiographic catheter-guided deep engagement of Swartz sheath in GCV was conducted to support the ablation catheter.

Definition of the Location of DGCV-AIV Origin

The DGCV-AIV origin of VAs was identified by mapping and ablation outcomes combined with retrograde venography of the coronary venous system. In our study, DGCV-AIV refers to the anatomy in the distal portion of the great cardiac vein, including four regions: DGCV1, DGCV2, summit-CV, and AIV. DGCV1 is defined as the segment of DGCV at the epicardium of the anterolateral wall of mitral annulus and DGCV2 as the segment of DGCV transecting the epicardial LV outflow region bounded by the bifurcation between the left anterior descending artery and left circumflex artery and continued to DGCV1. Anterior interventricular vein (AIV) refers to the vein going along the

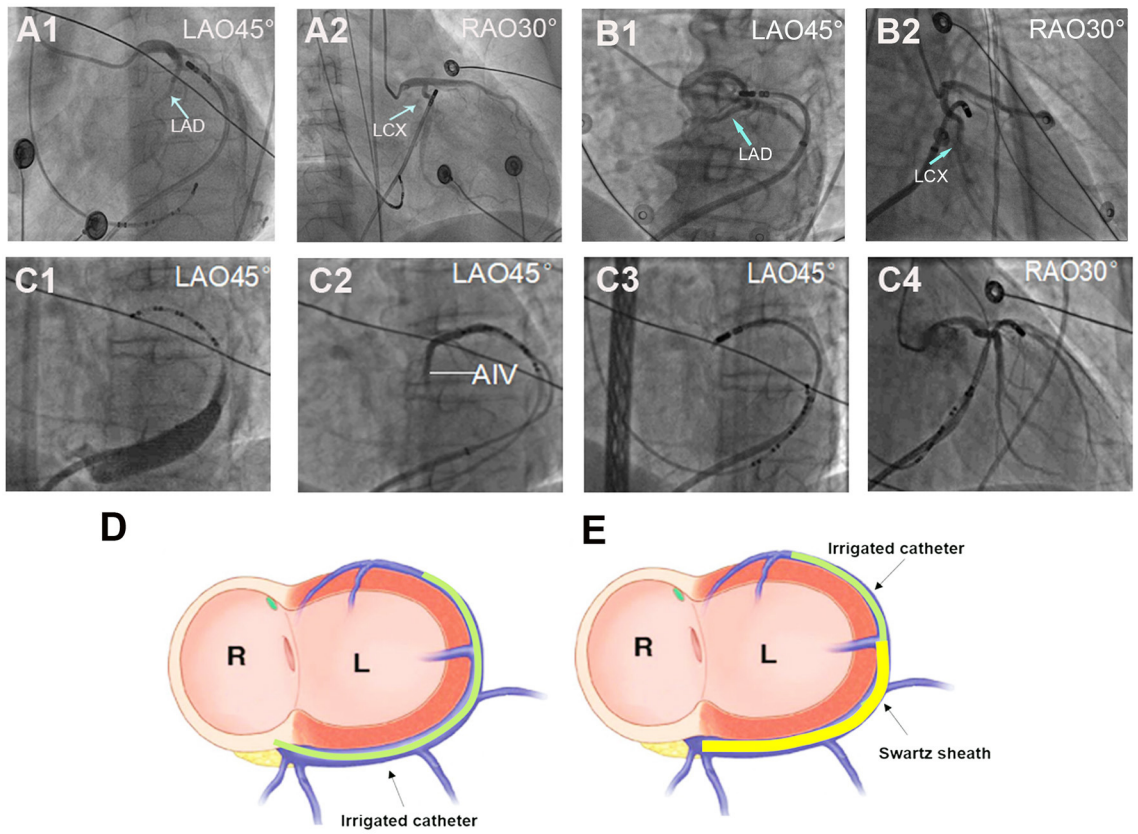

FIGURE 1 | Different approaches for ablation catheter reaching target sites in DGCV. **(A)** Manipulation of the ablation catheter in GCV by non-Swartz sheath support (NS) approach. **(A1,A2)** The tip of the catheter was delivered to DGCV from the ostium of the coronary sinus directly. **(B)** Manipulation of the ablation catheter in GCV by Swartz sheath support (SS) approach. **(B1,B2)** The tip of the catheter was delivered to summit-CV with support from Swartz sheath in the GCV. **(C)** Super smooth guidewire and left coronary angiographic catheter-guided deep engagement of Swartz sheath in GCV. **(C1)** Due to the blockage of the Vieussens valve (shown by coronary venography), even with the support of Swartz sheath, the catheter tip could not reach the middle part of GCV. **(C2)** The hydrophilic coated guide wire and Judkin's 4-left coronary catheter were delivered through a Swartz sheath and passed the Vieussens valve and reached the DGCV. **(C3,C4)** The guided guide wire and coronary catheter, the Swartz sheath was advanced alternately and passed the Vieussens valve, then the guidewire and Jukin's catheter was exchanged with ablation catheter to perform mapping and ablation in DGCV. **(D)** Schema of NS approach for DGCV-AIV VAs. Targeting DGCV-AIV VAs via advancing ablation catheter from the ostium of coronary sinus directly. **(E)** Schema of SS approach for DGCV-AIV VAs. Targeting DGCV-AIV VAs via advancing ablation catheter from the ostium of the coronary sinus with the support from Swartz sheath. LAD, left anterior descending artery; LCX, left circumflex artery. LAO, left anterior oblique; RAO, right anterior oblique.

anterior interventricular groove from cardiac apex to bottom, turning posteriorly and continuing as DGCV2. Summit-CV refers to the communicating vein (CV) between the aortic and pulmonary annulus, which is the extended tributary of the DGCV located distal to the origin of the AIV, see **Figure 2**.

Anatomic Obstacles for Catheter Manipulation in GCV

For catheter ablation of DGCV-AIV VAs, a thorough understanding of CVS anatomy is essential (1, 2). The coronary sinus is located at the posterior and inferior part of the epicardial mitral valve and, collecting the blood from the CVS, ends in the right atrium. There is a small folded tissue known as the Thebesian valve at the ostium of the coronary sinus, which might occasionally be an obstacle to catheterization. A small left atrial vein named Marshall (or Marshall ligament) is the remnant of the embryonic left superior cardinal vein and drains into the coronary sinus. It is at the point where the Marshall vein drains into the coronary sinus that the coronary sinus turns into the great cardiac vein, 29.15% of patients have a well-developed Vieussens valve at this site that might preclude ablation catheter advancement. The GCV goes along the lateral portions of the mitral valve and extends into DGCV at the epicardium of the anterolateral portion of the mitral annulus. It is reasonable to believe that a curved GCV morphology may limit the advancement of a catheter. DGCV turns into AIV beneath the aortic valve cusp at the left ventricular summit. The angle between AIV and DGCV2 has great individual variability. It is observed that an acute angle between AIV and DGCV2 would prevent the ablation catheter from reaching proximal AIV, on the contrary, an obtuse angle would facilitate catheter performing mapping and ablation in proximal AIV. Communicating vein refers to the very thin veins between the GCV and conus branch that drains to the small cardiac vein,

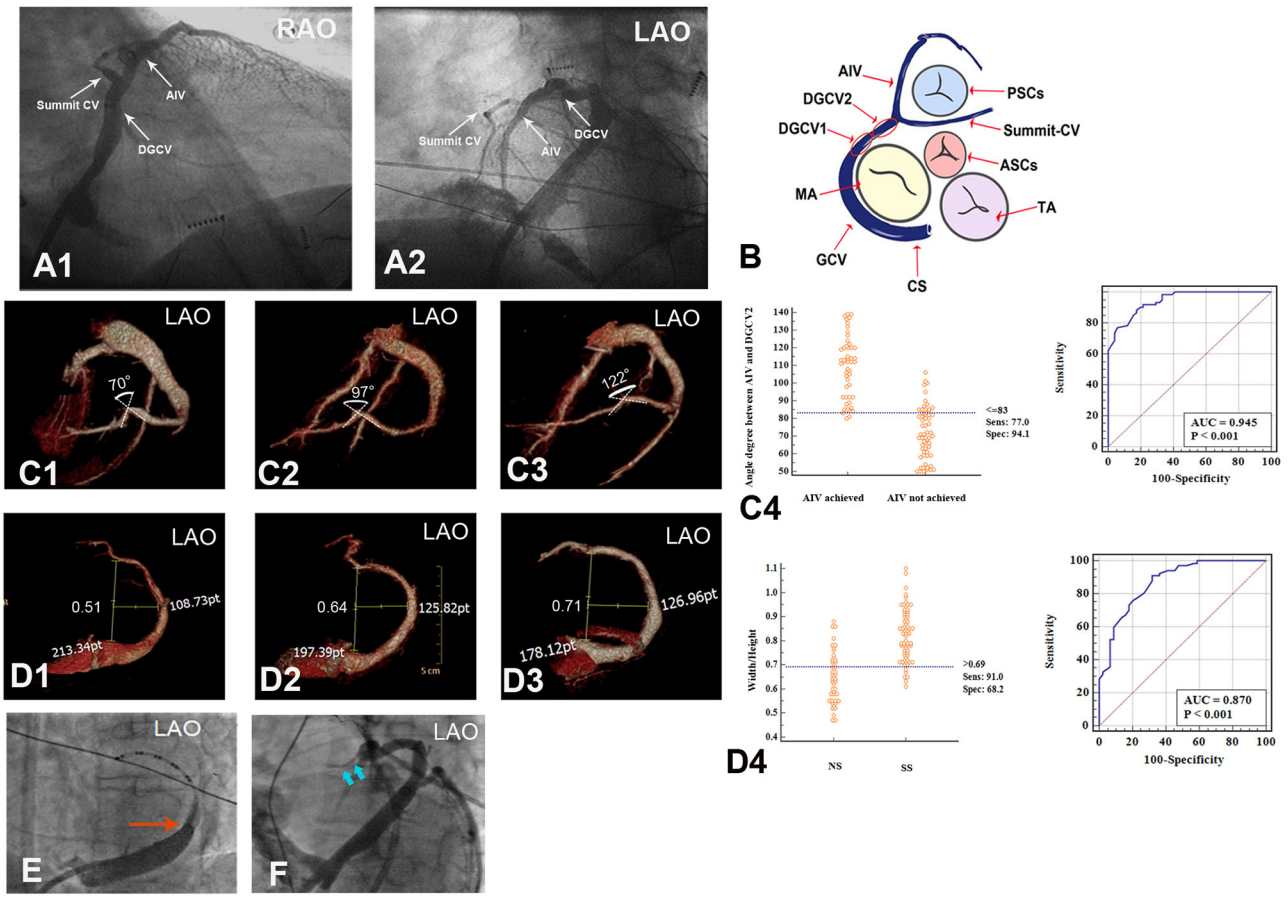

FIGURE 2 | Anatomy of DGCV-AIV and anatomic obstacles preventing catheterization in GCV. **(A,B)** Anatomy of DGCV-AIV. **(C,D)** Anatomic obstacles preventing catheterization in GCV. **(D)** Angle formed between DGCV and AIV, and an angle <83° prevented the ablation catheter from advancing from DGCV into AIV. **(E)** Different morphology of GCV, and Width/Hight>0.69 more favored the application of the SS approach. **(E)** Venous valve (Vieussens valve) in GCV. **(F)** Thin lumen of summit-CV. DGCV, distal great cardiac vein; AIV, anterior interventricular vein; summit-CV, communicating vein in the left ventricular summit. RVOT, right ventricular outflow tract; LVOT, left ventricular outflow tract; TA, tricuspid annulus; MA, mitral annulus; CS, coronary sinus.

and Summit-CV is a distinct CV that is located between the aortic and pulmonary annulus, distal to the transitional area between the GCV and the AIV, and in close association with the superior portion of the LV summit. Previous studies have revealed summit-CV can be the source of idiopathic ventricular arrhythmias. However, the very thin lumen of this vessel usually limits the detailed mapping and ablation in this region. Above all, hampering of venous valves (Thebesian valve and Vieussens valve), deflections of GCV, acute angle between DGCV and AIV, the thin lumen of Summit-CV, are all potential anatomic factors preventing catheter ablation of DGCV-AIV VAs. Therefore, any method, which could assist ablation catheter overcoming these anatomic obstacles, would contribute to the successful ablation of DGCV-AIV VAs **Figure 2**.

Follow-Up

Each patient returned for evaluation in the hospital's outpatient department of cardiology 1-month after treatment. Twelve-lead ECG and 24-h Holter monitoring were performed at the 3-month follow-up visit. All patients received coronary CT angiography using 128-slice dual-source CT 3-months later to detect the long-term effect of ablation in DGCV-AIV to an adjacent coronary artery. Meanwhile, the anatomy of the coronary venous system was evaluated in each case using maximum intensity projection and volume rendering technique multi-planar reformation reconstructions. The angle between AIV and DGCV, and width/ height of GCV in each patient was measured by three radiologists independently, a mean value was adopted for statistical analysis. The height of GCV was defined as the maximal vertical distance from the beginning of AIV to the proximal GCV. The width of GCV was defined as the maximal transversal distance from lateral GCV to the maximal vertical line.

Statistical Analysis

Continuous variables are expressed as mean ± SD. Continuous variables were compared using a *t*-test if a normal distribution was assumed or using a Mann-Whitney U test if a normal

distribution was not assumed. Categorical variables were compared using the χ^2-test. A 2-tailed $P < 0.05$ was considered significant.

RESULTS

The 123 consecutive cases of DGCV VAs undergoing mapping and ablation in our center were retrospectively reviewed in this study, shown in **Figure 3**. NS approach and SS approaches were attempted in 123 and 79 cases, respectively. By NS approach, DGCV-AIV target site reaching was only obtained in 44 VAs (30.89%, 44/123) with successful ablation in 38 VAs (30.89%, 38/123) VAs. Via SS approach, DGCV-AIV target site reaching was obtained in 67 VAs (84.81%, 67/79) with successful ablation in 60 VAs (75.95%, 60/79). In 12 VAs, target sites failed to be reached by both NS approach and SS approach, the hydrophilic coated guide wire, and left coronary angiographic catheter-guided deep engagement of Swartz sheath in GCV to support ablation catheter was applied. In this way, the irrigated catheter was delivered to distal sites of DGCV-AIV. Among these 12 VAs, target sites were achieved in 7 VAs (58.33%, 7/12) with successful ablation in 5 cases (41.67%, 5/12). There were no significant differences in catheter tip reaching coronary sinus, proximal GCV, or middle GCV by NS approach and SS approach. Of note, some distal sites of GCV (DGCV1, DGCV2, AIV, Summit-CV) could be more possibly reached by catheter tip via SS approach, shown in **Table 1**. A successful ablation case of DGCV-AIV VAs by SS approach post failed NS approach was shown in **Figure 4**.

Due to the obstacle of venous valves of CVS, middle GCV could not be reached in 13 VAs and in 7 VAs by NS approach and SS approach, respectively. Nevertheless, via the hydrophilic coated guidewire and left coronary angiographic catheter-guided deep engagement of Swartz sheath in GCV, the obstacle of the venous valve was overcome. As the guidewire went through the venous valves smoothly, the angiographic catheter advanced to the distal portion of CVS along the guide wire, which provided a backup force for the Swartz sheath and facilitate the Swartz sheath to reach the middle GCV.

By NS approach, the catheter tip accessed DGCV2 in 43 patients, among which, catheter tip could achieve AIV in only 21 patients. Via SS approach, catheter tip accessed DGCV2 in 69 patients, and the catheter tip could further achieve AIV in 30 patients. CTV of CVS 3-month post-RFCA compared the patients of AIV reached by catheter tip with the patients of AIV not reached (51 VAs: $72.05 \pm 14.62^\circ$ vs. 61 VAs: $108.73 \pm 17.61^\circ$). The angle between AIV and DGCV2 $\leq 83^\circ$ had a sensitivity of 94.1%, specificity of 77.0%, and accuracy of 94.5% for identifying the inaccessibility from DGCV2 to AIV, no matter SS approach or NS approach used, shown in **Figure 2**.

Whether the CVS morphology would affect the catheter manipulation approach selected was also investigated. In 44 VAs with target sites reached by the NS approach, a smaller Width/Height of CVS was more found. On the contrary, in 67 VAs with target sites reached by the SS approach, a relatively larger Width/Height of CVS was observed. A W/H of CVS>0.69 had a sensitivity of 91.0%, specificity of 68.2%, and accuracy of 87% for identifying a SS approach application, shown in **Figure 2**, **Table 2**.

Electrophysiological Mapping and Ablation

A series of mapping and ablation parameters of successful ablated DGCV-AIV VAs by NS approach and by SS approach were also compared. There were no significant differences in the local ventricular activation time relative to the QRS onset (V-QRS), ventricular capture ratio, pace-match leads, procedure time, RF duration, number of RF lesions, and fluoroscopic time. The operation time in CVS by SS approach was slightly longer than by NS approach, shown in **Table 3**.

Complications during the procedure by the NS approach and the SS approach were also compared. There were no significant

TABLE 1 | Comparison of Catheter tip reaching sites and success rate between two manipulation methods (Cases, %).

	Group		
	NS approach ($n = 123$)	**SS approach ($n = 79$)**	**-Value**
Coronary sinus	123 (100.00%)	79 (100.00%)	>0.05
Proximal GCV	114 (92.68%)	74 (93.67%)	>0.05
Middle GCV	110 (93.50%)	72 (91.14%)	>0.05
DGCV1	49 (39.84%)	70 (88.61%)	<0.00
DGCV2	43 (34.96%)	69 (87.34%)	<0.00
AIV	21 (17.07%)	30 (37.97%)	<0.00
Summit-CV	2 (1.63%)	7 (8.86%)	<0.05
Reaching target sites	44 (35.77%)	67 (84.81%)	<0.00
Successful ablation	38 (30.89%)	60 (75.75%)	<0.00

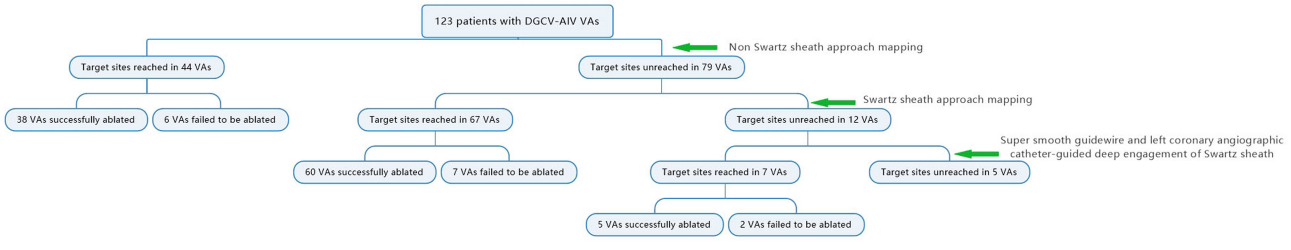

FIGURE 3 | Flowchart of mapping and ablation procedure in this study.

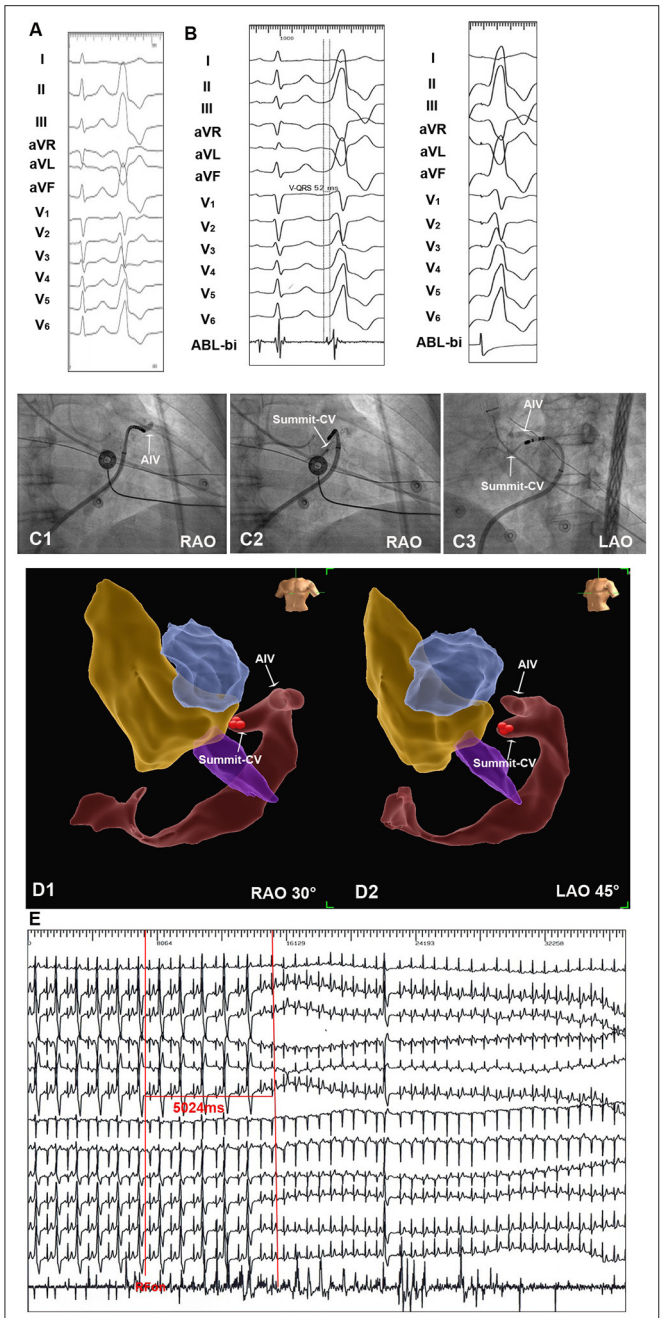

FIGURE 4 | An example of successful ablation of premature ventricular complex (PVC) originating from Summit-CV by SS approach. **(A)** Twelve-lead ECG 3 morphology of the clinical PVC. The PVC showed R wave in II, III, aVF, V4-V6, rS morphology in lead V1, the precordial transition zone of PVC was earlier than sinus beat. **(B)** By NS approach, the irrigated catheter could reach the distal portion of GCV. SS approach was then applied in this patient. By SS approach, the irrigated catheter reached the target site in summit-CV. The local ventricular activation time recorded at the summit-CV preceded the onset of the QRS complex by 52 ms, and a perfect pace-match was achieved by pacing at summit-CV. **(C1–C3)** Fluoroscopic view of the target site in summit-CV. **(D1,D2)** Three-dimension view of target site in Summit-CV. **(E)** Radiofrequency energy delivered on target site for 5 seconds led to an acute disappearance of target PVCs.

TABLE 2 | Reasons for failure of reaching target sites (Cases,%).

	Group		
	NS approach (*n* =123)	**SS approach (*n* =79)**	***P*-Value**
Obstacle of Venous valves	13	7	>0.05
Narrow angle between DGCV2 and AIV (>83°)	22/43	33/69	>0.05
Failure to reach Summit-CV	121	72	<0.05
Width/Height ratio>0.69	14/44	60/67	<0.05

TABLE 3 | Comparison of electrophysiological study and radiofrequency catheter ablation of successful ablated VAs between two manipulation methods.

	Group		
	NS approach (*n* = 38)	**SS approach (*n* = 60)**	***P*-Value**
V-QRS, ms	−34.52 ± 6.73	−34.87 ± 5.66	>0.05
Ventricular capture	32 (84.21%)	55 (84.61%)	>0.05
Pace match leads	11.22 ± 1.34	11.40 ± 1.65	>0.05
Procedure time, min	64.18 ± 12.64	67.11 ± 15.09	>0.05
Operation in CS, min	32.63 ± 5.27	40.72 ± 4.43	<0.05
RF duration, s	147.65 ± 58.61	142.03 ± 61.37	>0.05
No. of RF lesions	1.74 ± 0.58	1.77 ± 0.64	>0.05
Fluoroscopic time, min	10.98 ± 4.98	11.98 ± 5.33	>0.05

TABLE 4 | Comparison of complications between these two manipulation methods (Cases,%).

	Group		
	NS approach (*n* = 123)	**SS approach (*n* = 79)**	***P*-Value**
Coronary vein dissection	2	3	>0.05
Coronary vein rupture	1*	2#	>0.05
Cardiac tamponade	0	2#	>0.05
Delayed pericardial effusion	1*	0	>0.05
Coronary artery injury	1	1	>0.05
Coronary artery spasm	0	1	>0.05
Death	0	0	>0.05
Total complications	4 (3.25%)	7 (8.86%)	>0.05

**the same patients in the manipulation without long sheath group; #the same patients in the manipulation with long sheath group.*

differences in complications between these two groups (4/123, 3.25% vs. 7/79, 8.86%, $p > 0.05$). Via SS approach, coronary vein dissection happened on three patients and coronary vein rupture happened on two patients. The two patients of coronary vein rupture developed cardiac tamponade but turned into hemodynamic stability post-emergent pericardiocentesis. One patient has severe chest pain with CAG showing an acute irreversible 50% coronary stenosis in LAD, another patient had

an episode of chest tightness, and coronary angiography revealed coronary spasm of LCx, relieved by intravenous nitroglycerin. By NS approach, coronary vein dissection happened on two patients and coronary vein rupture occurred on one patient. Coronary vein rupture caused delayed pericardial effusion but without hemodynamic instability, thus pericardiocentesis was not performed. Coronary spasm occurred on one patient but was relieved by intravenous nitroglycerin, shown in **Table 4**.

DISCUSSION

Major Findings

This study reports for the first time that VAs arising from DGCV-AIV can be mapped and ablated by the Swartz sheath support approach with high efficiency and success rate compared to the non-Swartz sheath support approach. Width/height of coronary venous system>0.69 favored a SS approach. However, an angle between DGCV and AIV<83° indicated an inaccessible AIV by ablation catheter.

RFCA VAs Arising From DGCV-AIV

A total of 2768 VAs received RFCA in our cardiac lab, and 4.44% VAs (123/2768) were found arising from the region of DGCV-AIV. Successful ablation was achieved in 102 patients (102/123). As is well-known, DGCV-AIV is the epicardial part of LVOT, the myocardium near the DGCV-AIV can be a source of idiopathic VAs. Yamada T et al. studied 27 consecutive patients with VAs originating from the epicardial LVOT and achieved successful ablation within the DGCV in 14 patients (5). Hachiya H et al. also reported successful catheter ablation of idiopathic VAs originating from the AIV (6). More recently, Yuki K et al. reported that 14 patients were found to have summit-CV VAs and successful ablation was achieved in 10 (71%) patients (7). Therefore, VAs arising from DGCV-AIV were not a rare phenomenon and catheter ablation is an effective treatment for DGCV-AIV VAs.

Catheter Ablation Approach for DGCV-AIV VAs

Previous studies have revealed that one key point for successful ablation of DGCV-AIV VAs is the structure of DGCV-AIV being sufficiently accessed and mapped. However, the existence of anatomic obstacles in the coronary venous system limited the ablation catheter manipulation and access to the target sites in this region. In some cases, even advancing the ablation catheter to the proximal GCV is difficult. In our study, due to the obstacle of venous valves, the catheter tip could not reach the proximal-middle GCV by NS approach and SS approach in seven patients. One study reported in one patient with DGCV VAs, because of the tortuous course of GCV, catheter ablation could not access the optimal target site of VAs (8). The deflectable sheath and contact force ablation catheter was then advanced alternately, overcoming the deflection of GCV, leading to a deep engagement of catheter tip to DGCV, and achieving successful ablation consequently. However, this method had its limitations and might not be widely applied to most patients. In patients with a coronary venous system smaller in size, it could be challenging to manipulate the contact force catheter and steerable sheath, as both of which were much larger than the conventional irrigated catheter and sheath in diameter. Besides, the much harder characteristics of steerable sheath and contact force catheter may more easily cause coronary vein dissection and rupture. Another study also reported anatomic obstacles that restrained successful ablation of DGCV-AIV VAs (7). Due to the very distal portion of DGCV are usually very thin and frequently inaccessible to an ablation catheter, Kazutaka A et al. delivered a 2F microcatheter into the vein as a landmark of the ablation sites and performed ablation in the nearby endocardial structures. However, by this approach, the elimination of these VAs usually requires ablation at multiple sites at adjacent structures and because of indirect ablation, the efficacy of RFCA was usually limited and more complications unpredictable. In our research, we detected that in a situation of a narrow elliptical shape of CVS (Width/Height>0.69), SS approach ensured a powerful backup force for ablation catheter, which could assist the catheter tip in overcoming partial anatomic impediments of the coronary venous system and reach the target sites in DGCV-AIV more easily, contributing to a relatively higher success rate of RFCA. Thus, it was more favorable than the NS approach when RFCA of DGCV-AIV VAs. Nonetheless, we found an acute angle between AIV and DGCV was in fact an anatomic obstacle difficult to overcome no matter whether an NS approach or SS approach was applied, for which, the appropriate manipulation approach remains to be investigated. In addition, It should be noted that when catheter ablation of DGCV-AIV VAs, anatomic obstacles are not the only factors that restrain successful ablation. In clinical practice, successful ablation of DGCV-AIV VAs is associated with a network of factors, including origin sites (epicardial but not intramural), distance to adjacent coronary artery (distal but not proximal), impedance (not too high to limit energy delivery) during ablation and so on. In our study, failed ablation happened on 15 patients with good target sites accessed by catheter tip. The reasons underlying the failure are mostly the factors mentioned above.

Complications of Swartz Sheath Support Approach for DGCV-AIV VAs

Of note, a relatively higher rate of cardiac vein dissection and rupture was observed in the SS approach. We speculated that while the SS approach application provided a better backup for catheter manipulation, it also increased the contact force of the catheter tip to the coronary vein, contributing to a higher incidence of coronary vein damage.

In our study, coronary injury was found in both groups. Though the safe distance from the catheter tip to the adjacent coronary artery has been demonstrated by coronary angiography, coronary injury is still a potential complication, which could not be neglected.

Study Limitations

As the study was retrospective research, results need to be confirmed by prospective studies. Further studies with multi-center cooperation and a larger sample size are needed to confirm the findings.

CONCLUSION

VAs arising from DGCV-AIV is not a rare phenomenon. For catheter ablation of DGCV-AIV VAs, the Swartz sheath support approach facilitates the access of target sites and improves the success rate of RFCA.

DATA AVAILABILITY STATEMENT

The original contributions presented in the study are included in the article/supplementary material, further inquiries can be directed to the corresponding authors.

ETHICS STATEMENT

The studies involving human participants were reviewed and approved by Second Affiliated Hospital and Yuying Children's Hospital's Ethics Committee. The patients/participants provided their written informed consent to participate in this study. Written informed consent was obtained from the individual(s) for the publication of any potentially identifiable images or data included in this article.

AUTHOR CONTRIBUTIONS

CZ and J-FL designed and drafted the original research. CZ, W-QL, Y-JW, Q-QJ, F-ZL, JL, and J-FL performed the follow-up and data analysis for the study. All authors approved it for publication.

FUNDING

This work was supported by the Wenzhou Municipal Science and Technology Commission (grant no. ZY2020018), the Zhejiang Provincial Natural Science Foundation (grant no. LY21H020011), and the National Natural Science Foundation of China (grant no. 82070333). The funders had no role in study design, data collection, and analysis, decision to publish, or preparation of the manuscript.

REFERENCES

1. Habib A, Lachman N, Christensen KN, Asirvatham SJ. The anatomy of the coronary sinus venous system for the cardiac electrophysiologist. *Europace.* (2009) 11(Suppl. 5):v15–21. doi: 10.1093/europace/eup270
2. Chen YH, Lin JF. Catheter ablation of idiopathic epicardial ventricular arrhythmias originating from the vicinity of the coronary sinus system. *J Cardiovasc Electrophysiol.* (2015) 26:1160–7. doi: 10.1111/jce.12756
3. Liao Z, Zhan X, Wu S, Xue Y, Fang X, Liao H, et al. Idiopathic ventricular arrhythmias originating from the pulmonary sinus cusp: prevalence, electrocardiographic/electrophysiological characteristics, and catheter ablation. *J Am Coll Cardiol.* (2015) 66:2633–44. doi: 10.1016/j.jacc.2015.09.094
4. Ouyang F, Mathew S, Wu S, Kamioka M, Metzner A, Xue Y, et al. Ventricular arrhythmias arising from the left ventricular outflow tract below the aortic sinus cusps: mapping and catheter ablation via transseptal approach and electrocardiographic characteristics. *Circ Arrhythm Electrophysiol.* (2014) 7:445–55. doi: 10.1161/CIRCEP.114.001690
5. Yamada T, McElderry HT, Doppalapudi H, Okada T, Murakami Y, Yoshida Y, et al. Idiopathic ventricular arrhythmias originating from the left ventricular summit: anatomic concepts relevant to ablation. *Circ Arrhythm Electrophysiol.* (2010) 3:616–23. doi: 10.1161/CIRCEP.110.939744
6. Hachiya H, Hirao K, Nakamura H, Taniguchi H, Miyazaki S, Komatsu Y, et al. Electrocardiographic characteristics differentiating epicardial outflow tract-ventricular arrhythmias originating from the anterior interventricular vein and distal great cardiac vein. *Circ J.* (2015) 79:2335–44. doi: 10.1253/circj.CJ-15-0476
7. Komatsu Y, Nogami A, Shinoda Y, Masuda K, Machino T, Kuroki K, et al. Idiopathic ventricular arrhythmias originating from the vicinity of the communicating vein of cardiac venous systems at the left ventricular summit. *Circ Arrhythm Electrophysiol.* (2018) 11:e005386. doi: 10.1161/CIRCEP.117.005386
8. Kumagai YU, Arimoto T, Iwayama T, Hashimoto N, Watanabe T, Kubota I. Contact force-guided deep engagement with a steerable sheath in the distal great cardiac vein: a case report. *Pacing Clin Electrophysiol.* (2016) 39:507–10. doi: 10.1111/pace.12826

Conflict of Interest: The authors declare that the research was conducted in the absence of any commercial or financial relationships that could be construed as a potential conflict of interest.

Publisher's Note: All claims expressed in this article are solely those of the authors and do not necessarily represent those of their affiliated organizations, or those of the publisher, the editors and the reviewers. Any product that may be evaluated in this article, or claim that may be made by its manufacturer, is not guaranteed or endorsed by the publisher.

frontiers in Cardiovascular Medicine

ORIGINAL RESEARCH
published: 27 January 2022
doi: 10.3389/fcvm.2021.793903

Experimental Findings and Clinical-Pathologic Correlation of Radiofrequency Catheter Ablation at the Left Ventricle Para-Hisian Region

Zuyi Fu[1†], Zili Liao[1†], Jinlin Zhang[2], Xianzhang Zhan[1], Weidong Lin[1], Fang Zhou Liu[1], Xi Su[2], Hai Deng[1], Xianhong Fang[1], Hongtao Liao[1], Hongyue Wang[3], Shulin Wu[1], Yumei Xue[1,4] and Feifan Ouyang[1,2,5*]*

[1] Department of Cardiology, Guangdong Provincial People's Hospital, Guangdong Academy of Medical Sciences, Guangzhou, China, [2] Department of Cardiology, Wuhan Asian Heart Hospital, Wuhan, China, [3] Department of Pathology, National Center for Cardiovascular Diseases, Fuwai Hospital, Chinese Academy of Medical Sciences and Peking Union Medical College, Beijing, China, [4] Southern Medical University, Guangzhou, China, [5] Universitäres Herz- und Gefäßzentrum, University Hospital Eppendorf, Hamburg, Germany

Background: Catheter ablation target at the site with large His activation in the left ventricle poses a high risk of atrioventricular (AV) block. We aimed to identify far-field (FF) and near-field (NF) His activation at left upper septum (LUS).

Methods: Three-D mapping of the aortic root and left ventricle was performed in 12 dogs. Two sites located at either the base or apex of the triangle interposed between the hinges of the the noncornary coronary cusp (NCC) - right coronary cusp (RCC) were chosen for a single radiofrequency (RF) application. Bipolar and unipolar pacing with different outputs at both sites was attempted to discern NF and FF His activation.

Results: The sites chosen for NF and FF ablation were located at the base and apex of the triangle, which were 8.03 ± 1.18 mm (group 1) and 3.42 ± 0.61 mm (group 2) away from the RCC-NCC junction. Lower A/V ratios were found in group 1. Pacing could not differentiate NF from FF His activation. In group 1, ablation resulted in III degree AV block in all 6 dogs, whereas neither PR prolongation nor AV block occurred in group 2. Pathologic examination of group 1 showed complete/partial necrosis of the His bundle (HB) and left bundle branch in all 6 dogs. In group 2, no necrosis of the HB was seen in the 6/6 dogs.

Conclusion: Anatomical localization in the triangle of RCC-NCC junction can help differentiate NF from FF His activation.

Keywords: his bundle, 3-D anatomical, catheter ablation, pathology, pacing

OPEN ACCESS

Edited by:
Tamas Szili-Torok, Erasmus Medical Center, Netherlands

Reviewed by:
Yoshifumi Fukushima, Juntendo University, School of Medicine, Japan
Evgeny Lyan, University Medical Center Schleswig-Holstein, Germany
Hussam Ali, MultiMedica Holding SpA (IRCCS), Italy

***Correspondence:**
Feifan Ouyang
f.ouyang@uke.de
Yumei Xue
xymgdci@163.com

[†] These authors have contributed equally to this work and share first authorship

Specialty section:
This article was submitted to Cardiac Rhythmology, a section of the journal Frontiers in Cardiovascular Medicine

Received: *12 October 2021*
Accepted: *22 December 2021*
Published: *27 January 2022*

Citation:
Fu Z, Liao Z, Zhang J, Zhan X, Lin W, Liu FZ, Su X, Deng H, Fang X, Liao H, Wang H, Wu S, Xue Y and Ouyang F (2022) Experimental Findings and Clinical-Pathologic Correlation of Radiofrequency Catheter Ablation at the Left Ventricle Para-Hisian Region. Front. Cardiovasc. Med. 8:793903. doi: 10.3389/fcvm.2021.793903

INTRODUCTION

Understanding the anatomy and identification of near-field (NF) and far-field (FF) His activation of the Para-Hisian (PH) area is critical for catheter ablation of PH arrhythmias (1, 2). Catheter ablation targeted at the site with a large His activation in the left ventricle (LV) can lead to a high risk of atrioventricular (AV) block, often abortion of procedures or targeting of neighboring sites

associated with high recurrence rates. Our previous studies demonstrated that (1) the His potential with either FF or NF activation is widely distributed in the right PH region, and the NF or FF His activation can be identified using systematic pacing maneuvers; (2) ablation at the site with FF His activation can be safely performed without injuring the AV conduction system (AVCS) (1, 2). Our strategy is widely used to guide radiofrequency (RF) ablation of right-sided PH arrythmias including PH accessory pathways and ventricular arrhythmias. However, it was unknown whether this strategy can be extrapolated to left upper septal ablation. The aim of this study was to investigate the distribution of His activation at the left upper septum (LUS) below the noncornary coronary leaflet (NCL)- right coronary leaflet (RCL) junction, to identify FF and NF His activation within the region using pacing techniques, to deliver a single RF ablation at the apex or base of the triangle interposed between the hinges of the NCL and RCL of the aortic root and finally to correlate with clinical and pathological characteristics of AVCS injury in the canine model. We include a case of successful ablation of a left PH accessory pathway in a patient with previous failed ablation attempts.

METHOD

Electrophysiological Procedure

Twelve mongrel dogs with a weight of 27.1 ± 3.5 kg (range 22.0–33.5 kg) were anesthetized and intubated with an endotracheal tube and mechanically ventilated as previously reported (1). High frequency/low tidal volume with a volume of 200 ml and a frequency of 30 breaths per minute (bpm) was used during mapping and ablation in the left PH region. Standard limb and V1, V3 and V5 leads of the surface ECG were continuously monitored and documented throughout the entire procedure. Subsequently, two 6F catheters were placed into the coronary sinus (CS) and at the right ventricle under fluoroscopic guidance *via* the right jugular vein and left femoral vein, respectively. All bipolar intracardiac electrograms were filtered at 30–500 Hz and recorded using a LABSYSTEM^{TM} EP recording system (Bard, Boston-Scientific, MA, USA). Programmed atrial stimulation from the CS was performed to determine the antegrade conduction over the AVCS.

Three-Dimensional Electro-Anatomical Map

3-D electro-anatomical mapping (CARTO, Biosense Webster, CA, USA) of the LV was performed as previously reported (3). In brief, mapping was performed using a 7.5F D-curve catheter with a 3.5-mm irrigated-tip electrode (Navistar Thermo-Cool; Biosense Webster, Diamond Bar, CA). Initially, the aortic root was mapped via a retrograde approach to identify the noncornary coronary cusp (NCC), right coronary cusp (RCC) and left coronary sinuses (LCC), to highlight the anatomical location of LUS in the LV. Subsequently, high-density mapping of the LV was performed at the LUS including identification of the HB, left bundle branch(LBB) and proximal branch of the LBB during sinus rhythm (SR) (**Figure 1**). The transseptal approach with an 8.5F SL1 long sheath (St Jude, Minneapolis, MN, USA) was attempted to reach the upper septal region with a reverse S curve of the ablation catheter (**Figures 1D,E**) (3). Activation mapping was performed as previously reported (1). The site of the His potential in the LV, which, defined as the potential with the longest interval from the Purkinje potential to the ventricular activation as well as an atrial activation, was tagged on the 3-D map (**Figure 1A**).

Pacing Protocol at the Region With His Activation

Unipolar and bipolar pacing from the mapping catheter was performed as previously reported (1). The pacing protocol consisted of different pacing currents (20, 10 and 5 mA) at different pulse widths (2, 1 and 0.5 ms). Pacing with a cycle length of 400–450 ms was only performed at the sites with His activation within the LUS below the NCC-RCC junction. The resultant paced QRS morphologies were showed as **Figure 2**. The following parameters were analyzed on the recording system at the paced sites: (1) the amplitude of atrial and ventricular potentials, and the A/V amplitude ratio; (2) the amplitude of His potential; and (3) the H-QRS, the stimulus-to-QRS and the QRS duration during pacing and SR.

Radiofrequency Ablation Protocol

RF energy was delivered as previously reported (1). Before ablation, a 5F catheter was positioned in the right ventricle apex for back-up pacing if AV block occurred. In every dog, only a single application of irrigated RF energy was delivered in power-controlled mode with a power of 30 W and a flow rate of 17 mL/min and maintained for 60 seconds.

In this study, two sites with His activation within LUS below the NCC-RCC junction were chosen for a single RF application. The anatomical site was located at the base of the triangle between the hinges of the RCC and NCC in 6 dogs (group 1) and at the apex of that in 6 dogs (group 2). During RF delivery, the PR interval, abnormal ventricular ectopy or rhythm and catheter movement were continuously monitored. An abnormal ventricular ectopy or rhythm was defined as originating from Purkinje system if a distinct Purkinje activation preceded the QRS during RF ablation. AH and HV intervals were repeatedly measured immediately after the procedure in cases of no AV block. Also, the distance between the targeted site in the LV and the NCC-RCC junction was measured on the 3-D map.

For those dogs with third-degree AV block, a single chamber Sigma permanent ventricular pacemaker was implanted, being programmed to VVI mode with a rate of 120 beats per minute.

Follow-Up

All dogs were kept alive with continuous monitoring for 12–14 days to investigate whether AV and bundle branch (BB)

Abbreviations: AV, atrioventricular; AVCS, AV conduction system; BB, bundle branch; CS, coronary sinus; FF, far-field; IMS, interventricular membranous septum; LBB, left bundle branch; LCC, left coronary sinuses; LUS, left upper septum; LV, left ventricle; NCC, noncornary coronary cusp; NCL, noncornary coronary leaflet; NF, near-field; PB, penetrating bundle; RBB, right BB; RBBB, RBB block; RCC, right coronary cusp; RCL, right coronary leaflet; RF, radiofrequency; SR, sinus rhythm.

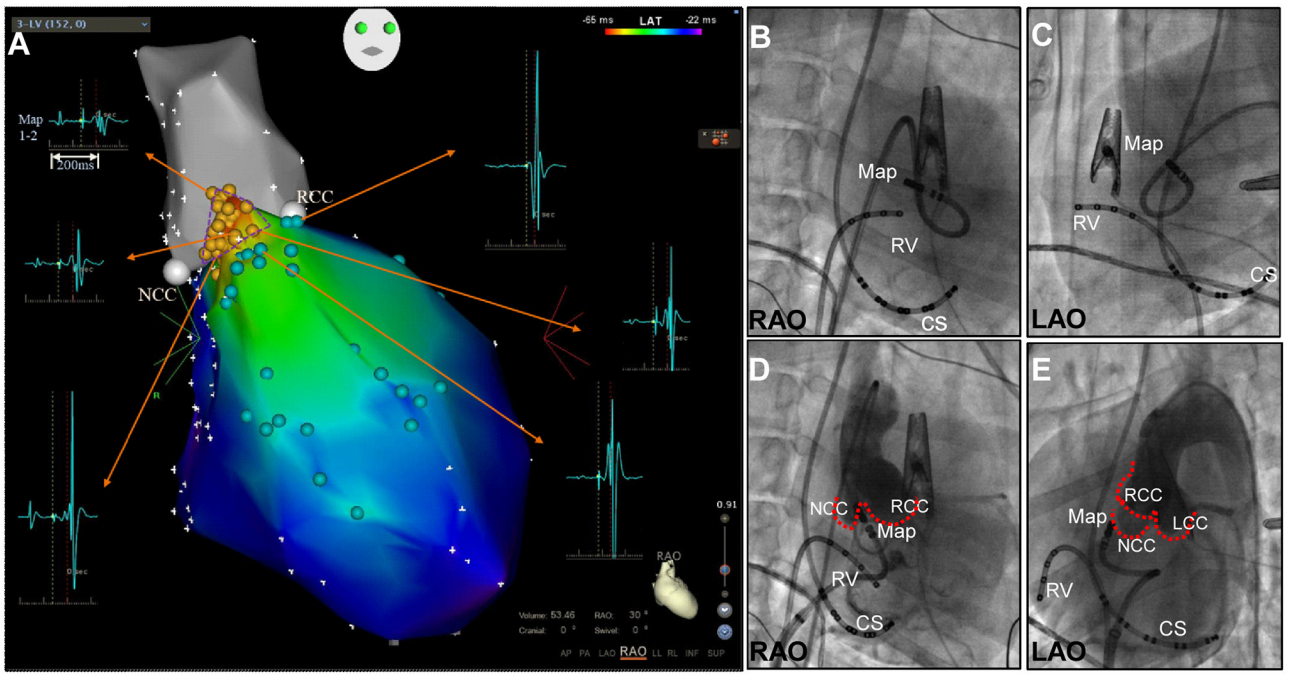

FIGURE 1 | (A) Three-dimensional mapping of the aortic root (grey) and upper septal region in the left ventricle in right anterior oblique (RAO) view. A small triangular area with His activation was found between the NCC and RCC. His activation (yellow points), bundle branch potential and branches (light green points). **(B-E)** Fluoroscopic right anterior oblique (RAO) and left anterior oblique (LAO) views demonstrating mapping at the apex of the NCC-RCC junction via the retrograde transaortic approach **(B,C)** and transseptal approach with the reverse S-curve **(D,E)**. CS, coronary sinus; LCC, left coronary cusp; Map, mapping catheter; NCC, non-coronary cusp; RCC, right coronary cusp; RV, right ventricle.

block persisted, and then sacrificed for pathological examination. Standard and V1, V2 and V3 leads of surface ECGs were recorded under anesthesia with intramuscular administration of ketamine hydrochloride (6 mg/kg) and continuous mask ventilation before sacrificing.

Pathologic Examination

Pathologic examination was performed as previously reported (1). All tissue sections were stained with hematoxylin and eosin and Masson trichrome using routine protocols. The ablation lesion and its related conduction tissue injury were histologically determined at the tissue section with the maximum ablation injury (**Figure 3**) (3). In this study, the HB was defined as including the penetrating bundle (PB) within the septum and BB, which extends from the PB to the beginning of the junction of the LBB and right BB (RBB).

Statistical Analysis

Data are expressed as the mean ± SD or medians with minimum and maximum values. For comparison between groups, the Mann-Whitney *U*-test was used for the continuous variables. A two-sided $P < 0.05$ was considered statistically significant. Analyses were performed using IBM SPSS Statistics 22.

RESULTS

Basic Electrophysiological and Mapping Data

There was no statistical difference in the baseline AH, HV intervals and QRS duration during SR between the two groups. LV mapping was performed via only the transaortic approach in 6 (#4, #5 and #6 in group 1, #2, #4 and #6 in group 2) and via both transaortic and transseptal approaches in the other 6 dogs. High-density maps in the aortic root and around the LUS below the NCC-RCC junction were successfully achieved with 51 ± 13 (range 33–74) points and 56 ± 25 (range 24–104) points. A small triangular area with His activation was found below the NCC-RCC junction in all 12 canine models. This small triangular area measured 0.950 ± 0.197 cm∧2 (range 0.6–1.2 cm∧2) via an only transaortic approach and 0.933 ± 0.334cm∧2 (range 0.6–1.5cm∧2) via both transaortic and transseptal approaches ($P = 0.805$). The distance between the apex of the triangle and the middle base of the triangle was 8.95 ± 2.32 mm in these 12 dogs. The amplitude of atrial, His and ventricular activation were 0.70 ± 0.50 mV, 0.51 ± 0.35 mV, and 1.41 ± 0.85 mV at the apex of the triangle, and 0.42 ± 0.33 mV, 0.37 ± 0.20 mV, and 4.45 ± 3.70 mV at the middle base of the triangle, respectively. An FF His activation was recorded above the NCC-RCC junction in all 12 dogs, with the amplitude of 0.22 ± 0.12 mV.

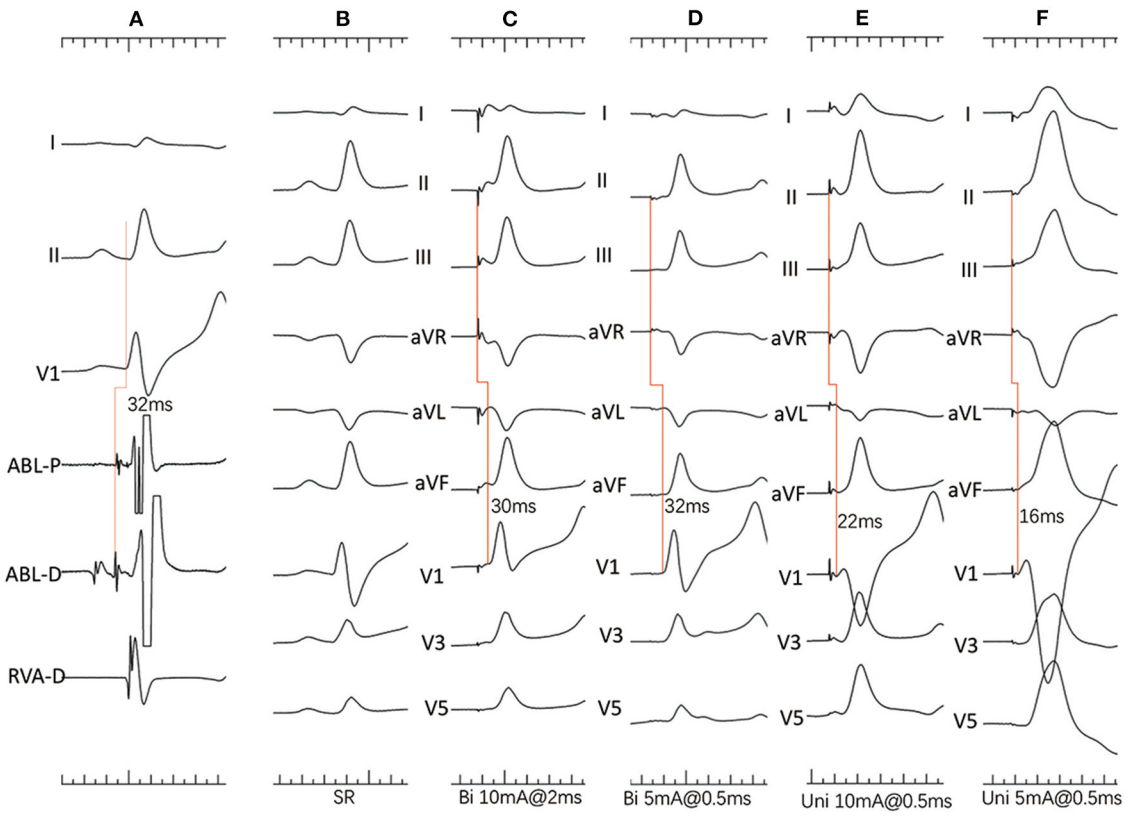

FIGURE 2 | (A–F) Dog #2 (group 2). **(A)** Surface ECG leads I, II, V1, and intracardiac recordings from a quadrupolar catheter in the right ventricle and mapping catheter (ABL) at the apex of the NCC-RCC junction. Note that the H-V interval is 30ms with atrial and His activation on distal electrodes. **(B)** Surface 12-lead ECG during sinus rhythm (SR). **(C)** Bipolar pacing with 10 mA, 2 ms shows slightly different morphology from SR with narrow QRS duration, indicating both myocardial and His capture. **(D)** Bipolar pacing with 5 mA, 0.5 ms shows paced QRS morphology identical to that during SR and a long stimulus to QRS interval indicating pure HB capture. **(E)** Unipolar pacing with 10 mA, 0.5 ms shows narrow QRS complexes with short stimulus-to-QRS interval, indicating both myocardial and His capture. **(F)** Unipolar pacing with 5 mA, 0.5 ms shows wide QRS complexes indicating only myocardial capture.

Pacing Protocol at the Apex and Middle Buttom of the Triangle With His Activation

Two sites were chosen for ablation after completing the pacing protocol. One was located at the base of the triangle between the hinges of the RCC and NCC 8.03 ± 1.18 mm away from the apex (group1) and the other was at the apex 3.42 ± 0.61 mm away from the RCC-NCC junction ($P = 0.004$) (**Table 1**). The His and atrial amplitudes were not significantly different between both groups. However, the amplitude of ventricular activation was significantly larger in group 1 ($P = 0.01$), with a lower A/V ratio ($P = 0.01$). The pacing protocol was performed via transaortic approach in three and transseptal approach in three in each group.

In group one, the minimal output required to capture the HB with bipolar pacing was 5 mA/0.5 ms in all six dogs, and with unipolar pacing was 5 mA/0.5 ms in three dogs and 10 mA/0.5 ms in the remaining 3 dogs. Bipolar paced QRS duration and Stimulus-to-QRS intervals were 96.00 ± 7.48 ms and 32.00 ± 2.83 ms, whereas unipolar paced QRS duration and Stimulus-to-QRS intervals were 96.80 ± 5.22 ms and 28.80 ± 8.67 ms. In dog #3, minimal output during unipolar pacing resulted in simultaneous atrial capture. Pure HB capture was observed in five with minimal bipolar pacing output and in one dog with minimal unipolar pacing output.

In group 2, the minimal output required to capture the HB with bipolar pacing was 5 mA/0.5 ms in 3, 10 mA/0.5 ms in 1, 10 mA/1 ms in 1 and 10 mA/2 ms in one dog. Whereas the minimal output required to capture the HB with unipolar pacing was 10 mA/0.5 ms in 3, 10 mA/1 ms in 2 and 10 mA/2 ms in 1 dog. Bipolar paced QRS duration and Stimulus-to-QRS intervals were 92.67 ± 12.24 ms and 30.33 ± 4.46 ms. Unipolar paced QRS duration and Stimulus-to-QRS intervals were 100.67 ± 15.47 ms and 26.00 ± 7.48 ms. Pure HB capture was observed in 3 dogs with bipolar pacing and none with unipolar pacing.

There was no significant difference in paced output between bipolar and unipolar pacing in both groups. Also, the paced QRS duration and Stimulus-to-QRS interval in both groups were not significantly different with bipolar or unipolar pacing.

Irrigated RF Ablation

In group 1, a single RF application was delivered at the middle base of the triangle interposed between the hinges of the RCC

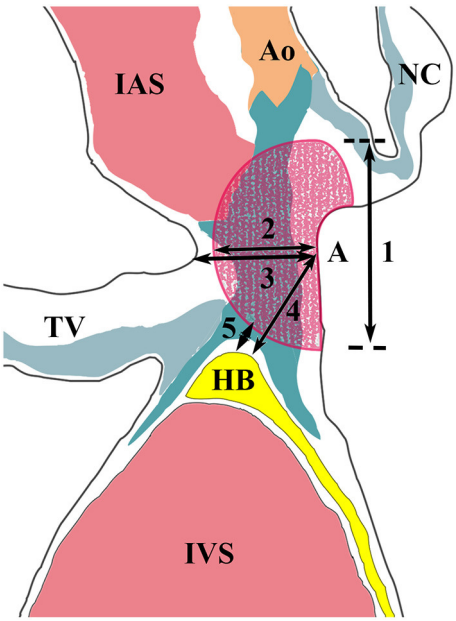

FIGURE 3 | Measurements of the ablation lesion and its related conduction tissue injury. Segments 1 and 2 represent the diameter and depth of the ablation lesion. Segment 3 represents the thickness of the interventricular septum at the ablation site. Segment 4 shows the distance between the ablation site and the His bundle. Segment 5 represents the shortest distance between them. Ao, aorta; HB, His bundle; IAS, interatrial septum; IVS, interventricular septum; NC, non-coronary leaflet; TV, tricuspid valve.

TABLE 1 | Eletrophysiologic study, mapping, and ablation data.

	Gruop1	Gruop2	*P* values
AH interval (ms)	62 ± 16	53 ± 10	0.15
HV interval (ms)	32 ± 2	33 ± 5	0.93
Wenckenbach cycle (ms)	262 ± 40	242 ± 43	0.47
Local amplitude at targeted site (mV) Atrial activation	0.24 ± 0.13 (0.13–0.48)	0.34 ± 0.26 (0.14–0.79)	0.75
Ventricular activation	2.40 ± 1.76 (0.54–4.39)	0.52 ± 0.26 (0.28–0.99)	0.01
A/V ration	0.15 ± 0.09 (0.07–0.24)	0.79 ± 0.81 (0.22–2.38)	0.01
His activation	0.28 ± 0.19 (0.15–0.65)	0.25 ± 0.15 (0.05–0.44)	1.00
The targeted site to the NCC-RCC apex (mm)	8.03 ± 1.18 9.4) (6.5–9.4)	3.42 ± 0.61 (2.5–4.3)	0.04

*Abbreviations as in **Figure 1**.*

and NCC. RF energy resulted in immediate Purkinje-associated ventricular rhythm, with a narrow QRS morphology in one, wide QRS morphology with RBB block(RBBB) and superior axis in three and alternating narrow and wide QRS morphology in 2 dogs. III degree AV block was observed after cessation of the junctional rhythm in all 6 dogs (**Figure 4A**). A slow junctional escape rhythm with cycle lengths of 1,358 ± 537 ms (616–2096 ms) was recorded after the ablation. A VVI pacemaker with HR set at 120 bpm was immediately implanted via the right jugular vein.

In group 2, a single RF application was delivered at the apex of the triangle. PR prolongation and AV block was not observed during the single RF ablation. However, Purkinje-associated junctional beats or salvos were infrequently observed in 3 dogs. In dog #2, RBBB and left anterior fascicle block developed 28.8s after ablation via a transaortic approach and persisted until the end of the procedure (**Figure 4B**). In dog #5, via a transseptal approach, the RBBB and left anterior fascicle block were seen 47.4s following the start of ablation, and completely recovered 4.0s after stopping the RF application. At the end of the procedure, HV intervals were repeatedly measured and remained unchanged from baseline in all 6 dogs.

Follow-Up

In group 1, dog #1 had undergone pacemaker implantation and died suddenly 1 day after ablation. Pathological examination found a myxoma on each side of the interatrial septum near the inferior margin of the fossa ovalis. The right myxoma was ruptured with a short stump at the fossa ovalis. The long section (56 mm length, 4–10 mm width) had embolized into the right ventricular outflow tract. It was most likely due to the transseptal approach. The left-sided myxoma (50 mm length, 4–10mm width) remained intact. In the other 5 dogs, ECG recordings showed persistent paced rhythm with heart rate of 120 beats/min and AV dissociation.

In group 2, PR prolongation and AV block was not observed in any dogs. In dog #2, RBBB with left anterior fascicle block remained even on Day 14 post ablation.

Pathologic Findings

Pathological examination was performed 12–14 days after ablation in both groups except dog #1 from group 1, who underwent pathological assessment 1 day after the ablation. Focal hemorrhage was found only in the tricuspid valve in 2/5 dogs in group 1 and 1/6 in group 2. Infective endocarditis was found on the tricuspid valve and left ventricular outflow tract in 1/5 from group 1 and 1/6 from group 2.

In group 1 where all dogs had persistent AV block (all at the infra nodal site), coagulative necrosis occurred just below the interventricular membranous septum (IMS) and extended into the PB,BB and LBB in dogs #3–#6 (**Figures 5A,B**). In dog #1, coagulative necrosis occurred infero-posterior to the IMS extended inferiorly and anteriorly and resulted in complete necrosis of the PB/BB and LBB and in dog #2, the lesion occurred in the IMS leading to complete necrosis of the PB/BB and incomplete necrosis of the LBB. However, there was no injury in the AVN and RBB in all 6 dogs of this group.

In group 2, coagulative necrosis was not found in dogs #4 and #6 with a transaortic approach. Coagulative necrosis was found at the postero-superior region of the IMS without any injury of the AVCS in dog #1. Coagulative necrosis was found below the NCC and extended anteriorly and superiorly, which resulted in complete necrosis of the RBB within the septum, and complete injury of the proximal left anterior fascicle, in

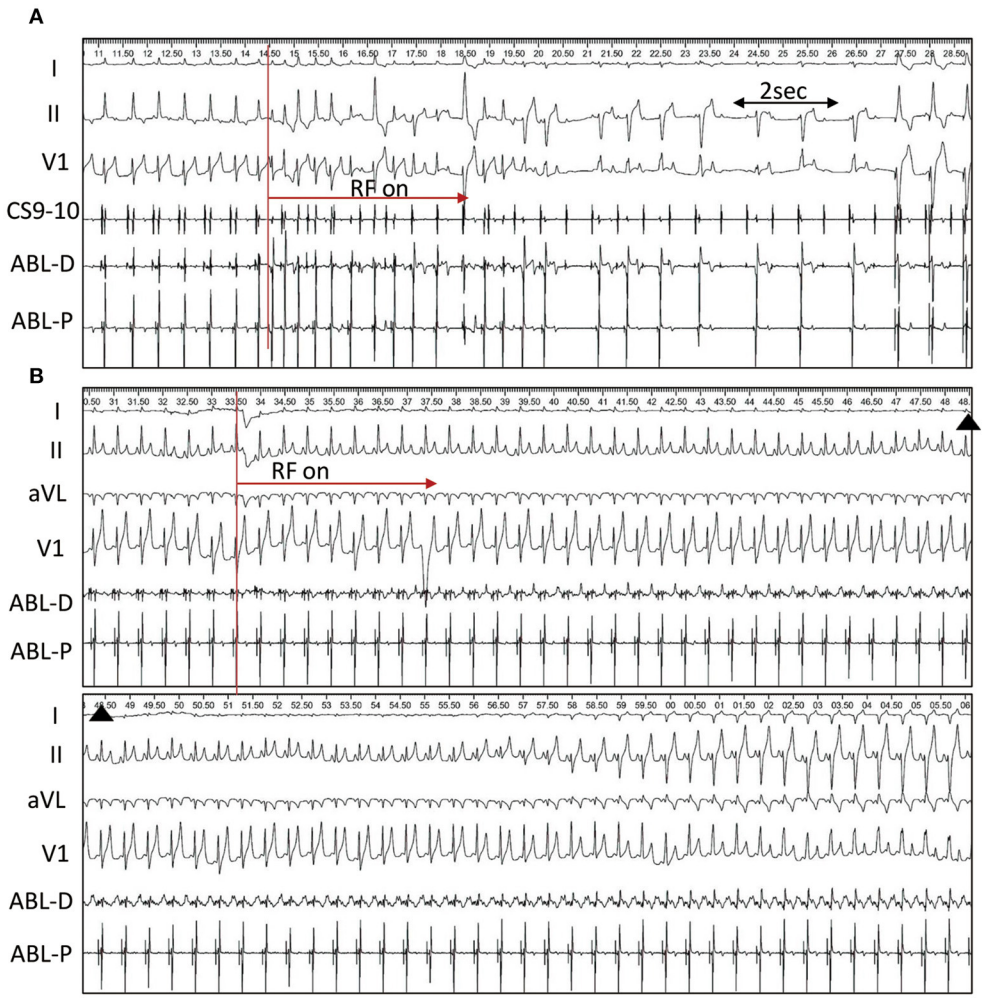

FIGURE 4 | Single RF application at the triangle. **(A)** Radiofrequency (RF) Ablation in dog #4 (group 1). RF energy delivery results in immediate alternating narrow and wide QRS junctional beats, and complete AVB occurs at 4.4s after ablation followed by ventricular paced rhythm. **(B)**, Ablation in dog #2 (group 2). Right bundle branch block and left anterior fascicular block occurs 28.8s after ablation and persists until the end of the procedure.

dog #2 with persistent RBBB and left anterior fascicle block after ablation (**Figures 5C,D**). In dog #5 with transient RBBB and left anterior fascicle block, coagulative necrosis was found at the IMS and extended to the upper margin of the RBB and resulted in partial necrosis of the RBB without involvement of the LBB.

There was no difference in the length of IMS (3.6 ± 0.6 vs. 3.3 ± 0.4; $P = 0.292$), the PB (5.22 ± 1.05 mm vs. 5.07 ± 1.57 mm; $P = 0.463$), the BB (5.33 ± 0.71 mm vs. 5.70 ± 1.13 mm; $P = 0.747$) and ablation lesion width (6.55 ± 1.17 mm vs. 5.08 ± 1.38 mm; $P = 0.109$) between the groups. However, the lesions in group 1 were markedly deeper than that in group 2 (5.20 ± 2.43 mm vs. 2.40 ± 0.87 mm; $P = 0.025$), which may be due to thicker tissue at the ablation sites in group 1 (5.10 ± 1.75 mm vs. 3.44 ± 1.15 mm; $P = 0.078$). In group 1, RF-related complete AV block demonstrated different levels of PB/BB necrosis.

Left Para-Hisian Accessory Pathway

A 32-year-old male presented with recurrent paroxysmal supraventricular tachycardia. Twelve-lead ECG in SR showed supra-paraseptal ventricular preexcitation. A transthoracic echocardiogram was normal. Two previous ablations at the right PH region and NCC failed to eliminate the antegrade and retrograde conduction of the accessory pathway, and RBBB developed after the second ablation. At the third procedure, the accessory pathway with a large His activation was successfully eliminated by ablation via a transseptal approach (**Figure 6**). Angiography of the aorta confirmed the position of catheter located at the apex of the IMS. No junctional beats occurred during ablation and the HV interval remained stable to that during tachycardia. No preexcitation on surface ECG or evidence of tachycardia-related symptoms was documented off antiarrhythmic drugs during a follow-up of 30 months.

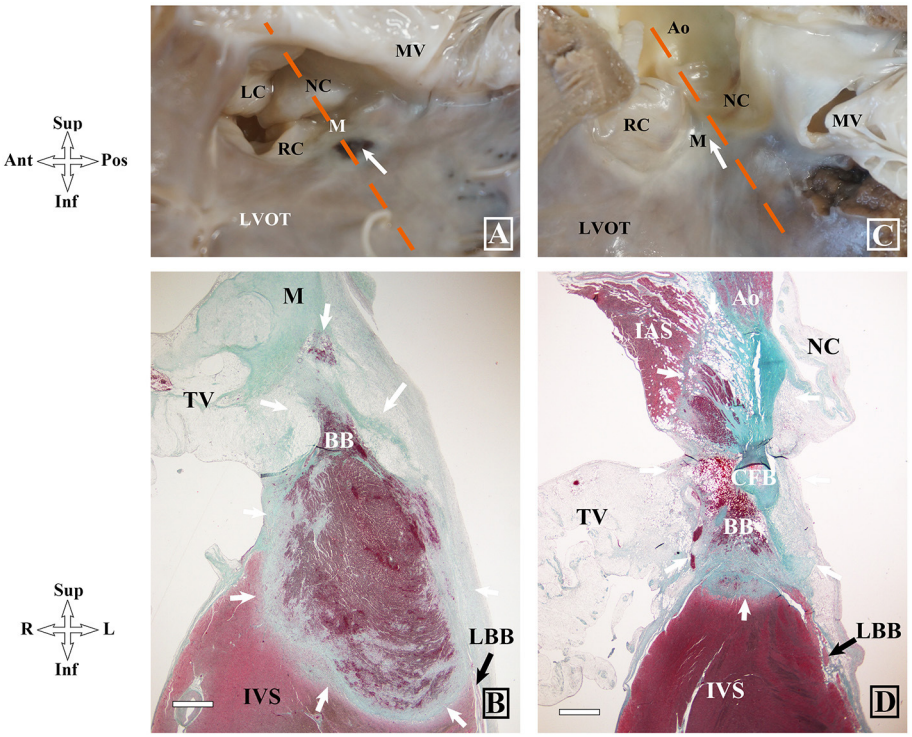

FIGURE 5 | Gross and histopathologic images of different locations of ablation lesions and related injuries on atrioventricular conduction system in dog hearts after radiofrequency delivery. **(A,B)** Coagulative necrosis is shown at the left upper septum below the IMS in dog #5 (group1). **(C,D)** Complete necrosis in the IMS in dog #2 (group2). BB, bundle branch; IMS, interventricular membranous septum; LAF, left anterior fascicle; LBB, left bundle branch; PB, penetrating bundle; RBB, right bundle branch; RC, right coronary leaflet; LC, left coronary leaflet.

DISCUSSION

This study describes the methods to identify the anatomical distribution of the left HB, and assesses the clinical-pathological correlation when RF application is targeted at LUS below the NCL-RCL junction.

Anatomical Distribution of the Left His Activation on 3-D Mapping

The LUS leans to the aortic valves. It is here the common atrioventricular conduction bundle emerges from the central fibrous body to pass along the base of the membranous septum and the crest of the muscular ventricular septum (4). In both the human and canine hearts, the atrioventricular node is uniformly located at the apex of the inferior pyramidal space. It is the presence or absence of the inferoseptal recess, therefore, that is the major difference between the two species. In turn, in canine and the minority of human hearts, a more extensive nonbranching bundle skirts half of the noncoronary aortic sinus (5). Our pathologic results showed that the length of IMS in canine was shorter than that in human heart, according closely with previous study (5, 6). The landmark for the site of the atrioventricular conduction bundle is the central fibrous body that adjoins the interleaflet triangle interposed between the hinges of RCL-NCL. From here, the LBB descends in the subendocardium and usually branches into three main fascicles.

Given the thin HB, the HB potential should not be recorded in a large area as frequently shown in 3D mapping. In this study, a triangular area (0.9 cm∧2) with a discrete His potential was found below the RCL-NCL junction using high-density mapping, via both the transaortic and transseptal approach. The anatomical distribution of the His activation was inconsistent with the anatomical assessment that the left His runs along the septal crest. The most possible explanation is FF vs. NF His activation at this area.

Identification of Near-Field and Far-Field His Activation in the Left Ventricle

Our previous studies have demonstrated that NF or FF His activation can be identified using systematic pacing maneuvers in the right PH region (1, 2). However, in this study, unipolar and bipolar pacing both failed to discern NF and FF His activation in the left PH region. There was some overlap between group 1 and group 2 in the minimal output required to capture NF His activation. In addition, de and colleagues' histological study have shown that the nonbranching bundle are significantly longer in dog than in man (5). The great proportion of the AV conduction axis skirts the noncoronary sinus of the aortic root within the right atrial vestibule. According to the above-mentioned results, we can speculate that the pacing protocol used in our study might unable distinguish NF and FF His activation in the left PH region in dog. Due to the inability to differentiate NF from FF His

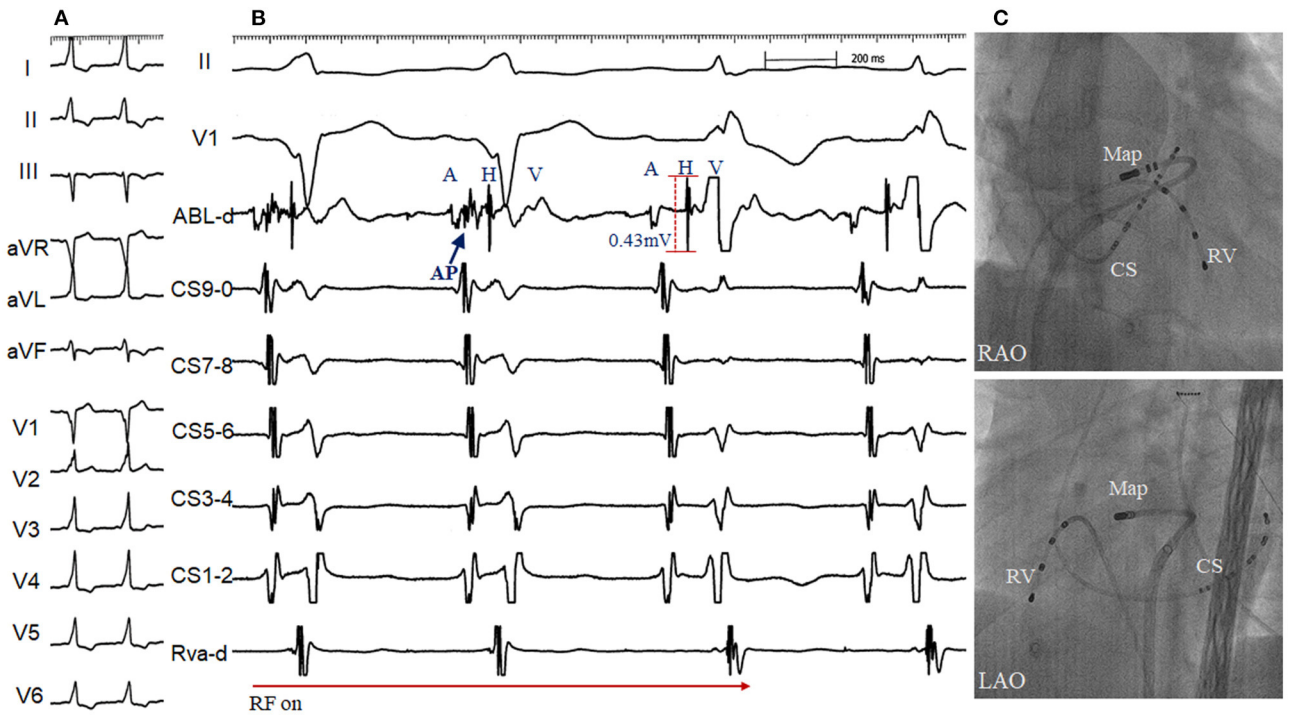

FIGURE 6 | Radiofrequency (RF) delivery **(A)** and fluoroscopic image **(C)** at the apex of the interventricular membranous septum via transseptal approach in a patient with supra-paraseptal ventricular preexcitation **(B)** and 2 failed RF attempts at the right para-Hisian region and non-coronary cusp (Right bundle branch block developed after the second ablation). The accessory pathway blocked within 2s during the first RF application, starting with 15W and up-titrated to 30 W. Note a distinct accessory pathway (AP) and large His activation (amplitude 0.43 mV) was recorded at the successful site. ABL, ablation catheter; RV, right ventricle. Abbreviations as in **Figure 1**.

activation at the triangle, we hypothesized that the His activation at the apex of the triangle was FF activation and NF was located at the base of the triangle. Then, similar to our previous study in the right PH region, a single RF energy was attempted to delivery at the two sites with His activation for confirming NF and FF His activation.

In this study, patho-histologic assessment 12–14 days after ablation showed clear coagulative necrosis with a diameter of 5–7 mm, consistent with previous animal studies. In the 6 dogs from group 1, RF-induced coagulative necrosis of the PB/BB and LBB in 5 dogs and complete necrosis of the PB/BB and incomplete necrosis of the LBB in 1, which resulted in total AV block and was consistent with the findings on the surface ECG. In group 2, RF resulted in no AV block in all 6 dogs. No complete coagulative necrosis occurred at the PB and proximal BB except in one dog, which was proved without changed HV interval before and after ablation. The mechanism of damage to the RBB and left anterior fascicle may be associated with direct thermal effect or lesion expansion generated by RF energy ablation as well as slight catheter dislocation during ablation. On the other contrary, no evidence of RF-induced lesion with an energy of 30 w was found in 2 dogs. However, the diameter of coagulative necrosis in the remaining 4 dogs was similar to that in the 6 dogs of group 1. The above results indicated that poor contact of ablation catheter with transaortic approach may be related with no RF-induced lesion.

Compared with group 1, we found a larger atrial electrogram and higher A/V ratios vs. group 2 compared to these in groups. It can be explained by anatomical findings that the apex of the triangle is closer to the atrium and the base is closer to interventricular myocardium.

Clinical Implication of Catheter Ablation Close to the Left His Bundle Region

The critical concern of ablation close to the left HB region is durable injury of the AVCS, and AV conduction disturbances requiring permanent pacemaker implantation are not uncommon (7). In addition, the risk of severe conduction abnormalities can be influenced by anatomical variation of the conduction system and baseline disturbances. Our observation highlights a potential way to minimize AV injury during ablation close to the triangle between the hinges of NCL-RCL. The first step is to identify the anatomical location of the triangle, which is completely covered with NF-and FF-His activations. The atrial amplitude and AV ratio can also indirectly help identify the anatomical location. The second step is to initially deliver RF with low energy which can be up-titrated at the apex when it is necessary to ablate these arrythmias. The AV interval and junctional response should be continuously monitored.

Our case with a patient with the left PH AP further demonstrated our ablation strategy that RF application with low

energy can be safely delivered at the apex of the triangle in spite of a large His activation (0.43 mV). On the other hand, no change on surface ECG and HV interval does not mean no pathological injury of the left-HB system. Finally. it needs further study whether our method can also be extrapolated into mechanical or transcatheter aortic valve replacement procedure to minimize or avoid AV block.

Study Limitations

In the study, a steerable 7.5F, D-curve catheter with a 3.5-mm irrigated-tip electrode was used for mapping and pacing in in the study. No high-resulation catheter such as PentaRay, Orion catheter were used. However, it may be very difficult to reach the region in small hearts. Secondly, the AVCS in dogs differs from the that in humans. It need further investigation whether our experimental data can be extratrasplated into clinical practice in humans, especially in the elderly patients. Finally, because intracardiac echocardiography was not used to identify the valvar leaflet in aortic root, we used "cusp" to show the catheter location in the method and results.

CONCLUSION

The His activation can be widely distributed in the LUS below the RCL-NCL junction. It was difficult to differentiate the NF-and FF-His activation using pacing technique at the region. However, anatomical location of His activation in the triangle between the hinges of RCL-NCL can help identify the NF- from FF-His activation, which was consistent with clinical-pathological finding with a single RF application at apex or base of the triangle of that in canine model. This important information can provide an objective evidence to guide catheter ablation in arrhythmias originating from in LPH area.

DATA AVAILABILITY STATEMENT

The original contributions presented in the study are included in the article/supplementary material, further inquiries can be directed to the corresponding authors.

ETHICS STATEMENT

The studies involving human participants were reviewed and approved by Ethic Committee of Wuhan Asian Heart Hospital. The patients/participants provided their written informed consent to participate in this study. The animal study was reviewed and approved by the Institutional Animal Care and Use Committee at Guangdong Provincial People's Hospital. Written informed consent was obtained from the individual(s) for the publication of any potentially identifiable images or data included in this article.

AUTHOR CONTRIBUTIONS

All authors listed have made a substantial, direct, and intellectual contribution to the work and approved it for publication.

FUNDING

The study was partially supported by Science and Technology Program of Guangdong Province, China (No. 2014B070705005 to SW), National Key Research and Development Project (No. 2018YFC1312502), and Science and Technology Planning Program of Guangdong Province, China (No. 2019B020230004 to SW).

REFERENCES

1. Xue Y, Zhan X, Wu S, Wang H, Liu Y, Liao Z, et al. Experimental, pathologic, and clinical findings of radiofrequency catheter ablation of para-hisian region from the right ventricle in dogs and humans. *Circ Arrhythm Electrophysiol*. (2017) 10:e005207. doi: 10.1161/CIRCEP.116.005207
2. Luo S, Zhan X, Ouyang F, Xue Y, Fang X, Liao H, et al. Catheter ablation of right-sided para-hisian ventricular arrhythmias using a simple pacing strategy. *Heart Rhythm*. (2019) 16:380–7. doi: 10.1016/j.hrthm.2018.09.015
3. Ouyang F, Mathew S, Wu S, Kamioka M, Metzner A, Xue Y, et al. Ventricular arrhythmias arising from the left ventricular outflow tract below the aortic sinus cusps: mapping and catheter ablation via transseptal approach and electrocardiographic characteristics. *Circ Arrhythm Electrophysiol*. (2014) 7:445–55. doi: 10.1161/CIRCEP.114.001690
4. Anderson RH, Ho SY. The architecture of the sinus node, the atrioventricular conduction axis, and the internodal atrial myocardium. *J Cardiovasc Electrophysiol*. (1998) 9:1233–48. doi: 10.1111/j.1540-8167.1998.tb00097.x
5. de Almeida MC, Macías Y, Tretter JT, Sánchez-Quintana D, Cabrera JA, Spicer DE, et al. Similarities and differences in the arrangement of the atrioventricular conduction axis in the canine compared to the human heart. *Heart Rhythm*. (2021) 18:1990–8. doi: 10.1016/j.hrthm.2021.07.065
6. Hamdan A, Guetta V, Klempfner R, Konen E, Raanani E, Glikson M. et al. Inverse relationship between membranous septal length and the risk of atrioventricular block in patients undergoing transcatheter aortic valve implantation. *JACC Cardiovasc Interv*. (2015) 8:1218–28. doi: 10.1016/j.jcin.2015.05.010
7. Sousa J, el-Atassi R, Rosenheck S, Calkins H, Langberg J, Morady F. Radiofrequency catheter ablation of the atrioventricular junction from the left ventricle. *Circulation*. (1991) 84:567–71. doi: 10.1161/01.CIR.84.2.567

Conflict of Interest: The authors declare that the research was conducted in the absence of any commercial or financial relationships that could be construed as a potential conflict of interest.

Publisher's Note: All claims expressed in this article are solely those of the authors and do not necessarily represent those of their affiliated organizations, or those of the publisher, the editors and the reviewers. Any product that may be evaluated in this article, or claim that may be made by its manufacturer, is not guaranteed or endorsed by the publisher.

frontiers in Cardiovascular Medicine

ORIGINAL RESEARCH
published: 02 March 2022
doi: 10.3389/fcvm.2022.844320

A Systemic Mapping Approach for Right and Left Parahisian Ventricular Arrhythmias Ablation

Ling-cong Kong†, Tian Shuang†, Zheng Li, Zhi-guo Zou, Wen-long Jiang, Jun Pu and Xin-hua Wang**

Department of Cardiology, Ren Ji Hospital, Shanghai Jiao Tong University School of Medicine, Shanghai, China

Background: Catheter ablation for parahisian ventricular arrhythmias (PHVA) is technically challenging and associated with increased risks of atrioventricular block (AVB). We developed a systemic mapping approach to improve the efficacy and safety of PHVA ablation.

Methods: Forty-three patients (29 males; average age 65.8 ± 10.5 years) with PHVAs were enrolled. A systemic mapping approach comprising differential electrocardiogram, sequential mapping, and ablation beneath/above the septal leaflet of the tricuspid valve (SLTV) and at the neighboring/contralateral regions (the aortic root and sub-aortic valve region) was applied for PHVA. The effectiveness and safety of this approach was evaluated at 1 year's follow-up.

Results: Sequential ablation beneath the SLTV (B-SLTV) succeeded in 24 (66.7 %) of 36 with right PHVA and ablation above the SLTV succeeded in 6 of the remaining 12 with failed B-SLTV ablation. Target-His bundle (HB) distance > 4.5 mm significantly predicted successful right PHVA ablation (OR 1.703; 95% CI 1.084–2.676, $P = 0.02$). "Seeming" right PHVA by electrocardiogram in 4 and apparent left PHVA in 3 was successfully ablated at the sub-aortic parahisian region. At 1 year's follow-up, 27 (75%) of 36 patients with right PHVA and 6 (85.7%) of 7 patients with left PHVA were free of PHVA recurrence off anti-arrhythmic drugs. The total success rate was 76.7% by using the systemic mapping approach for PHVA. One patient with A-SLTV ablation underwent pacemaker implantation due to complete AVB.

Conclusions: The systemic mapping approach was effective and safe for treating PHVA. The target-HB distance was a significant predictor for right PHVA ablation.

Keywords: parahisian ventricular arrhythmias, systemic mapping approach, radiofrequency ablation, atrioventricular block, the septal leaflet of the tricuspid valve

OPEN ACCESS

Edited by:
Andreas Metzner, University Heart and Vascular Center, University Medical Center Hamburg-Eppendorf, Germany

Reviewed by:
Hui-Nam Pak, Yonsei University Health System, South Korea
Steven Markowitz, Cornell University, United States

****Correspondence:***
Xin-hua Wang
ttwwxh@126.com
Jun Pu
pujun310@hotmail.com

† These authors have contributed equally to this work

Specialty section:
This article was submitted to Cardiac Rhythmology, a section of the journal Frontiers in Cardiovascular Medicine

Received: *28 December 2021*
Accepted: *04 February 2022*
Published: *02 March 2022*

Citation:
Kong LC, Shuang T, Li Z, Zou ZG, Jiang WL, Pu J and Wang XH (2022) A Systemic Mapping Approach for Right and Left Parahisian Ventricular Arrhythmias Ablation. Front. Cardiovasc. Med. 9:844320. doi: 10.3389/fcvm.2022.844320

HIGHLIGHTS

- The systemic mapping approach comprising differential ECG, mapping and ablation beneath/above the SLTV and the neighboring/contralateral regions was effective and safe for treating right and left parahisian VAs.
- B-SLTV ablation succeeded in two thirds of patients with right parahisian VAs.
- Target-HB distance > 4.5 mm could predict successful ablation of right parahisian VAs.

BACKGROUND

Most idiopathic ventricular arrhythmias (VAs) [pre-mature ventricular contraction (PVC) and ventricular tachycardia (VT)] originate from the right ventricular outflow tract (RVOT), and can be eliminated by radiofrequency (RF) catheter ablation effectively (1, 2). Parahisian VA (PHVA), defined as the earliest activation exhibiting His potential or <1 cm away from the His bundle (HB) of the right or left ventricular side (3), are less commonly seen, with the prevalence of 3–9% in all idiopathic VAs (4, 5). Catheter ablation for PHVA is technically challenging because the septal leaflet of the tricuspid valve (SLTV) hampers catheter tip-tissue contacts by the "above SLTV (A-SLTV)" approach. In contrast to RVOT-VAs, PHVAs ablation is associated with compromised effectiveness and higher risks of conduction system injury (5–8).

A novel technical improvement is to curve the catheter tip reversely and place it beneath the SLTV (B-SLTV) to acquire good proximity to the basal interventricular septum (9, 10). The B-SLTV approach might be superior to the A-SLTV approach in terms of effectiveness and safety, and was recommended for PHVAs ablation in recent studies (10, 11); Nevertheless, catheter ablation might fail even by the B-SLTV approach in a considerable proportion of patients (11). In this scenario sequential mapping at the A-SLTV region, the neighboring left parahisian area or the aortic root might help to improve the outcomes (12). These findings reminded us to propose a systemic mapping approach for PHVAs ablation. This study was carried out to evaluate the effectiveness and safety of this approach in a consecutive cohort of patients with right and left PHVAs.

METHOD

Study Population

Forty-three patients (29 males; average age 65.8 ± 10.5 years) with PHVAs were enrolled to undergo catheter ablation from January 2017 to September 2020. PHVAs were diagnosed according to surface electrocardiograms (ECGs) (3–5), which typically manifested QRS discordance in inferior leads (lead II/III/aVF), "QS"/"Qr"/"qR"pattern in lead V1, and precordial transition earlier than lead V3/V4 (**Figure 1A**). Inclusion criteria were symptomatic monomorphic VAs; daily PVC burden >10% or total PVC exceeding 10,000 per day or concomitant with VT of identical morphology; refractory or intolerance to at least one antiarrhythmic drug (AAD), including beta-blockers, Class Ic and Class III AADs. Exclusion criteria were ischemic heart disease; primary cardiomyopathy; prior cardiac surgery; congenital heart disease. All patients provided written informed consent for the ablation.

Abbreviations: PHVA, parahisian ventricular arrhythmias; PVC, premature ventricular contraction; VA, ventricular arrhythmia; VT, ventricular tachycardia; RF, radiofrequency; HB, the His bundle; RVOT, the right ventricular outflow tract; AVB, atrioventricular block; SLTV, the septal leaflet of the tricuspid valve; AAD, antiarrhythmic drug.

The Protocol of Systemic Mapping Approach for PHVAs

The protocol of systemic mapping approach was shown in **Figure 1B**. Briefly, it could be described as three steps. Step 1: Pre-judgement of left or right PHVAs according to the QRS morphology in lead V1 and precordial transitional zone (13). The "R"/"qR(s)" pattern in V1 and precordial transitional zone ≤ V1 indicated a left PHVA. The "QS"/"rS" pattern in V1 and precordial transitional zone ≥ V2 indicated a right PHVA. Step 2: Initial ablation based on the results of parahisian mapping. For right PHVA, the B-SLTV approach was performed in all patients. For left PHVA, ablation was performed above or below the aortic valve based on the mapping results. Step 3: Subsequent mapping and ablation if the initial ablation failed, including A-SLTV ablation and anatomical ablation at the contralateral parahisian region and the adjacent structures.

Electrophysiological Mapping

The procedures were performed in fasting state and under local analgesia. A decapolar catheter was positioned within coronary sinus (CS) *via* left femoral vein or left subclavian vein. A 3.5 mm saline-irrigated catheter with or without contact-force sensing (Thermocool Navistar or SmartTouch Thermocool Navistar, Biosense Webster, CA, USA) was used for geometry reconstruction, mapping and ablation. If spontaneous VAs was insufficient for mapping, intravenous infusion of isopreterenol (2–5 μg/min) was used to provoke the clinical VAs. The result of activation mapping was displayed on the geometry in color-coded manner. The site with the highest amplitude of His potential was tagged as the "HB." Pace mapping was applied with the output just higher than the diastolic capture threshold. A matched pace mapping was defined as the morphology of paced QRS identical to that of the clinical VAs in at least 11 of 12 leads.

EP Mapping at the Preferential Regions

For right PHVAs, the B-SLTV region was preferentially mapped. To access to the subvalvular area, the ablation catheter was introduced to the right ventricle *via* a Swartz sheath (SR0 type, St. Jude Medical, MN, USA), then curved reversely and clockwise rotated the catheter and pulled it back toward the tricuspid annulus, to form catheter inversion configuration (**Figures 2A–C**). The position of the catheter tip was judged by fluoroscopy and confirmed by intracardiac echocardiography (ICE) imaging (CARTO Sound, Biosense Webster, CA, USA) (**Figures 2D,H**). For left PHVAs, the mapping catheter was advanced in the left ventricle *via* trans-aortic retrograde approach to map the left parahisian region and the septal region of mitral annulus (**Figure 3**).

The earliest activation site was tagged on the geometry and served as the initial ablation target if it was >4 mm away from the HB, and if the HB-Right bundle branch (RBB) capture threshold by pacing at the earliest activation site was higher than that at the HB site (14). However, in case of the earliest activation <4 mm away from the HB, or if HB-RBB was captured with lower threshold at this site than the HB, attempt of ablation could be tried under close monitoring of junctional rhythm/AV conduction (**Figure 4**).

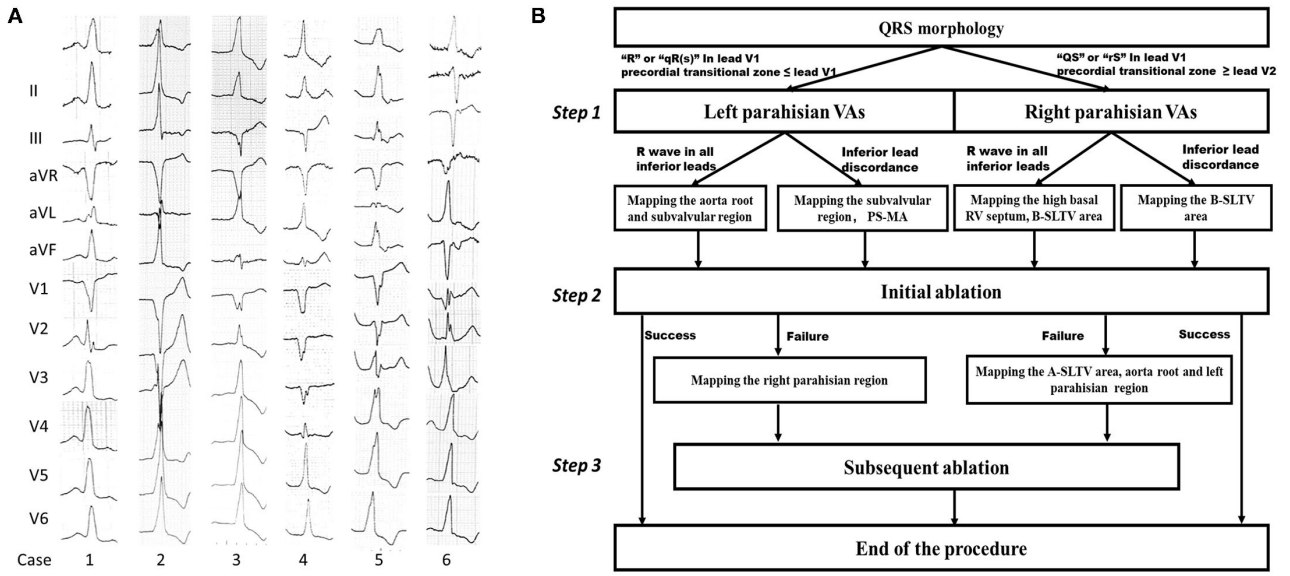

FIGURE 1 | Examples of PHVA electrocardiograms and the flow chart of the systemic mapping approach. **(A)** Typical twelve-lead electrocardiographic manifestation of parahisian VAs. Right parahisian VAs were diagnosed in Case 1–5, and left parahisian VA in Case 6. Note there were positive "R" waves/or QRS discordance in inferior leads, a "QS" wave in lead V1, precordial transition in lead V2–V4 for right parahisian VAs, and a "qR" wave in lead V1 and precordial transition in lead V1–V2 for left parahisian VA. **(B)** The flow chart of the systemic mapping approach for right and left parahisian VA.

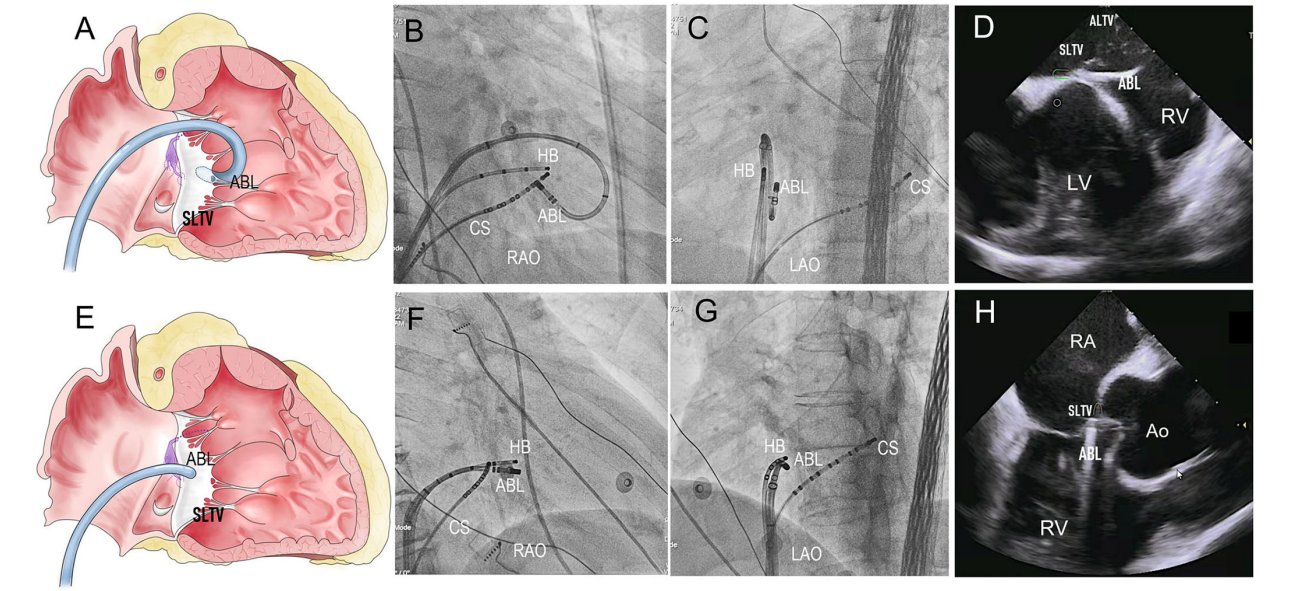

FIGURE 2 | The Catheter placement in the B-SLTV and A-SLTV approach. **(A)** The schematic diagram illustrating the catheter tip was reversely curved beneath the SLTV (RAO view). **(B,C)** The fluoroscopic images showing the catheter was reversely curved beneath the SLTV through a long sheath (RAO and LAO view). **(D,H)** The ultrasonic images confirmed the catheter placement beneath the SLTV. **(E)** The schematic diagram showing the catheter tip was directly placed above the SLTV (RAO view). **(F,G)** The fluoroscopic images showing the catheter tip was placed directly above the SLTV (RAO and LAO view). HB, the His bundle; CS, coronary sinus; ABL, the ablation catheter; SLTV, the septal leaflet of the tricuspid valve; ALTV, the anterior leaflet of the tricuspid valve; RA, the right atrium; RV, the right ventricle; LV, left ventricle; RAO, right anterior oblique; LAO, left anterior oblique.

Subsequent EP Mapping at Other Regions

If the attempt of B-SLTV ablation failed or was withdrawn due to safety concerns, the A-SLTV region (**Figures 2E–G**), contralateral parahisian regions and the neighboring structures (i.e., the coronary cusps at the aortic root) were mapped to search for an earlier activation site than the initial one, or the adjacent

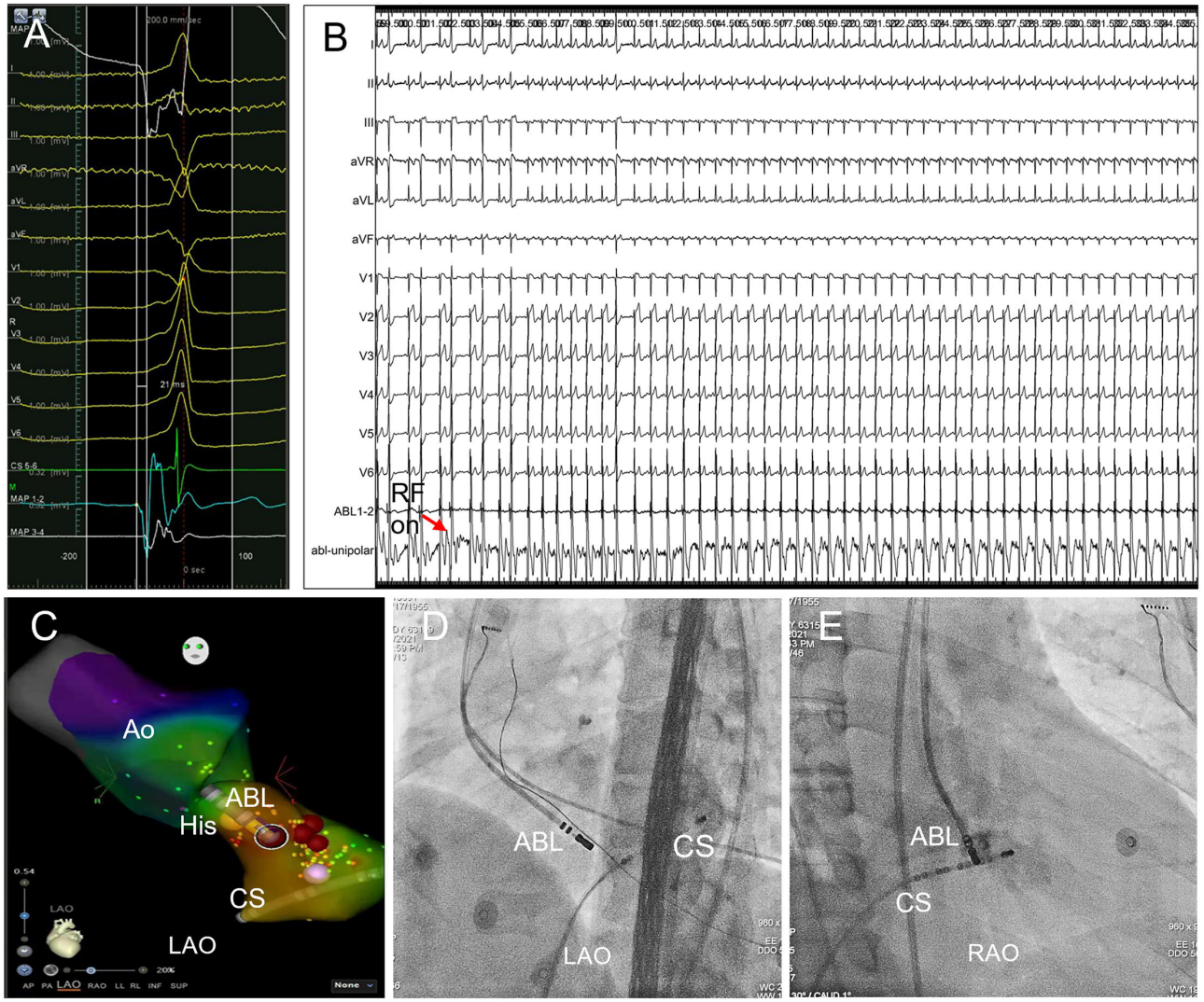

FIGURE 3 | Trans-aortic retrograde ablation of left PHVA. **(A)** Tracings were unipolar MAP1, twelve-lead surface ECG, CS_{5-6}, bipolar MAP_{1-2}, MAP_{3-4}. The local bipolar electrogram at the ablation target preceded the QRS onset by 21 ms with a sharp "QS" unipolar electrogram. **(B)** RF ablation 30W, 60s at the sub-aortic ablation target successfully eliminated the left PHVA without causing PR prolongation or AVB. **(C)** Activation mapping of the left PHVA region and the aortic root. The catheter tip was positioned at the ablation target ≈3 mm below the HB in the left ventricle. Ablation attempt (30W, 10 s) was not effective at other sites slightly away from the ablation target. Red dots represented ablation lesions. **(D,E)** The catheter placement at the left parahisian region on LAO and RAO fluoroscopic projection. Ao, the aorta; HB, the His bundle; CS, coronary sinus; ABL, the ablation catheter; RAO, right anterior oblique; LAO, left anterior oblique.

site that was just opposite to the initial lesion. They were served as a better target for subsequent ablation, or as a suitable target for anatomical ablation.

RF Ablation Settings

Once the initial ablation target was determined, irrigated RF ablation was applied for lesion creation. Typically, RF energy delivery commenced at 20W (saline-irrigation speed 17 ml/min, contact force 8–20 g if applicable), and was gradually titrated to 35–45 W (saline-irrigation speed 20–25 ml/min, contact force 8–20 g if applicable) if no sign of AV conduction injury was observed (5–10). If the clinical VAs were suppressed within 15 s, RF energy delivery was prolonged for 90–120 s, otherwise RF ablation was suspended, and re-mapping was performed. RF ablation was terminated immediately in case of PR prolongation or rapid junctional rhythm, which foreboded impending AV block (AVB).

Procedural success was deemed if no clinical VAs recurred at the end of 30 min's observation period with the challenge of intravenous isoproterenol infusion (2–5 μg/min).

Post-ablation Management and Follow-Up

Patients were discharged the next day after the procedure and were regularly followed up at the outpatient clinic for 1 year. All AADs were withdrawn if no symptomatic VAs were detected. Surface ECG and 24 h Holter monitoring were

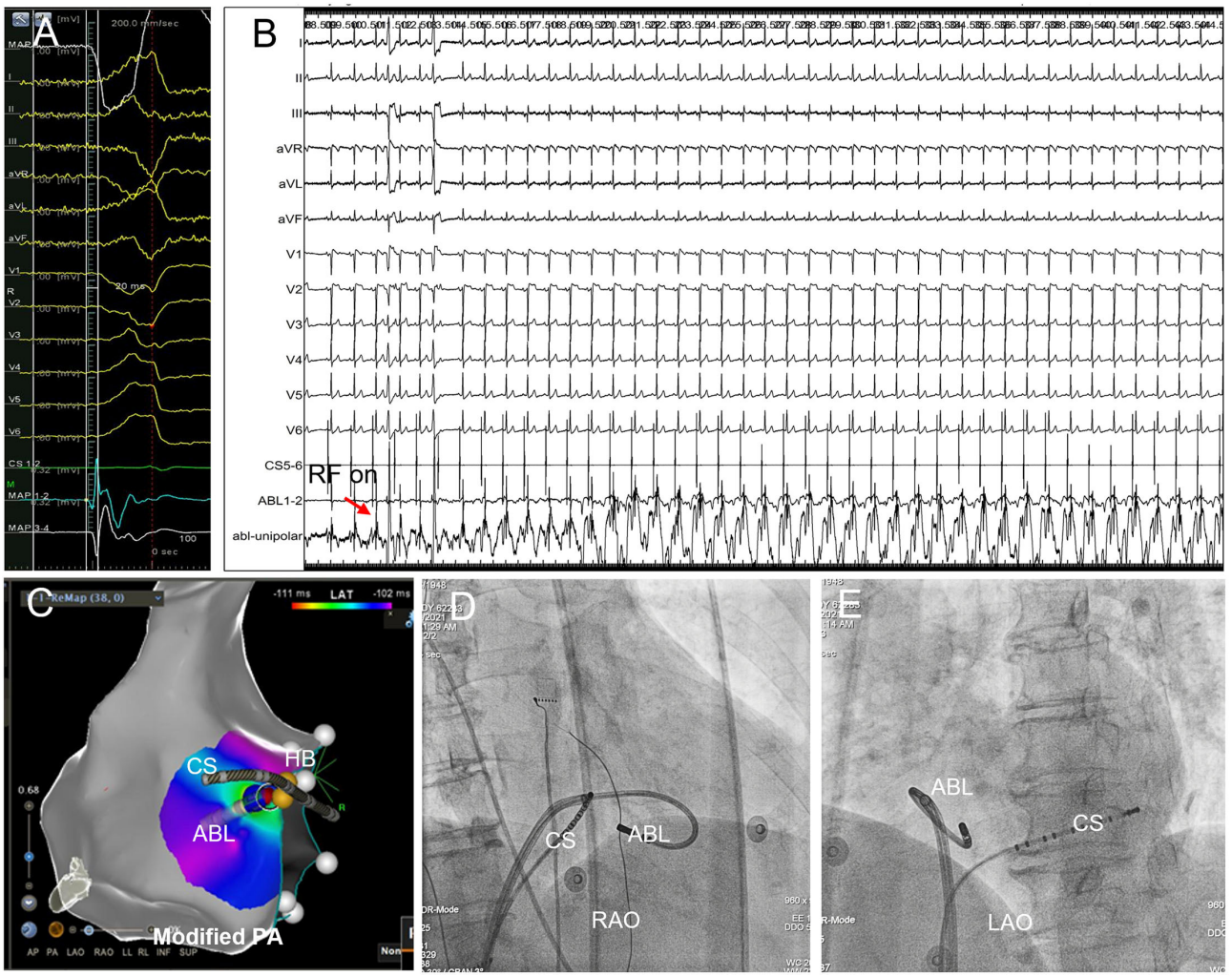

FIGURE 4 | Successful B-SLTV ablation of right PHVA with the ablation target extremely close to the HB. **(A)** Tracings were unipolar MAP_1, twelve-lead surface ECG, CS_{1-2}, bipolar MAP_{1-2}, MAP_{3-4}. The local bipolar electrogram at the ablation target preceded the QRS onset by 20 ms with a sharp "QS" unipolar electrogram. **(B)** Saline-irrigated RF energy delivery 35W, 90s at this site successfully abolished the PVC, without junctional rhythm or AV conduction impairment. **(C)** The catheter tip was positioned beneath the SLTV ≈ 2 mm away from the HB. The blue dot represented the ablation lesion. **(D,E)** The B-SLTV placement of the ablation catheter was displayed on RAO and LAO projection. HB, the His bundle; CS, coronary sinus; ABL, the ablation catheter. PA, postero-anterior; RAO, right anterior oblique; LAO, left anterior oblique.

performed at 3, 6, and 12 months after the procedure, and were performed whenever the patient experienced symptoms suggesting a VA recurrence.

Clinical success was defined as absence of clinical PHVAs on surface ECGs and reduction of clinical VAs burden by more than 90% on 24 h Holter monitoring compared with the recording prior to the procedure at the end of 1 year's follow-up off AADs.

Statistical Analysis

Continuous variables with normal distribution were expressed as mean ± standard deviation (SD) or as median and range otherwise. They were compared by Student's *t*-test if the variance was equal, or by Mann–Whitney *U*-test otherwise. Category variables were expressed as counts and percentage (%), and were compared with χ^2 or Fisher's exact test. Multivariate binary logistic regression analysis was applied to detect the independent predictors for successful right PHVA ablation, which were described as odds ratio (OR) and 95% confidence interval (CI). A receiver operating characteristic (ROC) analysis was applied to determine the cut-off value for predicting successful right PHVA ablation. A two-tailed $P < 0.05$ was considered statistically significant. Statistical analysis was performed by IBM SPSS Statistics 19.0 for Windows (IBM Corporation, Somers, NY, USA).

RESULTS

The baseline demographic parameters in all patients and in those with right / left PHVAs were listed in **Table 1**, respectively.

TABLE 1 | Patients' baseline characteristics.

Parameters	Total	Right parahisian VA	Left parahisian VA
Cases (*N*)	43	36	7
Age (years)	65.8 ± 10.5	65.7 ± 11.2	66.4 ± 5.1
Male, *n* (%)	29 (67.4)	23 (63.9)	6 (85.7)
24-h PVC count	17,603 ± 7,072	16,878 ± 7,028	21,331 ± 6,528
History of PVC (months)	5.0 (4.0, 8.0)	5.0 (4.0, 7.8)	6.0 (3.0, 24.0)
Comorbidities			
Hypertension, *n* (%)	18 (41.8)	15 (41.6)	3(42.9)
Diabetes mellitus, *n* (%)	5 (11.6)	4 (11.1)	1(14.3)
Mild coronary atherosclerosis, *n* (%)	2 (4.7)	2 (5.6)	0
LVEF 40–50%	3 (7.0)	2 (5.6)	1 (14.3)
Presenting arrhythmia			
Isolated PVC, *n* (%)	42 (97.7)	35 (97.2)	7 (100)
PVC/NSVT, *n* (%)	1(2.3)	1 (2.8)	0
AAD use			
Beta-Blocker, *n* (%)	20 (46.5)	17 (47.2)	3 (42.9)
Class Ic drug, *n* (%)	19 (44.2)	15 (41.7)	4 (57.1)
Sotalol, *n* (%)	10 (23.3)	8 (22.2)	2 (28.6)
Amiodarone, *n* (%)	6 (14.0)	6 (16.7)	0 (0)

PVC, premature ventricular complex; NSVT, non-sustained ventricular tachycardia; LVEF, left ventricular ejection fraction; AAD, antiarrhythmic drug.

There were 18 patients with hypertension, 5 with type 2 diabetes mellitus, 2 with mild coronary artery atherosclerosis detected by computed tomographic angiography, and 3 with left ventricular ejection fraction 40–50%. Forty-two patients presented with isolated PVCs and 1 with concomitant non-sustained VT. An average of 1.3 ± 0.5 AADs were used per patient. The clinical VA was primarily diagnosed as left PHVA in 3 patients and as right PHVA in the remaining 40 patients based on the ECG. PHVA was successfully ablated from the left side in 4 of 40 patients with ECG-diagnosed right PHVA, and was re-grouped as left PHVA. Totally there were 36 with right PHVA and 7 with left-sided VA.

Right PHVA Ablation

RF ablation by the B-SLTV approach succeeded in 24 (66.7%) of 36 patients with right PHVA, and failed in the remaining 12 patients (**Figure 5**). The electrocardiographic and procedural data were compared between successful and unsuccessful B-SLTV ablation in **Table 2**. There was significant greater target -HB distance and lower prevalence of junctional beats in patients with successful B-SLTV ablation than in those without. ECG morphologies, the local ventricular activation preceding QRS onset (V-QRS), proportion of small HB potential at the target, average RF power, RF duration, number of RF delivery and fluoroscopy time were comparable between successful and unsuccessful B-SLTV ablation.

Among the electrocardiographic and procedural parameters, target-HB distance was the only factor that could predict successful B-SLTV ablation for right PHVA (OR 1.703; 95% CI 1.084–2.676, $P = 0.02$). ROC analysis showed target-HB distance cutoff value was 4.5 mm (sensitivity 66.7% and specificity 83.3%; Area under the curve = 0.773, 95% CI 0.614–0.931, $P = 0.01$). There was no significant difference in RF power and duration between cases with target-HB distance > 4.5 mm and those with target-HB distance ≤ 4.5 mm (35.0 ± 2.3 vs. 36.0 ± 3.4 W, $P = 0.34$; 155.5 ± 38.1 vs. 146.3 ± 34.2 s, $P = 0.76$, respectively).

Subsequent ablation in 12 patients with unsuccessful B-SLTV ablation was listed in detail in **Supplementary Table 1**. A-SLTV ablation successfully abolished the clinical VA in 6 of them. Totally procedural success was achieved in 30 (83.3%) of 36 patients with right PHVA. The remaining 6 patients experienced ablation failure even after thorough mapping and ablation at the neighboring structures (RVOT and three coronary cusps at the aortic root) and the left- parahisian region.

Left PHVA Ablation

Sub-aortic valve ablation was successful in all seven patients with left PHVA. In each of 4 patients with failed right parahisian ablation, the V-QRS time at the left-sided target was greater than that at the right-sided target (27 vs. 24, 31 vs. 29, 16 vs. 14, 33 vs. 31 ms, respectively). Compared with right PHVA, left PHVA exhibited higher proportion of precordial transition ≤lead V2 and lower proportion of QS shape in lead V1 on ECG recordings (**Table 2**). The procedural parameters were comparable except that the target-HB distance was greater in left sided group than that in right-sided group.

Complications

Mechanical injury caused right bundle branch block in 6 patients during catheter manipulation in the RV, which recovered in all of them within 24 h post-ablation. Transient high degree AVB occurred during A-SLTV ablation 4 mm below the HB in 1 patient, and resolved completely after immediate ablation suspension. However, this patient underwent pacemaker implantation due to complete AV block one-month post-ablation.

Follow-Up Results at 1 Year

At the end of 12 months' follow-up, clinical success was achieved in 27 (75%) of 36 patients with right PHVA and in 6 (85.7%) of 7 patients with left PHVA. In this PHVA cohort, totally the clinical success was achieved in 33 (76.7%) of 43 patients off AADs by using this systemic mapping approach.

DISCUSSION

Major Findings

In this retrospective study we firstly proposed and evaluated a novel systemic mapping approach for PHVA ablation, which was a combination of ablation at the B-SLTV/A-SLTV region, the neighboring structures and the contralateral parahisian regions. Secondly the target-HB distance was the only predictor for right PHVA ablation among all the procedural parameters and

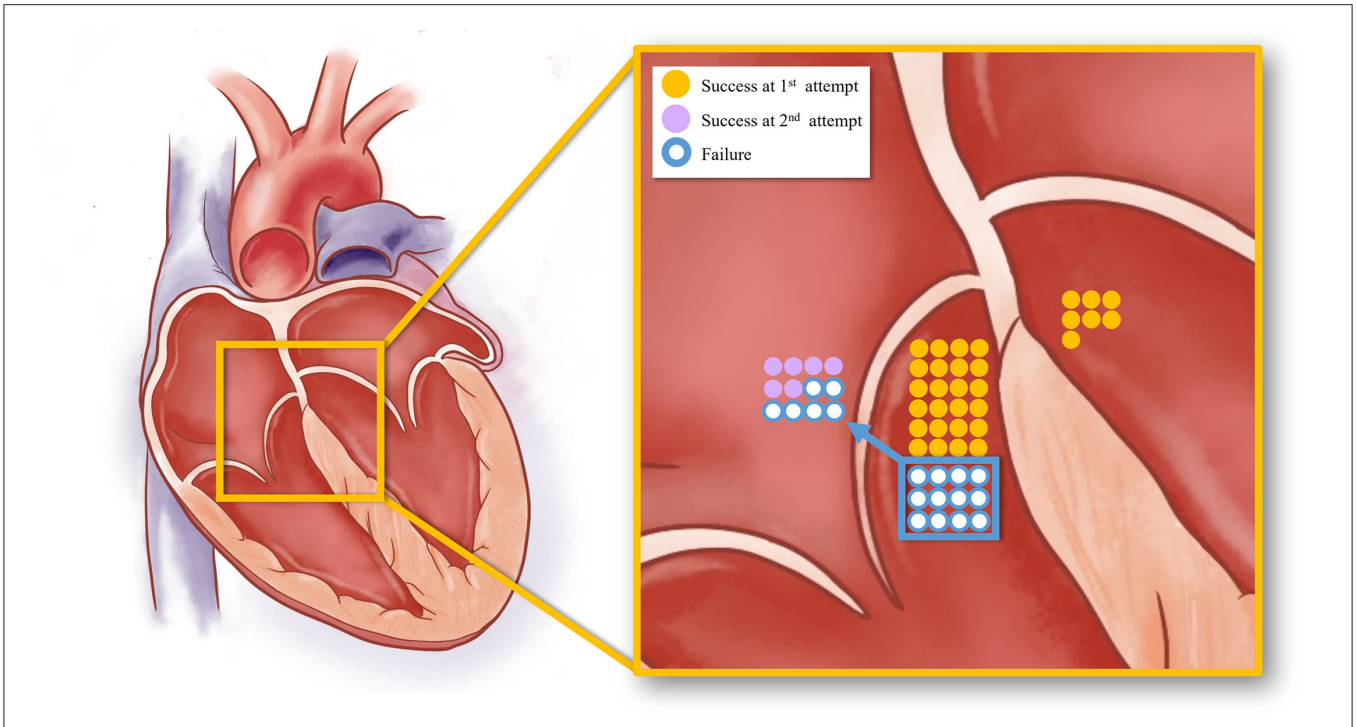

FIGURE 5 | The schematic diagram showing the acute procedural results of right and left PHVA ablation. The yellow dots represented successful cases by the B-SLTV approach and those by trans-aortic retrograde ablation. The purple dots represented success cases by the adjunctive A-SLTV approach. White dots represented cases with ablation failure.

TABLE 2 | Comparison of right and left parahisian VA ablation.

	Right parahisian VA ablation (n = 36)			Left parahisian VA ablation (n = 7)
	Total	**Successful B-SLTV (n = 24)**	**Unsuccessful B-SLTV (n = 12)**	
ECG morphology				
QS pattern in lead V1, *n* (%)	33 (91.7)$^{\$}$	23 (95.8)	10 (83.3)	2 (28.6)$^{\$}$
Precordial transition ≤ lead V2, *n* (%)	14 (38.9)$^{\#}$	8 (33.3)	6 (50.0)	6 (85.7)$^{\#}$
Inferior lead negative/discordance, *n* (%)	27 (75.0)	18 (75.0)	9 (75.0)	7 (100.0)
Procedural parameters				
V-QRS, ms	24.8 ± 7.4	25.1 ± 7.1	24.1 ± 8.4	24.1 ± 5.7
Target-HB distance, mm	5.1 ± 2.3‡	5.8 ± 2.3*	3.7 ± 1.7*	7.4 ± 1.8‡
Small HBP at the target, *n* (%)	11(30.6)	5 (20.8)	6 (50)	2 (28.6)
Junctional beats, *n* (%)	10 (27.8)	2 (8.3)*	8 (66.7)*	2 (28.6)
RF power (W)	35.5 ± 3.0	35.1 ± 1.9	36.3 ± 4.3	36.9 ± 3.1
Number of RF delivery	3.6 ± 1.3	3.3 ± 1.2	4.0 ± 1.3	4.0 ± 1.2
RF duration (s)	150.6 ± 35.9	149.2 ± 37.2	153.4 ± 34.5	165.7 ± 41.5
Fluoroscopy time (s)	519.5 ± 352.7	441.6 ± 270.1	675.5 ± 451.1	346.1 ± 108.3

$^{\$}P = 0.001$; $^{\#}P = 0.04$; $^{‡}P = 0.02$ for comparison between right PHRA and left PHRA.
**P < 0.05 for comparison between successful B-SLTV and unsuccessful B-SLTV group.*
RF, radiofrequency; HBP, the His bundle potential.

this value exceeding 4.5 mm predicted successful ablation. This informative result might provide us a useful tool to estimate the effectiveness in advance and avoid excessive risks of AVB during the procedure.

Challenges and Obstacles for PHVAs Ablation

In one anatomical study it was found that the HB ran superficially without a layer of myocardial coat (the "naked" HB) in one

fifth of the subjects (15). In another study it was found that the distal compact atrioventricular node (AVN) and the proximal HB had no surrounding myocardial layer (16). In this scenario RF ablation in close proximity to the AVN-HB was associated with increased risk of AVB. This severe complication became a major challenge for PHVA ablation. The major anatomical obstacle that was faced during right PHVA ablation was the SLTV. The "shield effect" of the SLTV prevented direct energy delivery to the basal myocardium. Furthermore, the movement of the SLTV might cause displacement of catheter tip, leading to insufficient lesion creation.

Technical Innovations in PHVA Ablation

In the early days, the conventional A-SLTV approach was initially used for right PHVA ablation in several small-volume studies (6–8), with modest effectiveness and safety results. Later on, the application of cryo-energy failed to demonstrate better efficacy and safety in right PHVA ablation, compared with RF energy (17). In that study, cryoablation succeeded in only 4 of 10 patients with PHVA with the cost of pacemaker implantation in 1 patient complicated with three-degree AVB. The potential advantages of cryo- over RF energy comprised reversible cryo-mapping with a temperature of −30°C, reduced risk of damage to the surrounding tissue and better catheter stability. However, the size of ice ball was bigger than that of the catheter tip during cryoablation at a temperature of −70°C, which might reduce the distance threshold to avoid AVB. Furthermore, the A-SLTV rather than the B-SLTV approach was applied in that study. The latter might be more useful to improve the effectiveness as well as safety for PHVA ablation, which would be discussed below.

In recently years, the novel B-SLTV ablation (also known as "catheter inversion" technique, "reversed C-curve technique," etc.) began to be applied for PHVA ablation, with a high success rate of 88% reported in a latest cohort study of 28 cases (11). The advantages of the B-SLTV approach over the conventional A-SLTV approach lay in two aspects: one was better catheter tip-tissue contact and more efficient energy delivery; the other was less risk of AVB, which was demonstrated in an animal study. It that study, the B-SLTV ablation carried less risk of AVB in experimental dogs compared with the A-SLTV ablation (18).

Judgement of B-SLTV placement of the catheter tip was vital for the B-SLTV approach. Although the fluoroscopic catheter inversion configuration indicated correct placement, it was doubtful that the catheter tip was at the right place in some cases. At this time the B-SLTV positioning could be judged by the fluoroscopic sign of catheter "fixation" while pulling it back, and could be further confirmed by ICE imaging (shown in **Figures 2D,H**). Even if the catheter tip was placed at the B-SLTV area, a contact-force sensing catheter was preferable and sometimes clockwise rotation of the catheter was needed to ensure appropriate catheter tip-tissue contact.

Rationale for a Systemic Mapping Approach for Right PHVA Ablation

Despite the important advantages, the B-SLTV approach was not the end of story in the course of right PHVA ablation. It might not be able to abolish left parahisian foci, intramural foci, or foci extremely close to the AVN-HB. In our cohort, the procedural success could only be achieved in 66.7% of the patients by the B-SLTV approach. The "seemingly" right PHRA turned out to be left PHVA in a small proportion of the patients. Similar to RVOT VA ablation, VA with a left-sided origin might breakout from a right-sided exit through a preferential conduction pathway (19, 20), exhibiting the ECG of a right-sided VA. In our study the earliest local activation time at the left side preceding the one at the right side supported the existence of preferential conduction. Apparently, the B-SLTV approach was not effective for left PHVAs and left parahisian ablation was necessitated. Furthermore, to abolish intramural foci, RF ablation in the contralateral region might be necessary, rather than repeated B-SLTV ablation. Moreover, to ablate the ectopic focus extremely close to the AVN-HB, the B-SLTV approach was not always effective or safe and the A-SLTV approach/anatomical ablation at the neighboring structures might be effective (11, 12). The adjunctive A-SLTV approach succeeded in 6 of 12 cases who experienced B-SLTV ablation failure in our study. Among 6 cases with adjunctive A-SLTV ablation success, the target-HB distance was only 2 mm in 2 cases. This result indicated that different catheter tip orientation and trivial adjustment of the target site might help to improve the ablation results on certain occasions, though the risk of AVB should be carefully balanced.

Predictors for Successful PHVA Ablation

There were no electrocardiographic predictors (such as QRS shape in lead V1 and the inferior leads, precordial transition, etc.) identified for successful PHVA ablation. However, among all the procedural parameters, we found only the target-HB distance > 4.5 mm could predict successful right PHVA ablation. We believed this finding might serve as a useful tool to estimate the effectiveness ahead of ablation and avoid excessive risks of AVB if the target-HB distance was markedly shorter than 4.5 mm.

Study Limitations

Several major limitations existed in our study. Firstly, this study was a retrospective, single-arm cohort study and included limited patients. The effectiveness and safety of the systemic mapping approach should be tested in a prospective, controlled, and large-scale clinical trials. However, given the fairly low prevalence of PHVA, all the published literature were mainly case reports or small case series reports, lacking randomized controlled studies. Secondly, it was possible that PHVA abolished at left side after failed at right side originated from an intramural focus rather than a true left side focus. However, as was the case in RVOT VA, the existence of preferential conduction might increase the difficulties in identifying left or right out-flow tract VAs. The earliest local activation time at the left-sided target preceding the one at the right-sided target supported the existence of preferential conduction in our study. There might be no gold standard for defining right, intramural and left foci, and the response to ablation might be a practical one. Successful ablation at the contralateral parahisian region or the adjacent structures justified the

application of s systemic mapping approach in complex PHVA ablation.

CONCLUSIONS

The systemic mapping approach was effective and safe for treating right and left PHVAs. The ablation target-HB distance was a significant predictor for right PHVA ablation.

DATA AVAILABILITY STATEMENT

The raw data supporting the conclusions of this article will be made available by the authors, without undue reservation.

AUTHOR CONTRIBUTIONS

XW conceptualized the systemic mapping approach for PHVA ablation. LK, XW, and TS drafted the manuscript. LK drew the figures and illustrations. ZL were involved in clinical data collection. ZZ and WJ were involved in data processing. JP revised the manuscript. All authors have read and approved the final manuscript.

FUNDING

This study was supported by funds from Shanghai Natural Science Foundation Project (Grant No. 18ZR1423400), National Science Fund for Distinguished Young Scholars (81625002), and Shanghai Outstanding Academic Leaders Program (18XD1402400). These funds were not used in study designing or data collection/processing.

SUPPLEMENTARY MATERIAL

The Supplementary Material for this article can be found online at: https://www.frontiersin.org/articles/10.3389/fcvm.2022.844320/full#supplementary-material

REFERENCES

1. Miller JM, Pezeshkian NG, Yadav AV. Catheter mapping and ablation of right ventricular outflow tract ventricular tachycardia. *J Cardiovasc Electrophysiol.* (2006) 17:800–2. doi: 10.1111/j.1540-8167.2006.00519.x
2. Dixit S, Gerstenfeld EP, Callans DJ, Marchlinski FE. Electrocardiographic patterns of superior right ventricular outflow tract tachycardias: distinguishing septal and free-wall sites of origin. *J Cardiovasc Electrophysiol.* (2003) 14:1–7. doi: 10.1046/j.1540-8167.2003.02404.x
3. Enriquez A, Tapias C, Rodriguez D, Liang J, Marchlinski F, Saenz L, et al. How to map and ablate parahisian ventricular arrhythmias. *Heart Rhythm.* (2018) 15:1268–74. doi: 10.1016/j.hrthm.2018.02.028
4. Ban J, Chen Y, Park H, Kim D, Lee D, Park Y, et al. Idiopathic ventricular arrhythmia originating from the para-hisian area: prevalence, electrocardiographic and electrophysiological characteristics. *J Arrhythm.* (2014) 30:48–54. doi: 10.1016/j.joa.2013.04.007
5. Enriquez A, Pathak RK, Santangeli P, Liang JJ, Al Rawahi M, Hayashi T, et al. Inferior lead discordance in ventricular arrhythmias: A specific marker for certain arrhythmia locations. *J Cardiovasc Electrophysiol.* (2017) 28:1179–1186. doi: 10.1111/jce.13287
6. Yamauchi Y, Aonuma K, Takahashi A, Sekiguchi Y, Hachiya H, Yokoyama Y, et al. Electrocardiographic characteristics of repetitive monomorphic right ventricular tachycardia originating near the His-bundle. *J Cardiovasc Electrophysiol.* (2005) 16:1041–8. doi: 10.1111/j.1540-8167.2005.40787.x
7. Komatsu Y, Taniguchi H, Miyazaki S, Kusa S, Takayama K, Kakita K, et al. Two distinct electrocardiographic forms of idiopathic ventricular arrhythmia originating in the vicinity of the His bundle. *Europace.* (2012) 14:1778–85. doi: 10.1093/europace/eus160
8. Komatsu Y, Otomo K, Taniguchi H, Kakita K, Takayama K, Fujiwara H, et al. Catheter ablation of ventricular arrhythmias arising from the right ventricular septum close to the His bundle: features of the local electrogram at the optimal ablation site. *J Cardiovasc Electrophysiol.* (2011) 22:878–85. doi: 10.1111/j.1540-8167.2011.02014.x
9. Zeljko HM, Yue A. Catheter inversion technique for ablation of parahisian accessory pathway. *Europace.* (2015) 17:1707. doi: 10.1093/europace/euv254
10. Clemens M, Peichl P, Kautzner J. Catheter ablation of idiopathic ventricular ectopy in the vicinity of the His bundle under the septal leaflet of the tricuspid valve. *Europace.* (2015) 17:1370. doi: 10.1093/europace/euv084
11. Sun J, Zhang PP, Wang QS, Xu QF, Wang ZQ, Yu Y, et al. Catheter ablation of ventricular arrhythmias originating from the para-Hisian region with reversed C-curve technique. *J Cardiovasc Electrophysiol.* (2019) 30:2377–2386. doi: 10.1111/jce.14170
12. Yamada T, McElderry HT, Doppalapudi H, Kay GN. Catheter ablation of ventricular arrhythmias originating in the vicinity of the His bundle: significance of mapping the aortic sinus cusp. *Heart Rhythm.* (2008) 5:37–42. doi: 10.1016/j.hrthm.2007.08.032
13. Zhang SQ, Zheng C, Li YC, Ji KT, Yin RP, Lin JF, et al. Common and distinctive electrocardiographic characteristics and effective catheter ablation of idiopathic ventricular arrhythmias originating from different areas of ventricular septum adjacent to atrioventricular annulus. *J Cardiovasc Electrophysiol.* (2018) 29:1104–12. doi: 10.1111/jce.13638
14. Luo S, Zhan X, Ouyang F, Xue Y, Fang X, Liao H, et al. Catheter ablation of right-sided para-Hisian ventricular arrhythmias using a simple pacing strategy. *Heart Rhythm.* (2019) 16:380–7. doi: 10.1016/j.hrthm.2018.09.015
15. Kawashima T, Sasaki H. A macroscopic anatomical investigation of atrioventricular bundle locational variation relative to the membranous part of the ventricular septum in elderly human hearts. *Surg Radiol Anat.* (2005) 27:206–13. doi: 10.1007/s00276-004-0302-7
16. Mulpuru SK, Cha YM, Asirvatham SJ. Synchronous ventricular pacing with direct capture of the atrioventricular conduction system: functional anatomy, terminology, and challenges. *Heart Rhythm.* (2016) 13:2237–46. doi: 10.1016/j.hrthm.2016.08.005
17. Miyamoto K, Kapa S, Mulpuru SK, Deshmukh AJ, Asirvatham SJ, Munger TM, et al. Safety and efficacy of cryoablation in patients with ventricular arrhythmias originating from the para-Hisian region. *JACC Clin Electrophysiol.* (2018) 4:366–73. doi: 10.1016/j.jacep.2017.12.013
18. Kato R, Matsumoto K, Goktekin O, Matsuo H, Watanabe H, Takahama M. Parahisian radiofrequency catheter ablation in dogs: comparison of the above-valve and below-valve approaches. *J Interv Card Electrophysiol.* (2000) 4:359–68. doi: 10.1023/A:1009814803581
19. Yamada T, Murakami Y, Yoshida N, Okada T, Shimizu T, Toyama J, et al. Preferential conduction across the ventricular outflow septum in ventricular arrhythmias originating from the aortic sinus cusp. *J Am Coll Cardiol.* (2007) 50:884–91. doi: 10.1016/j.jacc.2007.05.021
20. Yamada T, Platonov M, McElderry HT, Kay GN. Left ventricular outflow tract tachycardia with preferential conduction and multiple exits.

Circ Arrhythm Electrophysiol. (2008) 1:140–2. doi: 10.1161/CIRCEP.108.778563

Conflict of Interest: The authors declare that the research was conducted in the absence of any commercial or financial relationships that could be construed as a potential conflict of interest.

Publisher's Note: All claims expressed in this article are solely those of the authors and do not necessarily represent those of their affiliated organizations, or those of the publisher, the editors and the reviewers. Any product that may be evaluated in this article, or claim that may be made by its manufacturer, is not guaranteed or endorsed by the publisher.

frontiers in Cardiovascular Medicine

ORIGINAL RESEARCH
published: 31 March 2022
doi: 10.3389/fcvm.2022.816237

Premature Ventricular Contractions From the Left Anterior Fascicle: Electrocardiographic and Electrophysiological Characteristics, Mapping Strategy, and Immediate and Long-Term Catheter Ablation Results

Hongwu Chen[1†], Fangyi Xiao[2†], Weizhu Ju[1], Gang Yang[1], Fengxiang Zhang[1], Kai Gu[1], Mingfang Li[1], Hailei Liu[1], Zidun Wang[1], Dinesh Sharma[3], Kejiang Cao[1] and Minglong Chen[1]*

[1] Cardiology Division, The First Affiliated Hospital of Nanjing Medical University, Nanjing, China, [2] Department of Cardiology, The First Affiliated Hospital of Wenzhou Medical University, Wenzhou, China, [3] Division of Cardiology, Naples Community Hospital, Naples, FL, United States

Background: Left anterior fascicle (LAF) premature ventricular contractions (PVC) are rarely reported. We described the electrocardiographic and electrophysiological characteristics of PVCs originating from LAF and evaluated the results of catheter ablation.

Methods: The baseline AH and HV intervals were recorded during normal sinus rhythm (NSR), and the HV interval of LAF-PVC was measured during the procedure. During the index procedure, the conduction interval from the earliest Purkinje potential (PP) site to the His was labeled as time A, the conduction interval from the earliest site to the onset of the QRS as time B, then the HV interval during NSR (HV_{NSR}) is A + B, and the HV interval during PVC (HV_{PVC}) is B-A; a predicted PP time was calculated using HV_{NSR} and HV_{PVC}. The calculated formula is as follows: Predicted target PP = (HV_{NSR} + HV_{PVC})/2. During the repeat procedure, the mapping strategy only focuses on the earliest retrograde PP due to the injury or block of LAF sustained at the index procedure.

Results: Notably, 24 patients with LAF-PVC were included. The ECG characteristics of PVC exhibited right bundle branch block (RBBB) morphology with right-axis deviation (RAD) in 18 patients and only RAD in 6 patients. The QRS durations of NSR and PVC were 78.8 ± 7.9 and 106.8 ± 12.3 ms, respectively. There was no significant difference between the predicted and mapped PP site (31.5 ± 8.1 vs. 30.6 ± 7.8 ms; $P = 0.17$). There was a significant difference between the mean axis deviation before and after ablation (46.3 ± 25.4° vs. 18.3 ± 44.1°; $P = 0.001$); however, only 10 patients had a complete LAF block. Eight patients had a recurrence, the QRS morphology of LAF-PVC became narrower (95.9 ± 17.2 vs. 105.3 ± 16.9 ms, $P = 0.003$), and 4 patients's PVC QRS morphology was similar to NSR. During the repeat procedure, the earliest

OPEN ACCESS

Edited by:
Frank Heinzel,
Charité Universitätsmedizin Berlin, Germany

Reviewed by:
Martin Manninger,
Medical University of Graz, Austria
Maurizio Giuseppe Lunati,
Niguarda Ca' Granda Hospital, Italy

***Correspondence:**
Minglong Chen
chenminglong@njmu.edu.cn

[†] These authors have contributed equally to this work and share first authorship

Specialty section:
This article was submitted to Cardiac Rhythmology, a section of the journal Frontiers in Cardiovascular Medicine

Received: 16 November 2021
Accepted: 03 March 2022
Published: 31 March 2022

Citation:
Chen H, Xiao F, Ju W, Yang G, Zhang F, Gu K, Li M, Liu H, Wang Z, Sharma D, Cao K and Chen M (2022) Premature Ventricular Contractions From the Left Anterior Fascicle: Electrocardiographic and Electrophysiological Characteristics, Mapping Strategy, and Immediate and Long-Term Catheter Ablation Results. Front. Cardiovasc. Med. 9:816237. doi: 10.3389/fcvm.2022.816237

retrograde PP interval was longer than the index procedure in four patients (12.0 ± 1.9 vs. 37.8 ± 1.1 ms; $P < 0.001$).

Conclusion: The target PP site for ablation of the LAF region can be calculated using the HV interval during NSR and PVC at the index procedure. The mapping strategy at repeat procedures focused on the earliest retrograde PP interval.

Keywords: left anterior fascicle, premature ventricular contraction, presystolic purkinje potential, recurrence, catheter ablation

INTRODUCTION

Ventricular arrhythmias (VAs) arising from the left Purkinje system can be classified into left posterior fascicular, left anterior fascicular, and left upper septal (1–4). Idiopathic left ventricular tachycardia (ILVT) originating from the left posterior tachycardia is common. It can be treated with radiofrequency ablation with a high success rate, while VAs originating from the left anterior fascicle (LAF) are rare. LAF premature ventricular contractions (LAF-PVC) can be abolished by mapping using a point-to-point strategy (3) or targeting the earliest Purkinje potential (PP) (2). In this study, we investigated the following:

(1) the relationship between the predicted origin site based on our measurement and the mapped target site during LAF-PVC,
(2) electrocardiographic characteristics of LAF-PVC,
(3) the reason for recurrence and the mapping strategy during the repeat procedure.

MATERIALS AND METHODS

Patient Population

From January 2011 to September 2020, 27 consecutive patients (12 men, mean age 43.5 ± 17.9 years) refractory to 1.4 ± 1.0 antiarrhythmic drugs with LAF-PVC were prospectively enrolled in this study. The PVC electrocardiogram was recorded after enrollment. No patients had evidence of episodes of ventricular tachycardia. A flowchart of the study population was presented (**Figure 1**). The local institutional review board approved the study protocol, and all patients provided written informed consent.

Electrophysiological Study

No patients were on amiodarone before enrollment. All antiarrhythmic drugs were discontinued for at least five half-lives before the procedure. An electrophysiological study was performed after overnight fasting in a mildly sedated state. In patients with LAF-PVC, one 6F quadripolar catheter (Diag, St. Jude Medical, Inc.) was positioned in His-bundle *via* a left femoral vein approach; a 6F decapolar catheter (Diag, St. Jude Medical, Inc.) was positioned in the coronary sinus *via* the left femoral vein for endocardial reference if an EnSite Velocity System was used. An ablation catheter guided by 3-dimensional (3-D) electroanatomic mapping (EnSite Velocity System, St Jude Medical Inc., St Paul, MN, United States; or CARTO TM, Biosense-Webster Inc., Diamond Bar, California United States) was introduced into the left ventricle (LV) *via* a retrograde aortic approach for mapping and ablation. Intracardiac electrograms were recorded using a digital electrophysiological recording system (EP-workmate Electrophysiology, St. Jude Medical, Inc., St Paul, MN, United States or LabSystem, Bard Electrophysiology, Lowell, MA, United States) and were filtered from 30 to 300 Hz.

The baseline AH and HV intervals were recorded during normal sinus rhythm (NSR). In patients with LAF-PVC, the HV and coupled interval during PVC were measured. If LAF-PVC did not occur at baseline, then isoproterenol infusion (1–4 μg/min) was given to increase the heart rate by 30%. If the LAF-PVC was non-inducible, the case was excluded.

According to previous studies, the origin of LAF-PVC is located in the LAF at the site of the earliest retrograde PP (1, 2, 5), and the myocardial breakthrough site is adjacent to the LAF during PVC (5). The mapping strategy during the index procedure developed from our center has been previously described (1). In brief, the conduction interval from the earliest PP site to His was labeled as time A, the conduction interval from the earliest site to the onset of the QRS was delineated as time B, the HV interval during NSR (HV_{NSR}) was A + B, the HV interval during PVC (HV_{PVC}) was B-A, and the predicted target PP (B) was calculated from the HV_{NSR} and HV_{PVC}. The calculated formula is as follows: Predicted target PP = (HV_{NSR} + HV_{PVC})/2. During the repeat procedure, the mapping strategy focused on the earliest retrograde PP due to the injury or block of LAF.

Mapping and Ablation

Left ventricle geometry and activation mapping *via* a retrograde approach were created by 3-D mapping (CARTO system, Biosense-Webster Inc., Diamond Bar, CA; or EnSite Velocity System, St Jude Medical Inc., St Paul, MN, United States). Activation mapping during PVC was performed along the LAF to identify the earliest PP by 3D activation mapping. As a result, radiofrequency ablation energy utilizing a 4-mm non-irrigated catheter was delivered at the earliest PP during PVC. The power output was titrated to 30 W with a maximum target temperature of 50–60°C for 60–120 s. If the origin site was closer to the distal left bundle branch, the power output was started at 10 W

Abbreviations: ECG, electrocardiogram; ILVT, idiopathic left ventricular tachycardia; LAF, left anterior fascicle; LAF-PVC, LAF premature ventricular contractions; LPF, left posterior fascicle; LV, left ventricle; NSR, normal sinus rhythm; PP, Purkinje potential; PVC, premature ventricular contractions; RAD, right axis deviation; RBBB, right bundle branch block; VAs, ventricular arrhythmias.

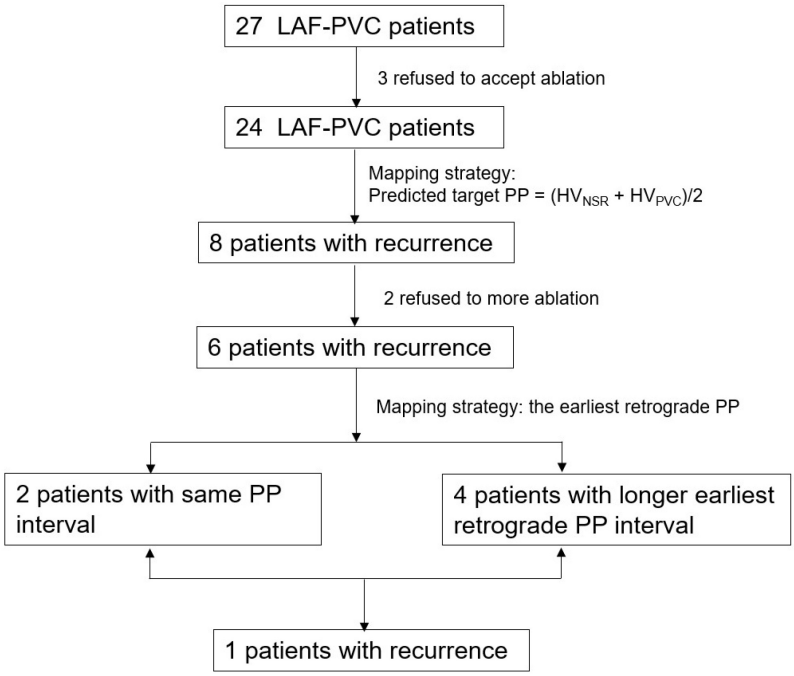

FIGURE 1 | A flowchart of the study population. PVC, premature ventricular contractions; LAF, left anterior fascicle.

and titrated to 20 W to avoid left bundle branch injury. Acute procedural success was defined as the termination of the LAF-PVC during ablation and the absence of arrhythmias within 30 min of the final radiofrequency ablation application despite programmed electrical stimulation with isoproterenol infusion.

Follow-Up

Surface ECGs and 24-h Holter recordings were performed regularly following the procedure and then at 3 and 6 months after discharge. Furthermore, an ECG was performed anytime if patients experienced palpitations.

Statistical Analysis

Data were analyzed using SPSS 18.0. Continuous variables are expressed as the mean ± SD. Then, the Mann-Whitney two-sample test examined group differences for continuous data. The categorical variables were compared with the chi-square test. A *P-value* of <0.05 was considered statistically significant.

RESULTS

Patient Characteristics

Among the 27 patients, three patients were excluded because two patients were non-inducible, and one patient had common iliac artery dissection while introducing an ablation catheter to the LV. The remaining 24 patients (10 men, mean age 40.7 ± 17.2 years) were enrolled in this study. The mean PVC burden and coupled interval were 18.8 ± 7.7% and 503.7 ± 63.1 ms, respectively. Their mean left ventricular ejection fraction and left ventricular diastolic diameter were 64.1 ± 3.2% and 46.0 ± 3.9 mm, respectively.

All patients had clinical palpitations for a mean of 39.9 ± 43.7 months. Eleven patients had no history of using verapamil, and only six of the remaining patients (46%) were sensitive to verapamil. The ECG characteristics of PVC exhibited right bundle branch block (RBBB) morphology with right axis deviation (RAD) in 18 patients and only RAD in 6 patients (**Table 1**); the mean axis deviation was 46.3 ± 25.4°. The QRS pattern of the LAF-PVC was roughly shaped like qR in leads II, III, and aVF. Interestingly, the QRS pattern of the LAF-PVC in V_1 was demonstrated as rs (2 cases), rS (2 cases), Rs (2 cases), rsr′ (2 cases), and rsR′ (16 cases). The QRS durations of NSR and PVC were 78.8 ± 7.9 and 106.8 ± 12.3 ms, respectively. The mean ratio of QRS duration with NSR and PVC was 0.74 ± 0.06.

Mapping and Ablation Left Anterior Fascicle-Premature Ventricular Contractions During the Index Ablation Procedure

According to the inferior leads of ECG, all PVC patients had an origin from the LAF. The mean AH, HV interval during NSR, and HV interval during LAF-PVC were 88.6 ± 14.5 ms, 47.7 ± 6.0 ms, and 15.7 ± 12.4 ms, respectively (**Table 2**). There was no significant difference between the predicted and mapped values (31.5 ± 8.1 vs. 30.6 ± 8.0 ms; $P = 0.17$), and three patients had differences in predicted and mapped values due to unstable ABL catheters. The acute success rate was 100% during the procedure. Eight patients had a recurrence, six of

TABLE 1 | Baseline characteristics of patients with premature ventricular contractions originated from the left anterior fascicle.

No.	Sex	Age (years)	Diagnosis	History (M)	PVC burden (%)	Morphology	LVDd	LVEF (%)	Numbers of AAD (N)	Verapamil	Follow up (M)
1	M	21	LAF-PVC	12	17.8	RAD	49	63.7	1	+	96
2	F	31	LAF-PVC	24	20.0	RBBB/RAD	48	62.1	1	–	87
3	M	50	LAF-PVC	12	19.8	RBBB/RAD	40	63	1	NO	77
4	F	15	LAF-PVC	120	20.5	RBBB/RAD	41	69.9	0	NO	77
5	F	57	LAF-PVC	120	11.0	RAD	42	65	1	NO	65
6	F	46	LAF-PVC	14	17.0	RBBB/RAD	43	62.1	3	NO	63
7	M	48	LAF-PVC	46	13.6	RBBB/RAD	40	66.2	1	NO	62
8	F	38	LAF-PVC	24	22.9	RAD	49	60	1	+	51
9	M	24	LAF-PVC	24	20.6	RBBB/RAD	40	62.1	1	–	49
10	F	23	LAF-PVC	12	14.4	RBBB/RAD	46	64	1	NO	49
11	F	40	LAF-PVC	60	19.9	RBBB/RAD	47	68	2	NO	48
12	F	51	LAF-PVC	4	12.4	RBBB/RAD	50	70.4	0	NO	46
13	M	71	LAF-PVC	180	49.0	RAD	46	66.9	2	+	42
14	M	19	LAF-PVC	12	12.6	RBBB/RAD	49	63.7	0	–	40
15	M	27	LAF-PVC	4	12.5	RBBB/RAD	45	59	3	+	37
16	M	74	LAF-PVC	24	14.8	RAD	48	67.4	4	+	37
17	F	38	LAF-PVC	6	12.8	RBBB/RAD	44	62.1	1	NO	25
18	F	37	LAF-PVC	36	12.7	RBBB/RAD	49	60.1	1	NO	23
19	F	38	LAF-PVC	3	22.0	RBBB/RAD	41	60.2	0	NO	19
20	M	75	LAF-PVC	60	28.8	RBBB/RAD	54	62.1	2	+	18
21	F	59	LAF-PVC	84	22.1	RBBB/RAD	49	63.7	1	–	17
22	M	20	LAF-PVC	24	12.6	RAD	49	69	1	–	16
23	F	46	LAF-PVC	24	18.2	RBBB/RAD	43	61.2	2	–	15
24	F	29	LAF-PVC	29	22.9	RBBB/RAD	52	65.9	3	–	3
Mean		40.7		39.9	18.8		46.0	64.1	1.4		44.2
STD		17.2		43.7	7.7		3.9	3.2	1.0		24.8

AAD, anti-arrhythmic drugs; LAF, left anterior fascicle; LVDd, left ventricle diastolic diameter; LVEF, left ventricular ejection fraction; M, months; N, number; PVC, premature ventricular contractions; NA, no available; RAD, right axis deviation; RBBB, right bundle branch block; +, sensitivity to verapamil; –, not sensitivity to verapamil.

whom recurred at an average of 1.3 ± 0.5 days after the index procedure. Three patients with different predicted and mapped values had a recurrence of PVC (**Table 2**); five patients with the same values had a recurrence. All patients without recurrence had the same predicted and mapped earliest PP interval, as illustrated in **Figure 2**. In patients with recurrence, the QRS morphology of NSR had slight changes; however, the QRS morphology of PVC became narrower than the basic pattern (95.9 ± 17.2 vs. 105.3 ± 16.9, $P = 0.003$), and four patients had a similar QRS morphology of PVC compared with NSR. There was a significant difference in the mean axis deviation before and after ablation during NSR (46.3 ± 25.4° vs. 18.3 ± 44.1°; $P = 0.001$); however, only ten patients had a complete LAF block. Furthermore, there was no significant difference between the mean axis deviation in the successful and unsuccessful groups after the index ablation procedure (16.7 ± 46.7° vs. 32.3 ± 31.7°; $P = 0.45$).

Mapping and Ablation Left Anterior Fascicle-Premature Ventricular Contractions During the Second Ablation Procedure

Eight patients who had documented recurrence of LAF-PVC were recommended to undergo a repeated ablation procedure. Six patients consented to the second ablation. All eight patients had a narrower LAF-PVC QRS duration compared with the index procedure (102.0 ± 13.1 vs. 83.6 ± 8.4; $P = 0.0003$), and five patients had the change of LAF-PVC QRS morphology in lead V_1, three patients PVC-QRS morphology changed from rsR′ to rS, one from Rs to rS, one from Rs to rs; the remaining three patients had the similar morphology.

Figure 3 shows an example of the failed case in patient 5, who refused repeat ablation. During the first procedure, the AH_{NSR}, HV_{NSR}, and HV_{PVC} intervals were 91, 56, and 34 ms, respectively; the axis deviation was 45°. The predicted value was 45 ms, and the earliest PP interval was also mapped with 45 ms; however, the radiofrequency energy was delivered at the distal site (32 ms), the QRS duration ratio of NSR/PVC after ablation increased from 0.68 to 0.93, and the axis deviation increased to 58°.

During the repeat procedure of the six consented patients, the earliest retrograde PP interval during PVC was mapped. Four patients had different predicted and mapped values. The earliest retrograde PP interval during PVC was mapped to the vicinity of the LAF, to a similarly located site of the index procedure in four cases. The earliest retrograde PP interval was longer than the index procedure (12.0 ± 1.9 vs. 37.8 ± 1.1; $P < 0.001$) (**Figures 4**, **5**).

Figure 4 (patient 22) shows that the HV_{NSR} interval was the same as that of the first procedure, while the HV_{PVC} interval was 20 ms; the QRS duration after ablation decreased from 96

TABLE 2 | Electrophysiological characteristics and follow-up result after the index ablation procedure.

No.	Age	NSR QRS duration	PVC QRS duration	NSR/PVC QRS ratio	PVC pattern*	Coupled interval (ms)	Axis before ablation	Axis after ablation	AH-SR (ms)	HV-SR (ms)	HV-PVC (ms)	Predicted PP site (ms)	Mapped PP site (ms)	NSR PP site (ms)	LAF block	Success
1	21	80	100	0.80	qR/rs	560	67	11	96	53	38	45	45	45	+	+
2	31	80	120	0.67	qR/rsR′	460	−8	−13	90	42	12	27	27	27	−	+
3	50	90	120	0.75	qR/rsR′	464	55	64	84	52	24	38	38	38	−	+
4	15	65	98	0.66	qR/rsR′	564	63	53	75	45	15	30	30	30	−	−
5	57	80	118	0.68	qR/Rs	544	45	58	100	56	34	45	32	32	+	−
6	46	80	120	0.67	qR/rsR′	480	46	NA	92	55	6	30	20	20	+	−
7	48	104	132	0.79	qR/rsR′	520	48	50	100	35	25	30	30	30	−	+
8	38	80	106	0.75	qR/rs	620	21	30	96	46	12	29	29	29	+	−
9	24	82	100	0.82	qR/rsR′	520	21	11	110	46	22	34	34	34	−	+
10	23	63	82	0.77	qR/rsR′	596	73	68	100	50	25	37	40	40	+	−
11	40	84	106	0.79	qR/rsR′	596	43	−7	106	50	0	25	25	25	−	−
12	51	76	96	0.79	qR/rsR′	428	73	63	84	52	16	34	34	34	−	+
13	71	82	106	0.77	qR/rS	528	67	−7	66	50	42	46	46	46	+	+
14	19	80	106	0.75	qR/rsR′	426	30	11	116	54	0	27	27	27	−	+
15	27	74	96	0.77	qR/rsR′	460	81	80	100	40	20	30	30	30	+	+
16	74	80	108	0.74	qR/Rs	484	−18	−90	68	46	10	28	28	28	−	+
17	38	72	88	0.82	qR/rsR′	484	82	53	66	54	12	33	33	33	+	+
18	37	70	90	0.78	qR/rsR′	440	60	54	80	49	11	30	30	30	−	−
19	38	80	118	0.68	qR/rsR′	545	60	60	80	48	20	34	34	34	+	+
20	75	80	110	0.73	qR/rsR′	480	30	−42	108	52	26	39	39	39	+	+
21	59	78	128	0.61	qR/rsR′	404	47	−22	68	38	−8	10	10	10	−	+
22	20	72	96	0.75	qR/rs	440	53	−30	74	54	10	32	32	32	−	−
23	46	76	110	0.69	qR/rsR′	612	15	21	80	40	5	22	22	22	−	+
24	29	82	108	0.76	qR/rsR′	434	56	−49	87	40	0	20	20	20	−	+
Mean	40.7	78.8	106.8	0.74		503.7	46.3	18.3	88.6	47.7	15.7	31.5	30.6	30.6		
STD	17.2	7.9	12.3	0.06		63.1	25.4	44.1	14.5	6.0	12.4	8.1	8.0	8.0		

LAF, left anterior fascicle; NA, no available; PVC, premature ventricular complex; NSR, normal sinus rhythm; TCL, tachycardia cycle length.
**The QRS pattern of PVC in leads II, III, and avF and the lead V1, respectively.*

to 80 ms; the PVC morphology was similar to baseline. The NSR-QRS morphology slightly changed; the same site was identified, and the earliest retrograde PP with 36 ms was mapped and had successful ablation using 3-D activation mapping. A schematic diagram demonstrates slow conduction within the LAF fiber, and the electrocardiogram reveals a left anterior block after successful ablation.

Figure 5 demonstrates that in patient 8, the HV_{NSR} interval was the same as that of the first procedure, while the HV_{PVC} interval was 28 ms. The QRS duration ratio of NSR/PVC increased from 0.75 to 0.95, and the PVC morphology was similar to the NSR-QRS morphology. The catheter was positioned at the same site with recordings of local anterior PP-the onset of a surface ECG interval of 38 ms during PVC compared with the index procedure.

Final Follow-Up Results

After a mean follow-up of 44.3 ± 24.8 months after the last ablation procedure, three patients had a recurrence and were prescribed metoprolol to control symptoms. All other patients had no arrhythmia recurrence.

Complications

No complications were observed in the study patients during the perioperative period.

DISCUSSION

Major Finding

This is the first report of the long-term follow-up results of LAF-PVC in a relatively large sample. Our study found that the target site can be calculated by the HV interval during NSR and PVC. Locations of recurrent PVCs in repeat procedures were anatomically close to the ablation sites during the index procedure even though the QRS morphology of the PVC is different compared with the index procedure. The QRS morphology of LAF-PVC is dependent on how slow conduction over LAF occurs in recurrence patients. If the conduction velocity is slightly slower over LAF, the PVC morphology might be similar, but the QRS duration becomes narrower; if the conduction velocity is rebalanced over both left fascicles, the PVC-QRS morphology might be similar to NSR.

The Anatomy of the Left Anterior Purkinje System

Basic histological studies or postmortem examination have demonstrated that the left His-Purkinje system is a fan-like structure with a bifascicular structure or three major divisions; which means left posterior fascicle (LPF) and LAF with or without left middle fascicle (6–8). Long et al. elucidated the entire left His-Purkinje system in the human heart during NSR

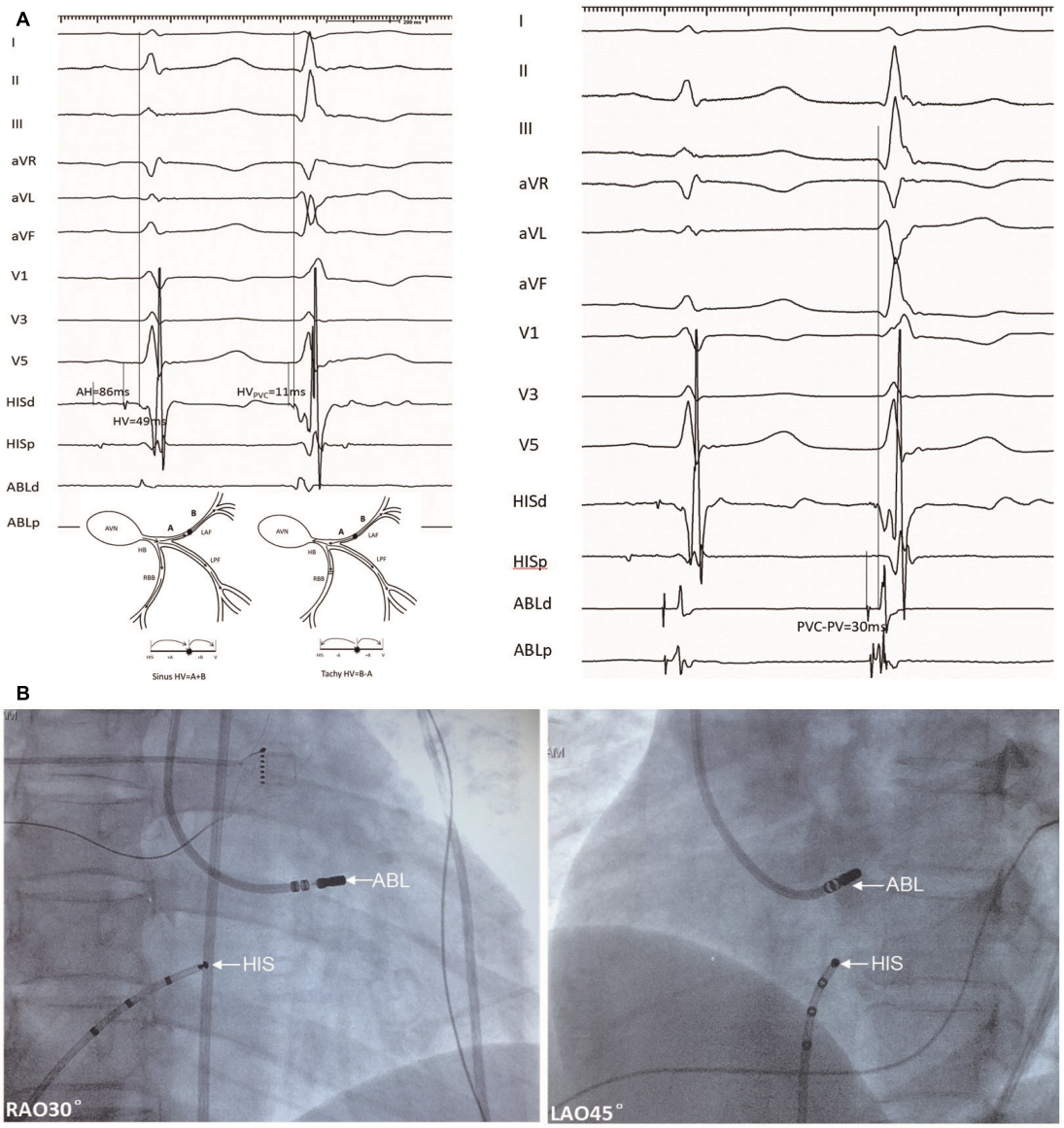

FIGURE 2 | An example of a target ablation site for a PVC originating from the LAF (Patient 18). **(A)** Left panel, HV intervals during NSR and PVC with mapping electrode positioned at the His bundle were 49 and 11 ms, respectively. Right panel, the catheter was positioned at the target site with a recording interval of 30 ms during PVC between local fascicular potential (PP) and surface ECG, this is equal to the predicted value. **(B)** Fluoroscopy of LAF-PVC target. PVC, premature ventricular contractions; LAF, left anterior fascicle; NSR, normal sinus rhythm; ABL, ablation electrode; H-V, His bundle to the onset of surface ventricular activation; RAO, right anterior oblique; and LAO, left anterior oblique.

(5). Their study demonstrated that 92% of patients bifurcated into LAF and LPF divisions. Furthermore, the length of LAF was shorter than that of LPF. They also identified that the activation time of LAF was shorter than that of LPF in 24 patients, who presented preferential conduction over LAF with a single ventricular breakthrough site.

The Mechanism of Different QRS Morphology in Recurrent Patients

Left ventricular arrhythmia originating from the left posterior fascicle is common. The QRS morphology shows RBBB and left axis deviation (9). Ventricular arrhythmia with QRS morphology similar to that of NSR or incomplete RBBB was demonstrated to arise from the left upper septum (4). In our study, all patients shared small q waves and tall R waves in inferior leads, and most of the patients (74%) showed incomplete RBBB in the V_1 lead. The mechanism might be preferential conduction over LAF. In patients with proximal LAF origin, the QRS morphology of V_1 was similar to that of the NSR electrocardiogram at baseline. In the patients with recurrence, the PVC-QRS duration was narrower (102.0 ± 13.1 vs. 83.6 ± 8.4; P = 0.0003), and five patients had a change in LAF-PVC QRS morphology in lead V_1. Three patients had PVC-QRS

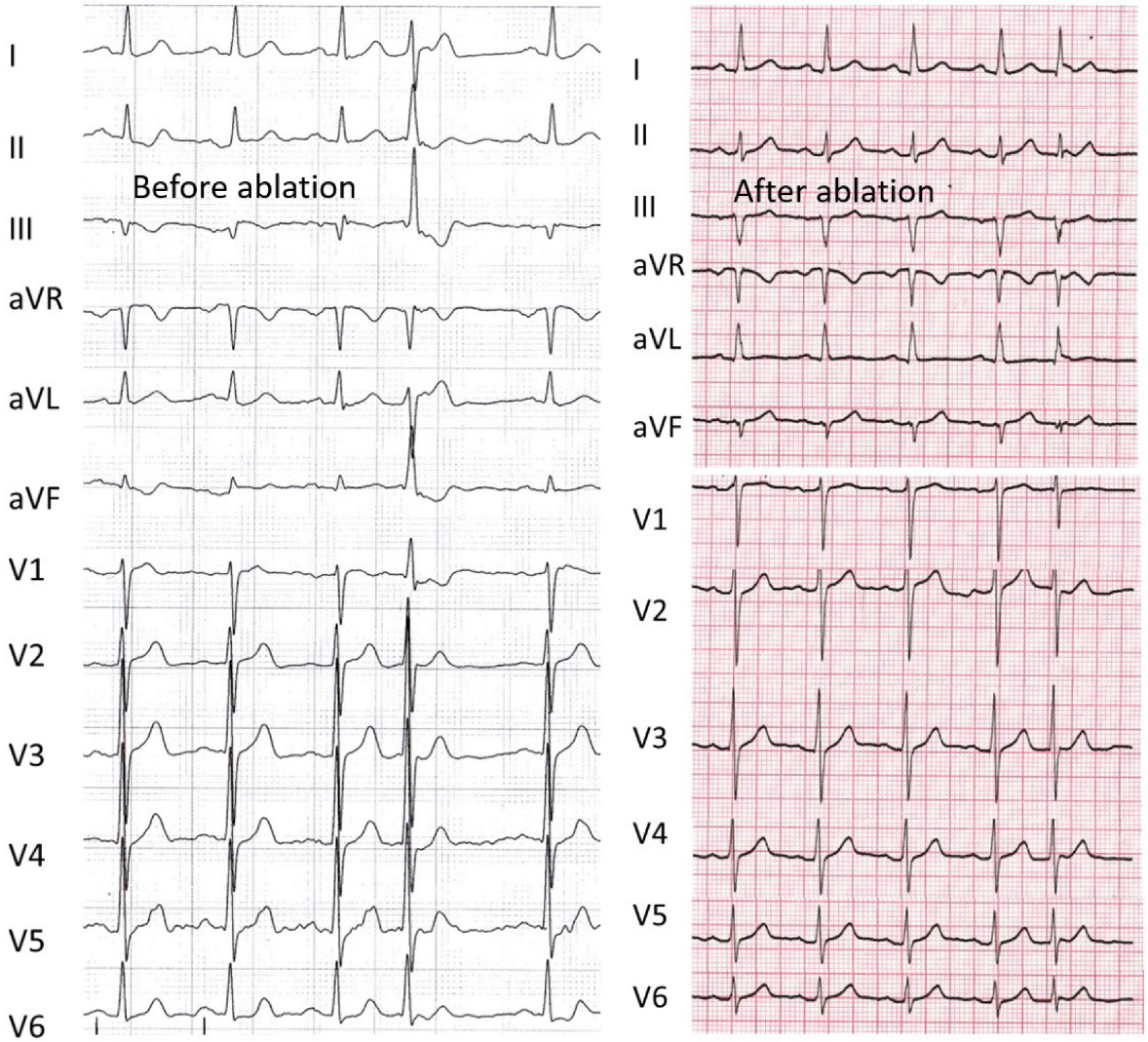

FIGURE 3 | An example of a failed case that refused more procedures (Patient 5). Left panel, the axis deviation was 45° before ablation, and radiofrequency energy was delivered at the distal site. Right panel, the patient had recurrence after the index procedure, the QRS duration ratio of NSR/PVC after ablation increased from 0.68 to 0.93, and the axis deviation increased to 58°. The abbreviations are as in **Figure 2**.

morphology that changed from rsR′ to rS, one from Rs to rS, and one from Rs to rs. The similarity between PVC-QRS morphology during the index and repeat procedure was identified in three patients. This phenomenon might be explained as follows:

1. Ineffective ablation lesions.
2. If there was slower conduction, which means the preferential conduction was still over LAF than LPF, the PVC-QRS duration was slightly narrower with a similar morphology after the index ablation.
3. If there was further slower conduction over LAF, which led to rebalancing conduction over both left fascicles, the PVC-QRS duration was narrower, and the PVC morphology was similar to that of NSR.
4. If there was block conduction over LAF, we can speculate that the PVC-QRS morphology might show left axis deviation.

Previous studies have demonstrated changes in QRS morphology in recurrent patients with idiopathic left posterior ventricular tachycardia. Zhang et al. recently reported that upper septal ventricular tachycardia is identified in recurrent patients with the previous ablation of typical ILVT, which led to narrow QRS morphology (10). Other studies also had similar findings (4, 11). Their mechanism of recurrence is reentry or a new focal origin. However, in our study, the recurrent patients had the same origin. The change in QRS morphology depends on the conduction velocity over LAF, different from previous studies (4, 10, 11).

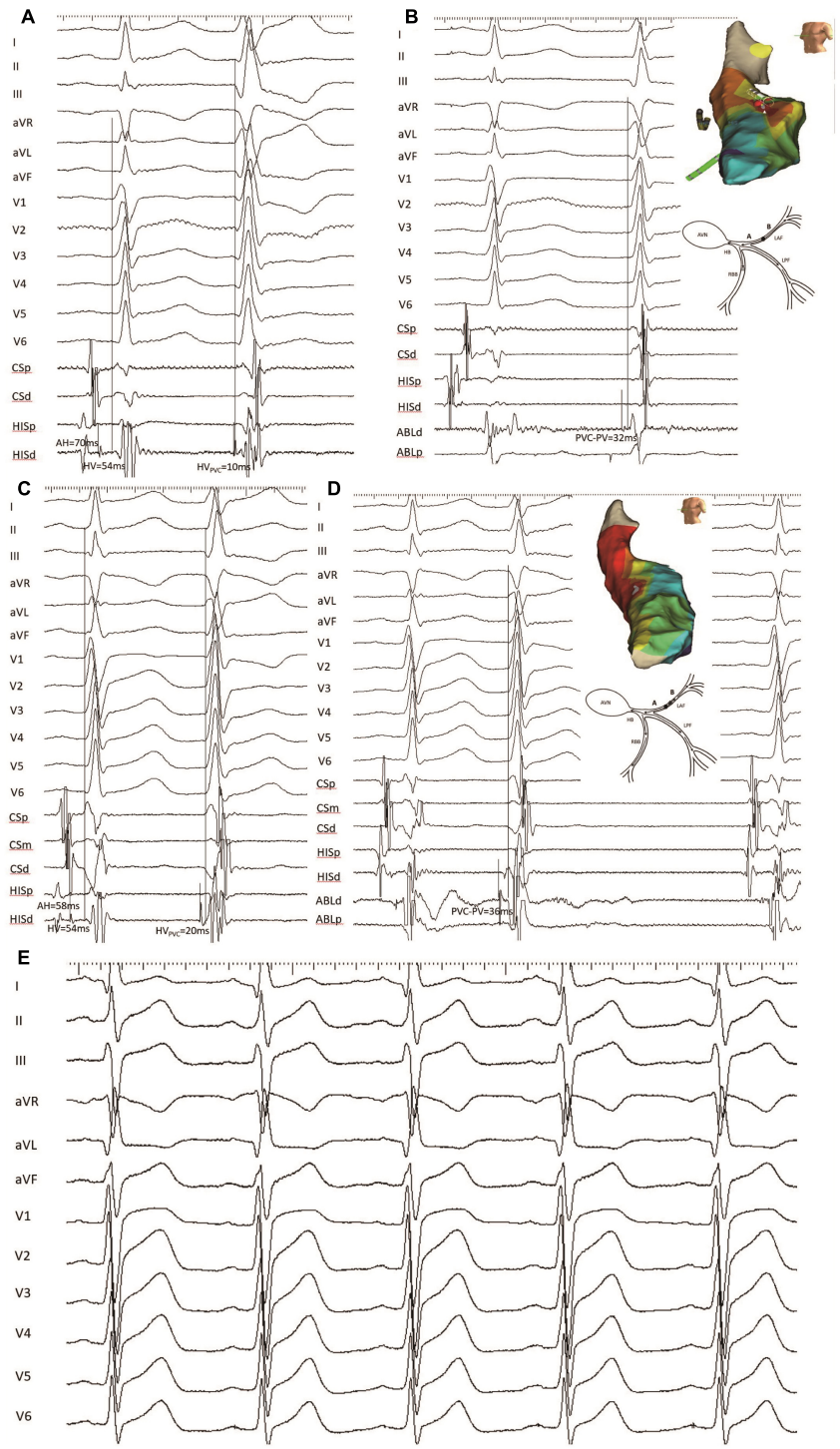

FIGURE 4 | An example of a failed patient with LAF-PVC who underwent a repeat ablation procedure (patient 22). **(A)** HV interval during NSR and PVC with mapping electrode positioned at the His bundle was 54 and 10 ms, respectively. **(B)** The target site was mapped with recordings of local fascicular potential-the onset of the QRS interval of 32 ms during PVC. Three-dimensional activation mapping of the left anterior area showed the target site, and a schematic diagram showed conduction within the Purkinje system. **(C)** During the repeat procedure, the HV_{NSR} interval was the same as that during the first procedure, while the HV_{PVC} interval was 20 ms; the QRS duration after ablation decreased from 96 to 80 ms, and the axis deviation increased to 21°. Note that NSR-QRS morphology had a slight change, and the QRS duration of PVC was slightly narrower than that before ablation. **(D)** The same site was identified, and the earliest retrograde PP with 36 ms was mapped and had successful ablation. Three-dimensional activation mapping of the left anterior area showed the target site and a schematic diagram showing the slow conduction within the LAF fiber. It is noted that the target PP was sharp during PVC, while the PP was fragmented during NSR. **(E)** The electrocardiogram showed the left anterior block after successful ablation. CS, coronary sinus; PP, Purkinje potential; the other abbreviations are as in **Figure 2**.

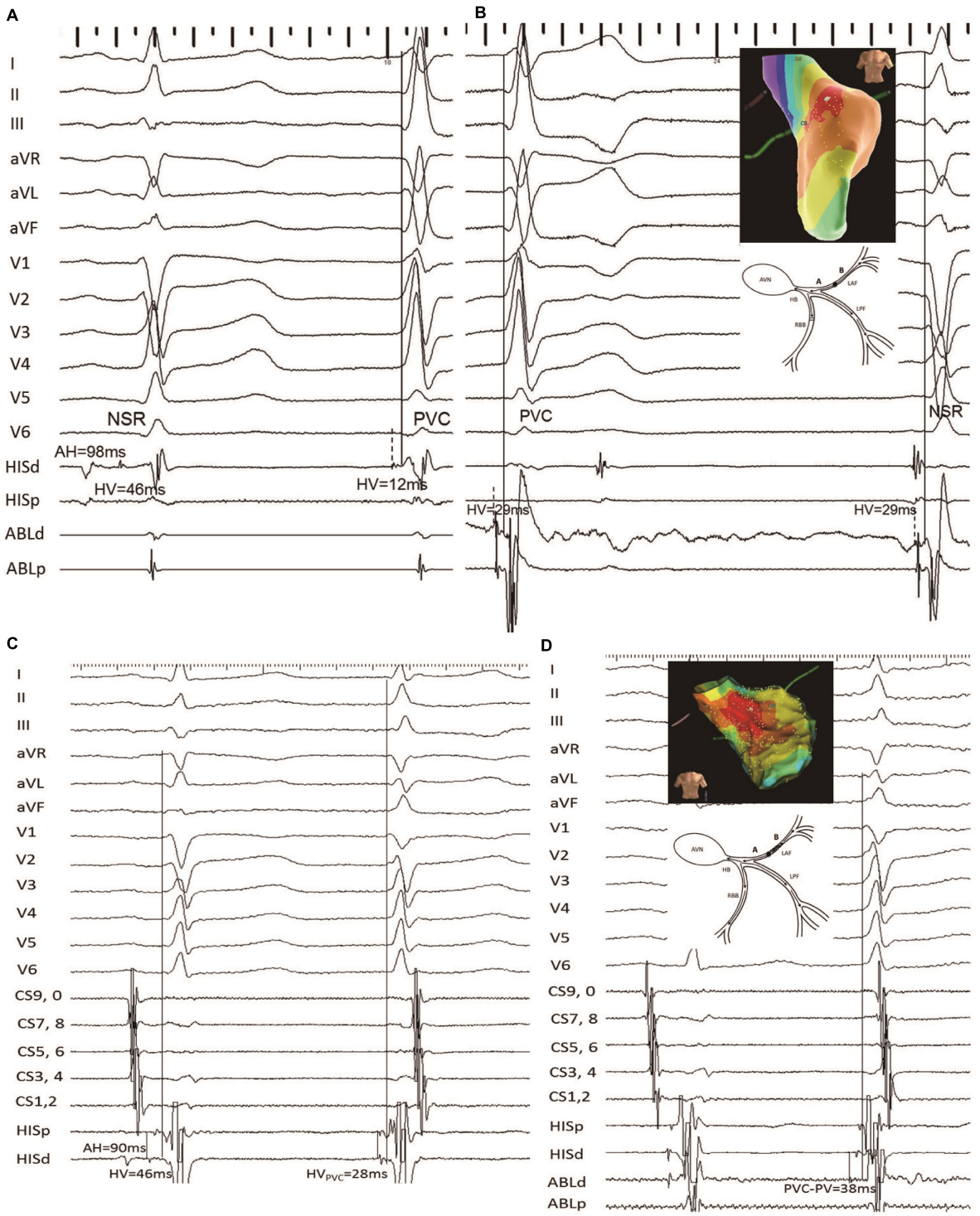

FIGURE 5 | Another example of failed LAF-PVC case (patient 8). **(A)** The HV intervals during SNR and PVC with the mapping electrode positioned at the His bundle were 46 and 12, respectively; it is noted that the predicted value was 29 ms. **(B)** The catheter was positioned at the target site with recordings of local anterior PP-the onset of surface ECG interval of 29 ms during PVC. Three-dimensional activation mapping of the left anterior area shows the target site. **(C)** The HV_{NSR} interval was the same as that of the first procedure, while the HV_{PVC} interval was 28 ms; the QRS duration ratio of NSR/PVC increased from 0.75 to 0.95; and the QRS morphology of PVC was similar to the NSR-QRS morphology. **(D)** The earliest retrograde PP with 38 ms was mapped and had successful ablation. Three-dimensional activation mapping of the left anterior area showed the target site and a schematic diagram showing the slow conduction within the LAF fiber, which might explain the reason for the narrower QRS. It is noted that the target PP was fragmented during PVC. CS, coronary sinus; the other abbreviations are as in **Figure 2**.

The Mapping and Ablation Strategy for Left Anterior Fascicle-Premature Ventricular Contractions

During the index procedure, a previous study showed a simple point-to-point mapping strategy along with the left anterior fiber in two cases. If the earliest activation time was mapped, the target site was identified. They also found that the target site's fascicular potential to ventricle interval is identical during NSR and PVC (3). Recently, Wang et al. (2). reported a selective method in three cases. They found that the target site should be identified by the earliest presystolic PP but not the earliest ventricular activation mapping in patients with LAF-PVC. Our previous study (1) showed a straightforward method with a formula to identify the target site in a series of patients with ILVT. The calculated formula is as follows: Predicted target PP = $(HV_{NSR} + HV_{PVC})/2$. This study also proves this formula in patients with LAF-PVC, and the success rate was 76% (16/21). All three cases had recurrence with different predicted and mapped values during the index procedure and the repeat procedure (3/3, 100%). One of the cases had recurrence with narrower PVC-QRS morphology (**Figure 3**). Patients with the same predicted and mapped values who had recurrence might have poor contact.

The earliest PP is suggested in previous studies during the repeat procedure with recurrence LAF-PVC cases (10, 11). However, no study has focused on LAF-PVC or mentioned the reasons for recurrence. Our study is the first to describe the mapping strategy with the earliest retrograde PP in a series cohort of patients with LAF-PVC. This method is simple but effective for identifying the target site. The QRS morphology depends on the LAF conduction characteristics; our study showed that PVC-QRS could be similar to NSR during the repeat procedure despite the same LAF site of origin, not near the His area. However, if we focused on the His region according to narrower PVC-QRS morphology, an unnecessary third-degree atrioventricular block might occur, and the LAF-PVC would also recur. In this study, the earliest retrograde PP was mapped in the LAF region in recurrent cases, and the success rate was 83% (5/6), even though the PVC-QRS morphology differed.

The ablation endpoint in ILVT was controversial. Some studies demonstrated that a complete LPF block is associated with a high procedural success rate (12, 13); others showed that LPF block is not necessary for success (14, 15). In patients with LAF-PVC, controversy also exists. A previous study demonstrating changes in the QRS axis and morphology noted in two cases indicated proximal LAF block (3). In our study, there was a significant difference in the mean axis deviation before and after ablation (46.3 ± 25.4° vs. 18.3 ± 44.1°; $P = 0.002$). However, LAF block was only identified in ten cases (41.7%). Therefore, we can speculate that the LAF block was unnecessary to predict success even though there were changes in the QRS axis or morphology. The LAF block was just a byproduct following LAF region ablation.

Limitations

First, this study involved only a small number of patients due to rare cases of LAF-PVC. Second, we used the formula to predict the origin site; however, the ventricular breakthrough site may affect the HV interval during NSR, which could lead to incorrect calculation of the predicted location. Third, we did not analyze the PVC mechanism; and fourth, verapamil was prescribed in 13 patients, and verapamil sensitivity was only identified in six patients.

CONCLUSION

The target PP site for ablation of the LAF region can be calculated using the HV interval during NSR and PVC. During the repeat procedures, the earliest retrograde PP should be targeted.

DATA AVAILABILITY STATEMENT

The original contributions presented in the study are included in the article/supplementary material, further inquiries can be directed to the corresponding author.

ETHICS STATEMENT

The studies involving human participants were reviewed and approved by the local institutional review board. Written informed consent to participate in this study was provided by the participants' legal guardian/next of kin.

AUTHOR CONTRIBUTIONS

MC and HC participated in the design of this study. HC, FX, WJ, GY, and FZ mapped and ablated all the cases. ML, KG, ZW, and HL collected and performed the statistical analysis. HC and FX wrote the first draft of the manuscript. DS revised the manuscript. MC and KC monitored this study. All authors provided input on data analysis and interpretations, participated in multiple revisions of the manuscript, approved the final version of the manuscript, and agreed to be accountable for all aspects of the work.

FUNDING

This study was supported by the National Natural Science Foundation of China (grant number: 82170322) and the Special Foundation for Clinical Science and Technology of Jiangsu Province (grant number: BE2017754).

ACKNOWLEDGMENTS

We thank Yumin Sun for providing one case from the Department of Cardiology at Shanghai Jing'an Central Hospital. We also thank Weiming Wang for providing one case from the Department of Cardiology at the Third Affiliated Hospital of Soochow University.

REFERENCES

1. Chen H, Zhang F, Yang B, Shehata M, Ju W, Yang G, et al. A novel method to identify the origin of ventricular tachycardia from the left fascicular system. *Heart Rhythm.* (2016) 13:686–94. doi: 10.1016/j.hrthm.2015.12.003
2. Wang YF, Xu Q, Luo HD, Yu JW, Qu BM, Wang LH. Catheter ablation of premature ventricular contractions arising from left anterior fascicle guided by an earliest presystolic Purkinje potential. *Int J Cardiol.* (2016) 221:280–2. doi: 10.1016/j.ijcard.2016.07.095
3. Ma W, Wang X, Cingolani E, Thajudeen A, Gupta N, Nageh MF, et al. Mapping and ablation of ventricular tachycardia from the left upper fascicle: how to make the most of the fascicular potential? *Circ Arrhythm Electrophysiol.* (2013) 6:e47–51. doi: 10.1161/CIRCEP.113.000249
4. Guo XG, Liu X, Zhou GB, Sun Q, Yang JD, Luo B, et al. Clinical, electrocardiographic, and electrophysiological characteristics of left upper septal fascicular ventricular tachycardia. *Europace.* (2018) 20:673–81. doi: 10.1093/europace/euw429
5. Long DY, Dong JZ, Sang CH, Jiang CX, Tang RB, Yan Q, et al. Isolated conduction within the left His-Purkenje system during sinus rhythm and idiopathic left ventricle tachycardia: findings from mapping the whole conduction system. *Circ Arrhythm Electrophysiol.* (2013) 6:522–7. doi: 10.1161/CIRCEP.113.000293
6. Suma K. Sunao Tawara: a father of modern cardiology. *Pacing Clin Electrophysiol.* (2001) 24:88–96. doi: 10.1046/j.1460-9592.2001.00088.x
7. Myerburg RJ, Stewart JW, Hoffman BF. Electrophysiological propertiesf the canine peripheral A-V conducting system. *Circ Res.* (1970) 26:361–78. doi: 10.1161/01.res.26.3.361
8. Kulbertus HE. Concept of left hemiblocks revisited. A histopathological and experimental study. *Adv cardiol.* (1975) 14:126–35. doi: 10.1159/000397645
9. Nogami A, Naito S, Tada H, Taniguchi K, Okamoto Y, Nishimura S, et al. Demonstration of diastolic and presystolic Purkinje potentials as critical potentials in a macroreentry circuit of verapamil-sensitive idiopathic left ventricular tachycardia. *J Am Coll Cardiol.* (2000) 36:811–23. doi: 10.1016/s0735-1097(00)00780-4
10. Liu Y, Fang Z, Yang B, Kojodjojo P, Chen H, Ju W, et al. Catheter ablation of fascicular ventricular tachycardia: long-term clinical outcomes and mechanisms of recurrence. *Circ Arrhythm Electrophysiol.* (2015) 8:1443–51. doi: 10.1161/CIRCEP.115.003080
11. Talib AK, Nogami A, Morishima I, Oginosawa Y, Kurosaki K, Kowase S, et al. Non-reentrant fascicular tachycardia: clinical and electrophysiological characteristics of a distinct type of idiopathic ventricular tachycardia. *Circ Arrhythm Electrophysiol.* (2016) 9:e004177. doi: 10.1161/CIRCEP.116.004177
12. Luo B, Zhou G, Guo X, Liu X, Yang J, Sun Q, et al. Long-term outcome of catheter ablation for left posterior fascicular ventricular tachycardia with the development of left posterior fascicular block and characteristics of repeat procedures. *Int J Cardiol.* (2017) 236:203–8. doi: 10.1016/j.ijcard.2017.01.152
13. Kataria V, Yaduvanshi A, Kumar M, Nair M. Demonstration of posterior fascicle to myocardial conduction block during ablation of idiopathic left ventricular tachycardia: an electrophysiological predictor of long-term success. *Heart Rhythm.* (2013) 10:638–45. doi: 10.1016/j.hrthm.2013.01.001
14. Fishberger SB, Olen MM, Rollinson NL, Rossi AF. Creation of partial fascicular block: an approach to ablation of idiopathic left ventricular tachycardia in the pediatric population. *Pacing Clin Electrophysiol.* (2015) 38:209–15. doi: 10.1111/pace.12551
15. Wissner E, Menon SY, Metzner A, Schoonderwoerd B, Nuyens D, Makimoto H, et al. Long-term outcome after catheter ablation for left posterior fascicular ventricular tachycardia without development of left posterior fascicular block. *J Cardiovasc Electrophysiol.* (2012) 23:1179–84. doi: 10.1111/j.1540-8167.2012.02377.x

Conflict of Interest: The authors declare that the research was conducted in the absence of any commercial or financial relationships that could be construed as a potential conflict of interest.

frontiers | Frontiers in Cardiovascular Medicine

ORIGINAL RESEARCH
published: 25 May 2022
doi: 10.3389/fcvm.2022.910042

Ablation of Outflow Tract Arrhythmias in Patients With and Without Structural Heart Disease—A Comparative Analysis

Ruben Schleberger[1,2], Jan Riess[1], Anika Brauer[1], Hans O. Pinnschmidt[3], Laura Rottner[1,2], Fabian Moser[1], Julia Moser[1], Shinwan Kany[1], Ilaria My[1], Marc D. Lemoine[1,2], Bruno Reissmann[1], Christian Meyer[4,5], Andreas Metzner[1], Feifan Ouyang[1,6], Paulus Kirchhof[1,7] and Andreas Rillig[1]*

[1] Department of Cardiology, University Heart and Vascular Center Hamburg, University Medical Center Hamburg-Eppendorf, Hamburg, Germany, [2] DZHK (German Center for Cardiovascular Research), Partner Site Hamburg/Kiel/Lübeck, Berlin, Germany, [3] Institute of Medical Biometry and Epidemiology, Center of Experimental Medicine, University Medical Center Hamburg-Eppendorf, Hamburg, Germany, [4] Department of Cardiology, Cardiac Neuro- and Electrophysiology Research Consortium, Protestant Hospital Düsseldorf, Düsseldorf, Germany, [5] Cardiac Neuro- and Electrophysiology Research Consortium, Medical Faculty, Heinrich Heine University Düsseldorf, Düsseldorf, Germany, [6] Hong Kong Asian Medical Group, Hong Kong, China, [7] Institute of Cardiovascular Sciences, University of Birmingham, Birmingham, United Kingdom

Introduction: Catheter ablation of ventricular arrhythmias emerging from the ventricular outflow tracts and adjacent structures is very effective and considered almost curative in patients without structural heart disease (SHD). Outcomes of patients with SHD undergoing ablation of outflow tract arrhythmias are not known.

Methods: Consecutive patients (2019–2021) undergoing catheter ablation of ventricular arrhythmias in a single high-volume center were retrospectively analyzed. Patients with ablation of outflow tract arrhythmias were identified and divided in individuals with and without SHD. Procedural parameters and acute outcome were compared.

Results: We identified 215 patients with outflow tract arrhythmias (35.3% female, mean age 58.3 ± 16.0 years). Of those, 93 (43.3%) had SHD. Patients with SHD and outflow tract arrhythmias were older (65.0 ± 12.8 vs. 53.3 ± 16.3 years; $p < 0.001$), more often male (82.8 vs. 50.0%; $p < 0.001$) and had more comorbidities than patients without SHD (arterial hypertension: 62.4 vs. 34.4%, $p < 0.001$; diabetes: 22.6 vs. 8.2%, $p = 0.005$; chronic lung disease: 20.4 vs. 7.4%, $p = 0.007$). Outflow tract arrhythmias in patients with SHD had their origin more often in the left ventricle (68.8 vs. 53.3%, $p = 0.025$). The acute success rate was similar in both patient groups (93.4 vs. 94.2%, $p = 0.781$). Patients with SHD were discharged later {median length of hospital stay with SHD 5 [6 (interquartile range)] days, without SHD 2 [4] days, $p < 0.001$}. Periprocedural complications were numerically more frequent in patients with SHD [with SHD 12 (12.9%), without SHD 8 (6.6%), $p = 0.154$].

OPEN ACCESS

Edited by:
Francesco Santoro, University of Foggia, Italy

Reviewed by:
Christian Hendrik Heeger, University Heart Center Luebeck, Germany
Christian Sohns, Heart and Diabetes Center North Rhine-Westphalia, Germany
Florian Straube, Heart Center Munich-Bogenhausen, Cardiology and Internal Intensive Care Medicine, Germany

***Correspondence:**
Ruben Schleberger
r.schleberger@uke.de

Specialty section:
This article was submitted to Cardiac Rhythmology, a section of the journal Frontiers in Cardiovascular Medicine

Received: *31 March 2022*
Accepted: *15 April 2022*
Published: *25 May 2022*

Citation:
Schleberger R, Riess J, Brauer A, Pinnschmidt HO, Rottner L, Moser F, Moser J, Kany S, My I, Lemoine MD, Reissmann B, Meyer C, Metzner A, Ouyang F, Kirchhof P and Rillig A (2022) Ablation of Outflow Tract Arrhythmias in Patients With and Without Structural Heart Disease—A Comparative Analysis. Front. Cardiovasc. Med. 9:910042. doi: 10.3389/fcvm.2022.910042

Conclusion: Outflow tract arrhythmia ablation has a high success rate irrespective of the presence of SHD. Longer hospital stay and potentially a higher risk of periprocedural complications should be considered when discussing this treatment option with patients.

Keywords: catheter ablation, outflow tract arrhythmia, procedural outcome, structural heart disease, ventricular tachycardia, premature ventricular complexes

INTRODUCTION

Despite advances in mapping and ablation technology, catheter ablation of ventricular arrhythmias remains difficult (1). Acute and long-term outcome vary depending on patient selection (2–5). Large substrates and multiple origins of ventricular tachycardias (VT) are reasons for a low success rate, especially in patients with structural heart disease (SHD) (6). Subtypes with excellent outcome are ventricular arrhythmias emerging from the right ventricular outflow tract and -to a lesser extent- also from the left ventricular outflow tract including its adjacent structures like aortic cusps, aortomitral continuity and left ventricular summit (7–10). Many patients present with such outflow tract arrhythmias and SHD. These arrhythmias are considered more difficult to treat by ablation due to presence of myocardial substrate areas and might differ from idiopathic outflow tract arrhythmias because of a reentry rather than focal mechanism (11). Whether the outcome of outflow tract arrhythmias in patients with SHD is comparable to that in patients without SHD is not known. We therefore analyzed procedural outcomes in a large series of patients undergoing ablation of outflow tract arrhythmias with and without SHD.

METHODS

Study Design

Consecutive patients presenting for ablation of ventricular arrhythmias at our tertiary care center between January 2019 and October 2021 were retrospectively analyzed. Patients with insufficient available procedural data were excluded from analysis (see **Figure 1**). Data collection and analysis were approved by the ethics committee of the Medical Association Hamburg. All patients gave written informed consent to data analysis and procedure.

Patients with outflow tract arrhythmias were identified and classified as patients with or without SHD. All patients had cardiac imaging (e.g., echocardiography, cardiac magnetic resonance imaging or computer tomography before the procedure). SHD was defined as history of or present evidence of abnormal systolic or diastolic ventricular function or more than mild abnormality of cardiac dimensions and diameters, abnormalities of myocardial texture, known coronary artery disease, higher than mild valve regurgitation or any valve stenosis or congenital heart disease. Baseline parameters, procedural characteristics and acute outcome were analyzed.

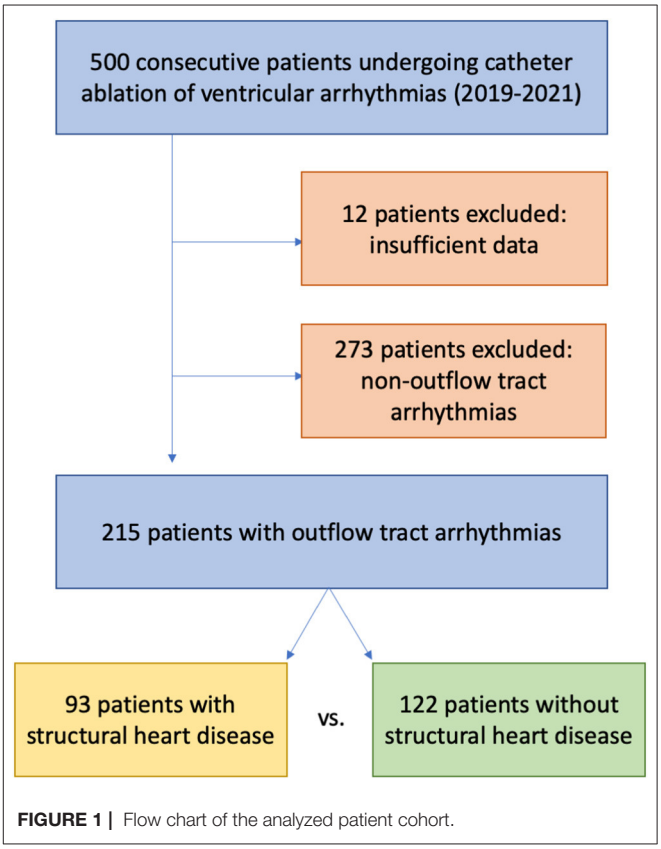

FIGURE 1 | Flow chart of the analyzed patient cohort.

Electrophysiological Evaluation and Instrumentation

The procedures were performed under conscious sedation or general anesthesia. Reversible causes of arrhythmia were excluded before the procedure. Detailed procedural methods have been described before (12). Electroanatomical three-dimensional mapping was performed using the Carto mapping system (Carto® 3 System, Biosense Webster, Irvine, CA, USA). Unfractionated heparin was administered intravenously to maintain an activated clotting time >300 s in patients with left ventricular access, all others received a heparin bolus of 3.000 IE in the beginning of the procedure. At first an electroanatomical voltage map was acquired with a steerable single-tip ablation catheter (THERMOCOOL®, D- or F-Type, 2-5-2 mm spacing, Biosense Webster) or a multipolar mapping catheter (PENTARAY™ NAV eco Catheter, Biosense Webster) through retrograde (aortic) and/or antegrade (transseptal) access (13). Local abnormal ventricular activity, including fractionated

TABLE 1 | Baseline characteristics of patients with outflow tract arrhythmias.

Variable	All ($n = 215$)	With structural heart disease ($n = 93$)	Without structural heart disease ($n = 122$)	*p*-value
Age (years)	58.3 ± 16	65.0 ± 12.8	53.3 ± 16.3	<0.001
Body-mass-index (kg/m^2)	27.3 ± 5.5	28.6 ± 6.1	26.2 ± 4.8	0.001
Gender (male)	64.2%	82.8%	50.0%	<0.001
Admission type				0.036
Elective	75.8%	68.8%	81.1%	
Urgent	24.2%	31.2%	18.8%	
Admission ward				0.133
Normal ward	93.5%	90.3%	95.9%	
Intermediate care	2.8%	5.4%	0.8%	
Intensive care	3.7%	4.3%	3.3%	
Critical events before admission				
Electrical storm	16.7%	16.7%	16.7%	1.000
Acute heart failure	10.7%	17.2%	5.7%	0.013
Structural heart disease	43.3%	100.0%	0.0%	
Ischemic		43.0%		
Non-ischemic		57.0%		
LV-EF (%)	50 ± 14	40 ± 14	57 ± 8	<0.001
TAPSE (mm)	21.1 ± 5.5	20.7 ± 5.9	23.3 ± 4.8	0.001
ICD	20.0%	41.9%	3.3%	<0.001
CRT-D	9.8%	21.5%	0.8%	
Pacemaker	1.9%	2.2%	1.6%	1.000
Comorbidities				
Arterial hypertension	46.5%	62.4%	34.4%	<0.001
Diabetes mellitus	14.4%	22.6%	8.2%	0.005
Chronic kidney disease	26.0%	41.9%	13.9%	<0.001
Chronic lung disease	13.0%	20.4%	7.4%	0.007
Chronic liver disease	4.2%	6.5%	2.5%	0.180
Atrial Fibrillation	20.9%	31.2%	13.1%	0.002
CHA_2DS_2-VASc score	2.1 ± 1.6	3.2 ± 1.4	1.3 ± 1.3	<0.001
Laboratory results				
Creatinine (mg/dl)	1.1 ± 0.4	1.2 ± 0.5	0.9 ± 0.2	<0.001
Glomerular filtration rate (ml/min/1.73 m^2; CKD-EPI)	76.3 ± 22.1	65.7 ± 21.0	84.5 ± 19.5	<0.001
GOT (U/l)	25.3 ± 11.6	27.2 ± 13.0	23.8 ± 10.3	0.025
GPT (U/l)	32.4 ± 35.6	36.7 ± 50.6	29.2 ± 16.8	0.170
INR	1.1 ± 0.4	1.3 ± 0.6	1 ± 0.3	<0.001
Hemoglobin (g/dl)	13.9 ± 1.5	13.8 ± 1.6	14 ± 1.4	0.414
Leucocytes (Mrd/l)	7.3 ± 2.1	7.4 ± 2.3	7.2 ± 1.9	0.786
Thrombocytes (Mrd/l)	221.7 ± 58.7	204.1 ± 56.6	235 ± 56.9	<0.001
Potassium (mmol/l)	4.1 ± 0.4	4.2 ± 0.4	4.1 ± 0.4	<0.001
Antiarrhythmic drugs at admission				
Flecainide	4.2%	5.5%	3.3%	0.501
Betablockers	68.1%	83.5%	56.6%	<0.001
Amiodarone	8.5%	18.7%	0.8%	<0.001
Anticoagulation				
DOAC	9.9%	17.6%	4.1%	0.002
Vit. -K- antagonists	6.1%	9.9%	3.3%	0.079
Platelet inhibitors	23.9%	45.1%	8.2%	<0.001

Data are presented as per cent or mean ± standard deviation. $p < 0.05$ is considered statistically significant. Electrical storm was defined as three or more episodes of sustained ventricular arrhythmias in 24 h.

CKD-EPI, chronic kidney disease epidemiology collaboration; CRT-D, cardiac resynchronisation therapy defibrillator; DOAC, direct oral anticoagulant; GOT, glutamic-oxaloacetic transaminase; GPT, glutamate pyruvate transaminase; ICD, implanted cardioverter-defibrillator, INR, international normalized ratio; LV-EF, left ventricular ejection fraction; No., number; PVC, premature ventricular complex; TAPSE, tricuspid annular plane systolic excursion; Vit., vitamin.

and late potentials as well as areas of scar, were marked whenever appropriate and later considered for ablation. In line with previous studies for scar demarcation a bipolar endocardial voltage of 0.5/1.5 mV with individual adaptation was chosen (12, 14). All voltage maps were generated during sinus rhythm or paced rhythm from coronary sinus or right ventricle. In case of presumed VT a 6 French quadripolar diagnostic catheter, placed in the right ventricular apex was used to induce VT by programmed stimulation with a fixed stimulation protocol consisting of three basic cycle lengths (510, 440, 370 ms) and up to three added extra stimuli (lowest coupling interval 200 ms). In patients presenting with VT at the beginning of the procedure, activation/entrainment mapping was conducted before substrate mapping. Pace mapping and activation mapping was performed at the operator's discretion, especially in patients presenting for ablation of premature ventricular complexes (PVC). In case of absence of PVC or non-inducibility of VT, sedation was reduced and/or orciprenaline was administered continuously until a 20% increase of the baseline heartrate was achieved. Then stimulation was repeated. Radiofrequency current was used for complete abolition of all abnormal electrograms including fractionated potentials, highly fractionated potentials, late potentials, and fractionated late potentials in patients with abnormal myocardial substrate (15, 16). Radiofrequency current was applied with a maximum power of 45 Watts (upper temperature limit was set to 48°C) at an irrigation rate of 17–30 mL per min. If the ablation site was in possible proximity to the coronary arteries, coronary angiography was performed for visualization before ablation. Subsequently, targeted regions were remapped to demonstrate elimination of the respective electrograms. We aimed to achieve the combined procedural endpoint of VT non-inducibility, freedom from spontaneous PVC and substrate modification. In patients that required initial orciprenaline infusion due to absence of spontaneous arrhythmia, infusion was repeated at the end of procedure to confirm ablation success. At the end of the procedure, all sheaths were removed, and the puncture site was compressed manually until complete haemostasis was achieved. Consequently, a compression bandage was applied. An Angio-Seal™ device (Terumo Interventional Systems, Terumo Europe,

TABLE 2 | Procedural parameters of patients with outflow tract arrhythmias.

Variable	All ($n = 215$)	With structural heart disease ($n = 93$)	Without structural heart disease ($n = 122$)	*p*-value
Clinical target				
PVC	83.3%	72.0%	91.8%	<0.001
VT	25.6%	34.4%	18.9%	0.012
Outflow tract origin				
RVOT	49.3%	43.0%	54.1%	0.130
LVOT	60.0%	68.8%	53.3%	0.025
Procedure duration (minutes)	132.3 ± 62.1 122.5 (91)	150.5 ± 61.7 142 (84)	118.7 ± 59.1 105 (72)	<0.001
Fluoroscopy duration (seconds)	760.1 ± 559.2 641.5 (690.5)	963.1 ± 617.0 826 (730)	608.3 ± 458.7 429 (562)	<0.001
Fluoroscopy dose (cGycm^2)	605 ± 1,309 279 (492)	952 ± 1,873 568 (770)	343 ± 461 186 (288)	<0.001
Radiofrequency energy duration (seconds)	661.4 ± 559.7 465 (682)	833.3 ± 643.6 621 (974)	534.7 ± 451.2 360.5 (407)	<0.001
Contrast dye (milliliters)	10.4 ± 18.0	12.6 ± 18.4	8.8 ± 17.6	0.087
No. of VTs induced	1.9 ± 1.5	2.0 ± 1.5	1.6 ± 1.4	0.140
No. of targeted PVCs	1.5 ± 1.1	1.7 ± 1.2	1.4 ± 1.1	0.033
Previous ablation for ventricular arrhythmia	22.3%	32.3%	14.8%	0.003
Thereof of same target(s)	42.6%	51.7%	27.8%	0.137
General anesthesia	4.2%	6.5%	2.5%	0.180
Catecholamines during procedure	4.2%	7.6%	1.6%	0.041
ECMO/Impella during procedure	0.9%	2.2%	0%	0.186
Epicardial approach	1.4%	2.2%	0.8%	0.580
Ablation in RV	55.8%	50.5%	59.8%	0.212
Ablation in LV	56.3%	64.5%	50.0%	0.038
Ablation in CS	13.5%	17.2%	10.7%	0.226

Data are presented as per cent, mean ± standard deviation or median (IQR). $p < 0.05$ is considered statistically significant.

CS, coronary sinus; ECMO, extracorporeal membrane oxygenation; LV, left ventricle; LVOT, left ventricular outflow tract; No., number; PVC, premature ventricular complex; RV, right ventricle; RVOT, right ventricular outflow tract; VT, ventricular tachycardia.

Löwen, Belgium) was used at the operator's discretion according to the manufacturer's instructions.

All patients were connected to telemetry monitoring on a specialized heart rhythm ward or intensive/intermediate care ward for at least 18 h after the procedure. The monitor records were reviewed by a physician before discharge and PVC, or VT episodes were analyzed and quantified. In case of suspected recurrence, Holter ECG was performed.

After discharge, amiodarone and other antiarrhythmic drugs were continued at the operator's discretion. A recurrence was defined as any sustained VT or recurrence of the targeted PVC documented by device interrogation or ECG.

The electronic patient charts were reviewed by a senior electrophysiologist for the acquisition of patient characteristics, procedural parameters, and acute outcome.

Statistical Analysis

Descriptive statistics are presented as count and percentage for categorical variables and as mean ± standard deviation or median [interquartile range (IQR)] for continuous variables. The distribution of numeric values was assessed visually using histograms. The baseline and treatment characteristics of patients with and without SHD were compared with Fisher's exact test or Mann-Whitney *U*-test, as appropriate. Cox proportional hazards models were used to assess the relationships between covariates and length of stay or procedure duration. Uni- as well as multivariable Cox-regression analyses were performed. In the multivariable analyses, the grouping variable "structural heart disease" was forced into the model equations while all other covariates were selected following the forward-stepwise variable selection method. Hazard ratios with 95% confidence intervals as well as Wald *P*-values are presented in forest plots. The reported *p*-values are used as descriptive measures only. Significance level α was set to 5%. Statistical analyses were performed using SPSS v. 28.0.1.0 (IBM corporation, USA).

RESULTS

Total Study Population

A total of 500 patients were identified. Twelve had insufficient data (**Figure 1**). The patients were male in 71.7% (350/488) and had a mean age of 61.1 ± 15 years. Baseline characteristics of the total cohort are presented in **Supplementary Table 1**.

Patients With Outflow Tract Arrhythmias

Baseline Parameters

Outflow tract arrhythmias were identified and treated in 215/488 patients (44.1% of the entire cohort, **Figure 1**). Those patients were of male gender in 64.2% (138/215) and had a mean age of 58.3 ± 16 years. 43.3% (93/215) had SHD, 43.0% (40/93) of those showing ischemic heart disease (**Supplementary Table 2**). Further baseline parameters of patients with outflow tract arrhythmias are presented in **Table 1**. Patients with SHD presenting for ablation of outflow tract arrhythmias were older (65.0 ± 12.8 vs. 53.3 ± 16.3 years; $p < 0.001$) und more often of male gender [82.8% (77/93) vs. 50.0% (61/122); $p < 0.001$] than patients without SHD. They were more frequently transferred with urgency to our center [31.2% (29/93) vs. 18.8% (23/122); $p = 0.036$]. Left and right ventricular systolic function was reduced in comparison to patients with outflow tract arrhythmias without

TABLE 3 | Acute outcome of patients with outflow tract arrhythmias.

Variable	All ($n = 215$)	With structural heart disease ($n = 93$)	Without structural heart disease ($n = 122$)	*p*-value
Acute success	94.0%	93.4%	94.2%	0.781
Periprocedural complication	9.3%	12.9%	6.6%	0.154
Groin complications	6.5%	9.7%	4.1%	
Pericardial tamponade	0.5%	0%	0.8%	
Periprocedural death	0.5%	1.1%	0.0%	0.433
Reablation during stay	2.3%	4.3%	0.8%	0.168
Recurrence during stay	12.1%	16.1%	9.0%	0.140
Discharge to other hospital	1.4%	2.3%	0.8%	0.572
Length of stay (total; nights)	4.9 ± 5.7 2 (4)	6.5 ± 7.1 5 (6)	3.8 ± 4.1 2 (4)	<0.001
Postinterventional acute heart failure	1.4%	3.3%	0.0%	0.077
Postinterventional acute kidney injury	3.8%	7.7%	0.8%	0.022
Antiarrhythmic drugs at discharge				
Flecainide	3.4%	1.1%	5.0%	0.133
Betablockers	67.8%	85.1%	55.4%	<0.001
Amiodarone	6.7%	16.1%	0.0%	<0.001

Data are presented as per cent, mean ± standard deviation or median (IQR). $p < 0.05$ is considered statistically significant.

SHD (left ventricular ejection fraction: 40 ± 14 vs. 57 ± 8; $p < 0.001$ and TAPSE 20.7 ± 5.9 vs. 23.3 ± 4.8 mm; $p = 0.001$). A higher percentage of patients with SHD also had comorbidities like arterial hypertension, diabetes, and chronic kidney disease (**Table 1**).

Procedural Parameters

Patients with SHD were more likely to be treated for VT than patients without SHD [34.4% (32/93) vs. 18.9% (23/122); $p = 0.012$]. Furthermore, ablation in SHD patients was performed more frequently in the left ventricle [64.5% (60/93) vs. 50.0% (61/122); $p = 0.038$; see details of ablation sites in **Supplementary Table 3**]. Procedure duration [142 (84) vs. 105 (72) min; $p < 0.001$] as well as fluoroscopy and energy delivery time were longer in patients with SHD (**Table 2**). The number of inducible VT or PVC targeted differed only slightly between groups. Three patients (two with SHD) had an epicardial ablation.

Procedural Outcome of Patients With and Without Structural Heart Disease

The acute success rate was high in both groups with 93.4% (86/93) vs. 94.2% (115/122) (SHD vs. no SHD; $p = 0.781$). Early recurrences of the targeted arrhythmia were observed in 16.1% (15/93) vs. 9.0% (11/122; $p = 0.140$) and there was a numerically higher rate of reablations during the stay in patients with SHD [4.3% (4/93) vs. 0.8% (1/122); $p = 0.168$].

Periprocedural complications occurred in 12.9% (12/93) vs. 6.6% (8/122) of patients (SHD vs. no SHD; $p = 0.154$). Complications of the groin were seen more often in patients with SHD [9.7% (9/93) vs. 4.1% (5/122); for details see **Supplementary Table 4**]. There was no significant association between a retrograde aortic mapping approach and groin complications: arterial groin puncture was performed in 60.7% (128/211) of all patients and 66.7% (10/15) of patients with groin complications ($p = 0.787$). A pericardial tamponade that required drainage with a pigtail catheter was observed in one

TABLE 4 | Uni- and multivariable analysis.

Variable	Influencing factors	Hazard ratio	Confidence interval	*p*-value
(A) Univariate analysis				
Procedural duration				
	Structural heart disease	0.594	0.439–0.804	<0.001
Length of hospital stay				
	Structural heart disease	0.696	0.517–0.936	0.017
Periprocedural complications				
	Structural heart disease	2.107	0.927–4.796	0.076
(B) Multivariable analysis				
Procedure duration				
	Age	1.015	1.003–1.027	0.001
	Female gender	1.457	1.027–2.069	0.035
	Structural heart disease	0.656	0.461–0.936	0.02
	VT ablation	0.621	0.416–0.926	0.02
	LV ablation	0.585	0.431–0.795	<0.001
Length of hospital stay				
	Age	0.988	0.979–0.998	0.018
	Female gender	1.441	1.017–2.042	0.040
	Structural heart disease	0.966	0.687–1.359	0.844
	VT ablation	0.404	0.268–0.608	<0.001

*Uni- (**A**) as well as multivariable (**B**) Cox-regression analyses were performed. Lower hazard ratio stands for association with longer procedure duration as well as longer hospital stay, while higher hazard ratio goes along with shorter procedure duration, length of stay and a higher likelihood of periprocedural complications. In the multivariable analyses, the grouping variable "structural heart disease" was forced into the model equations while all other covariates were selected following the forward-stepwise variable selection method. The initial model for procedure duration consisted of age, body-mass-index, left ventricular ejection fraction, female gender, structural heart disease, VT ablation, procedure under general anesthesia and LV ablation. The initial model for length of hospital stay consisted of age, body-mass-index, left ventricular ejection fraction, gender, structural heart disease, VT ablation, procedure under general anesthesia, LV ablation and postoperative intermediate or intensive care treatment. Hazard ratios with 95% confidence intervals as well as Wald p-values are displayed. P-values <0.05 are regarded statistically significant.*

LV, left ventricle; VT, ventricular tachycardia.

patient without SHD (0.8%). A full list of all complications is provided in **Supplementary Table 4**. One patient with cardiac sarcoidosis died during the post-interventional stay due to progressive heart failure (**Table 3**).

The median duration of stay was 5 (6) nights for patients with SHD and 2 (4) nights for otherwise healthy patients ($p < 0.001$). Changes in antiarrhythmic medication at discharge were insignificant in both groups compared to the initial admission (see **Supplementary Figure 1**).

In the univariate analysis, SHD was associated with a longer procedure duration as well as a longer hospital stay and there was a trend toward higher likelihood of periprocedural complications (**Table 4A**). The multivariable analysis confirmed this result regarding procedure duration, but not regarding length of stay. Additionally, ablation of VT instead of PVC and ablation within the left ventricle were identified as factors independently associated with a longer procedure duration, while female gender and higher age were associated with a shorter procedure duration. Regarding the length of stay, higher age and VT ablation were associated with a longer stay, while female gender was associated with a shorter stay at the hospital (**Table 4B**; **Figures 2**, **3**).

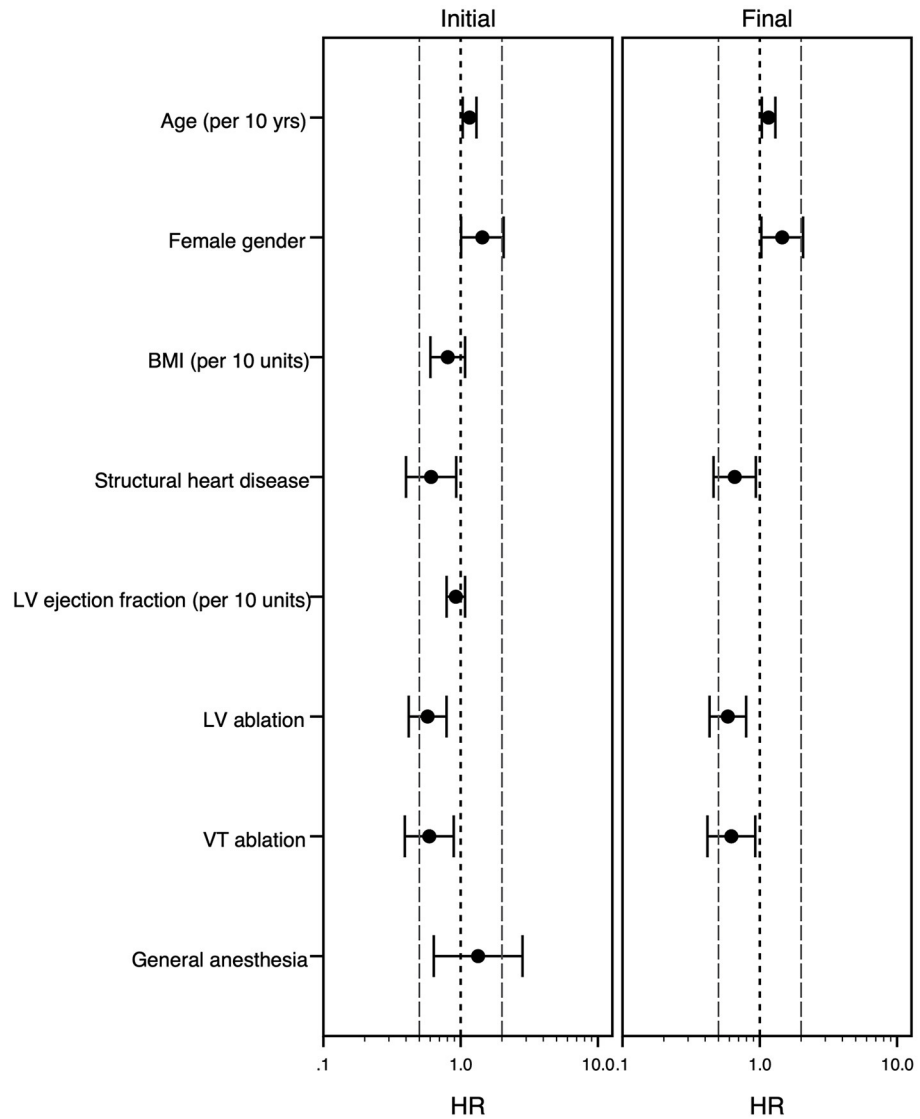

FIGURE 2 | Forest plot of the multivariable Cox model analyzing risk factors for longer procedure duration. The multivariable Cox-regression analysis is displayed. Hazard ratio <1 stands for association with longer procedure duration, while hazard ratio >1 goes along with shorter procedure duration. The initial model (left panel) and final model (right panel) is shown. The grouping variable "structural heart disease" was forced into the model equations, all other covariates were selected following the forward-stepwise variable selection method. For age, body mass index and left ventricular ejection fraction the effect of an increase of 10 years/kg/m^2/% is shown. Hazard ratios (point) with 95% confidence intervals (whiskers) are displayed. BMI, body mass index (kg/m^2); HR, hazard ratio; LV, left ventricle; VT, ventricular tachycardia, yrs., years.

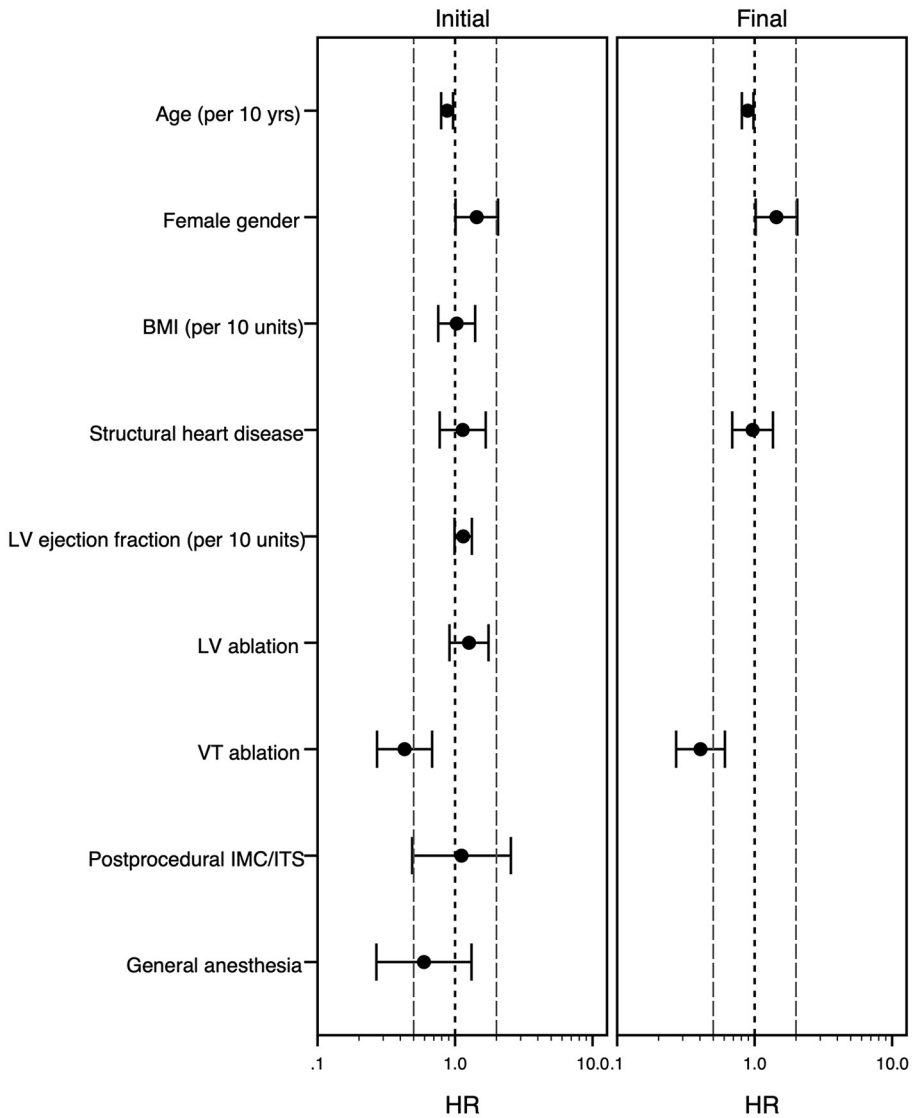

FIGURE 3 | Forest plot of the multivariable Cox model analyzing risk factors for longer hospital stay. The multivariable Cox-regression analysis is displayed. Hazard ratio <1 stands for association with longer hospital stay, while hazard ratio >1 goes along with shorter stay. The initial model (left panel) and final model (right panel) is shown. The grouping variable "structural heart disease" was forced into the model equations, all other covariates were selected following the forward-stepwise variable selection method. For age, body mass index and left ventricular ejection fraction the effect of an increase of 10 years/kg/m^2/% is shown. Hazard ratios (point) with 95% confidence intervals (whiskers) are displayed. BMI, body mass index (kg/m^2); HR, hazard ratio; IMC/ITS, intermediate care unit/intensive care unit; LV indicates left ventricle; VT, ventricular tachycardia, yrs., years.

DISCUSSION

The main findings of the present study are:

- Outflow tract arrhythmias are common in patients with SHD. Those patients presenting for ablation are older, more often male and have more comorbidities than patients with idiopathic ventricular arrhythmias.
- The acute procedural success of outflow tract arrhythmia ablation is similar in patients with and without SHD.
- Outflow tract arrhythmias in patients with SHD have their origin more often in the left ventricle than outflow tract arrhythmias in patients without SHD.
- The median duration of hospital stay was 3 days longer in patients with SHD than in patients without SHD. Patients with SHD had numerically more periprocedural complications.

The present study shows that almost half of the patients being treated for outflow tract arrhythmias also suffer from underlying SHD. The evidence available on outflow tract arrhythmias in patients with SHD is still limited, as those patients have so far often been excluded from most clinical trials. Our study is the first, to compare the procedural

parameters and acute outcome of outflow tract arrhythmias in patients with and without SHD. A proper prediction of those parameters seems to be especially relevant in times with restricted availability of hospital capacities due to the COVID-19 pandemic.

Two previous publications investigated the origin and outcome of ventricular arrhythmias unrelated to myocardial substrate in patients with SHD, showing, that "idiopathic arrhythmias" remote from abnormal myocardial substrate do occur in those patients and have an acceptable ablation outcome (17, 18). Arrhythmias associated with abnormal myocardial substrate on the other hand tend to have a worse ablation outcome, but several other confounding factors such as the accessibility of area of origin of the arrhythmia might be important (4). The procedural parameters and ablation outcome of outflow tract arrhythmias, representing a typical location of idiopathic arrhythmias, but also an area that might be affected by abnormal myocardial substrate remains unclear. This is especially relevant for patients with non-ischemic cardiomyopathy, as areas of fibrosis can sometimes be found associated to the outflow tracts in those individuals during magnetic resonance imaging (11, 19, 20).

According to our analysis, patients with SHD presenting with outflow tract arrhythmias differ in most baseline parameters from patients without SHD. In brief, they are older, more often male and have higher counts of comorbidities like arterial hypertension and diabetes. Factors, recently proven to be relevant indicators of 1-year mortality and recurrence like left ventricular function, prior ICD implantation and previous ablation (I-VT score) were observed more often in comparison to patients without SHD (21). In our cohort, rates of complications and intrahospital death were comparable to previously published large trials. The higher amount of groin complications in the SHD group might be attributed to a slightly higher percentage of arterial punctures in this group in combination with more patients on oral anticoagulation for treatment of atrial fibrillation. Furthermore, a higher body-mass-index might play a role, even if experiences from catheter ablation of atrial fibrillation only showed an effect for the morbidly obese (22).

Procedures in the SHD group took on average 32 min longer than procedures in otherwise healthy patients. This can potentially be explained by differences during the sedation as well as the ablation procedure itself. Furthermore, there was a higher amount of VT and arrhythmias with origin in the left ventricle and in these patients an arterial access and invasive blood pressure monitoring was used. At last, in patients with SHD there was a trend to more VT morphologies and PVCs to be targeted during the procedure. The latter might be caused by the myocardial substrate itself being a source of a variety of arrhythmias, while the mechanism of arrhythmia in otherwise healthy patients was most likely automaticity or triggered activity (23).

The acute success rate was equally high in both groups, which fits with results from previous studies that show good acute success rates for patients with SHD, even if the long-term results were less optimal (4). Early recurrences occurred numerically more often in patients with SHD without reaching statistical significance.

The overall length of the hospital stay was 5 nights (median) for patients with SHD and thus longer than in patients without SHD. Recently published data on ablation of non-ischemic VT shows a similar duration of stay (24). The difference between groups might be caused by comorbidities (7.7% of acute kidney failure and 3.3% cardiac decompensation) in the SHD group, but also by a longer surveillance after femoral artery puncture. The multivariable analysis suggests that higher age and ablation of VT are independent factors associated with a longer hospital stay. However, those factors also seem to be associated with a generally sicker patient collective which requests a more extent periprocedural surveillance period. Female gender was interestingly associated with shorter procedure duration as well as hospital stay, potentially reflecting, that female patients were younger and had less comorbidities than male patients.

LIMITATIONS

The data for this analysis has been derived from a single center registry and was analyzed retrospectively. Our results should therefore be considered as hypothesis generating and might not be applicable to the general population.

CONCLUSION

This analysis shows that patients presenting with outflow tract arrhythmias and coexisting SHD have a higher burden of risk factors and comorbidities that might be relevant for ablation procedures than patients without SHD. The acute success rate was high, irrespective of the presence of SHD, but a longer hospital stay and potentially a higher risk of periprocedural complications should be considered when discussing this treatment option with patients.

DATA AVAILABILITY STATEMENT

The raw data supporting the conclusions of this article will be made available by the authors, upon reasonable request.

ETHICS STATEMENT

The studies involving human participants were reviewed and approved by Ethics Committee of the Medical Association Hamburg. The patients/participants provided their written informed consent to participate in this study.

AUTHOR CONTRIBUTIONS

RS and JR were involved in data generation, data collection, study design, statistical analysis, and manuscript preparation. AB was involved in data generation, data collection, and manuscript preparation. HP was involved in study design,

statistical analysis, and manuscript preparation. LR, FM, JM, SK, IM, ML, BR, CM, AM, FO, PK, and AR were involved in data generation, data analysis, and manuscript preparation. All authors contributed to the article and approved the submitted version.

SUPPLEMENTARY MATERIAL

The Supplementary Material for this article can be found online at: https://www.frontiersin.org/articles/10.3389/fcvm.2022.910042/full#supplementary-material

REFERENCES

1. Priori SG, Blomstrom-Lundqvist C, Mazzanti A, Blom N, Borggrefe M, Camm J, et al. 2015 ESC Guidelines for the management of patients with ventricular arrhythmias and the prevention of sudden cardiac death: The Task Force for the Management of Patients with Ventricular Arrhythmias and the Prevention of Sudden Cardiac Death of the European Society of Cardiology (ESC) Endorsed by: Association for European Paediatric and Congenital Cardiology (AEPC). *Eur Heart J.* (2015) 36:2793–867. doi: 10.1093/eurheartj/ehv316
2. Latchamsetty R, Yokokawa M, Morady F, Kim HM, Mathew S, Tilz R, et al. Multicenter outcomes for catheter ablation of idiopathic premature ventricular complexes. *JACC Clin Electrophysiol.* (2015) 1:116–23. doi: 10.1016/j.jacep.2015.04.005
3. Dinov B, Fiedler L, Schönbauer R, Bollmann A, Rolf S, Piorkowski C, et al. Outcomes in catheter ablation of ventricular tachycardia in dilated nonischemic cardiomyopathy compared with ischemic cardiomyopathy: results from the Prospective Heart Centre of Leipzig VT (HELP-VT) Study. *Circulation.* (2014) 129:728–36. doi: 10.1161/CIRCULATIONAHA.113.003063
4. Kumar S, Romero J, Mehta NK, Fujii A, Kapur S, Baldinger SH, et al. Long-term outcomes after catheter ablation of ventricular tachycardia in patients with and without structural heart disease. *Heart Rhythm.* (2016) 13:1957–63. doi: 10.1016/j.hrthm.2016.07.001
5. Al-Khatib SM, Stevenson WG, Ackerman MJ, Bryant WJ, Callans DJ, Curtis AB, et al. 2017 AHA/ACC/HRS guideline for management of patients with ventricular arrhythmias and the prevention of sudden cardiac death: a report of the American College of Cardiology/American Heart Association Task Force on Clinical Practice Guidelines and the Heart Rhythm Society. *Circulation*. (2018) 138:e272–391. doi: 10.1161/CIR.0000000000000614
6. Aliot EM, Stevenson WG, Almendral-Garrote JM, Bogun F, Calkins CH, Delacretaz E, et al. EHRA/HRS Expert Consensus on Catheter Ablation of Ventricular Arrhythmias: developed in a partnership with the European Heart Rhythm Association (EHRA), a Registered Branch of the European Society of Cardiology (ESC), and the Heart Rhythm Society (HRS); in collaboration with the American College of Cardiology (ACC) and the American Heart Association (AHA). *Heart Rhythm.* (2009) 6:886–933. doi: 10.1093/europace/eup098
7. Kim RJ, Iwai S, Markowitz SM, Shah BK, Stein KM, Lerman BB. Clinical and electrophysiological spectrum of idiopathic ventricular outflow tract arrhythmias. *J Am Coll Cardiol.* (2007) 49:2035–43. doi: 10.1016/j.jacc.2007.01.085
8. Tada H, Ito S, Naito S, Kurosaki K, Kubota S, Sugiyasu A, et al. Idiopathic ventricular arrhythmia arising from the mitral annulus: a distinct subgroup of idiopathic ventricular arrhythmias. *J Am Coll Cardiol.* (2005) 45:877–86. doi: 10.1016/j.jacc.2004.12.025
9. Yamada T, Kay GN. Anatomical consideration in catheter ablation of idiopathic ventricular arrhythmias. *Arrhythm Electrophysiol Rev.* (2016) 5:203–9. doi: 10.15420/aer.2016:31:2
10. Hayashi T, Liang JJ, Shirai Y, Kuo L, Muser D, Kubala M, et al. Trends in successful ablation sites and outcomes of ablation for idiopathic outflow tract ventricular arrhythmias. *JACC Clin Electrophysiol.* (2020) 6:221–30. doi: 10.1016/j.jacep.2019.10.004
11. Globits S, Kreiner G, Frank H, Heinz G, Klaar U, Frey B, et al. Significance of morphological abnormalities detected by MRI in patients undergoing successful ablation of right ventricular outflow tract tachycardia. *Circulation.* (1997) 96:2633–40. doi: 10.1161/01.CIR.96.8.2633
12. Nührich JM, Kaiser L, Akbulak R, Schäffer BN, Eickholt C, Schwarzl M, et al. Substrate characterization and catheter ablation in patients with scar-related ventricular tachycardia using ultra high-density 3-D mapping. *J Cardiovasc Electrophysiol.* (2017) 28:1058–67. doi: 10.1111/jce.13270
13. Ouyang F, Mathew S, Wu S, Kamioka M, Metzner A, Xue Y, et al. Ventricular arrhythmias arising from the left ventricular outflow tract below the aortic sinus cusps: mapping and catheter ablation *via* transseptal approach and electrocardiographic characteristics. *Circ Arrhythm Electrophysiol.* (2014) 7:445–55. doi: 10.1161/CIRCEP.114.001690
14. Viswanathan K, Mantziari L, Butcher C, Hodkinson E, Lim E, Khan H, et al. Evaluation of a novel high-resolution mapping system for catheter ablation of ventricular arrhythmias. *Heart Rhythm.* (2017) 14:176–83. doi: 10.1016/j.hrthm.2016.11.018
15. Ghanbari H, Baser K, Yokokawa M, Stevenson W, Della Bella P, Vergara P, et al. Noninducibility in postinfarction ventricular tachycardia as an end point for ventricular tachycardia ablation and its effects on outcomes: a meta-analysis. *Circ Arrhythm Electrophysiol.* (2014) 7:677–83. doi: 10.1161/CIRCEP.113.001404
16. Tsiachris D, Silberbauer J, Maccabelli G, Oloriz T, Baratto F, Mizuno H, et al. Electroanatomical voltage and morphology characteristics in postinfarction patients undergoing ventricular tachycardia ablation: pragmatic approach favoring late potentials abolition. *Circ Arrhythm Electrophysiol.* (2015) 8:863–73. doi: 10.1161/CIRCEP.114.002551
17. Schleberger R, Jularic M, Salzbrunn T, Hacke C, Schwarzl JM, Hoffmann BA, et al. Outcome of catheter ablation of non-reentrant ventricular arrhythmias in patients with and without structural heart disease. *Eur J Med Res.* (2020) 25:4. doi: 10.1186/s40001-020-0400-y
18. Ellis ER, Shvilkin A, Josephson ME. Nonreentrant ventricular arrhythmias in patients with structural heart disease unrelated to abnormal myocardial substrate. *Heart Rhythm.* (2014) 11:946–52. doi: 10.1016/j.hrthm.2014.03.012
19. Piers SR, Tao Q, van Huls van Taxis CF, Schalij MJ, van der Geest RJ, Zeppenfeld K. Contrast-enhanced MRI-derived scar patterns and associated ventricular tachycardias in nonischemic cardiomyopathy: implications for the ablation strategy. *Circ Arrhythm Electrophysiol.* (2013) 6:875–83. doi: 10.1161/CIRCEP.113.000537
20. Tian J, Ahmad G, Mesubi O, Jeudy J, Dickfeld T. Three-dimensional delayed-enhanced cardiac MRI reconstructions to guide ventricular tachycardia ablations and assess ablation lesions. *Circ Arrhythm Electrophysiol.* (2012) 5:e31–5. doi: 10.1161/CIRCEP.111.968636
21. Vergara P, Tzou WS, Tung R, Brombin C, Nonis A, Vaseghi M, et al. Predictive score for identifying survival and recurrence risk profiles in patients undergoing ventricular tachycardia ablation: the I-VT score. *Circ Arrhythm Electrophysiol.* (2018) 11:e006730. doi: 10.1161/CIRCEP.118.006730
22. Providência R, Adragão P, de Asmundis C, Chun J, Chierchia G, Defaye P, et al. Impact of body mass index on the outcomes of catheter ablation of atrial fibrillation: a european observational multicenter study. *J Am Heart Assoc.* (2019) 8:e012253. doi: 10.1161/JAHA.119.012253

23. Nagashima K, Tedrow UB, Koplan BA, Michaud GF, John RM, Epstein LM, et al. Reentrant ventricular tachycardia originating from the periaortic region in the absence of overt structural heart disease. *Circ Arrhythm Electrophysiol.* (2014) 7:99–106. doi: 10.1161/CIRCEP.113.000870
24. Nascimento Matos D, Cavaco D, Carmo P, Carvalho M, Rodrigues G, Carmo J, et al. Ventricular tachycardia ablation in nonischemic cardiomyopathy. *EP Europace*. (2021) 23(Suppl. 3):362. doi: 10.1093/europace/euab116.362

Conflict of Interest: The authors declare that the research was conducted in the absence of any commercial or financial relationships that could be construed as a potential conflict of interest.

Publisher's Note: All claims expressed in this article are solely those of the authors and do not necessarily represent those of their affiliated organizations, or those of the publisher, the editors and the reviewers. Any product that may be evaluated in this article, or claim that may be made by its manufacturer, is not guaranteed or endorsed by the publisher.

frontiers | Frontiers in Cardiovascular Medicine

TYPE Original Research
PUBLISHED 10 October 2022
DOI 10.3389/fcvm.2022.950401

OPEN ACCESS

EDITED BY
Minglong Chen,
The First Affiliated Hospital of Nanjing Medical University, China

REVIEWED BY
Yap-Hang Chan,
The University of Hong Kong, Hong Kong SAR, China
Christian Hendrik Heeger,
University Heart Center Luebeck, Germany

*CORRESPONDENCE
Jianping Li
lijianping03455@pkufh.com
Jing Zhou
zhoujing1232004@sina.com

SPECIALTY SECTION
This article was submitted to Cardiac Rhythmology, a section of the journal Frontiers in Cardiovascular Medicine

RECEIVED 22 May 2022
ACCEPTED 22 September 2022
PUBLISHED 10 October 2022

CITATION
Li K, Lv P, Wang Y, Fan F, Ding Y, Li J and Zhou J (2022) Electrocardiographic criteria for localization of ventricular premature complexes from the inferior right ventricular outflow tract. *Front. Cardiovasc. Med.* 9:950401. doi: 10.3389/fcvm.2022.950401

Electrocardiographic criteria for localization of ventricular premature complexes from the inferior right ventricular outflow tract

Kang Li, Pinchao Lv, Yuchuan Wang, Fangfang Fan, Yansheng Ding, Jianping Li* and Jing Zhou*

Department of Cardiology, Peking University First Hospital, Beijing, China

Background: The ventricular premature complexes (PVCs) originating from the superior right ventricular outflow tract (RVOT) have high success rates by catheter ablation. It may not be the same when the origin is in the inferior RVOT.

Objective: To identify electrocardiographic (ECG) characteristics that predict the site for successful ablation of PVCs originating in the inferior RVOT.

Methods: Of 309 consecutive patients with symptomatic PVCs despite medical therapy, 124 had PVCs originating from the RVOT, and 107 RVOT cases without structural heart disease and no bundle branch block in sinus rhythm were enrolled in the study. Among them, 74 have a superior RVOT origin, and 33 have an inferior RVOT origin.

Results: The proportion with multiple morphologies of PVC was significantly higher in the inferior RVOT group than in the superior RVOT group (24.24 vs. 6.76%, $P = 0.011$). The QRS duration of PVCs with an inferior RVOT origin was more expansive than PVCs with a superior RVOT origin (162.42 ± 19.69 ms vs. 140.90 ± 11.30 ms; $P < 0.001$). Furthermore, the QRS wave in V1 in patients in the inferior RVOT group was more likely to have a negative delta wave at the onset of the QRS (27.27 vs. 1.39%, $P < 0.001$). We found that the areas under the receiver-operating characteristic curve (AUCs) for PVC diagnosis with an inferior RVOT origin ranged from 0.812 to 0.841 depending on ECG features, with the highest AUC for the QRS duration of PVCs and the amplitude of R waves in lead II. These ECG indices had good predictability for judging the origin of PVCs in the RVOT; the best threshold for the QRS duration of PVCs was 145 ms, and the best thresholds for the amplitude of R waves in leads II, III, and aVF were 1.35, 1.35, and 1.15 mV, respectively.

Conclusion: When evaluating a patient with PVCs, the source is likely to be the inferior RVOT if the ECG presentation conforms to the morphological characteristics of the RVOT, meanwhile, the QRS wave is relatively broad and polymorphic, and the main waves in limb leads (II, III, and aVF) are upward with low amplitude.

KEYWORDS

ventricular premature complexes, inferior right ventricular outflow tract, catheter ablation, electrocardiogram, algorithms

Introduction

Ventricular premature complexes (PVCs) in patients with structurally normal hearts usually originate from the right ventricular outflow tract (RVOT). Catheter ablation is an excellent treatment option for these PVCs, with a success rate of >80% and few significant complications (1). The RVOT is bounded by the supraventricular crest and the pulmonic valve (2). Previous studies have demonstrated that the origin of PVCs from the RVOT is mostly above or below the pulmonary sinus cusp (3). Moreover, Zhang et al. reported that reverse U-curve ablation above the pulmonary sinus cusp could improve the treatment success rate (4). However, there are still some cases of failure or recurrence of PVCs from the RVOT after catheter ablation, especially when the origin is remote from the pulmonary annulus. In patients with failed ablation of idiopathic left bundle branch block (LBBB) and PVCs with an inferior axis morphology, the most frequent origin is still in the RVOT, followed by an intramural focus and the pulmonary artery (5, 6). In these patients, the septum of the inferior RVOT is a site where ablation occasionally fails. The septal papillary muscles, abundant trabeculae, and moderator band intersect at the junction of the smooth-walled pulmonary infundibulum and the large trabecular inflow tract, making it difficult for the catheter to attach (6).

The electrocardiogram (ECG) in patients with PVCs originating from the RVOT shows the characteristics of LBBB and an inferior axis morphology (7). However, the ECG characteristics of inferior RVOT have rarely been described. ECG-guided prediction of localization of RVOT has important procedural implications concerning the selection of catheter and auxiliary sheath, procedure time, and risk of complications. In this study, we sought to identify ECG characteristics that can predict the site for successful ablation of PVCs originating from the inferior RVOT.

Methods

Study population

This is a retrospective study. Between January 2016 and December 2020, 309 consecutive patients at Peking University First Hospital were identified to have symptomatic PVCs despite medical therapy. One hundred and twenty-four of these patients had PVCs originating in the RVOT. Among these RVOT cases, 107 patients without structural heart disease and no bundle branch block in sinus rhythm, were enrolled in the study. Left and right ventricular function was assessed by echocardiography before catheter ablation in all patients. From April 2019 onwards, we used intracardiac echocardiography (ICE) in PVC ablations.

ECG evaluation

Twelve-lead ECGs of symptomatic PVCs were analyzed for bundle branch block morphology, axis, QRS width, notching in V1–V6, R-wave pattern in V1 and V2 (rS, QS), and the precordial transition point from predominantly negative S-wave to predominantly positive R-wave deflection. Early QRS transition was defined as a transition in V3 or earlier and late transition as a transition in V4 or V5. Notching was defined as deflections in the QRS complex aside from a triphasic pattern.

Electrophysiological study

All patients underwent invasive electrophysiologic testing under local anesthesia in an awake state after providing written informed consent. Antiarrhythmic medications were discontinued at least five half-lives before the procedure, and beta-blockers and calcium channel blockers were withheld for at least 3 days. The right ventricle was mapped via the standard femoral approach. Intravenous isoproterenol (up to 10 μg/min for 5–10 min) was administered as necessary to induce ectopy.

Definition of superior and inferior RVOT

We considered a superior RVOT origin to be within 1 cm above or below the pulmonary annulus. An inferior RVOT origin is between the supraventricular crest and the pulmonary infundibulum and more than 1 cm away from the pulmonary annulus (8).

Mapping and ablation

Three-dimensional electroanatomic mapping (Carto; Biosense Webster Inc., Diamond Bar, CA, USA) was performed during all procedures. A 6-F steerable decapolar catheter (Dynamic XT; Boston Scientific, Marlborough, MA, USA) was advanced into the coronary sinus. An 8.5-F long sheath (St Jude Medical, St Paul, MN, USA) was used to facilitate and stabilize the mapping catheter. In 15 patients (7 patients in the superior RVOT group, and 8 patients in the inferior RVOT group), a 10-F ICE catheter (SoundStar; Biosense Webster Inc.) was advanced to the right ventricle to assist with mapping and ablation and monitor for complications. Mapping and radiofrequency ablation were performed through an open irrigated ablation catheter (Thermocool SmartTouch or Navistar; Biosense Webster Inc.). Anatomic and activation mapping was performed simultaneously using the three-dimensional Carto mapping system. The earliest point of activation during clinical PVCs was targeted for ablation. If PVC suppression was observed during ablation, additional

radiofrequency energy was applied at or adjacent to the successful ablation site. Radiofrequency energy was applied for at least 45–60 sec per site using 30–35 W. The number of lesions delivered was in the range of 5–9. Patients were monitored for a minimum of 15–30 min after the last radiofrequency application to eliminate PVCs. Patients were monitored overnight on the day of the procedure and discharged on the following day. The procedural endpoint was the complete elimination of clinical PVCs following catheter ablation. Suppression of the PVC burden by >80% on 24-h Holter monitoring immediately after the procedure was defined as an immediate success.

Follow-up

Patients were followed up for 3 months post-ablation. A 24-h Holter monitor was performed 1 and 3 months after the procedure. The PVC burden and episodes of ventricular arrhythmia were tracked and recorded. All patients underwent routine echocardiographic evaluation immediately after ablation and 3 months later. Long-term success was defined as a reduction in PVC burden of >80% at 3 months after ablation.

Statistical analysis

Data for continuous variables that were normally distributed are shown as the mean ± standard deviation and those with a skewed distribution as the median (interquartile range). Differences in continuous data were compared between patients with a superior RVOT origin and those with an inferior RVOT origin using the Student's *t*-test or the Kruskal–Wallis rank-sum test as appropriate. Categorical data are shown as the number (percentage) and were compared between the two groups using the chi-squared test. Receiver-operating characteristic (ROC) curve analyses were used to assess the ability of various ECG features to predict an inferior RVOT origin. All statistical analyses were performed using Empowerstats software (version 2.0; Empowerstats, Greenwood Village, CO, USA) and R software (version 3.4.3; R Foundation for Statistical Computing, Vienna, Austria). All analyses were two-sided, and a P-value < 0.05 was considered statistically significant.

Results

Patient characteristics

The patient demographics, clinical characteristics, and ECG features are shown in Table 1. Seventy-four patients (27 male, 47 female, mean age 47.30 ± 12.86 years) had PVCs with a superior RVOT origin (the superior RVOT group), and 33 (9 male, 24 female, mean age 45.58 ± 15.98 years) had PVCs with an inferior RVOT origin (the inferior RVOT group). There was no significant between-group difference in patient age or sex. Furthermore, all patients had a left ventricular ejection fraction within the normal range (mean, 64.63 ± 7.10% in the inferior RVOT group vs. 65.77 ± 6.94% in the superior RVOT group, $P = 0.435$).

ECG features

Patients in the inferior RVOT group were significantly more likely to have multiple morphologies (24.24 vs. 6.76%, $P = 0.011$). The PVC burden was seemingly slightly higher in the inferior RVOT group than in the superior RVOT group (24.93 ± 9.05 vs. 22.87 ± 10.25%, $P = 0.346$). Generally, PVCs with a superior RVOT origin have an inferior axis with LBBB morphology and a late R/S transition in the precordial leads (7). Therefore, a QRS duration <140 ms suggests a PVC with a septal origin, whereas a QRS duration >140 ms favors a free wall origin. However, the QRS wave of PVCs originating from the inferior RVOT does not conform to this rule. Due to the complex anatomic structure of the inferior RVOT, the QRS wave of PVCs originating from this site may be broad and multiform.

Although the morphology of the QRS wave of PVCs was consistent with the characteristics of origin in the RVOT, there were significant differences in QRS amplitude in leads II, III, and aVF between the inferior and superior RVOT groups (see Table 1). The QRS amplitude in the limb leads was lower for PVCs with an inferior RVOT origin than for those with a superior RVOT origin.

Although there was no significant statistical difference in the QRS duration of sinus rhythm between the two groups, PVCs with an inferior RVOT origin were more expansive than those with a superior RVOT origin (QRS duration, 162.42 ± 19.69 ms vs. 140.90 ± 11.30 ms; $P < 0.001$). Furthermore, the QRS wave in the limb leads for PVCs with an inferior RVOT origin was significantly more likely to be with a negative delta wave at the onset of the QRS wave in V1, somewhat like W-P-W (27.27 vs. 1.39%, $P < 0.001$).

The anterior septum was the most common site of origin of PVCs, accounting for 42.42% of PVCs in the inferior RVOT group (14 patients) and 50% of those in the superior RVOT group (37 patients) (see Table 2). In addition to the above ECG features, there was a between-group difference in transition in the precordial leads when the PVCs originated in the anterior septum, in that most of the PVCs arising from the anterior septum transited in V4 and V5 in the inferior RVOT group (78.57%) but transited in V3 and V4 in the superior RVOT group (94.44%) ($P = 0.036$).

Radiofrequency ablation

The earliest site of activation of PVCs was 29.3 ± 5.1 ms ahead of the QRS complex in the inferior RVOT group and

TABLE 1 Patient characteristics and ECG features of PVCs in the superior RVOT group and in the inferior RVOT group.

	Superior RVOT ($N = 74$)	Inferior RVOT ($N = 33$)	P
Gender (Female %)	63.51	72.73	0.352
Age	47.30 ± 12.86	45.58 ± 15.98	0.555
PVC burden in 24h Holter (%)	22.87 ± 10.25	24.93 ± 9.05	0.346
LVEF (%)	65.77 ± 6.94	64.63 ± 7.10	0.435
ECG features			
Multiform PVCs (%)	6.76	24.24	0.011
The amplitude of lead II (mV)	1.72 ± 0.45	1.21 ± 0.33	<0.001
The amplitude of lead III (mV)	1.62 ± 0.53	0.99 ± 0.46	<0.001
The amplitude of lead aVF (mV)	1.65 ± 0.48	1.09 ± 0.40	<0.001
QRS duration (ms) in sinus rhythm	94.14 ± 10.71	93.55 ± 10.12	0.789
QRS duration (ms) of PVCs	140.90 ± 11.30	162.42 ± 19.69	<0.001
A notch of QRS in Limb leads (%)	30.56	48.48	0.076
A negative delta wave at the onset of the QRS in V1 (%)	1.39	27.27	<0.001
Induced by isoproterenol (%)	16.67	18.18	0.848
Support with long sheath (%)	31.94	51.52	0.055
Successful rate (%)	95.95	87.88	0.199

ECG, electrocardiographic; LVEF, left ventricular ejection fraction; PVC, premature ventricular complexes; RVOT, right ventricular outflow tract; ICE, intracardiac echocardiography.

TABLE 2 Electrocardiographic characteristics of PVCs originating in the anterior septum in the superior RVOT group and in the inferior RVOT group.

	Anterior septum of the superior RVOT ($N = 37$)	Anterior septum of the inferior RVOT ($N = 14$)	P
PVC burden in 24 h Holter (%)	25.10 ± 11.62	24.48 ± 9.54	0.863
ECG features			
Multiform PVCs (%)	5.41	7.14	1.000
The amplitude of lead II (mV)	1.62 ± 0.32	1.34 ± 0.37	0.009
The amplitude of lead III (mV)	1.57 ± 0.41	1.23 ± 0.47	0.013
The amplitude of lead aVF (mV)	1.59 ± 0.35	1.31 ± 0.40	0.018
QRS duration (ms) in sinus rhythm	94.35 ± 12.10	93.64 ± 7.43	0.839
QRS duration(ms) of PVCs	139.03 ±10.54	156.43 ± 13.36	<0.001
A notch of QRS in Limb leads (%)	25.00	35.71	0.449
A negative delta wave at the onset of the QRS in V1 (%)	0	21.43	0.019
Induced by isoproterenol (%)	16.67	21.43	0.697
Support with long sheath (%)	30.56	42.86	0.410
Successful rate (%)	94.59	78.57	0.120

ECG, electrocardiographic; LVEF, left ventricular ejection fraction; PVC, premature ventricular complexes; RVOT, right ventricular outflow tract.

27.2 ± 7.0 ms in the superior RVOT group ($P = 0.572$). Therefore, catheter ablation was performed at the site of the earliest activity.

Overall, the ablation success rate was slightly lower for PVCs in the inferior RVOT group than those in the superior RVOT group (87.88 vs. 95.95%, $P = 0.199$). However, there was a difference but it did not reach a statistical significance in the ablation success rate if the PVCs arose from the anterior septum (78.57% in the inferior RVOT group vs. 94.59% in the superior RVOT group, $P = 0.120$) (see Table 2).

It is worth noting that long sheath support was used to maintain the stability of the ablation catheter more often in the inferior RVOT group than in the superior RVOT group (51.52 vs. 31.94%, $P = 0.055$).

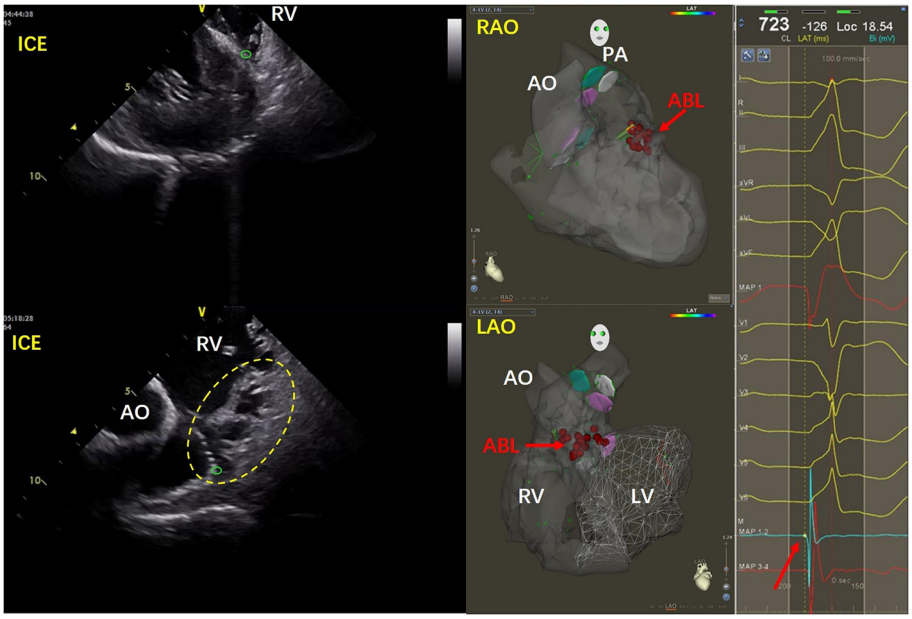

FIGURE 1
Images for a patient with PVCs that originated from the inferoanterior septum in the inferior RVOT. In the ICE image on the **left**, the tip of the ablation catheter is indicated by the green circle. Abundant trabeculae can be seen in the yellow dotted line area. The tip of the ablation catheter is visible embedded at the intersection of the muscle trabeculae at their junction with the smooth conus of the pulmonary artery. The red arrow in the middle three-dimensional image shows the ablation target. On the **right** side of the figure, the red arrow indicates the early potential at the ablation site. ABL, ablation; AO, aorta; ICE, intracardiac echocardiography; LAO, left anterior oblique; LV, left ventricle; PA, pulmonary artery; RAO, right anterior oblique; RV, right ventricle.

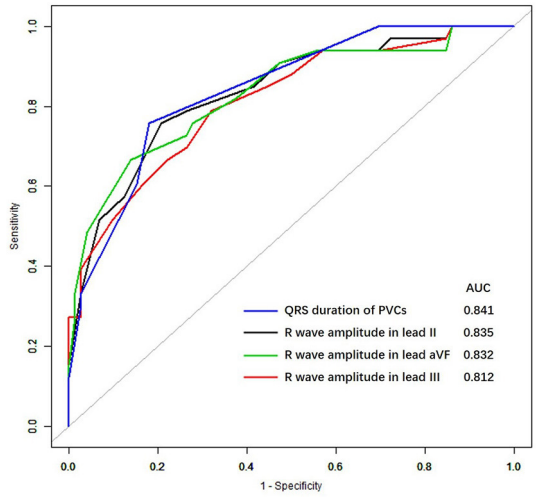

FIGURE 2
Receiver-operating characteristic curves for premature ventricular complexes in the inferior right ventricular outflow tract. AUC, the area under the receiver-operating characteristic curve.

Complex anatomy seen by ICE

The anatomy of the inferior RVOT is more complex than that of the superior RVOT because it includes the septal papillary muscles, abundant trabeculae, and the moderator band (7). Figure 1 shows a case in which the earliest excitation originated in the lower area of the anterior septum. The ICE image shows the tip of the ablation catheter embedded in the abundant trabeculae where the muscles intersect with the smooth-walled pulmonary infundibulum. In another case, the PVCs originated from the inferoanterior septum of the inferior RVOT. In Supplementary Video 1, the ICE image shows that the tip of the ablation catheter is located at the junction of the interventricular septum and the root of the moderator band. Supplementary Video 2 shows a case of PVCs originating from the middle part of the septum of the inferior RVOT. In the ICE image, the tip of the ablation catheter is inserted into the abundant muscle trabeculae.

Complications and follow-up

One patient in the inferior group developed pericardial tamponade, whose PVCs originated from the supraventricular crest, the posterior part of the inferior RVOT, where attachment of the catheter is challenging. The patient recovered after immediate pericardial drainage. It is noteworthy that the pericardial tamponade occurred before we started using ICE.

Furthermore, a complete right bundle branch block occurred after ablation in one further patient in the inferior RVOT group and two in the superior RVOT group (3.03 vs. 2.70%, $P = 0.448$).

During a mean follow-up of 8 ± 3 months, there was no statistical difference in the PVC recurrence rate between the inferior RVOT group and the superior RVOT group (9.09 vs. 8.11%, $P = 0.671$). All patients underwent routine echocardiography immediately following catheter ablation and at the 3-month follow-up. There was no change in the left ventricular ejection fraction or any evidence of new or worsening tricuspid regurgitation in any patient.

Diagnostic value of ECG algorithms for PVCs with an inferior RVOT origin

The areas under the ROC curves (AUCs) for all the previous ECG algorithms used to distinguish PVCs with an inferior RVOT origin from those with a superior RVOT origin were calculated and are shown in Figure 2.

We found that the AUCs for a diagnosis of an inferior RVOT origin were within the range of 0.812–0.841 for various ECG features, including the QRS duration of PVCs, the amplitude of R waves in lead II, III, and aVF; for which the AUC for the QRS duration of PVCs was the highest (0.841).

The ROC curves for the four ECG criteria that differentiated between PVCs of superior RVOT origin and those of inferior RVOT origin (maximum duration of the QRS, the R wave in lead II, the R wave in lead aVF, and the R wave in lead III) are shown in Figure 1. The sensitivities, specificities, positive and negative predictive values, and AUCs for the ability of these criteria to predict the site of origin in the RVOT are shown in Table 3. The R wave amplitude in lead III had the highest sensitivity (79%), and the R wave amplitude in lead aVF had the highest specificity (86%). The positive predictive value for identifying the RVOT region ranged from 53 to 68%, and the negative predictive value ranged from 85 to 88%.

Discussion

Main ECG findings

Although Xia et al. have reported ECG indices that can identify whether PVCs originate from the left ventricular outflow tract or the RVOT and Wang et al. have described ECG indices that identify PVCs that originate in the left ventricular outflow tract (9, 10), there is limited information on ECG indices for PVCs originating in the upper and lower RVOT.

PVCs originating from the inferior RVOT have a typical ECG pattern with an LBBB morphology and an inferior axis. Unlike PVCs with a superior RVOT origin that starts around the pulmonary annulus, the QRS of PVCs that originate from the inferior RVOT is upwards in the limb leads but has a lower amplitude and later R/S transition at V4∼V5 in the precordial leads.

PVC that originates in the septum of inferior RVOT is characterized by variable morphology, which is consistent with an origin in the RVOT septum but is relatively broad and pleomorphic. PVC originating from the anterior septum in the inferior RVOT often shows a negative delta wave at the onset of the QRS in V1 and polymorphism due to the crisscrossing of the septal papillary muscles, moderator band, and muscle trabeculae at this site. If the QRS wave of V2 is deep and concave, the PVCs may originate from the deep interventricular septum. However, the morphology of PVCs originating from the supraventricular crest of the inferior RVOT can also vary because early Purkinje potentials could be recorded here in some patients (11). A later R/S transition in the precordial leads means that ablation may be more difficult.

In summary, the ECG features of PVCs that originate in the inferior RVOT are as follows: (1) although the main waves of QRSs in leads II, III, and aVF are upward, they are relatively low or have S waves; (2) the negative wave is deep in V1–V3 and the R-wave transition is in V4–V5; (3) the QRS wave in V1 may have a negative delta wave at the onset of the QRS (somewhat like the W-P-W waveform); and (4) PVCs may be multiform, or the shape may change during ablation. Typical cases showing the characteristics of PVCs originating from different parts of the inferior RVOT are shown in Figure 3.

We found that the above ECG indices had good predictability for judging the origin of PVCs: (1) the best threshold for the QRS duration in PVCs was 145 ms. and (2) the best thresholds for the amplitude of R waves in leads II, III, and aVF were 1.35 mV, 1.35 mV, and 1.15mV. Thus, the general trend is consistent with the morphological characteristics of RVOT. Furthermore, the QRS wave of the PVCs has a low amplitude and wide duration, which points to an origin in the inferior RVOT.

Based on these ECG characteristics, we can infer the origin of PVCs and select appropriate catheters and additional tools to improve the success rate of ablation.

Anatomic characteristics of the inferior RVOT

The inferior RVOT is located above the supraventricular crest and below the pulmonary annulus. On the septal aspect, the supraventricular crest inserts between the limbs of the septomarginal trabeculation and the septal band. This muscular strap reinforces the septal surface of the right ventricle, breaking

TABLE 3 Best threshold analysis.

Test	Best threshold	Specificity	Sensitivity	Accuracy	Positive-PV	Negative-PV
R-wave amplitude in lead II	1.35 mV	0.792	0.758	0.781	0.625	0.877
R-wave amplitude in lead III	1.35 mV	0.681	0.788	0.714	0.531	0.875
R-wave amplitude in lead aVF	1.15 mV	0.861	0.667	0.800	0.688	0.849
QRS duration of PVCs	145 ms	0.819	0.758	0.800	0.658	0.881

Positive-PV, Positive predictive value; Negative-PV, Negative predictive value.

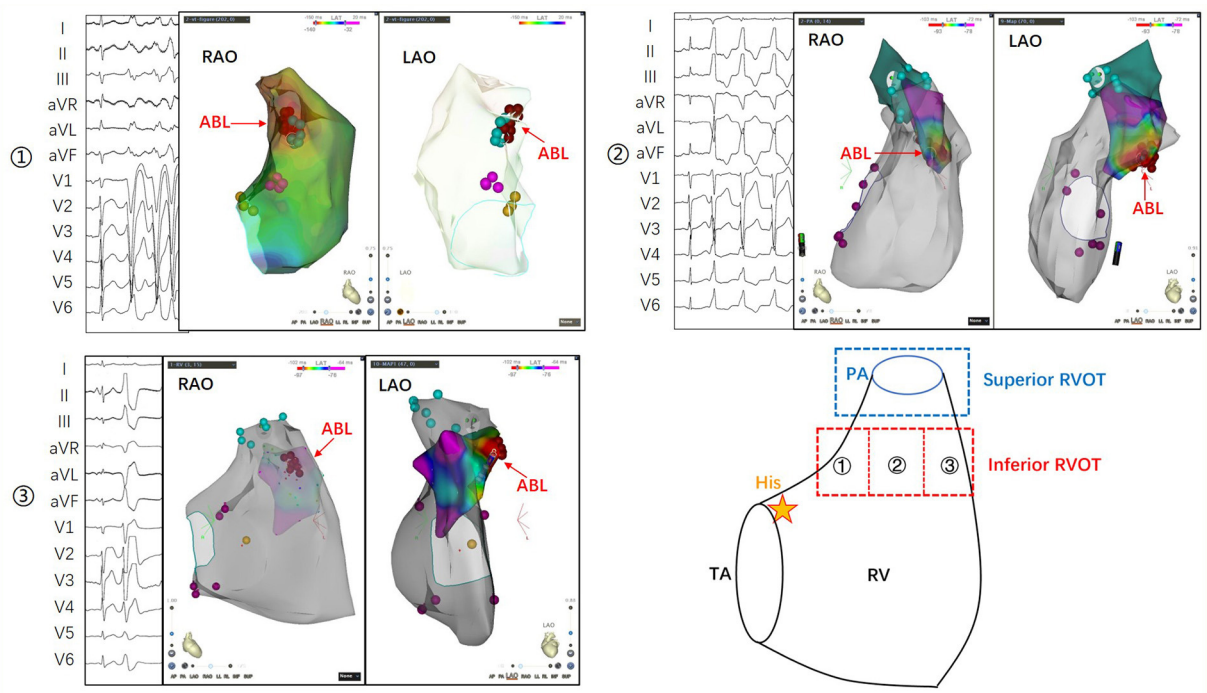

FIGURE 3
The inferior RVOT is between the supraventricular crest above the tricuspid annulus and the pulmonary annulus. Its lower portion is flush with His bundle, and its upper portion is more than 1 cm lower than the pulmonary annulus. ① The morphological characteristics of PVCs originating from the inferoposterior RVOT include a more comprehensive QRS, an R/S shape in leads II, III, and aVF, a positive main wave in leads I and aVL, and a shift in the R/S transition to between V4 and V5. ② The morphological characteristics of PVCs originating from the inferomedial RVOT include an upright but not tall QRS in leads II, III, and aVF, opposite main waves in leads I and aVL, and a shift of the R/S transition to between V3 and V4. ③ The morphological features of PVCs originating from the inferoanterior RVOT include an upright QRS in leads II, III, and aVF, and a negative main wave in leads I and aVL, indicating the origin of the septum. V1–V3 is QS-shaped, the beginning of the QRS in lead V1 is similar to the preexcitation wave, and the R/S transition is shifted to lead V5. PA, pulmonary artery; RAO, right anterior oblique; RV, right ventricle; RVOT, right ventricular outflow tract; TA, tricuspid annulus.

up at the apex to form the moderator band and anterior papillary muscles and giving rise to a further series of septoparietal trabeculations that run to the parietal ventricular wall (7). The anterior portion of the inferior RVOT is connected to the large inflow tract of muscle trabeculae, including the septal papillary muscles and the moderator band. The posterior part of the inferior RVOT contains the conus papillary muscles, supraventricular crest, and the upper edge of the tricuspid annulus. The interventricular septum is adjacent to the left anterior descending coronary artery, and the great cardiac vein runs in the anterior interventricular sulcus.

Ablation difficulties and techniques

When the ablation target site is located in the right anterior oblique projection, it is flush with or slightly higher than the His bundle. In this situation, there are several main ablation difficulties. First, catheter attachment is difficult. The use of a reversed U-curve ablation catheter is suitable for attachment at a site near the pulmonary annulus but not in the inferior RVOT. Second, there are interspaces between the muscle trabeculae, moderator band, papillary muscles, and the smooth-walled pulmonary conus, where it is difficult to insert a catheter

tip accurately without direct vision under ICE. Third, the left anterior descending coronary artery may be damaged by tightening the interventricular septum at its anterior and inferior portions. Fourth, the conduction system in the right bundle branch may be damaged by mechanical compression of the catheter or long sheath.

We recommend the following ablation techniques to overcome some of these difficulties. First, we suggest using a long sheath or steerable sheath to support the ablation catheter. A pressure-sensing ablation catheter can be used to prompt local attachment pressure, which is helpful when judging the attachment. ICE shows the anatomical structure and relationships in real-time, allowing the operator to adjust the moderator band and papillary muscles under direct vision. The tip may become embedded in the muscle trabeculae when the catheter adheres well due to the complex local anatomical structure. Therefore, careful tip pressure adjustment to 10–15 g is essential. If the impedance is still excessive, it is necessary to relax the high impedance limit of the radiofrequency apparatus and increase the heparin saline perfusion speed during catheter ablation. The discharge ablation requires gradual power titration, and PVCs originating from the inferior and anterior portions of the inferior RVOT need to be close to the ventricular septum. If severe pain occurs, the ablation procedure should be stopped because it may damage the left anterior descending coronary artery in the anterior interventricular sulcus or lead to rupture of the ventricular wall.

ICE helps with the judgment of the anatomical location and catheter attachment (12, 13). Furthermore, ICE can be helpful for identifying and confirming contact with the catheter and these endocavitary structures and should always be considered when these structures are potentially involved in the mechanism or substrate of an arrhythmia. Indeed, ICE can enhance the ability to perform successful endocardial mapping and ablation by direct visualization.

Conclusion

When evaluating a patient with PVCs, an ECG presentation that conforms to the morphological characteristics of RVOT, namely, the QRS wave is relatively broad and polymorphic and the primary waves in limb leads (II, III, and aVF) are upward and have low amplitude, we should consider the inferior RVOT as a likely origin.

Data availability statement

The original contributions presented in the study are included in the article/Supplementary material, further inquiries can be directed to the corresponding author/s.

Ethics statement

The studies involving human participants were reviewed and approved by the Ethics Committee of Peking University First Hospital. The patients/participants provided their written informed consent to participate in this study. Written informed consent was obtained from the individual(s) for the publication of any potentially identifiable images or data included in this article.

Author contributions

All authors listed have made a substantial, direct, and intellectual contribution to the work and approved it for publication.

Acknowledgments

We thank Liwen Bianji (Edanz) (www.liwenbianji.cn) for editing the English text of a draft of this manuscript.

Conflict of interest

The authors declare that the research was conducted in the absence of any commercial or financial relationships that could be construed as a potential conflict of interest.

Publisher's note

Supplementary material

The Supplementary Material for this article can be found online at: https://www.frontiersin.org/articles/10.3389/fcvm.2022.950401/full#supplementary-material

SUPPLEMENTARY VIDEO 1
A case in which PVCs originated from the inferoanterior septum of the inferior RVOT. The ICE image on the left shows the tip of the ablation catheter (red arrow) located at the junction of the interventricular septum and the root of the moderator band (pink arrow). The three-dimensional image in the middle shows an RAO projection in which the target can be seen in the inferoanterior portion of the inferior RVOT between the tricuspid annulus and the pulmonary annulus and an LAO projection in which the visual target is located at the root of the moderator band in the interventricular septum. The target map on the right shows the local fragmentation potential of multiple folds. ABL, ablation; ICE, intracardiac echocardiography; LAO, left anterior oblique;

LV, left ventricle; MB, moderator bundle; PA, pulmonary artery; RAO, right anterior oblique; RV, right ventricle.

SUPPLEMENTARY VIDEO 2

A case in which PVCs originated from the medial septum of the inferior RVOT. In the ICE image, the tip of the ablation catheter is inserted into the abundant muscle trabeculae. In the radiographic LAO projection, the tip of the ablation catheter is toward the medial septum. In the three-dimensional images, the RAO projection shows the target located in the anterior and upper portions of His bundle and in the middle of the lower RVOT. In the LAO projection, the target is in the ventricular septum. The effective target site shows the early and fragmentation potential. ABL, ablation; His, the bundle of His; ICE, intracardiac echocardiography; LAO, left anterior oblique; LV, left ventricle; MB, moderator band; PA, pulmonary artery; RAO, right anterior oblique; RV, right ventricle.

References

1. Ling Z, Liu Z, Su L, Zipunnikov V, Wu J, Du H, et al. Radiofrequency ablation versus antiarrhythmic medication for treatment of ventricular premature beats from the right ventricular outflow tract: prospective randomized study. *Circ Arrhythm Electrophysiol.* (2014) 7:237–43. doi: 10.1161/CIRCEP.113.000805

2. Cronin EM., Bogun FM, Maury P, Peichl P, Chen M, Namboodiri N, et al. 2019 HRS/EHRA/APHRS/LAHRS expert consensus statement on catheter ablation of ventricular arrhythmias. *Heart Rhythm.* (2020) 17:e2–e154. doi: 10.1016/j.hrthm.2019.03.002

3. Liao Z, Zhan X, Wu S, Xue Y, Fang X, Liao H, et al. Idiopathic ventricular arrhythmias originating from the pulmonary sinus cusp: prevalence, electrocardiographic/electrophysiological characteristics, and catheter ablation. *J Am Coll Cardiol.* (2015) 66:2633–44. doi: 10.1016/j.jacc.2015.09.094

4. Zhang J, Tang C, Zhang Y, Su X. Pulmonary sinus cusp mapping and ablation: A new concept and approach for idiopathic right ventricular outflow tract arrhythmias. *Heart Rhythm.* (2018) 15:38–45. doi: 10.1016/j.hrthm.2017.08.007

5. Yokokawa M, Good E, Crawford T, Chugh A, Pelosi F, Latchamsetty R, et al. Reasons for failed ablation for idiopathic right ventricular outflow tract-like ventricular arrhythmias. *Heart Rhythm.* (2013) 10:1101–8. doi: 10.1016/j.hrthm.2013.05.011

6. Yamada S, Chung FP, Lin YJ, Chang SL, Lo LW,Hu YF, et al. Electrocardiographic features of failed and recurrent right ventricular outflow tract catheter ablation of idiopathic ventricular arrhythmias. *J Cardiovasc Electrophysiol.* (2018) 29:127–37. doi: 10.1111/jce.13359

7. Ho SY, Nihoyannopoulos P. Anatomy, echocardiography, and normal right ventricular dimensions. *Heart.* (2006) 92 Suppl 1:i2–i13. doi: 10.1136/hrt.2005.077875

8. Yamada T. Idiopathic ventricular arrhythmias: Relevance to the anatomy, diagnosis, and treatment. *J Cardiol.* (2016) 68:463–71. doi: 10.1016/j.jjcc.2016.06.001

9. Xia Y, Liu Z, Liu J, Li X, Zhang H, Fu L, et al. Amplitude of QRS complex within initial 40 ms in V2 (V2 QRSi40): Novel electrocardiographic criterion for predicting accurate localization of outflow tract ventricular arrhythmia origin. *Heart Rhythm.* (2020) 17:2164–71. doi: 10.1016/j.hrthm.2020.07.006

10. Wang Y, Liang Z, Wu S, Han Z, Ren X. Idiopathic ventricular arrhythmias originating from the right coronary sinus: Prevalence, electrocardiographic and electrophysiological characteristics, and catheter ablation. *Heart Rhythm.* (2018) 15:81–9. doi: 10.1016/j.hrthm.2017.09.008

11. Santoro F, DI Biase L, Hranitzky P, Sanchez JE, Santangeli P, Perini AP, et al. Ventricular tachycardia originating from the septal papillary muscle of the right ventricle: electrocardiographic and electrophysiological characteristics. *J Cardiovasc Electrophysiol.* (2015) 26:145–50. doi: 10.1111/jce.12551

12. Enriquez A, Saenz LC, Rosso R, Silvestry FE, Callans D, Marchlinski FE, et al. Use of intracardiac echocardiography in interventional cardiology: working with the anatomy rather than fighting it. *Circulation.* (2018) 137:2278–94. doi: 10.1161/CIRCULATIONAHA.117.031343

13. Ehdaie A, Liu F, Cingolani E, Wan X, Chugh SS, Shehata M, et al. How to use intracardiac echocardiography to guide catheter ablation of outflow tract ventricular arrhythmias. *Heart Rhythm.* (2020) 17:1405–10. doi: 10.1016/j.hrthm.2020.02.037

frontiers | Frontiers in Cardiovascular Medicine

TYPE Original Research
PUBLISHED 13 October 2022
DOI 10.3389/fcvm.2022.868634

OPEN ACCESS

EDITED BY
Andreas Metzner,
University Medical Center
Hamburg-Eppendorf, Germany

REVIEWED BY
Armin Attar,
Shiraz University of Medical Sciences,
Iran
Emanuela Teresina Locati,
IRCCS San Donato Polyclinic, Italy

*CORRESPONDENCE
Yuegang Wang
wyg06@smu.edu.cn
Lichun Wang
wanglich@mail.sysu.edu.cn
Yumei Xue
xymgdci@163.com

†These authors have contributed equally to this work and share first authorship

SPECIALTY SECTION
This article was submitted to
Cardiac Rhythmology,
a section of the journal
Frontiers in Cardiovascular Medicine

RECEIVED 03 February 2022
ACCEPTED 16 September 2022
PUBLISHED 13 October 2022

CITATION
Qiu S, Sun Z, Li X, Li J, Huang X, Liu M, Bin J, Liao Y, Xiu J, Zha D, Xue Y, Wang L and Wang Y (2022) A novel and effective ECG method to differentiate right from left ventricular outflow tract arrhythmias: Angle-corrected V2S.
Front. Cardiovasc. Med. 9:868634.
doi: 10.3389/fcvm.2022.868634

A novel and effective ECG method to differentiate right from left ventricular outflow tract arrhythmias: Angle-corrected V2S

Shifeng Qiu[1,2,3†], Zhuhua Sun[4†], Xinzhong Li[1,2,3], Jianyong Li[1,2,3], Xiaobo Huang[1,2,3], Menghui Liu[5,6], Jianping Bin[1,2,3], Yulin Liao[1,2,3], Jiancheng Xiu[1,2,3], Daogang Zha[1,2,3], Yumei Xue[7,8*], Lichun Wang[5,6*] and Yuegang Wang[1,2,3*]

[1]Department of Cardiology, Nanfang Hospital, Southern Medical University, Guangzhou, China, [2]Guangdong Provincial Key Laboratory of Shock and Microcirculation, Nanfang Hospital, Southern Medical University, Guangzhou, China, [3]State Key Laboratory of Organ Failure Research, Nanfang Hospital, Southern Medical University, Guangzhou, China, [4]Department of Health Management, The Third Affiliated Hospital of Southern Medical University, Guangzhou, China, [5]Department of Cardiology, The First Affiliated Hospital of Sun Yat-sen University, Guangzhou, China, [6]Key Laboratory on Assisted Circulation, Ministry of Health, Guangzhou, China, [7]Guangdong Cardiovascular Institute, Guangdong Provincial People's Hospital, Guangdong Academy of Medical Sciences, Guangzhou, China, [8]Guangdong Provincial Key Laboratory of Clinical Pharmacology, Guangdong Provincial People's Hospital, Guangdong Academy of Medical Sciences, Guangzhou, China

Background and aims: Standard 12-lead electrocardiogram (ECG) patterns combined with the anatomical cardiac long-axis angle revealed by chest X-ray can prevent the influence of cardiac rotation, physical shape, and lead position, so it may be an ideal means to predict the origin of the outflow tract (OT) ventricular arrhythmias (OTVAs) for ablation procedures. The study explores the value of this strategy in identifying the origin of OTVA.

Methods: This study was conducted using a retrospective cohort and a prospective cohort of consecutive patients at two centers. The anatomical cardiac long-axis angle was calculated by measuring the angle between the cardiac long-axis (a line joining the apex to the midpoint of the mitral annulus) and the horizontal plane on a chest X-ray. The V2S angle was calculated as the V2S amplitude times the angle. We ultimately enrolled 147 patients with symptomatic OTVAs who underwent successful radiofrequency catheter ablation (RFCA) (98 women (66.7%); mean age 46.9 ± 14.7 years; 126 right ventricular OT (RVOT) origins, 21 left ventricular OT (LVOT) origins) as a development cohort. The new algorithm was validated in 48 prospective patients (12 men (25.0%); mean age 48.0 ± 15.8 years; 36 RVOT, 12 LVOT origins).

Results: Patients with RVOT VAs had greater V2S, long-axis angle, and V2S angle than patients with LVOT VA (all $P < 0.001$). The cut-off V2S angle obtained by receiver operating characteristic (ROC) curve analysis was 58.28 mV° for the prediction of RVOT origin (sensitivity: 85.7%; specificity: 95.2%; positive predictive value: 99.1%; negative predictive value: 52.6%). The AUC achieved using the V2S angle was 0.888 ($P < 0.001$), which was the highest among all indexes (V2S/V3R: 0.887 ($P < 0.016$); TZ index: 0.858 ($P < 0.001$); V1-2 SRd: 0.876 ($P < 0.001$); V3 transition: 0.651 ($P < 0.001$)). In the prospective cohort, the V2S angle had a high overall accuracy of 93.8% and decreased the procedure time ($P = 0.002$).

Conclusion: V2S angle can be a novel measure that can be used to accurately differentiate RVOT from LVOT origins. It could help decrease ablation duration and radiation exposure.

KEYWORDS

radiofrequency ablation, electrocardiogram, V2S, angle, ventricular outflow tract arrhythmias, cardiac long-axis

Introduction

Outflow tract (OT) ventricular arrhythmias (OTVAs), mainly composed of premature ventricular complexes (PVCs) or ventricular tachycardia (VT), are commonly encountered and sometimes harmful, as they can cause cardiomyopathy leading to dangerous conditions such as heart failure and sudden cardiac death (1, 2). Catheter ablation is a common curative therapy for OTVA patients with and without structural heart disease when drugs are ineffective or have unacceptable side effects (3, 4). Accurate prediction of a right ventricular outflow tract (RVOT) vs. left ventricular outflow tract (LVOT) origin of OTVA can direct the catheter ablation strategy, thereby reducing ablation duration and avoiding operative complications (5–7). Current algorithms that only rely on the standard 12-lead electrocardiogram (ECG) to identify OTVAs are limited to the cardiac rotation caused by the physical shape and cannot achieve the desired accuracy (8–10).

The amplitude and precordial transition of the 12-lead ECG depends on the cardiac depolarization vector axis and are influenced by the cardiac rotation and lead position. Even though the vectorcardiogram (VCG) can reflect electrical activation more accurately than scalar ECG in certain circumstances, this non-anatomical recording is still prone to error and takes more time (11, 12). Chest X-ray is simple and convenient in the clinic; more importantly, this imaging method can reflect anatomical characteristics and cardiac transposition and can be used to correct the recording differences caused by anatomical variations to a certain extent (13). Therefore, we hypothesized that 12-lead ECG combined with the anatomical cardiac long-axis calculated from the chest X-ray could more precisely predict the origin of OTVA.

In this study, we aimed first to develop a novel algorithm that took into account the anatomical cardiac long-axis plus 12-lead ECG to differentiate RVOT- from LVOT-origin VA. Second, we compared this algorithm with earlier methods of identifying OTVA and compared their accuracy in predicting LVOT vs. RVOT origin in a prospective cohort.

Materials and methods

The data, analytic methods, and study materials can be made available to other researchers for purposes of reproducing the results or replicating the procedure. This trial was approved by the Human Research Ethics Committee of Nanfang Hospital of Southern Medical University and the First Affiliated Hospital of Sun Yat-sen University (NFEC-2020-083).

Study design

This study was done in 2 parts: 1) a review and analysis of a retrospective cohort of premature ventricular contraction (PVC)/ventricular tachycardia (VT) patients who underwent successful radiofrequency catheter ablation (RFCA), whose aim was to develop a new diagnostic method to distinguish LVOT- from RVOT-origin PVC/VT, which we used to identify the origin of the interventricular septum and the coronary sinuses; and 2) an analysis of a prospective cohort for evaluating the validity of the new diagnostic method.

Study population

Consecutive patients who were indicated for OVTA ablation with ECG left bundle branch block (LBBB) morphology and transition in leads V2-V4 without structural abnormalities were recruited in two centers. Atypical LBBB morphologies, such as "annular" or "ostial" morphologies, were excluded. Patients with coronary heart disease, structural heart disease, paced rhythm, arrhythmogenic right ventricular cardiomyopathy, failed ablation, left ventricular ejection fraction (LVEF) of $< 50\%$, conduction disturbances in the underlying sinus rhythm, or a secondary cause of arrhythmias were excluded from the study. Additionally, those with a secondary possible cause of arrhythmias, such as electrolyte disturbance, impaired kidney, liver or thyroid function, or hematologic or rheumatological diseases, were excluded.

Electrocardiographic assessment

A 2-min standard surface 12-lead ECG was recorded during sinus rhythm and during PVC/VT at 25 mm/s speed (10 mm/mv amplitude) with chest and limb leads placed in standard positions in all patients. The ECG recording system was the FX-7402 (Fukuda Denshi, Inc., Tokyo, Japan) or the LabSystem Pro (Boston Scientific, Inc.). The morphologies of the sinus beats and OTVAs were analyzed on the same 12-lead ECG using electronic calipers. The following parameters were measured from the surface ECG of the first beat of PVC/VT: the S-wave amplitude in leads V1-V3, R-wave amplitude in leads V1-V3, and total QRS duration. Then, all the parameters above were normalized to the anatomical cardiac long-axis. The apex is clearly defined anatomically; the exact point used to locate the base has varied between studies, but the most convenient has been the atrioventricular rings (14). To determine the long-axis of the heart, we took a line from the center of the mitral valvar orifice to the left ventricular apex (13). The anatomical cardiac long-axis can be estimated by measuring the angle between the cardiac long-axis anatomically and the horizontal plane on chest radiography. In general, the cardiac long-axis angle is different in people of different physiques, in which taller, thinner people have an angle greater than 45 degrees (°), while shorter, heavier people have an angle less than 45° (13).

In our study, the S-wave in lead V2 of PVC/VT normalized to the cardiac long-axis, for calculating the angle practically, was termed the angle-corrected V2S (hereafter, V2S angle). Similarly, the S-wave in leads V1 and V3 and the R-wave in leads V1-V3 of PVC/VT normalized to the cardiac long-axis were termed the V1S angle, V3S angle, V1R angle, V2R angle, and V3R angle, respectively. For example, the V2S angle was calculated from the 12-lead surface ECG with this formula: V2S amplitude $\times$ angle (mV°) (**Figure 1**). QRS duration was measured in the lead with the widest QRS complex on the 12-lead surface ECG (15).

We compared our novel ECG criterion with several published ECG algorithms: 1) TZ index (16) = TZ score of the OTVA minus the TZ score of the sinus beat. The TZ score was graded in 0.5-point increments according to the site of the R-wave transition (e.g., TZ in V2 = 2 points, V2–V3 = 2.5 points, V3 = 3 points, and V3–V4 = 3.5 points). The cut-off value of the TZ index obtained by receiver operating characteristic (ROC) curve analysis was ≥ 0 for the prediction of RVOT origin. 2) V2S/V3R (10): the S-wave amplitude in lead V2 divided by the R-wave amplitude in lead V3 during the OTVA. The cut-off value of the V2S/V3R index obtained by ROC curve analysis was $>$ 1.5 mV for the prediction of RVOT origin. 3) The combined TZ index and V2S/V3R (8) were calculated with this formula: $Y = -1.15 \times (\text{TZ}) - 0.494 \times (\text{V2S/V3R})$. If the TZ index and V2S/V3R are ≥ -0.76, it predicts LVOT origin; 4) V1–V2 S-R difference (V1-2 SRd) (mV) (17): The S-R difference in V1-V2 on the 12-lead surface ECG was calculated with this formula: (V1S amplitude + V2S amplitude) – (V1R amplitude + V2R amplitude). If V1–2 SRd $>$ 1.625 mV, it predicts an RVOT origin. 5) V3 transition (18): An R-wave deflection interval in V3 ($>$ 80 ms) and an R-wave amplitude index in V1 ($>$ 0.3) predict an LVOT origin. 6) R wave amplitude in lead I (9): R amplitude $\geq$ 0.1 mV in lead I predicts an LVOT origin. 7) Initial r wave surface area (ISA) index (19): This index is measured by multiplying the R wave duration in milliseconds by the R wave amplitude in mV in the V1 (ISA V1) or V2 lead (ISA V1). If ISA $\geq$ 15, it predicts an LVOT origin. 8) V1R/V1S index (20): The R-wave amplitude is divided by the S-wave amplitude in the V1 lead during the OTVAs. An R-wave duration index $\geq$ 50% and an R/S-wave amplitude index $\geq$ 30% strongly suggest an ASC origin in patients with a typical LBBB morphology and an inferior axis.

Then, all ECG algorithms above were corrected for the anatomical cardiac long-axis. The TZ index corrected for the cardiac long-axis, for calculating by the angle practically, was termed the angle-corrected TZ index (hereafter, TZ index angle). The other corrected ones were termed V2S/V3R angle, combined TZ index and V2S/V3R angle, V1-2 SRd angle, V3 transition angle, R wave amplitude in lead I angle, ISA angle, and V1R/V1S angle.

All measurements were performed by 2 electrophysiologists who were blinded to the final diagnosis and the site of origin to eliminate interobserver variability and bias. Measurements were independently performed and reviewed by 3 physicians who were blinded to the PVC/VT site of origin.

Ablation protocol

All antiarrhythmic medications were suspended at least five half-lives before the ablation procedure. The ablation procedure

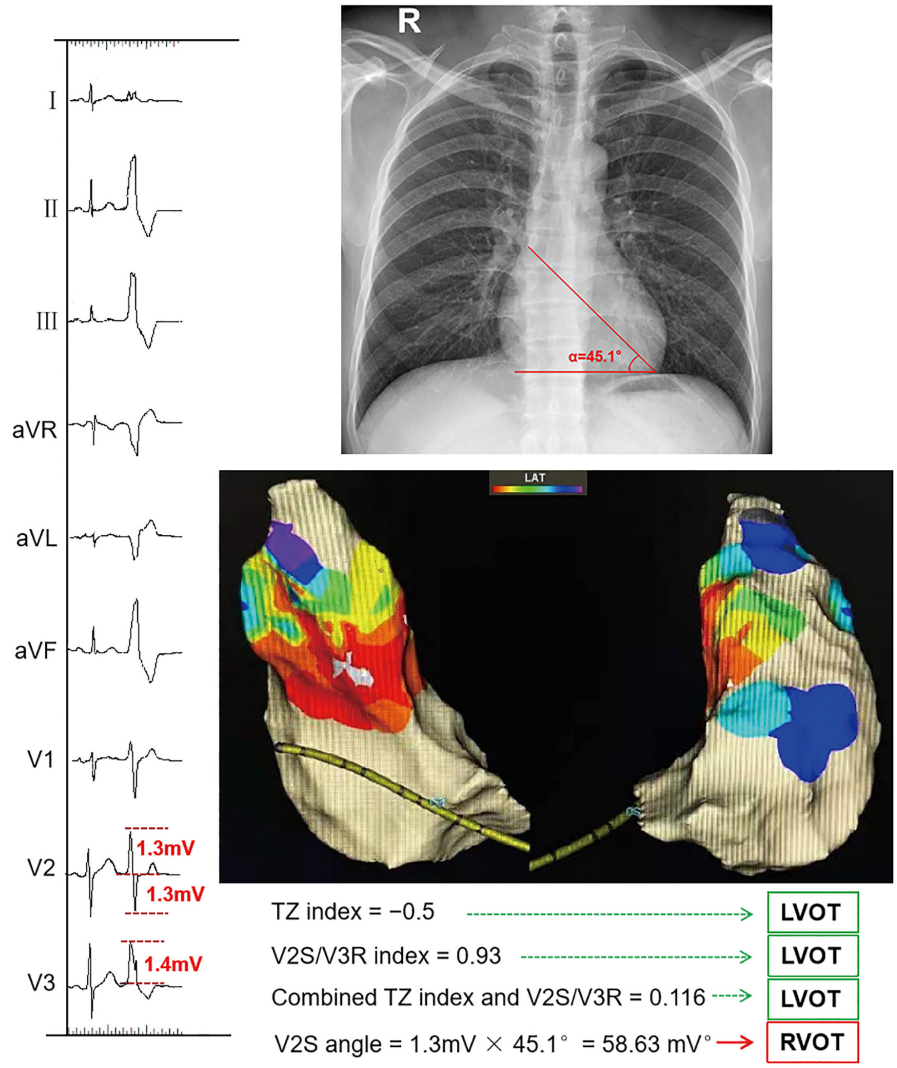

FIGURE 1
Example of calculating the V2S angle and several ECG algorithms. The TZ index was −0.5 according to the following formula: TZ score of OTVA minus TZ score of sinus beat (2−2.5 = −0.5). The V2S/V3R index was calculated with the following formula: V2S/V3R = 1.3 mV/1.4 mV = 0.93. The combined TZ index and V2S/V3R were calculated with the formula $Y = -1.15 \times (TZ) - 0.494 \times (V2S/V3R) = -1.15 \times (-0.5) - 0.494 \times 0.93 = 0.116$. These indexes indicate that this OTVA had a left ventricular outflow tract (LVOT) origin, though it was successfully ablated in the septal aspect of the right ventricular outflow tract (RVOT). The measurements of the V2S angle during the OTVAs are as follows: the S-wave amplitude in lead V2 is 1.3 mV. The angle (α) between the cardiac long-axis anatomically and the horizontal plane on chest radiography is 45.1°. The V2S angle was calculated with the following formula: (V2S × α) = 1.3 mv × 45.1° = 58.63 (mV°). The V2S angle was verified as accurate.

was performed without sedation. Conventional ablation was performed in 130 (88.4%) patients using a Marin 7 Fr 4-mm deflectable tip catheter (Medtronic Inc., Minneapolis, Minnesota, USA) with an Atak II RF generator (Medtronic Inc) and the Ensite NavX electroanatomic mapping system (St. Jude Medical Inc., St Paul, Minnesota, USA). The ablation was performed in temperature control mode with a target temperature of 43°C and a power limit of 40 W in the RVOT and LVOT (for 50 s) and with a target temperature of 43°C and a power limit of 40 W in the aortic root (for 30–45 s). VA ablation was performed with the CARTO electroanatomic mapping system (Biosense Webster, Diamond Bar, California, USA) in 17 (11.6%) patients to guide the ablation. In these patients, a 3.5-mm irrigated-tip catheter (Navistar, Biosense-Webster, Diamond Bar, California, USA) was used for mapping and ablation. Target ablation sites were chosen from the combination of activation mapping and pace mapping as described previously (21). If ablation failed, another target was chosen for ablation. Mapping and ablation of the LVOT area were performed *via* a retrograde aortic approach with a 100 IU/kg heparin bolus. If necessary, more doses were administered to maintain an

activated clotting time of 250–350 s. Acute procedural ablation success was defined as no spontaneous or induced clinical PVCs occurring within 30 min after the last radiofrequency energy application.

Statistical analyses

Statistical analyses were conducted using SPSS, version 19.0 (SPSS Inc., Chicago, IL, USA). Data are expressed as mean ± SD for continuous variables and as percentages for categorical variables. The Shapiro–Wilk test was used to test normality, in which a P-value > 0.05 indicated normally distributed data. Continuous variables that showed a normal distribution were compared using Student's t-test and ANOVA, whereas the Mann–Whitney U test and Kruskal–Wallis test were used for normally distributed samples. Categorical variables are expressed as numbers (percentage) and were compared using the chi-square test, except for those with $n \leq 5$ for 1 or more expected values, which were compared using Fisher's exact test. Multiple linear regression analysis was used to calculate the partial regression coefficient β and the 95% confidence interval (CI) for ECG characteristics and the angle.

Statistical significance was defined as a P-value < 0.05 for all comparisons. Pearson's and Spearman's correlation coefficients were calculated to examine the relationships between continuous variables. ROC curve analysis was performed to determine the cut-off value of the new diagnostic metric for differentiating LVOT from RVOT origins and calculate the sensitivity, specificity, positive predictive value (PPV), and negative predictive value (NPV).

Results

First, we retrospectively enrolled 178 patients with symptomatic frequent PVC/VT who underwent successful RFCA at Nanfang Hospital of Southern Medical University and The First Affiliated Hospital of Sun Yat-sen University hospitalized from February 2017 to May 2019, except for the patients who met the exclusion criteria below. We excluded 13 patients who originated from the tricuspid annulus or mitral annulus. Patients with underlying bundle branch block ($n = 3$), paced rhythm ($n = 1$), and failed ablation ($n = 3$) were excluded. Eleven patients who underwent redo procedures were also excluded. Therefore, 147 patients were successfully enrolled (49 men (33.3%); mean age 46.9 ± 14.7 years, 126 RVOT, 21 LVOT origins), all of whom underwent *de novo* ablation. ECG and exercise stress testing or coronary angiography demonstrated no evidence of structural heart disease in any patient, and all antiarrhythmic drugs were discontinued for at least 5 half-lives before the study. The local ethics committee approved the study protocol, and each patient gave written informed consent.

Second, an analysis of the prospective cohort for evaluating the validity of the new diagnostic method was performed in 48 patients from May 2019 to January 2020 (12 men (25.0%); mean age 48.0 ± 15.8 years, 36 RVOT, 12 LVOT origins).

The baseline characteristics of patients, including age, sex, body mass index (BMI), QRS duration, PVC burden of 24 h, documented episodes of VT, prior history of ablation, LVEF, and angle, were recorded for all patients (Table 1). LVEF was assessed using Simpson's equation in the apical 4-chamber view. The procedure time referred to the time of the operation from the beginning to the end of the patient on the operating table.

TABLE 1 Baseline characteristics of patients in retrospective and prospective cohorts.

	Retrospective cohort				Prospective cohort			
	All	**RVOT**	**LVOT**	***P*-value**	**All**	**RVOT**	**LVOT**	***P*-value**
Patients, n (%)	147	126 (85.8)	21 (14.2)	NA	48	36 (75.0)	12 (25.0)	NA
Age (y)	46.9 ± 14.7	45.6 ± 14.8	54.8 ± 12.1	0.004	48.0 ± 15.8	47.8 ± 15.6	48.8 ± 17.1	0.860
Male, n (%)	49 (33.3)	43 (34.1)	6 (28.6)	0.803	12 (25.0)	6 (16.7)	6 (50.0)	0.021
BMI, n (kg/m^2)	21.8 ± 2.3	22.0 ± 2.3	21.0 ± 2.3	0.072	20.8 ± 4.0	20.6 ± 4.3	21.5 ± 2.4	0.534
LVEF, n (%)	61.4 ± 9.1	61.9 ± 9.3	58.2 ± 7.3	0.080	63.1 ± 5.1	63.0 ± 5.2	63.6 ± 5.1	0.714
PVC burden, /24-h Holter (%)	21.5 ± 9.8	21.7 ± 10.4	20.3 ± 4.9	0.556	22.3 ± 10.5	21.0 ± 8.1	26.0 ± 15.6	0.154
Angle, n (°)	37.6 ± 8.5	38.6 ± 8.5	31.7 ± 5.9	<0.001	36.5 ± 8.8	38.8 ± 8.3	29.7 ± 6.4	0.001
Clinical arrhythmia, n (%)								
Frequent PVC	99 (67.3)	85 (67.5)	14 (66.7)	0.715	37 (77.1)	28 (77.8)	9 (75.0)	0.847
Non-SVT	13 (8.9)	11 (8.7)	2 (9.5)	0.346	3 (6.3)	2 (5.6)	1 (8.3)	0.737
Sustained VT	35 (23.8)	30 (23.8)	5 (23.8)	0.859	8 (16.7)	6 (16.7)	2 (16.7)	1.000
Prior RFCA	21 (14.3)	19 (15.1)	2 (9.5)	0.929	2 (4.2)	1 (2.8)	1 (8.3)	0.415

Data are expressed as mean ± SD. BMI, body mass index; LVEF, left ventricular ejection fraction; TZ, transitional zone; RVOT, right ventricular outflow tract; LVOT, left ventricular outflow tract; PVC, premature ventricular contraction; VT, ventricular tachycardia; V1-2 SRd, V1–V2 S-R difference.

Retrospective cohort analysis and development of a new diagnostic method

The baseline characteristics of 147 patients (49 men (33.3%); mean age 46.9 ± 14.7 years, 126 RVOT, 21 LVOT origins) are compared in Table 2. All patients were successfully ablated. Among patients with LVOT VA, all of the successful ablation sites were localized in the left or right coronary sinus. Among patients with RVOT VA, all of the successful ablation sites were localized in the interventricular septum RVOT.

There were no significant differences in sex (χ^2 = 0.361, P = 0.803) or LVEF (P = 0.080) between the two groups. Patients with RVOT VA were significantly younger ($P < 0.05$) than patients with LVOT VA. The V2S was found to be significantly higher in RVOT origins than in LVOT origins ($P < 0.001$). The

TABLE 2 Baseline patient characteristics and electrocardiographic characteristics of the retrospective cohort (n = 147).

	RVOT (n = 126)	LVOT (n = 21)	P-value	AUC	Cut-off	95% confidence interval		P-value
Age (years)	46 ± 15	55 ± 12	0.004					
Sex (Male, %)	43 (34.1)	6 (28.6)	0.803					
BMI (kg/m^2)	22.0 ± 2.3	21.0 ± 2.3	0.072					
LVEF (%)	61.9 ± 9.3	58.2 ± 7.3	0.080					
QRS duration (ms)	157.6 ± 20.6	150.8 ± 13.6	0.057					
PVC burden (%/24-h Holter)	21.7 ± 10.4	20.3 ± 4.9	0.556					
Patients had documented episodes of VT (n)	0.32 ± 0.79	0.29 ± 0.56	0.859					
Prior ablation history (n)	0.15 ± 0.36	0.14 ± 0.48	0.929					
ECG and angle related indicators								
V1S (mv)	1.26 ± 0.49	0.69 ± 0.32	<0.001	0.821	0.78	0.755	0.888	<0.001
V2S (mv)	1.82 ± 0.79	1.04 ± 0.59	<0.001	0.776	1.28	0.675	0.877	<0.001
V3S (mv)	0.93 ± 0.75	0.52 ± 0.56	0.018	0.693	0.63	0.571	0.816	0.005
V1R (mv)	0.26 ± 0.20	0.36 ± 0.22	0.030	0.362	0.85	0.239	0.485	<0.001
V2R (mv)	0.40 ± 0.33	0.91 ± 0.53	<0.001	0.183	2.30	0.085	0.280	<0.001
V3R (mv)	0.62 ± 0.43	1.46 ± 0.74	<0.001	0.143	4.30	0.059	0.228	<0.001
angle (°)	38.6 ± 8.5	31.7 ± 5.9	<0.001	0.750	31.5	0.638	0.862	<0.001
V1S angle (mV°)	44.95 ± 25.34	21.65 ± 9.78	<0.001	0.824	31.77	0.757	0.890	<0.001
V2S angle (mV°)	68.64 ± 29.85	31.80 ± 17.08	<0.001	0.888	58.28	0.831	0.945	<0.001
V3S angle (mV°)	35.18 ± 27.91	15.87 ± 16.73	<0.001	0.736	18.14	0.624	0.847	0.001
V1R angle (mV°)	9.82 ± 8.42	11.87 ± 8.58	0.306	0.425	9.15	0.297	0.554	0.274
V2R angle (mV°)	14.76 ± 10.96	29.95 ± 21.06	<0.001	0.247	91.20	0.128	0.365	0.061
V3R angle (mV°)	22.89 ± 14.47	48.08 ± 30.05	<0.001	0.205	136.30	0.098	0.313	<0.001
Several ECG algorithms								
V2S/V3R	4.81 ± 6.74	1.08 ± 1.05	0.013	0.887	1.40	0.812	0.961	<0.001
TZ index	0.43 ± 0.89	−0.79 ± 0.96	<0.001	0.858	−0.25	0.757	0.958	<0.001
Combined TZ index and V2S/V3R	−2.87 ± 3.55	0.37 ± 1.45	<0.001	0.088	−13.68	0.007	0.169	<0.001
V1-2 SRd (mv)	2.42 ± 1.08	0.46 ± 1.29	<0.001	0.876	0.73	0.795	0.957	<0.001
V3 transition	0.97 ± 0.18	0.67 ± 0.48	<0.001	0.651	0.50	0.505	0.796	0.027
R wave amplitude in lead I	28.87 ± 23.46	31.42 ± 22.73	0.644	0.457	2.67	0.315	0.598	0.524
ISA	22.35 ± 34.66	57.49 ± 40.28	<0.001	0.186	250	0.091	0.281	<0.001
ISA V1	2.11 ± 2.52	0.78 ± 1.16	0.019	0.723	0.36	0.605	0.841	0.001
ISA V2	0.36 ± 2.02	3.53 ± 9.28	0.001	0.151	42	0.045	0.257	<0.001
V1R/V1S index	0.39 ± 1.40	3.85 ± 11.40	0.001	0.313	−1.00	0.193	0.433	0.006

Data are expressed as mean ± SD. BMI, body mass index; LVEF, left ventricular ejection fraction; TZ, transitional zone; RVOT, right ventricular outflow tract; LVOT, left ventricular outflow tract; PVC, premature ventricular contraction; VT, ventricular tachycardia; V1-2 SRd, V1–V2 S-R difference.

angle ($P < 0.001$) and the V2S angle ($P < 0.001$) were found to be significantly greater in RVOT origins than in LVOT origins. There was no significant difference in BMI, QRS duration, PVC burden at 24 h, documented episodes of VT, or prior history of ablation between the two groups (all $P > 0.05$) (**Table 2**).

Linear regression analysis for ECG characteristics and angle

This study explored the effects of V1S, V2S, V3S, V1R, V2R, V3R, and angle on the ECG algorithm that we used to differentiate RVOT from LVOT origins by applying multiple linear regression analysis. The final multiple linear regression model constructed was statistically significant ($F = 14.278$, $P < 0.001$), and 38.9% of the variation in the dependent variable ECG algorithm could be explained by V1S, V2S, V3R, and angle (adjusted $R^2 = 0.389$). The regression coefficient β and 95% CI of each independent variable are shown in **Figure 2A**. ROC curve analysis for anatomic prediction of an RVOT origin was also studied. The area under the curve (AUC) of the V2S angle was 0.888, which was the highest among all studied indicators (**Figure 2B**).

Receiver operating characteristic curve analysis to determine the predictive value of the V2S angle for differentiating left ventricular outflow tract from right ventricular outflow tract

By analyzing the predictive accuracy of R- and S-wave amplitudes in leads V1 to V3 during PVC/VT multiplied by the angle in 147 patients, we found that the V2S angle was the best index. The AUC of the V2S angle was 0.888 ($P < 0.001$). In addition, the AUC of the V2S angle was greater than that of the TZ index (AUC = 0.887), V2S/V3R (AUC = 0.858), and V1-2 SRd (AUC = 0.876) (**Figure 3**).

The cut-off value of the V2S angle obtained by ROC curve analysis was 58.28 mV° for the prediction of RVOT origin (sensitivity: 85.7%; specificity: 95.2%; PPV: 99.1%; NPV: 52.6%) (**Table 3**), and the 95% confidence interval of the AUC was 0.831–0.945 (**Table 2**). A scatterplot diagram of the V2S angle against RVOT and LVOT origins is shown in **Figure 4A**.

Retrospective cohort analysis of several angle-corrected ECG algorithms

In the retrospective cohort ($n = 147$), several ECG algorithms from previous studies were corrected for the angle. Surprisingly, the AUCs of the angle-corrected ECG algorithms for differentiating LVOT from RVOT were all higher than those before correction (V2S/V3R angle vs. V2S/V3R = 0.916 vs. 0.887; the TZ index angle vs. the TZ index = 0.865 vs. 0.858; V1-2 SRd angle vs. V1-2 SRd = 0.912 vs. 0.876, etc.) (**Table 4**). The AUC of the V2S/V3R angle (AUC = 0.916) was the best, even greater than that of the V2S angle (AUC = 0.888) (**Figure 5**).

Prospective cohort analysis and validation of the new diagnostic method

A total of 48 consecutive patients with PVC/VT (12 men (25.0%); mean age 48.0 ± 15.8 years, 36 RVOT, 12 LVOT origins) with LBBB who underwent successful RFCA at Nanfang Hospital of Southern Medical University constituted the prospective cohort to test the validity of the new diagnostic method.

As in the retrospective cohort, there were no significant differences in baseline clinical characteristics between the 2 groups of PVC/VT origin ($P > 0.05$) in the prospective cohort, except there were more men in the LVOT group ($n = 6$, 50.0%) than in the RVOT group ($n = 6$, 16.7%) ($\chi^2 = 5.333$, $P = 0.021$). The detailed clinical characteristics of the prospective cohort are described in **Table 5**. Compared with LVOT origins, the V2S was found to be significantly higher ($P = 0.019$), the angle was significantly greater ($P = 0.001$), and the V2S angle was significantly greater in RVOT origins ($P = 0.001$).

In the prospective cohort, the sensitivity, specificity, PPV, and NPV of the V2S angle for predicting the RVOT origin over the LVOT origin were 97.2%, 83.3%, 94.6%, and 90.9%, respectively. The new diagnostic method had a high overall accuracy of 93.8% (**Figure 6**).

The differences in duration of the ablation procedure in the retrospective vs. prospective cohort

Overall, the procedure time in the prospective cohort ($n = 48$) (78.8 ± 31.8 min) was significantly shorter than that in the retrospective cohort ($n = 147$) (99.5 ± 40.8 min) due to the analysis of the V2S angle before RFCA ($P = 0.002$) (**Figure 7A**).

Specifically, for predicting RVOT origin, the procedure time in the prospective cohort in which the V2S angle was used ($n = 36$) (80.0 ± 32.0 min) was significantly shorter than that in the retrospective cohort in which the V2S/V3R or the TZ index was used before RFCA ($n = 128$) (102.6 ± 42.6 min) ($P = 0.004$). For predicting LVOT origin, the procedure time in the prospective cohort in which the V2S angle was used ($n = 12$) (75.2 ± 32.3 min) was shorter than that in the retrospective cohort in which the V2S/V3R or the TZ index was

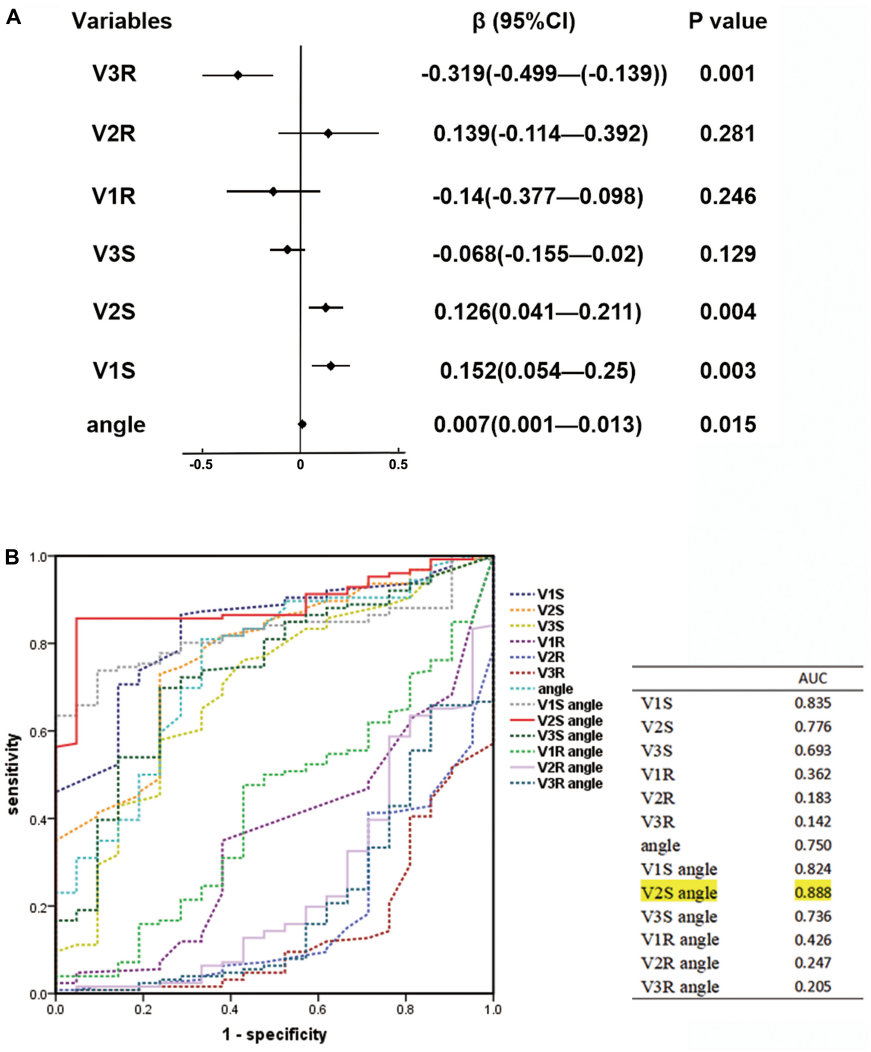

FIGURE 2
(A) Linear regression analysis for ECG characteristics and angle. The regression coefficient β and 95% CI of each independent variable are shown above. The final multiple linear regression model was statistically significant ($F = 14.278$, $P < 0.001$), and 38.9% of the variation in the dependent variable ECG algorithm could be explained by V1S, V2S, V3R, and angle (adjusted $R^2 = 0.389$). **(B)** Receiver operating characteristic (ROC) curve analysis for anatomic prediction of RVOT origin was also performed. The area under the curve (AUC) of the V2S angle was 0.888, which was the highest among all indicators.

used ($n = 19$) (78.7 ± 13.3 min), but the difference was not significant ($P = 0.675$) (**Figure 7B**).

Discussion

Main findings

In the current study, we developed a novel ECG criterion, the angle-corrected V2S, with an AUC of 0.88, making it the first ECG criterion proven to be predictive of LVOT and RVOT origins of VA. However, the V2S angle is only used to identify the origin of the interventricular septum and the coronary sinuses. The main finding of the present study is that a V2S angle ≥ 58.28 mV° predicted an RVOT origin with a sensitivity of 85.7% and specificity of 95.2% in the overall analysis (PPV: 99.1%, NPV: 52.6%). This means that the specific cut-off for differentiating LVOT from RVOT arrhythmias was confirmed in the prospective cohort. Compared with previous methods, such as 12-lead ECG and VCG, it is more accurate and time-saving and may be an ideal strategy for identifying OTVA. In addition, as reported previously, the V2S was found to be significantly higher in RVOT origins than LVOT origins in the present study ($P < 0.001$). The anatomical cardiac long-axis was found to be significantly greater in RVOT origins than LVOT origins ($P < 0.001$), which means that VA originating from the RVOT

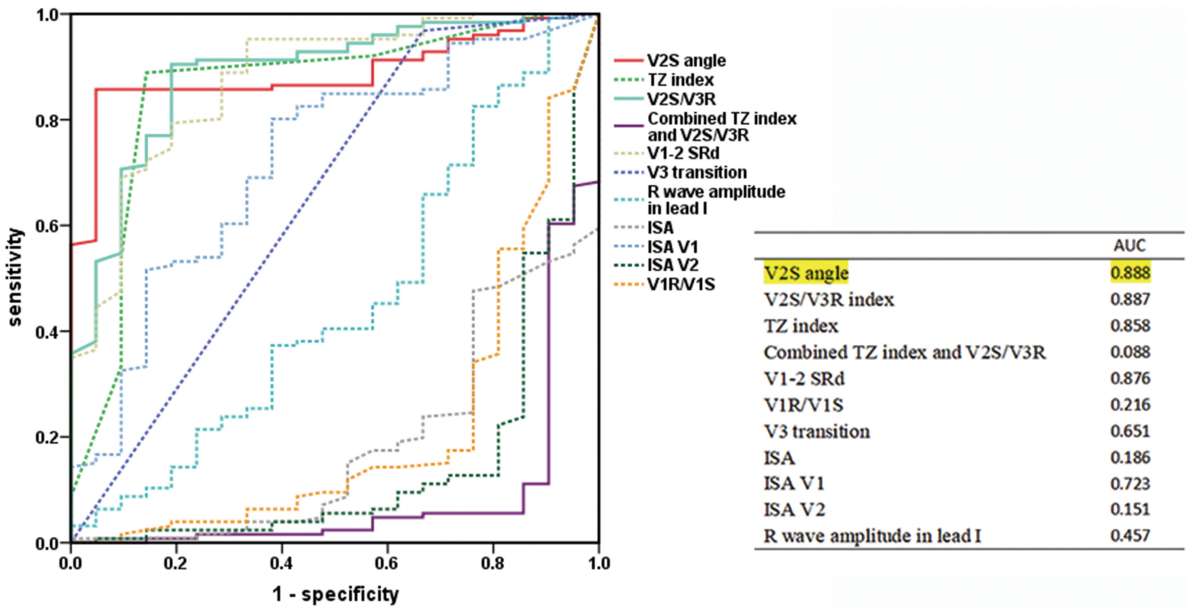

	AUC
V2S angle	0.888
V2S/V3R index	0.887
TZ index	0.858
Combined TZ index and V2S/V3R	0.088
V1-2 SRd	0.876
V1R/V1S	0.216
V3 transition	0.651
ISA	0.186
ISA V1	0.723
ISA V2	0.151
R wave amplitude in lead I	0.457

FIGURE 3
Predictive accuracy of the V2S angle and several ECG algorithms of previous studies. ROC curve analysis for anatomic prediction of RVOT origin. The AUC of the V2S angle was 0.888, which was the highest of all.

TABLE 3 Diagnostic indexes of ECG criteria for predicting RVOT origin.

	Sensitivity	Specificity	PPV	NPV
V2S angle ≥ 58.28 mV°	85.7%	95.2%	99.1%	52.6%
V2S/V3R > 1.5	89.7%	81.0%	96.6%	56.7%
TZ index ≥ 0	88.9%	81.0%	96.6%	54.8%
combined TZ index and V2S/V3R < −0.76	86.5%	23.8%	87.2%	22.7%
V1-2 SRd > 1.625	81.7%	28.6%	87.3%	20.7%
R wave amplitude in lead I ≥ 2.67 mV	99.2%	9.5%	52.3%	92.2%
ISA ≥ 250	0.8%	100.0%	100%	50.2%
ISA V1 ≥ 0.36	80.2%	61.9%	67.8%	75.8%
ISA V2 ≥ 42	0	100.0%	0	50.0%
V1R/V1S ≤ 0.3	82.5%	23.8%	86.7%	18.5%

PPV, positive predictive value; NPV, negative predictive value; BMI, body mass index; LVEF, left ventricular ejection fraction; TZ, transitional zone; RVOT, right ventricular outflow tract; LVOT, left ventricular outflow tract; PVC, premature ventricular contraction; VT, ventricular tachycardia; V1-2 SRd, V1–V2 S-R difference.

may be more likely to occur in taller, thinner people with a smaller angle on chest radiography.

Anatomical considerations and the V2S angle

The information provided by any particular form of electrocardiography obviously depends on the electrode configuration (number and positions of the electrodes utilized to sample the body surface potential distribution in space and time) (11). Anatomically, the aortic root occupies a central location within the heart, and the RVOT is located anteriorly and left of the aortic root (22). In patients whose hearts are normally positioned, the RVOT is located anterior to the LVOT at the level of the aortic cusps. The pulmonary valves are positioned approximately 1–2 cm superior to the aortic valves (23). Nikoo et al. (19) showed that the ISA index, defined as the highest value calculated in the V1 or V2 lead by multiplying the R wave duration in milliseconds by the R wave amplitude in terms of mV, is highly accurate and the most specific compared with other previously reported indexes in differentiating left from right outflow tract-originated VT/PVC. Regarding this anatomical background, V1 and V2 are the closest chest leads to the LVOT and RVOT, which are the best derivations to distinguish OTVAs. The closer

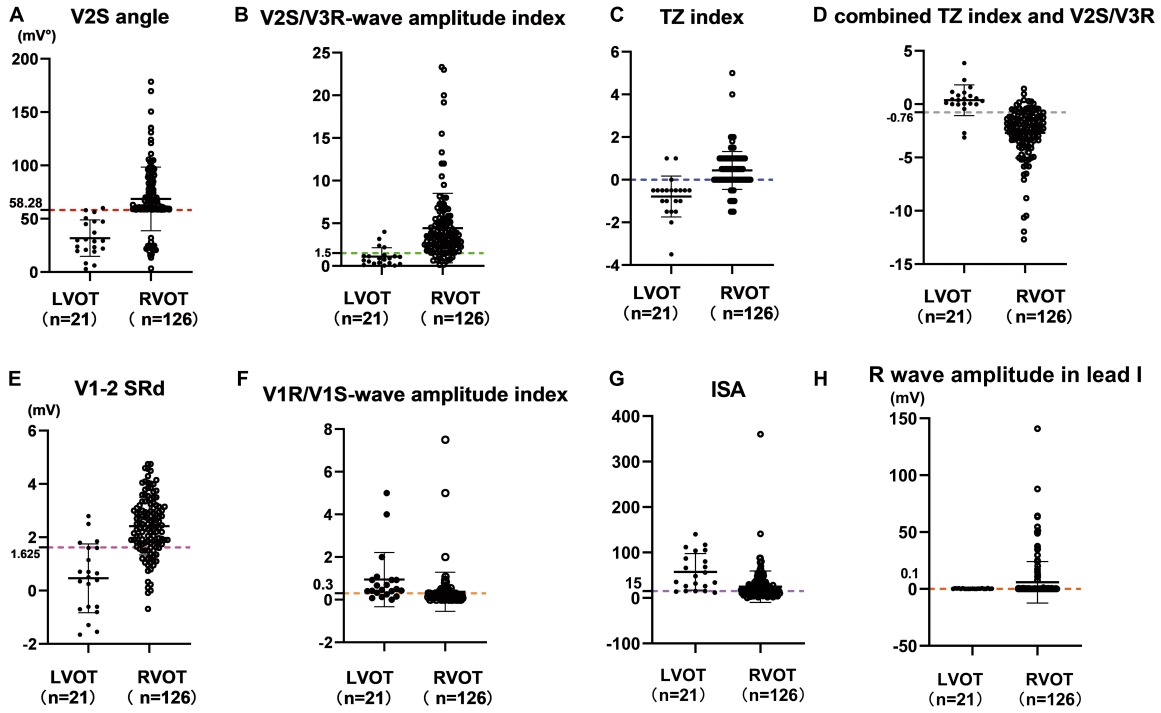

FIGURE 4
Scatterplot diagram of the V2S angle **(A)** and several ECG algorithms **(B–H)** between ventricular arrhythmias from RVOT and LVOT. The red dotted line indicates the optimal cut-off value of the V2S angle. The V2S angle of 58.28 mV° predicted the RVOT origin with 85.7% sensitivity and 95.2% specificity (PPV: 99.1%; NPV: 52.6%). Other diagnostic indexes for predicting RVOT origin (sensitivity, specificity, PPV, NPV) are shown in Table 3.

TABLE 4 The angle-corrected ECG algorithms applied to the retrospective cohort (n = 147).

	RVOT (n = 126)	LVOT (n = 21)	P-value	AUC	Cut-off	95% confidence interval		P-value
V2S/V3R angle (°)	186.18 ± 255.09	32.36 ± 2.73	<0.001	0.916	48.36	0.860	0.971	<0.001
TZ index angle (°)	17.30 ± 32.51	−27.93 ± 38.35	<0.001	0.865	−5.68	0.778	0.953	<0.001
Combined TZ index and V2S/V3R angle (°)	−111.87 ± 135.81	16.13 ± 52.10	<0.001	0.070	−508.28	0.009	0.132	<0.001
V1-2 SRd angle (mv°)	92.65 ± 43.86	11.62 ± 41.47	<0.001	0.912	52.71	0.853	0.971	<0.001
R wave amplitude in lead I angle (mv°)	0.13 ± 0.17	0.36 ± 0.30	<0.001	0.223	0.98	0.106	0.340	<0.001
ISA angle	9.33 ± 8.34	0.64 ± 2.92	<0.001	0.882	1.31	0.805	0.956	<0.001
V1R/V1S angle (°)	13.90 ± 46.48	119.80 ± 353.95	0.001	0.475	1565.00	0.338	0.612	0.717

Data are expressed as mean ± SD. BMI, body mass index; LVEF, left ventricular ejection fraction; TZ, transitional zone; RVOT, right ventricular outflow tract; LVOT, left ventricular outflow tract; PVC, premature ventricular contraction; VT, ventricular tachycardia; V1-2 SRd, V1–V2 S-R difference.

a focus of an impulse is to a lead, the greater the degree of S-wave amplitude in that lead. (17) This contiguity can be thought to result in higher R-wave amplitude and lower S-wave amplitude in the frontal leads V1 and V2 during OTVAs originating from the LVOT than those originating from the RVOT (24, 25). Therefore, it would be reasonable to develop an ECG algorithm using the S-wave amplitude in lead V1 or V2.

However, the location of the heart within the thorax varies significantly between individuals, which means that leads V1 and V2 are affected by different physiques. Analyzing previous research, such as on V2S/V3R and the TZ index, we speculate that the V2S amplitude is more meaningful than the V1S amplitude, taking into account the long cardiac axis. Compared with lead V1, lead V2 is the least influenced by the physique. Therefore, the V2S would be the best chest lead

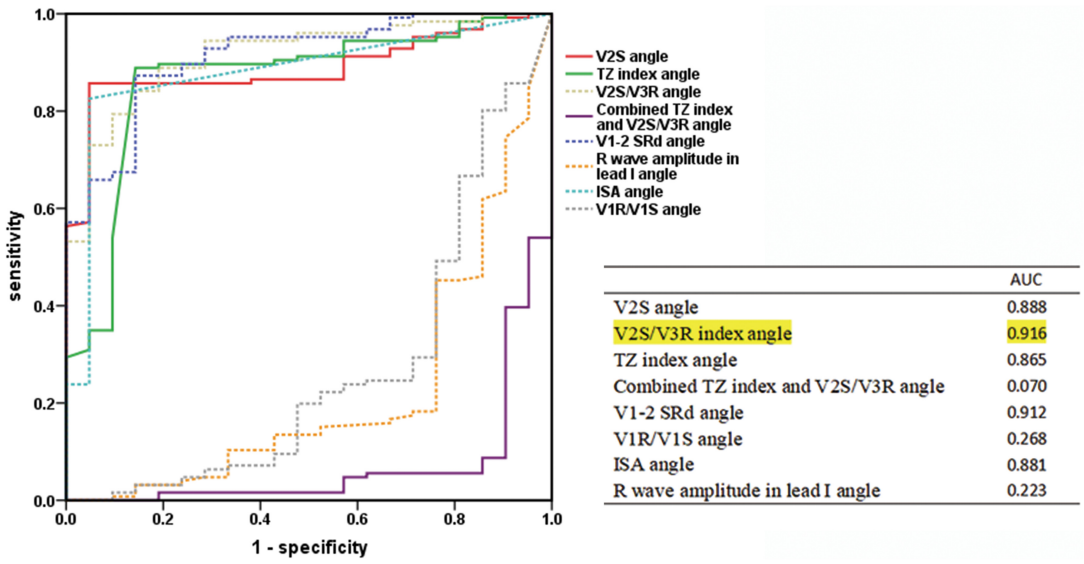

	AUC
V2S angle	0.888
V2S/V3R index angle	0.916
TZ index angle	0.865
Combined TZ index and V2S/V3R angle	0.070
V1-2 SRd angle	0.912
V1R/V1S angle	0.268
ISA angle	0.881
R wave amplitude in lead I angle	0.223

FIGURE 5
Receiver operating characteristic curve analysis of the V2S angle and the angle-corrected ECG algorithms. The predictive accuracy of several ECG algorithms was improved by correcting with the angle. The AUC of the V2S/V3R index angle (AUC = 0.916) was the highest of all, even greater than that of the V2S angle (AUC = 0.888).

to differentiate LVOT and RVOT in both taller, thinner and shorter, heavier people. Additionally, chest radiography can reflect anatomical characteristics and cardiac transposition and can be used to correct the recording differences caused by anatomical variations to a certain extent (13). Thus, through ECG and chest X-ray, the anatomical position of the heart can be located better and more accurately, and the deviation can be reduced as much as possible. The anatomical position of the heart can be reflected by locating the anatomical cardiac long-axis. To some extent, the use of the anatomical cardiac long-axis can correct for some factors, like the patient's physique, cardiac rotation, and respiratory variation. The anatomical cardiac long-axis can be reflected by measuring the angle between the cardiac long-axis anatomically and the horizontal plane on chest radiography. In brief, the long-axis angle can partly reflect the anatomical rotation and the position of the heart with its projection in the three spatial planes, thus giving rise to the vectorcardiographic loops in the respective planes (26). For example, the heart is overhanging in taller, thinner patients, so the angle on their chest X-ray is greater. If the heart is rotated clockwise, both the angle and the V2S amplitude will decrease. Accordingly, the V2S angle would be the best index among all indexes anatomically.

TABLE 5 Patient characteristics and electrocardiographic characteristics in the prospective cohort (n = 48).

	RVOT (n = 36)	LVOT (n = 12)	P-value
Age (years)	48 ± 16	49 ± 17	0.860
Sex (Male, %)	6 (16.7)	6 (50.0)	0.021
BMI (kg/m^2)	20.6 ± 4.3	21.5 ± 2.4	0.534
LVEF (%)	63.0 ± 5.2	63.6 ± 5.1	0.714
V2S (mv)	2.21 ± 0.76	1.53 ± 1.06	0.019
QRS duration (ms)	153.1 ± 24.5	150.8 ± 24.3	0.786
PVC burden before RF (%/24-h Holter)	21.0 ± 8.1	26.0 ± 15.6	0.154
PVC burden after RF (%/24-h Holter)	0.2 ± 1.1	0.4 ± 1.2	0. 649
Patient had any documented episode of VT (n)	0.25 ± 0.65	0.25 ± 0.62	1.000
Prior ablation history (n)	0.03 ± 0.17	0.08 ± 0.29	0.415
angle (°)	38.8 ± 8.3	29.7 ± 6.4	0.001
V2S angle (mV°)	84.49 ± 36.38	43.26 ± 33.55	0.001
V2S/V3R	3.46 ± 3.71	1.20 ± 1.69	0.048
TZ index	0.53 ± 0.99	−0.63 ± 0.53	<0.001

Data are expressed as mean ± SD. BMI, body mass index; LVEF, left ventricular ejection fraction; TZ, transitional zone; RVOT, right ventricular outflow tract; LVOT, left ventricular outflow tract; PVC, premature ventricular contraction; VT, ventricular tachycardia; V1-2 SRd, V1–V2 S-R difference.

Comparison with the previous indexes

Outflow tract ventricular arrhythmias mostly originate from the RVOT (27). Many studies have aimed to localize OTVAs. A combined model using the TZ index and V2S/V3R would be more accurate, but its clinical utility may be limited (28). We compared our criteria to previous indexes in our population. The cut-off value of the V2S/V3R index obtained by ROC curve

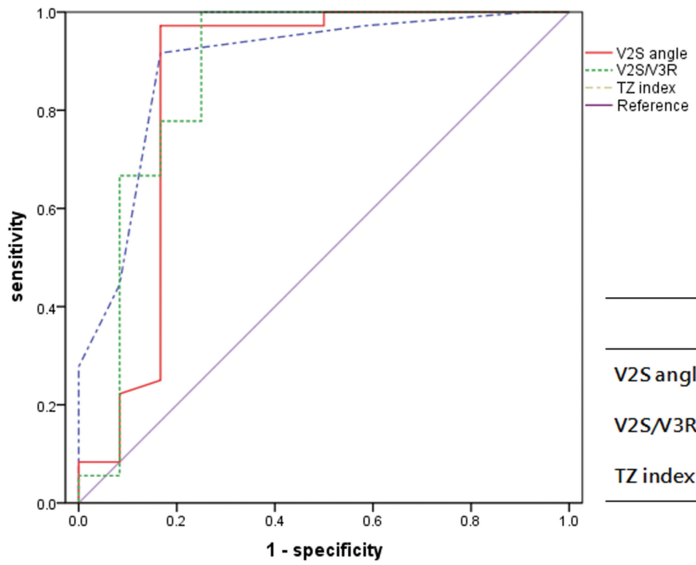

	AUC	95% confidence interval
V2S angle	0.851	0.672 – 1.000
V2S/V3R	0.875	0.720 – 1.000
TZ index	0.892	0.776 – 1.000

FIGURE 6
Receiver operating characteristic curve analysis for the anatomic prediction of OTVA origin with V2S angle and previous indexes in the prospective cohort. The AUC of V2S angle was 0.851, similar to that of V2S/V3R (0.875) and the TZ index (0.892).

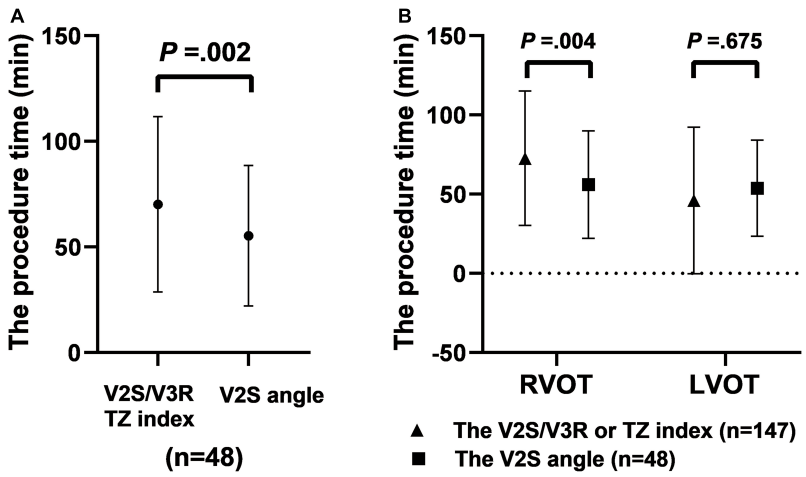

FIGURE 7
The procedure time when using different diagnostic indexes made up of ECG criteria for predicting RVOT origin. The procedure time with the V2S angle was shorter than with V2S/V3R or the TZ index before RFCA in the prospective cohort (n = 48) (P = 0.002) **(A)**. The procedure time in the prospective cohort (n = 48) with the V2S angle was shorter than that in the retrospective cohort (n = 147) with V2S/V3R or the TZ index **(B)**.

analysis was 1.40 for the prediction of RVOT origin (sensitivity: 89.7%, specificity: 81.0%, PPV: 96.6%, NPV: 56.7%), and its AUC was 0.887 ($P < 0.001$). The cut-off value of the TZ index obtained by ROC curve analysis was −0.25 for the prediction of RVOT origin (sensitivity: 88.9%, specificity: 81.0%, PPV: 96.6%, NPV: 54.8%), and its AUC was 0.858 ($P < 0.001$). There was no significant bias in the patient population of this study compared with those reported previously. The AUC of the V1-2 SRd was 0.876 ($P < 0.001$). The AUC of the V3 transition was 0.651 ($P < 0.001$). The combined TZ index and V2S/V3R (AUC = 0.088), the IAS (AUC = 0.186), and the V1R/V1S index (AUC = 0.313) were used for the prediction of LVOT origin. The cut-off value of the V2S angle obtained by ROC curve analysis was 58.28 mV° for the prediction of RVOT origin (sensitivity: 85.7%, specificity: 95.2%, PPV: 99.1%, NPV: 52.6%), and its AUC was 0.888 ($P < 0.001$) (Tables 2, 3). Scatterplot diagrams of several ECG algorithms between ventricular arrhythmias from RVOT and LVOT are shown in Figures 4B–H.

Therefore, our novel and simple ECG criterion, the V2S angle, seems to have a good AUC in the overall analysis. Since

the number of LVOT cases was relatively small, the NPVs of most of the methods were low. It should be noted that the specificity and sensitivity parameters will not practically help physicians find the arrhythmia site. Predictive value is of special importance in clinics (19). The V2S angle showed a non-significantly higher positive predictive value for RVOT-origin arrhythmias than V2S/V3R or the TZ index (99.1% vs. 96.6% vs. 96.6%). Overall, V2S angle, V2S/V3R, and the TZ index have similar accuracies and can be used interchangeably.

The V2S angle is a quantitative measure of the proximity of the focus of the impulse to lead V2. In our study, the V2S angle was significantly higher in VAs originating from the RVOT. With a cut-off value of 58.28 mV°, the V2S angle predicted an RVOT origin with 85.7% sensitivity and 95.2% specificity (PPV: 99.1%; NPV: 52.6%). We thought that some factors, such as the patient's physique, cardiac rotation, and respiratory variation, could be corrected by multiplying them by the anatomical cardiac long-axis. It is difficult to distinguish RVOT-originated VAs from LVOT-originated VAs with 100% precision. The QRS morphology of OTVAs can be affected by several factors, such as lead position, aortic deformities, obesity, the effect of medications, the effect on breasts in women, ventricular hypertrophy, chest wall deformities, and preferential conduction (16, 29, 30).

Comparison with several angle-corrected ECG algorithms

Several ECG algorithms of previous studies were corrected by multiplying them by the angle in the retrospective cohort (n = 147). Surprisingly, the AUCs of the angle-corrected ECG algorithms for differentiating LVOT from RVOT were all higher than those before correction: The AUC of the V2S/V3R angle was higher than that of V2S/V3R (0.916 vs. 0.887). The AUC of the TZ index angle was higher than that of the TZ index (0.865 vs. 0.858). The AUC of the V1-2 SRd angle was higher than that of the V1-2 SRd (0.912 vs. 0.876). The AUC of the V1R/V1S index angle was higher than that of the V1R/V1S index (0.268 vs. 0.216). However, the AUC of the combination of the TZ index and V2S/V3R angle was lower than that of the combination of the TZ index and V2S/V3R (0.070 vs. 0.088) (**Table 4**). The AUC of the V2S/V3R index angle (AUC = 0.916) was the best index of all, even greater than that of the V2S angle (AUC = 0.888) (**Figure 5**). However, the V2S angle is simpler and more convenient than the V2S/V3R index angle.

Therefore, most of the previous ECG algorithms, corrected by the anatomical cardiac long-axis angle, can improve accuracy for differentiating LVOT- from RVOT-origin VA. This is an interesting and very meaningful discovery. Other angle-corrected ECG algorithms need to be further validated, such as the V3R/V7 index (31), the V4/V8 ratio (32), and the V1-V3 transition index (33).

Clinical implications

Accurately predicting the origin of OTVT (the RVOT or LVOT) can optimize catheter ablation strategies, reduce ablation time, and reduce surgical complications. Therefore, the ability to more accurately predict an RVOT or LVOT origin of OTVA can have a significant impact on the ablation procedure.

In our study, under the condition of the same operator team and mapping system, the procedure time in the prospective cohort was shorter than that in the retrospective cohort due to the use of the V2S angle before RFCA (78.8 ± 31.8 min vs. 99.5 ± 40.8 min, P = 0.002). In particular, for predicting RVOT origin, the procedure time in the prospective cohort in which the V2S angle was used was significantly shorter than that in the retrospective cohort in which the V2S/V3R or the TZ index was used before RFCA (P = 0.004). However, there was no significant difference in the procedure time between the retrospective and prospective cohorts for predicting LVOT origin (P = 0.675) (**Figure 7**). This may be the reason for the small number of cases of LVOT origin. Therefore, future studies with larger sample sizes are needed.

It is well known that shortening the procedure time may improve RFCA efficiency and patient experience. However, it is worth noting that the procedure time may be affected by many factors, such as the operator's surgical style, mapping system and coordination of the surgical team, and even the degree of patient cooperation. Therefore, the V2S angle can provide a rapid and accurate diagnosis of the OTVA origin before catheter ablation, allowing us to develop a better procedural strategy (decreasing ablation duration and radiation exposure) and avoid any unnecessary arterial or venous punctures. Of course, further study of other novel methods for accurately differentiating RVOT from LVOT as the site of origin of VA is required for reducing the rates of recurrence and unnecessary ablation applications. VCG when used as an alternative form of ECG provides important spatial information about the electrical activity of the heart, which achieves higher sensitivity in the detection of some pathologies, such as myocardial infarction, ischemia, and hypertrophy. It may be interesting to combine the analysis of the V2S angle with other methodologies based on the VCG method, the inverse ECG method, or machine learning methods, and this approach holds promise in providing electro-anatomic identification of the site of origin of focal premature depolarization.

Study limitations

There were some limitations to this study. As a double-center study, the sample size was relatively small, and our results need to be confirmed in large, multi-center, prospective trials. Moreover, the algorithm used to identify the origin of the interventricular septum and the coronary sinuses cannot cover

the whole RVOT (including the free wall) or LVOT (including the subaortic valve). Further studies with a larger patient population are needed to verify its range of application. Because of the retrospective nature of our study, we did not have the chance to investigate the confounding factors that affect the QRS morphology of OTVAs, such as lead position, aortic deformities, obesity, the effect of breasts in women, ventricular hypertrophy, chest wall deformities, and preferential conduction. Finally, outside of chest X-ray, we may be able to correct the position of the heart *via* cardiac color Doppler ultrasound, cardiac magnetic resonance, and other examinations and take advantage of machine learning technology (34) to attain clinical-grade precision in the prediction of the LVOT or RVOT as the origin of VT with fewer applicability restrictions.

Conclusion

The V2S angle is a novel and simple ECG criterion for accurately differentiating RVOT- from LVOT-origin VA. The use of this simple ECG measurement could raise the accuracy of OTVA localization, and it could help decrease ablation duration and radiation exposure. This new method will hopefully improve mapping and ablation procedures.

Data availability statement

The raw data supporting the conclusions of this article will be made available by the authors, without undue reservation.

Ethics statement

The studies involving human participants were reviewed and approved by the Human Research Ethics Committee of Nanfang Hospital of Southern Medical University and the First Affiliated Hospital of Sun Yat-sen University. The patients/participants provided their written informed consent to participate in this study.

Author contributions

SQ, ZS, XL, JL, XH, and YW contributed to the conception and design of the study. SQ, ZS, ML, LW, and YW organized the database. SQ, ZS, XL, JL, XH, JB, YL, and YX searched for and collected the relevant literature. SQ, ZS, XL, JL, XH, JX, and DZ performed the statistical analysis. SQ and ZS wrote the first draft of the manuscript. XL, JB, YL, JX, DZ, YX, LW, and YW revised and finalized the manuscript. All authors contributed to the manuscript revision, read, and approved the submitted version.

Funding

This study was supported by grants from the National Key R&D Program of China (2018YFC1312803), the National Natural Science Foundation of China (81974266), and the Foundation of the President of Nanfang Hospital (Grants 2019Z002 and 2015A002).

Conflict of interest

The authors declare that the research was conducted in the absence of any commercial or financial relationships that could be construed as a potential conflict of interest.

Publisher's note

References

1. Saba MM, Li A. Mapping and ablation of ventricular outflow tract arrhythmias. *Card Electrophysiol Clin.* (2019) 11:597–607.

2. Chung FP, Chong E, Lin YJ, Chang SL, Lo LW, Hu YF, et al. Different characteristics and electrophysiological properties between early and late recurrences after acute successful catheter ablation of idiopathic right ventricular outflow tract arrhythmias during long-term follow-up. *Heart Rhythm.* (2014) 11:1760–9. doi: 10.1016/j.hrthm.2014.06.011

3. Cronin EM, Bogun FM, Maury P, Peichl P, Chen M, Namboodiri N, et al. 2019 HRS/EHRA/APHRS/LAHRS expert consensus statement on catheter ablation of ventricular arrhythmias. *Heart Rhythm.* (2020) 17:e2–154.

4. Liu Z, Jia YH, Ren L, Fang PH, Zhou GB, He J, et al. Multiple intercostal space electrocardiogram allows accurate localization of outflow tract ventricular arrhythmia origin. *Pacing Clin Electrophysiol.* (2016) 39:173–81. doi: 10.1111/pace.12781

5. Yamada T. Twelve-lead electrocardiographic localization of idiopathic premature ventricular contraction origins. *J Cardiovasc Electrophysiol.* (2019) 30:2603–17. doi: 10.1111/jce.14152

6. Enriquez A, Baranchuk A, Briceno D, Saenz L, Garcia F. How to use the 12-lead ECG to predict the site of origin of idiopathic ventricular arrhythmias. *Heart Rhythm.* (2019) 16:1538–44.

7. Efimova E, Dinov B, Acou WJ, Schirripa V, Kornej J, Kosiuk J, et al. Differentiating the origin of outflow tract ventricular arrhythmia using a simple, novel approach. *Heart Rhythm.* (2015) 12:1534–40.

8. He Z, Liu M, Yu M, Lu N, Li J, Xu T, et al. An electrocardiographic diagnostic model for differentiating left from right ventricular outflow tract tachycardia origin. *J Cardiovasc Electrophysiol.* (2018) 29:908–15.

9. Xie S, Kubala M, Liang JJ, Hayashi T, Park J, Padros IL, et al. Lead I R-wave amplitude to differentiate idiopathic ventricular arrhythmias with left bundle branch block right inferior axis originating from the left versus right ventricular outflow tract. *J Cardiovasc Electrophysiol.* (2018) 29:1515–22. doi: 10.1111/jce.13747

10. Yoshida N, Yamada T, Mcelderry HT, Inden Y, Shimano M, Murohara T, et al. A novel electrocardiographic criterion for differentiating a left from right ventricular outflow tract tachycardia origin: the V2S/V3R index. *J Cardiovasc Electrophysiol.* (2014) 25:747–53. doi: 10.1111/jce.12392

11. Man S, Maan AC, Schalij MJ, Swenne CA. Vectorcardiographic diagnostic & prognostic information derived from the 12-lead electrocardiogram: historical review and clinical perspective. *J Electrocardiol.* (2015) 48:463–75.

12. Sedaghat G, Ghafoori E, Waks JW, Kabir MM, Shvilkin A, Josephson ME, et al. Quantitative assessment of vectorcardiographic loop morphology. *J Electrocardiol.* (2016) 49:154–63.

13. Mori S, Anderson RH, Tahara N, Izawa Y, Toba T, Fujiwara S, et al. Diversity and determinants of the three-dimensional anatomical axis of the heart as revealed using multidetector-row computed tomography. *Anat Rec (Hoboken).* (2017) 300:1083–92. doi: 10.1002/ar.23564

14. Zaky A, Grabhorn L, Feigenbaum H. Movement of the mitral ring: a study in ultrasoundcardiography. *Cardiovasc Res.* (1967) 1:121–31. doi: 10.1093/cvr/1.2.121

15. Zhang F, Chen M, Yang B, Ju W, Chen H, Yu J, et al. Electrocardiographic algorithm to identify the optimal target ablation site for idiopathic right ventricular outflow tract ventricular premature contraction. *Europace.* (2009) 11:1214–20. doi: 10.1093/europace/eup231

16. Yoshida N, Inden Y, Uchikawa T, Kamiya H, Kitamura K, Shimano M, et al. Novel transitional zone index allows more accurate differentiation between idiopathic right ventricular outflow tract and aortic sinus cusp ventricular arrhythmias. *Heart Rhythm.* (2011) 8:349–56. doi: 10.1016/j.hrthm.2010.11.023

17. Kaypakli O, Koca H, Sahin DY, Karatas F, Ozbicer S, Koc M. S-R difference in V1-V2 is a novel criterion for differentiating the left from right ventricular outflow tract arrhythmias. *Ann Noninvasive Electrocardiol.* (2018) 23:e12516. doi: 10.1111/anec.12516

18. Cheng Z, Cheng K, Deng H, Chen T, Gao P, Zhu K, et al. The R-wave deflection interval in lead V3 combining with R-wave amplitude index in lead V1: a new surface ECG algorithm for distinguishing left from right ventricular outflow tract tachycardia origin in patients with transitional lead at V3. *Int J Cardiol.* (2013) 168:1342–8. doi: 10.1016/j.ijcard.2012.12.013

19. Nikoo MH, Taheri S, Attar A. A novel ECG criterion to differentiate left from right ventricular outflow tract premature complex. *Scand Cardiovasc J.* (2020) 54:139–45.

20. Ouyang F, Fotuhi P, Ho SY, Hebe J, Volkmer M, Goya M, et al. Repetitive monomorphic ventricular tachycardia originating from the aortic sinus cusp: electrocardiographic characterization for guiding catheter ablation. *J Am Coll Cardiol.* (2002) 39:500–8. doi: 10.1016/s0735-1097(01)01767-3

21. Arya A, Huo Y, Frogner F, Wetzel U, Sommer P, Gaspar T, et al. Effect of limb lead electrodes location on ECG and localization of idiopathic outflow tract tachycardia: a prospective study. *J Cardiovasc Electrophysiol.* (2011) 22:886–91. doi: 10.1111/j.1540-8167.2011.02012.x

22. Anderson RH. Clinical anatomy of the aortic root. *Heart.* (2000) 84:670–3.

23. Asirvatham SJ. Correlative anatomy for the invasive electrophysiologist: outflow tract and supravalvar arrhythmia. *J Cardiovasc Electrophysiol.* (2009) 20:955–68. doi: 10.1111/j.1540-8167.2009.01472.x

24. Hutchinson MD, Garcia FC. An organized approach to the localization, mapping, and ablation of outflow tract ventricular arrhythmias. *J Cardiovasc Electrophysiol.* (2013) 24:1189–97. doi: 10.1111/jce.12237

25. Suleiman M, Asirvatham SJ. Ablation above the semilunar valves: when, why, and how? Part I. *Heart Rhythm.* (2008) 5:1485–92.

26. Pastore CA, Samesima N, Pereira FH, Tobias N, Madaloso BA, Facin ME. Applicability of the electro-vectorcardiogram in current clinical practice. *Arq Bras Cardiol.* (2019) 113:87–99. doi: 10.5935/abc.20190095

27. Lavalle C, Mariani MV, Piro A, Straito M, Severino P, Della RD, et al. Electrocardiographic features, mapping and ablation of idiopathic outflow tract ventricular arrhythmias. *J Interv Card Electrophysiol.* (2019) 57:207–18.

28. Anderson RD, Kumar S, Parameswaran R, Wong G, Voskoboinik A, Sugumar H, et al. Differentiating right- and left-sided outflow tract ventricular arrhythmias. *Circ Arrhythm Electrophysiol.* (2019) 12:e7392.

29. Betensky BP, Park RE, Marchlinski FE, Hutchinson MD, Garcia FC, Dixit S, et al. The V(2) transition ratio: a new electrocardiographic criterion for distinguishing left from right ventricular outflow tract tachycardia origin. *J Am Coll Cardiol.* (2011) 57:2255–62. doi: 10.1016/j.jacc.2011.01.035

30. Yamada T, Murakami Y, Yoshida N, Okada T, Shimizu T, Toyama J, et al. Preferential conduction across the ventricular outflow septum in ventricular arrhythmias originating from the aortic sinus cusp. *J Am Coll Cardiol.* (2007) 50:884–91. doi: 10.1016/j.jacc.2007.05.021

31. Cheng D, Ju W, Zhu L, Chen K, Zhang F, Chen H, et al. V3R/V7 index: a novel electrocardiographic criterion for differentiating left from right ventricular outflow tract arrhythmias origins. *Circ Arrhythm Electrophysiol.* (2018) 11:e6243. doi: 10.1161/CIRCEP.118.006243

32. Zhang F, Hamon D, Fang Z, Xu Y, Yang B, Ju W, et al. Value of a posterior electrocardiographic lead for localization of ventricular outflow tract arrhythmias: the V4/V8 ratio. *JACC Clin Electrophysiol.* (2017) 3:678–86. doi: 10.1016/j.jacep.2016.12.018

33. Di C, Wan Z, Tse G, Letsas KP, Liu T, Efremidis M, et al. The V1-V3 transition index as a novel electrocardiographic criterion for differentiating left from right ventricular outflow tract ventricular arrhythmias. *J Interv Card Electrophysiol.* (2019) 56:37–43. doi: 10.1007/s10840-019-00612-0

34. Zheng J, Fu G, Abudayyeh I, Yacoub M, Chang A, Feaster WW, et al. A high-precision machine learning algorithm to classify left and right outflow tract ventricular tachycardia. *Front Physiol.* (2021) 12:641066. doi: 10.3389/fphys.2021.641066

frontiers | Frontiers in Cardiovascular Medicine

TYPE Original Research
PUBLISHED 21 November 2022
DOI 10.3389/fcvm.2022.879381

OPEN ACCESS

EDITED BY
Carlo de Asmundis,
University Hospital Brussels, Belgium

REVIEWED BY
Gaetano Thiene,
University of Padua, Italy
Avi Sabbag,
Sheba Medical Center, Israel

*CORRESPONDENCE
Weizhu Ju
juweizhu@126.com

†These authors have contributed equally to this work

SPECIALTY SECTION
This article was submitted to Cardiac Rhythmology, a section of the journal Frontiers in Cardiovascular Medicine

RECEIVED 19 February 2022
ACCEPTED 01 November 2022
PUBLISHED 21 November 2022

CITATION
Shi L, Wang C, Chen H, Yang G, Gu K, Li M, Chu M, Liu H, Wang Z, Ju W and Chen M (2022) Ventricular arrhythmias originating from the basal septum of the ventricle: Clinical and electrophysiological characteristics and a systematic ablation approach. *Front. Cardiovasc. Med.* 9:879381. doi: 10.3389/fcvm.2022.879381

Ventricular arrhythmias originating from the basal septum of the ventricle: Clinical and electrophysiological characteristics and a systematic ablation approach

Linsheng Shi[1,2†], Cheng Wang[3†], Hongwu Chen[3], Gang Yang[3], Kai Gu[3], Mingfang Li[3], Ming Chu[3], Hailei Liu[3], Zidun Wang[3], Weizhu Ju[3*] and Minglong Chen[3]

[1]Department of Cardiology, The Second Affiliated Hospital of Nantong University, Nantong, China, [2]Nantong School of Clinical Medicine, Kangda College of Nanjing Medical University, Nanjing, China, [3]Department of Cardiology, The First Affiliated Hospital of Nanjing Medical University, Nanjing, China

Background: There is a paucity of data about VAs clustered at the vicinity of the basal septum of the ventricle. We aimed to report and characterize the clinical and electrophysiological features of basal septum VAs and explore the systematic ablation approach.

Methods: A consecutive series of 51 patients who had their VAs successfully ablated at the basal septum of the ventricle was enrolled in this study. The basal septum was defined as the area 2 cm away from the septal annulus, the upper boundary was the site of the left or right His-Purkinje system, and the lower boundary was the borderline that separated away from the septum. RFCA was performed based on detailed activation mapping or pace mapping. Patients who underwent VA ablation from other areas of the tricuspid annulus (TA) and mitral annulus (MA) during the same period were enrolled as the control group.

Results: The patients with basal septum VAs were significantly older ($p < 0.01$) and had more comorbidities (hypertension and coronary artery disease) ($p < 0.01$). Meanwhile, the precordial R wave transition was significantly different in right side, left side and intramural foci group ($p < 0.001$). Acute procedural success was achieved in 44 patients (86.3%) in the study group and in 63 patients (95.5%) in the control group. After a median of 12 (6–36) months of follow-up, compared with VA recurrence in the control group (2 cases), 11 patients with basal septum VAs had recurrences ($p = 0.002$), while a delayed cure was observed in 3 in intramural foci group.

Conclusion: Based on the unique anatomical and electrophysiological characteristics, a systematic approach for VAs originating from the basal

septal area is warranted. Moreover, the follow-up data seemed to show a relative high recurrence rate for basal septal VAs during a period of time.

KEYWORDS

basal septum, ventricular arrhythmias, catheter ablation, anatomy, electroanatomic mapping

Introduction

Ventricular arrhythmias (VAs) in patients without structural heart disease have a predilection for specific anatomic structures. To date, numerous reports have described the ablation of VAs originating from a certain anatomical structure, such as the papillary muscles, the His-Purkinje system (His), the areas near the ventricular outflow tracts, and the annulus (1–5). This clustering feature makes it possible to estimate the exact locations before intracardiac mapping, consequently allowing preprocedure planning and potentially facilitating mapping and ablation. Till now, a relatively large data of VAs clustered at the vicinity of the basal septum of the ventricle are still limited (6–8). In the present study, we report a group of VAs clustered in the vicinity of the basal septum. Additionally, we characterize the clinical and electrophysiological features of basal septum VAs, as well as the elaboration of the systematic ablation approach.

Materials and methods

Patient

From February 2012 to April 2021, a consecutive series of 51 patients who had their VAs successfully ablated at the basal septal area was enrolled in this study. These patients were selected from a pool of 1,065 VAs patients referred to the First Affiliated Hospital of Nanjing Medical University. Patients ablated from other areas of the tricuspid annulus (TA) and mitral annulus (MA) during the same period were enrolled as controls. All patients provided written informed consent before the procedure, and the study protocol was approved by the Institutional Review Board of the First Affiliated Hospital of Nanjing Medical University.

Electrophysiological study, mapping and ablation of the ventricular arrhythmias

All procedures were performed under conscious sedation and local anesthesia. All antiarrhythmic medications were ceased for at least 5 half-lives before the procedure. If needed, a 6F quadripolar and a decapolar catheter were advanced into the high right atrium or right ventricle and coronary sinus, respectively. The isoproterenol challenge was performed to provoke clinical VAs in the absence of VAs during the session.

Three-dimensional mapping was performed using the CARTO (Biosense-Webster Inc., Diamond Bar, CA, USA) or EnSite Velocity (Endocardial Solutions, Inc., Minneapolis, MN, USA) systems. The right ventricle and left ventricle models were reconstructed using the roving catheter via the right femoral vein or right femoral artery with a retrograde aortic approach or a trans-septal approach. Detailed activation mapping was performed in the area of interest to identify the earliest activation site. Remapping at the bilateral side of the basal septum was performed in 18 patients whose initial ablation failed. Additionally, in some cases, pace mapping was performed with bipolar pacing in the lowest possible capture threshold.

Radiofrequency energy delivery was applied to the earliest activation sites using an irrigated ablation catheter (Navistar Thermocool, Biosense Webster, Diamond Bar, CA, USA or IBI Coolflex, St. Jude Medical, St. Paul, MN, USA). The maximum ablation power was adjusted between 20 and 50 W, depending on the proximity to the conduction system at the discretion of the operator. The temperature limit was set at 43°C, and the irrigation rate was 17–0 ml/min. Generally, the site where energy application was attempted would be regarded as an excellent target if the VAs disappeared in 10 s. Consequently, the energy delivery would be performed up to 90 s. If the ablation failed, a remapping was performed to identify the earliest activation site, and then another ablation attempt was made. In some situations, anatomical ablation on both sides of the septum was performed. The endpoint of the procedure was defined as the disappearance of spontaneous clinical arrhythmias and the lack of inducibility of the VA using the same drug provocation protocol as before ablation.

Ventricles were divided into 3 parts equally from the apex to base and the most basal part of the ventricle septum was considered as the basal septum. Moreover, the basal septum was defined as the area 2 cm away from the septal annulus, the upper boundary was the site of the left or right His, and the lower boundary was the borderline that separated from the septum. Those VAs with their earliest activation superior to the His point

were not enrolled; as such, no patient was found to need ablation at the right coronary cusp.

Two approaches, that is above-valve and under-valve approach, were used for the ablation of right septum. For the above-valve approach, a long-fixed sheath was used to stabilize the ablation catheter and the catheter was advanced to the above-valve region directly. For the under-valve approach, the catheter was made a big curve and pulled back to reach the TA from the ventricular side.

Follow-up

After the procedure, patients were sent back to the cardiovascular ward and monitored for at least 12 h. No anti-arrhythmia drugs were used. After discharge, patients were asked to perform pulse checks and undergo 24-h Holter monitoring 3, 6, and 12 months after ablation, with 3- and 6-month intervals post-procedure thereafter to reassess any recurrence of symptoms. During the follow-up, a decrease in PVC burden of over 90% or no recurrent VT was defined as no recurrence. A late cure was defined as the disappearance of the VAs as assessed by Holter after discharge during follow-up.

Statistical analysis

Continuous variables were expressed as the means ± standard deviations (normally distributed variables) or medians (25th, 75th percentiles). The normality of the distribution was assessed with the Shapiro–Wilk test. Comparisons between groups were performed with an unpaired Student's *t*-test or non-parametric test. Three group data were analyzed with one-way ANOVA. Categorical variables were expressed as numbers and percentages. The chi-square test or Fisher's exact test was employed to compare the categorical data. All tests were 2-sided, and a p value <0.05 was considered to indicate statistical significance. Statistical analyses were performed using SPSS 22.0.

Results

Patient characteristics

A total of 51 studied patients (study group) and 66 control patients (control group) were enrolled in the study. The baseline clinical characteristics are provided in **Table 1**. No significant differences were noted in sex, left ventricular ejection fraction (LVEF), or left ventricular end diastolic dimension (LVEDD) between the two groups (all $p > 0.05$). However, the patients in the study group were significantly older (59.6 ± 15.5 vs. 34.9 ± 17.3, $p < 0.01$) and had more comorbidities (hypertension and coronary artery disease) than those in the control group ($p < 0.001$). Before the ablation procedure, the patients in the two groups had taken 0.9 ± 0.7 types of medications, including β-blockers, propafenone, mexiletine, amiodarone, and traditional Chinese drugs, with no benefit. One patient in the study group was involved in an electrophysiological study and ablation procedure in another hospital.

ECG characteristics

As a result, tall R or RR' pattern waves were all found in leads I and aVL. In all but 5 patients, the surface ECG demonstrated an initial q or QS wave at lead V1, and the other 5 patients demonstrated an R or Rs pattern. There was a significant difference between Group 1, Group 2 and Group 3 in terms of the morphological features in the precordial lead (**Table 2**) ($p = 0.001$). The V1 lead showed a positive wave (qR type) in only one patient in Group 3, while in Group 2, a positive wave was found in 7/16 patients (QR, R, RS, or qR type). At the V1 lead, a QS type was found in 34/35 patients in Group 1, while it was found in 9/14 patients in Group 2 and 8/9 patients in Group 3 ($p = 0.001$). In Group 1, the precordial R wave transition occurred at or beyond V3 in 18 patients (64.3%); however, 2 patients in Group 2 exhibited the precordial R wave transition at or beyond V3 (14.3%), and 4 patients in Group 3 ($p < 0.001$).

Mapping and acute ablation outcome

First, an under-valve approach was used to locate the earliest activation of the VAs. In the study group, all of the earliest activations were located at the basal septum (40 patients on the right side and 11 patients on the left side), with a mean preceding time compared with the onset of the QRS wave of 25.4 ± 7.6 ms. A small, far-field "a" signal was recorded at the earliest activation in 45 patients.

In the first attempt of ablation, an under-valve approach was used to target the earliest activation at the basal septum in 40 patients on the right side (**Figure 1**). Successful ablation of PVCs was observed in 23 patients. Remapping at the bilateral side of the basal septum was performed in the 17 patients whose initial ablation failed. At this step, the procedure was canceled in one patient due to pericardial effusion. In the remaining 16 patients, the shift of the earliest activation to the contralateral side was observed in 13 patients, while no obvious existing shift was detected in another 3 patients. Consequently, ablation at the left side was performed in 13 patients, with the VAs abolished in 5 patients. Among the 8 patients, VAs was abolished by atrial side ablation at the area of the slow pathway in two cases. Finally,

TABLE 1 Comparisons of clinical and electrophysiological characteristics of VAs in basal septum (studied group) and other area of tricuspid annulus and mitral annulus (control group).

Variables	Study group (51)	Control group (66)	*P*-value
Age (years)	59.6 ± 15.5	34.9 ± 17.3	0.000
Gender (male)	31	37	0.233
Co-morbidity			
Hypertension	20	11	0.001
Coronary artery disease	15	0	0.000
Diabetes	4	2	0.177
Echocardiogram			
LVEF (%)	62.1 ± 5.3	63.7 ± 3.6	0.051
LVEDD (mm)	48.7 ± 3.9	48.70 ± 4.4	0.402
Burden	24,108.2 ± 12,126.8	23,384.1 ± 11,770.3	0.804
Medications			
Beta blockers	25	28	0.072
Class I agents	8	21	0.309
Traditional Chinese drug	13	4	0.019
Total success	36 (70.6%)	61 (90.9%)	0.001
Recurrence during follow up	11 (21.6%)	2 (3.0%)	0.002

Values are expressed as mean ± SD or number (percentage). LVEF, left ventricular ejection fraction; LVEDD, left ventricular end diastolic dimension.

TABLE 2 Comparisons of ECG and electrophysiological characteristics of VAs in basal septum between the right side (Group 1), left side (Group 2) and intramural foci (Group 3).

Variables	Group 1 (28)	Group 2 (14)	Group 3 (9)	*P*-value
ECG characteristics				
QRS type in V1				0.001
QS	28	7	8	
QR	0	1	0	
R	0	4	0	
RS	0	1	0	
qR	0	1	1	
Early QRS transition				0.000
(V1)	0	6	1	
(V2)	10	6	4	
(V3)	13	2	2	
(V4)	4	0	1	
(V5)	1	0	1	
Preceding time of the target	26.6 ± 7.8	23.5 ± 6.4	23.4 ± 5.7	0.313
Small "a" at the target	26	13	6	0.353
Total success	20 (71.4%)	11 (78.6%)	5 (55.6%)	0.499

Values are expressed as mean ± SD or number (percentage).

anatomical ablation at both sides of the septum was performed in 9 patients, with success achieved in two patients and failure in the other 7 patients due to the transient suppression effect of VAs by ablation (4 patients) and signs of atrial ventricular conduction impairment (3 patient).

Left-side ablation was initially performed in 11 patients (retrograde aortic approach in 8 patients and transseptal approach in 3 patients due to instability of the mapping catheter in the retrograde aortic approach), and it successfully eliminated the VAs in 11 patients. After remapping on both sides, one patient who failed ablation on the left side had the VA successfully ablated by right-side ablation under the valve.

The detailed ablation results are provided as a flowchart in Figure 1. The anatomical distribution of the VAs is delineated in Figure 2. Then, according to the site of successful ablation, patients were categorized into Group 1 (right side), Group 2 (left sight) and Group 3 (intramural foci).

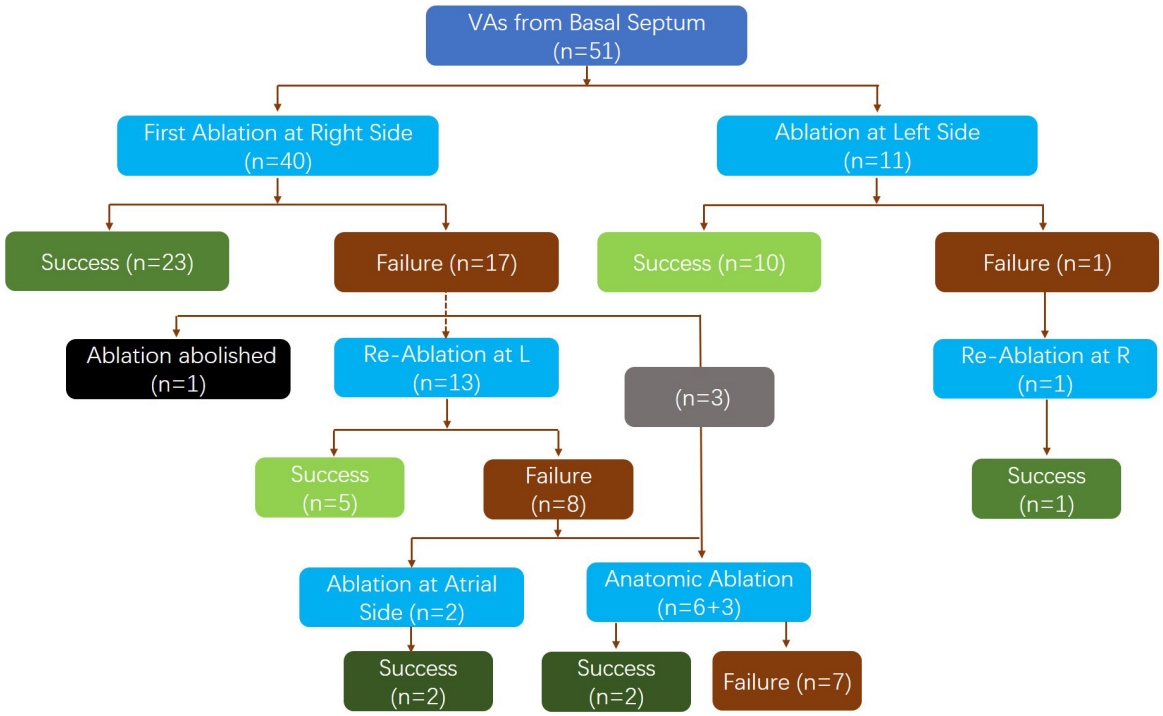

FIGURE 1
Flow chart of the detailed basal septum VA ablation results in acute term.

Acute and long-term outcomes

Acute procedural success was achieved in 44 patients (86.3%) in the study group and in 63 patients (95.5%) in the control group. After a median of 12 (6–36) months of follow-up, all anti-arrhythmia drugs were not used and 11 patients had a recurrence of their VAs, while a delayed cure was observed in 3 patients in the study group. There were 2 cases of recurrence in the control group (p = 0.002). In conclusion, success was achieved in 36 patients (70.6%) in the study group and 61 patients (90.9%) in the control group.

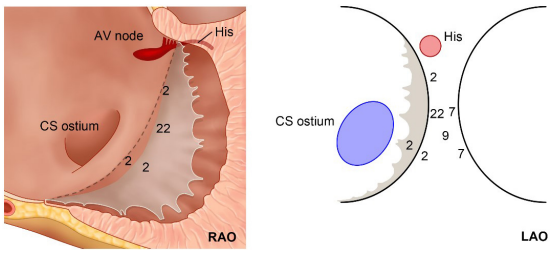

FIGURE 2
Schematic diagram of the anatomical distribution of the 51 cases of VAs.

Totally, junctional rhythm was observed in 5 patients during ablation, with no atrial ventricular block occurred after ceasing of burning in time. First-degree atrial ventricular block was observed in 2 patients during the procedure, in which the target site was close to the right His-bundle recording site (the distance was 6.0 and 5.5 mm, respectively), and they did not recover during the follow-up. Complete atrial ventricular block was observed in one patient 3 months after the procedure, with the ablation site at mid-septum under the valve.

Discussion

Major findings

In this study, we described the clinical, electrophysiological and ablation results of VAs ablated from the basal septum of the ventricle. We found that (1) VAs from the basal septum may represent a different group of VAs compared to VAs from other areas of the annulus; basal septum VAs manifest unique clinical characteristics and different ablation outcomes. (2) Compared with those originating in the tricuspid annulus (TA) and mitral annulus (MA), VAs originating from the basal septum of the ventricle had more recurrence. (3) Due to the deep location and multiple exits of this group of VAs, a systematic approach is needed, including under-valve or above-valve approaches for

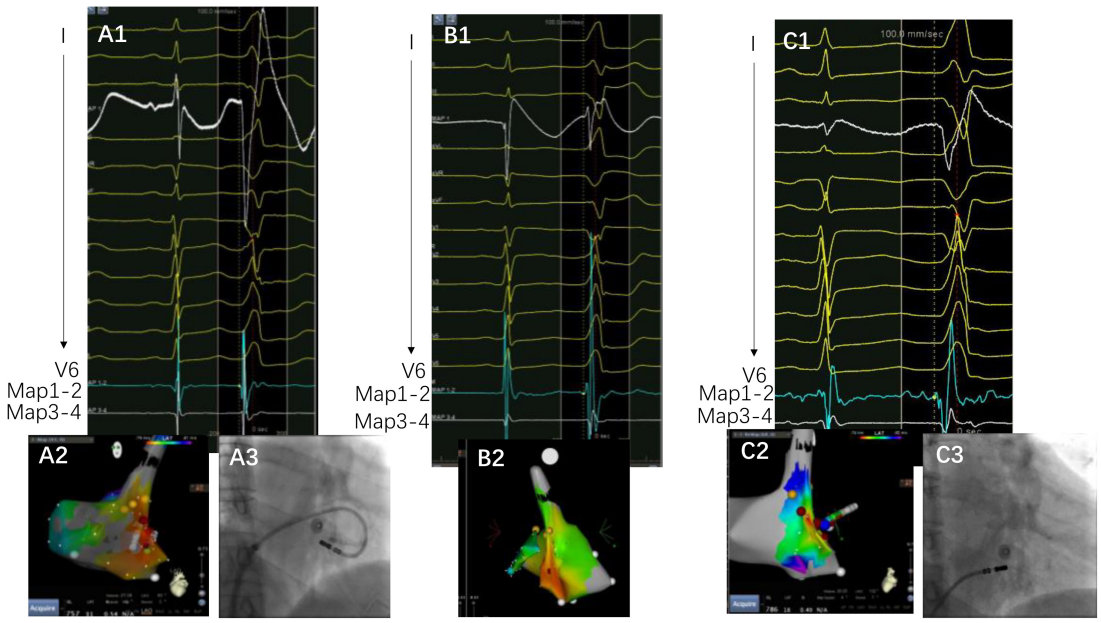

FIGURE 3
A case of VAs ablated from the low Koch's triangle. Panels **(A1–A3)** are target activation, three-dimensional map, and fluoroscopy image at the under-valve area, respectively. The target electrogram precedes the QRS onset by 14 ms, with a small "a" signal at the target electrogram. Panels **(B1,B2)** are the earliest activation and three-dimensional map, respectively. Notice that the target electrogram has a 6 ms prematurity compared with QRS onset without the "a" potential. Panel **(C1)** is the target electrogram at the low Koch's triangle preceding QRS onset with 28 ms. There is also an "a" potential at the target. The yellow points depict the area recording His in Panel **(C2)** and the blue point depicts the mapped activation. Notably, QRS demonstrates subtle changes after ablation on the right side of the under-valve area. Panels **(A3)** and **(C3)** depict the image contrast of the under-valve area and above valve area (low Koch's triangle).

the right side and retrograde aortic or transseptal approaches for the left side.

Anatomical considerations and ECG recognition

The basal septum delineated in the present study could be considered a combination of the farthest left part of the tricuspid annulus and the basal inferoseptal aspect of the left ventricular wall, i.e., the posterior-superior process of the left ventricle (PSP-LV). In some recent studies, the latter was delineated as the "basal inferoseptal left ventricle" (9). Theoretically, this area could also be considered the farthest right portion of the mitral annulus; however, most studies did not delineate the VAs originating here as the "septal mitral annulus," mostly because of the non-parallel position of the TA and MA. Based on the definition of the study, on the superior boundary of the basal septum lies the right fibrous trigone, and the inferior side was the upper end of the cardiac-crux area formed by the interventricular groove. Additionally, above this pyramidal structure lies the inferior wall of the right atrium, as well as the anteroinferior wall of the non-coronary cusp.

The complex anatomical arrangement has been translated into various VAs delineated by different groups. Hiroshi Tada et al. reported that the septum was the preferential site of origin for tricuspid annulus VAs (3). The latter has also been reported as the basal septum of the right ventricle for a distinct VA-originating structure by another group (10). Meanwhile, several studies have described the endocardial ablation of VAs from the left side, in which the structure was named "the basal infero-septal process of left ventricle" (7, 9), "left ventricular septum" (11), or "left ventricle adjacent to the membranous septum" (12). Additionally, the so-called basal infero-septal process has been successfully ablated from the atrial side (**Figure 3**) (13, 14).

In fact, these anatomical structures are very close to each other. Due to the neighboring topographic relationship, it is very difficult to differentiate these arrhythmias from each other before detailed mapping, and sometimes even attempted ablation. The tachycardias originating from these locations share several common ECG features, which have been shown in the present study. Almost all of the patients demonstrated an initial q or QS type wave at V1 with an abrupt reversal at V2, which has been identified as a sign of the septal accessory pathway in the ECG recognition of pre-excitation syndrome (2). Those patients eventually ablated from the right side demonstrated more QS type waves in V1; however, the QS type has little differential diagnosis value, as shown in **Table 1**. Nevertheless, if the ECG shows a more positive type (qR, R, RS), it is a predictive sign of warranting ablation from

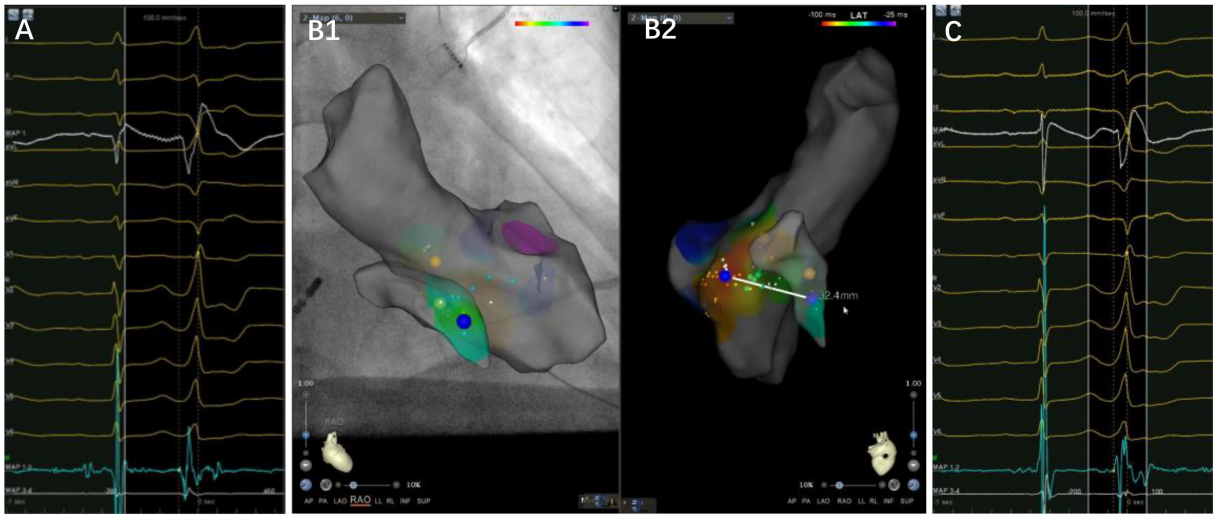

FIGURE 4
A case of premature ventricular complex ablated from the left side of the basal septum. Panels **(A–C)** are the left side target potential, three-dimensional map and the earliest activation at the under-valve area of right side, respectively. The target electrogram precedes the QRS onset by 36 ms, while the earliest activation on the right side only 14 ms, with a distance of 32.4 mm between them. Notice a small "a" potential at the target electrogram.

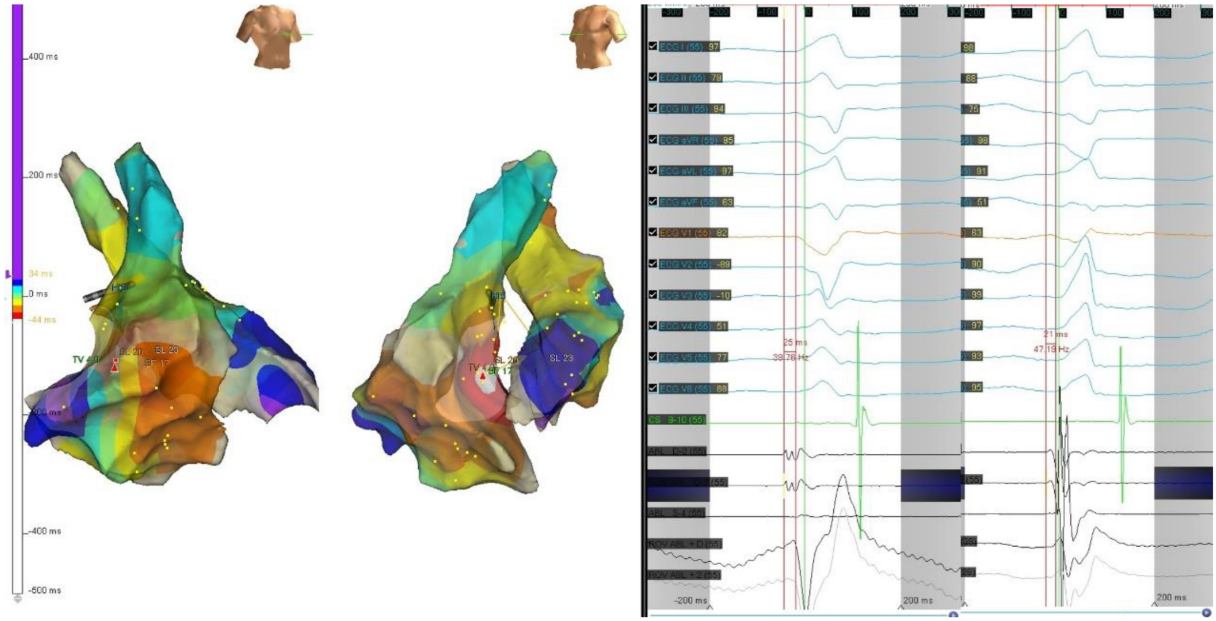

FIGURE 5
The precordial R wave transition occurred at V3 in ECG **(left)** before first ablation. Electroanatomic mapping in the right ventricle and the left ventricle, the earliest activation site was located at right basal septum with a preceding time compared with the onset of the QRS wave of 25 ms. After initial ablation failed, the precordial R wave transition occurred at V2 in ECG **(right)**. Remapping at the bilateral side of the basal septum was performed. The earliest activation site was located at left basal septum with a preceding time compared with the onset of the QRS wave of 21 ms. The PVC was successfully eliminated by ablation of both sides of basal septum.

the left side. Additionally, the two groups demonstrated a significant difference but an obvious overlap in terms of the reversal lead.

As such, we described these tachycardias together to distinguish these arrhythmias as an entity in the present study. From a clinical point of view, it has practical significance.

Electrophysiological findings and systematic approaches

It was found that the VAs was eliminated using the under-valve approach in 36 patients (70.6%) after a 12 month follow up. Additionally, most of the patients demonstrated a small "a" potential at the target site, which suggested that these tachycardias could be classified into a septal group of VAs from the annulus (**Figure 4**). Nevertheless, basal septal area VAs has unique characteristics compared with arrhythmias from other parts of the annulus due to the following facts. First, sequential ablation from both sides of the septum was required in 47% of patients due to the exit shift, which reflects a deep or even intramural location of the VA origin in some cases (**Figure 5**). When catheter ablation on the tricuspid valve is unsuccessful, a catheter inversion technique of the under-valve approach should be attempted for mapping and adequate contact and stability of the ablation catheter (15). In some situation, an anatomical ablation approach is also a valuable option in basal septum from intramural foci. Meanwhile, the impairment of AV conduction should not be ignored during RFCA delivered to this region. In our study, first-degree atrial ventricular block in the acute period and complete atrial ventricular block 3 months after the procedure were observed in two and one patients, respectively. Second, due to the apical displacement of the septal tricuspid valve relative to Koch's triangle, some VAs from the septal tricuspid annulus were successfully ablated from the low Koch's triangle with no complications (14). Third, in those patients that need left-side ablation, a combined strategy employing a retrograde aortic approach and a transseptal approach should be considered. Consequently, based on the unique anatomical and electrophysiological characteristics, a systematic approach for VAs originating from the basal septal area is warranted.

Limitations

First, this was a retrospective, single-center study. Second, the patients in the study group were found to be older than those in the control group, as well as more comorbidities including hypertension and coronary artery disease were found in basal septum VAs. It could not be determined whether the older age and more comorbidities accounted for the relative low success rate in the study group. To clarify this issue, systematical MRI imaging is needed to illuminate if a high progression of myocardial fibrosis at the basal septum due to the age and comorbidity occurred in the study group.

Conclusion

Based on the unique anatomical and electrophysiological characteristics of the basal septum, a systematic approach for VAs originating from this area is warranted. Moreover, the follow-up data seemed to show a relative high recurrence rate for basal septal VAs during a period of time.

Data availability statement

The original contributions presented in this study are included in the article/supplementary material, further inquiries can be directed to the corresponding author.

Ethics statement

The studies involving human participants were reviewed and approved by the Institutional Ethical Committee of the First Affiliated Hospital of Nanjing Medical University. The patients/participants provided their written informed consent to participate in this study.

Author contributions

LS and CW performed the clinical study and drafted the original manuscript. HC, GY, KG, ML, MCu, HL, ZW, and MCe interpreted and discussed the data. WJ reviewed and edited the manuscript. All authors contributed to the whole article and approved the final version of this manuscript.

Funding

This study was supported by Grant of Jiangsu Commission of Health (Grant No. LKM2022060), Science Foundation of Nantong City (Grant No. JC2021139), Research Innovation Team Project from Kangda College of Nanjing Medical School (Grant No. KD2022KYCXTD009), and Grant of Nantong Commission of Health (Grant No. MA2021013).

Conflict of interest

The authors declare that the research was conducted in the absence of any commercial or financial relationships that could be construed as a potential conflict of interest.

Publisher's note

References

1. Tada H, Ito S, Naito S, Kurosaki K, Kubota S, Sugiyasu A, et al. Idiopathic ventricular arrhythmia arising from the mitral annulus: a distinct subgroup of idiopathic ventricular arrhythmias. *J Am Coll Cardiol.* (2005) 45:877–86. doi: 10.1016/j.jacc.2004.12.025

2. Yamauchi Y, Aonuma K, Takahashi A, Sekiguchi Y, Hachiya H, Yokoyama Y, et al. Electrocardiographic characteristics of repetitive monomorphic right ventricular tachycardia originating near the His-bundle. *J Cardiovasc Electrophysiol.* (2005) 16:1041–8. doi: 10.1111/j.1540-8167.2005.40787.x

3. Tada H, Tadokoro K, Ito S, Naito S, Hashimoto T, Kaseno K, et al. Idiopathic ventricular arrhythmias originating from the tricuspid annulus: Prevalence, electrocardiographic characteristics, and results of radiofrequency catheter ablation. *Heart Rhythm.* (2007) 4:7–16. doi: 10.1016/j.hrthm.2006.09.025

4. Yamada T, Doppalapudi H, McElderry HT, Okada T, Murakami Y, Inden Y, et al. Electrocardiographic and electrophysiological characteristics in idiopathic ventricular arrhythmias originating from the papillary muscles in the left ventricle: relevance for catheter ablation. *Circ Arrhythm Electrophysiol.* (2010) 3:324–31. doi: 10.1161/CIRCEP.109.922310

5. Jia L, Yue-Chun L, Kang-Ting J, Na-Dan Z, Jia-Xuan L, Wen-Wu Z, et al. Premature ventricular contractions originating from the left ventricular septum: results of radiofrequency catheter ablation in twenty patients. *BMC Cardiovasc Disord.* (2011) 11:27. doi: 10.1186/1471-2261-11-27

6. Kotake Y, Campbell T, Bennett RG, Turnbull S, Huang K, Ross N, et al. Clinical and electrophysiological characteristics of ventricular tachycardias from the basal septum in structural heart disease. *JACC Clin Electrophysiol.* (2021) 7:1274–84. doi: 10.1016/j.jacep.2021.06.001

7. Li A, Zuberi Z, Bradfield JS, Zarif JK, Ward DE, Anderson RH, et al. Endocardial ablation of ventricular ectopic beats arising from the basal inferoseptal process of the left ventricle. *Heart Rhythm.* (2018) 15:1356–62. doi: 10.1016/j.hrthm.2018.04.029

8. Larsen TR, Shepard RK, Koneru JN, Cabrera JA, Ellenbogen KA, Padala SK. Electrocardiographic characteristics and ablation of ventricular arrhythmias originating from the basal inferoseptal area. *Europace.* (2021) 23:1970–9. doi: 10.1093/europace/euab189

9. Liang JJ, Shirai Y, Briceño DF, Muser D, Enriquez A, Lin A, et al. Electrocardiographic and electrophysiologic characteristics of idiopathic ventricular arrhythmias originating from the basal inferoseptal left ventricle. *JACC Clin Electrophysiol.* (2019) 5:833–42. doi: 10.1016/j.jacep.2019.04.002

10. Sasaki K, Sasaki S, Kimura M, Horiuchi D, Itoh T, Ishida Y, et al. Catheter ablation of ventricular arrhythmias arising from the basal septum of the right ventricle: characteristics and significance of junctional rhythm appearing during ablation. *J Interv Card Electrophysiol.* (2016) 45:159–67. doi: 10.1007/s10840-015-0095-0

11. Kusa S, Hachiya H, Iwasawa J, Ichihara N, Komatsu Y, Taniguchi H, et al. Ventricular arrhythmias with superior axis originating from the left ventricular septum: electrocardiographic characteristics predicting successful ablation and insights into their mechanism-observations from a small series of patients. *Europace.* (2015) 17:1587–95. doi: 10.1093/europace/euu396

12. Yamada T, Plumb VJ, McElderry HT, Doppalapudi H, Epstein AE, Kay GN. Focal ventricular arrhythmias originating from the left ventricle adjacent to the membranous septum. *Europace.* (2010) 12:1467–74. doi: 10.1093/europace/euq259

13. Santangeli P, Hutchinson MD, Supple GE, Callans DJ, Marchlinski FE, Garcia FC. Right atrial approach for ablation of ventricular arrhythmias arising from the left posterior-superior process of the left ventricle. *Circ Arrhythm Electrophysiol.* (2016) 9:e004048. doi: 10.1161/CIRCEP.116.004048

14. Briceño DF, Liang JJ, Shirai Y, Markman TM, Enriquez A, Lin A, et al. Clinical and electrophysiological characteristics of idiopathic ventricular arrhythmias originating from the slow pathway region. *Heart Rhythm.* (2019) 16:1421–8. doi: 10.1016/j.hrthm.2019.06.013

15. Kay GN, Yamada T. Anatomical consideration in catheter ablation of idiopathic ventricular arrhythmias. *Arrhythm Electrophysiol Rev.* (2016) 5:203–9. doi: 10.15420/aer.2016:31:2

Frontiers in
Cardiovascular Medicine

Innovations and improvements in cardiovascular treatment and practice

Focuses on research that challenges the status quo of cardiovascular care, or facilitates the translation of advances into new therapies and diagnostic tools.

Discover the latest Research Topics

See more →

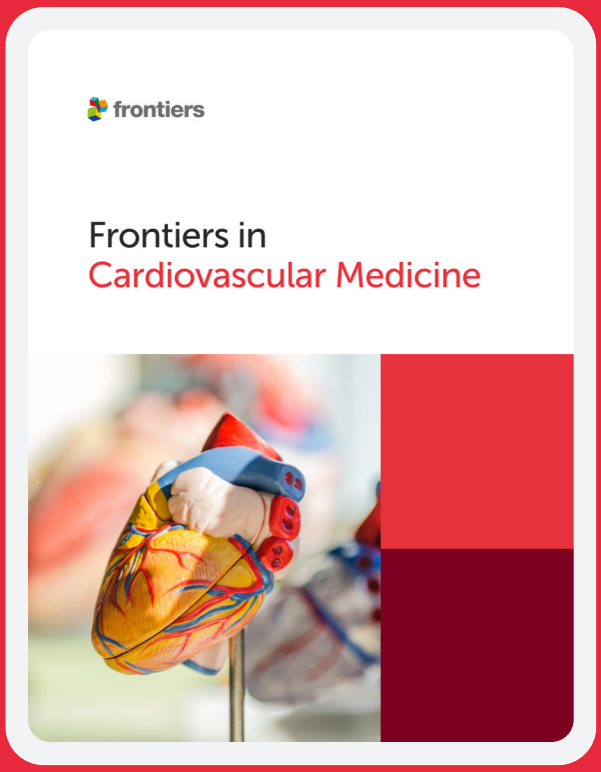

Frontiers

Avenue du Tribunal-Fédéral 34
1005 Lausanne, Switzerland
frontiersin.org

Contact us

+41 (0)21 510 17 00
frontiersin.org/about/contact